7. SITE 748[1]

Shipboard Scientific Party[2]

HOLE 748A

Date occupied: 13 March 1988

Date departed: 14 March 1988

Time on hole: 10 hr, 30 min

Position: 58°26.45′S, 78°58.89′E

Bottom felt (rig floor; m, drill pipe measurement): 1298.0

Distance between rig floor and sea level (m): 10.5

Water depth (drill pipe measurement from sea level, m): 1287.5

Total depth (rig floor; m): 1317.0

Penetration (m): 19.0

Number of cores (including cores with no recovery): 2

Total length of cored section (m): 19.0

Total core recovered (m): 19.25

Core recovery (%): 101

Oldest sediment cored:
Depth (mbsf): 19.0
Nature: diatom ooze and ice-rafted debris
Age: early Pliocene

HOLE 748B

Date occupied: 14 March 1988

Date departed: 15 March 1988

Time on hole: 1 day, 3 hr, 15 min

Position: 58°26.45′S, 78°58.89′E

Bottom felt (rig floor; m, drill pipe measurement): 1301.4

Distance between rig floor and sea level (m): 10.50

Water depth (drill pipe measurement from sea level, m): 1290.9

Total depth (rig floor; m): 1526.50

Penetration (m): 225.10

Number of cores (including cores with no recovery): 25

Total length of cored section (m): 225.10

Total core recovered (m): 190.15

Core recovery (%): 84

Oldest sediment cored:
Depth (mbsf): 206.10
Nature: nannofossil ooze
Age: middle Eocene
Measured velocity (km/s): 1.55

HOLE 748C

Date occupied: 15 March 1988

Date departed: 23 March 1988

Time on hole: 8 days, 11 hr, 45 min

Position: 58°26.45′S, 78°58.89′E

Bottom felt (rig floor; m, drill pipe measurement): 1301.0

Distance between rig floor and sea level (m): 10.50

Water depth (drill pipe measurement from sea level, m): 1290.5

Total depth (rig floor; m): 2236.00

Penetration (m): 935.00

Number of cores (including cores with no recovery): 87

Total length of cored section (m): 760.00

Total core recovered (m): 185.88

Core recovery (%): 24

Oldest sediment cored:
Depth (mbsf): 898.75
Nature: basalt cobble conglomerate
Age: undetermined
Measured velocity (km/s): undetermined

Hard rock:
Depth (mbsf): 935.00
Nature: altered basalt
Measured velocity (km/s): 4.580

Basement:
True basement not recovered

Principal results: Site 748 (proposed site SKP-3C) is a reentry site located on the Southern Kerguelen Plateau in the western part of the Raggatt Basin, east of Banzare Bank (58°26.45′S, 78°58.89′E, at a water depth of ~1290 m). The site was intended to recover an expanded section of Paleogene and Cretaceous sediments in order to decipher the tectonic and geologic history of this portion of the plateau.

An approach site survey located the site on *Rig Seismic* MCS line RS02-27 (100.2340, shot point 4150). Correlation of the *JOIDES Resolution* single channel line with existing data is clear and shows two major reflectors at the site that lie at 0.83 and 0.41 s two-way traveltime (TWT) below seafloor. Other reflectors deduced from seismic stratigraphy studies lie at 0.92, 0.61, 0.29, 0.16, and 0.09 s TWT below seafloor.

After coring the upper 215 m of the section via advanced hydraulic piston (APC) and extended core barrel (XCB) coring until refusal, the reentry hole was initiated using the rotary core barrel (RCB) and drilled to 550 m below seafloor (mbsf), at which point a model LH (Lamar Hayes) reentry minicone was deployed to take advantage of a calm weather window for that operation. The hole was continued to 742 mbsf, at which point a successful reentry procedure was conducted to change the bit. The hole was then drilled to a total depth of 935 m, where a failed flapper valve allowed massive backflow of sediments into the bottom hole assembly (BHA), preventing further operations (including logging) at this site.

Aside from the sediment recovered from the BHA, little material was trapped in cores (i.e., in core-catcher socks) taken over the basal

[1] Schlich, R., Wise, S. W., Jr., et al., 1989. *Proc. ODP, Init. Repts.*, 120: College Station, TX (Ocean Drilling Program).

[2] Shipboard Scientific Party is as given in the list of participants preceding the contents.

27 m of the hole, perhaps due to the malfunction of the flapper valve and/or to excessive ship heave. Nevertheless, average core recovery over the last 95 m prior to these problems was 70%; this is the deepest penetration yet achieved with a minicone upon reentry.

The following lithologic units were recognized at Site 748:

Unit I (0–13.3 mbsf): upper Pleistocene to lower Pliocene diatom ooze with radiolarian- and foraminifer-enriched intervals, dropstones, and ice-rafted debris.

Unit II (13.3–389.1 mbsf): upper Miocene to upper Paleocene nannofossil ooze, chalk, porcellanite, and chert divisible into two subunits.

Subunit IIA (13.3–180.6 mbsf): upper Miocene to middle Eocene nannofossil ooze with biosiliceous intervals.

Subunit IIB (180.6–389.1 mbsf): middle Eocene to upper Paleocene nannofossil ooze, chalk, porcellanite, and chert.

Unit III (389.1–898.8 mbsf): upper Paleocene to upper Albian–Turonian glauconitic packstones, wackestones, siltstones, and claystones, in part silicified and divided into three subdivisions.

Subunit IIIA (389.1–692.0 mbsf): upper Paleocene to upper Campanian glauconitic rud-, pack-, and grainstones, intermittently silicified, with intervals of abundant bryozoans, inoceramid prisms, and crinoid columnals, plus rare red algal debris.

Subunit IIIB (692.0–897.6 mbsf): upper Albian to Turonian sandstones, siltstones, and claystones.

Subunit IIIC (897.6–898.8 mbsf): basalt cobble conglomerate consisting of rounded, altered basalt cobbles and boulders, broken thick-walled mollusc fragments, and a matrix of glauconitic, calcareous siltstone. No baked contact is evident, but sparry calcite veins are common.

Unit IV (898.8–935.0 mbsf): highly altered basalt flow and underlying lithologies, undated but subdivided into two units.

Subunit IVA (898.8–902.2 mbsf): sparsely clinopyroxene and plagioclase phyric basalt, strongly weathered and altered.

Subunit IVB (902.2–935.0 mbsf): predominantly downhole cavings from Unit III plus some lithologies not encountered above. All of this material was recovered only as fragments in core-catcher socks or in the BHA; no intact cores were retrieved. Lithologies not observed previously are (1) red and green smectitic clay with goethite and hematite stains; (2) brown smectitic, sideritic clay with fine calcite and siderite veins; and (3) highly altered pieces of basalt that have vesicles filled with alteration minerals.

The basalt cored at 898.8 mbsf has compositional characteristics similar to intraplate, oceanic-island alkaline basalts and is thought to represent the last of a series of basalt flows that, for lack of core recovery, can only be inferred to lie within Subunit IVB. The Unit IV basalts are necessarily younger than those that form the true basement of the Raggatt Basin. These younger flows are strongly weathered, and some appear to be interlayered with siltstones and claystones derived from that weathering; wood fragments, if in place, denote the development of soils and vegetation on some flows. According to regional seismic data, true basement (located at 0.92 s TWT) was not penetrated at this site, but lay 150–200 m below the total depth (TD) of Hole 748C.

Beginning with the basal conglomerate, the first sediments deposited in the basin are glauconitic with up to 0.5% organic matter, denoting a restricted marine environment. No calcareous or siliceous microfossils are preserved, but shore-based palynological study dated them as late Albian–Cenomanian.

High glauconite contents (up to 20%) characterize the remainder of Unit III as do total organic contents between 0.2% and 0.6% (maximum 1.0%). These are mostly type III hydrocarbons composed of terrestrial and highly oxidized marine organic matter. Datable calcareous microfossils first occur at 711 mbsf and are followed a short distance upcore by a host of invertebrates. Some fossils, such as coralline red algae, serpulid worm tubes, and encrusting bryozoans, indicate periods of quite shallow paleodepths (up to the inner shelf). The inoceramid remains, which compose up to 80% of some intervals, are exceptionally well preserved and should provide reliable isotopic paleotemperature data. Some vertebrate teeth recovered belong to sharks and possibly to the giant swimming lizard, *Mosasaurus*.

Productivity and consequently sedimentation rates in this shallow, banklike environment were quite high (up to 60 m/m.y). Siliceous sponges as well as radiolarians, diatoms, and silicoflagellates contributed abundant biogenic silica that was ultimately responsible for the silicified layers in Subunit IIIA. The amount of glauconite produced over the entire 500-m-thick Unit III section is extraordinary, particularly in view of the high sedimentation rate.

Mesozoic calcareous nannofossil and planktonic foraminifer assemblages have a strong austral affinity, as at Site 747 to the north. Sedimentation was apparently continuous from the late Campanian into the early Maestrichtian, but a portion of the middle Maestrichtian is missing. The uppermost Maestrichtian and Danian are also missing (hiatus = ~6–7 m.y.). This latter gap in the record corresponds to a widespread regional disconformity, noted as the prominent reflector at 0.41 s TWT below seafloor on our seismic records, and thought to mark a major tectonic and erosional event that affected much of the plateau (i.e., see "Principal Results" section, "Site 747" chapter, this volume). Subsidence of Site 748 following this erosional event was quite rapid.

The upper Paleocene through middle Eocene pelagic carbonate and chert sequence is apparently continuous and was deposited in deeper waters (similar to present day) as subsidence had far outstripped the high sedimentation rate of 20 m/m.y. Regional seismic analysis shows that the Paleogene depocenter for the basin had shifted considerably toward the east as a consequence of the profound Maestrichtian tectonic event.

Full recovery (100%) in the upper 180 m of the section in Hole 748B provides an excellent Neogene calcareous-biosiliceous section with good paleomagnetic control that complements the one obtained at Site 747. The main elements of the magnetic polarity record from Anomaly Correlatives 1 to 18 (Pleistocene to late Eocene) have been recognized. Both the upper and lower epoch boundaries of the thick (65–70 m) Oligocene section are clearly defined by bio- and magnetostratigraphy (Anomaly Correlatives 6C and 13).

A striking occurrence of angular quartz sand, heavy minerals, and micas in the lowermost Oligocene denotes ice-rafted debris. This corresponds to early Oligocene glaciation documented in Prydz Bay by Leg 119 drilling and provides the most convincing evidence to date for the existence of a continental ice sheet on the Antarctic continent at this time. Several hiatuses are present in the Oligocene, and parts of the lower and middle Miocene are missing (hiatus = ~1–3 m.y.). Major hiatuses are identified in the upper Miocene–lower Pliocene (~4.0–8.5 Ma) and in the middle Miocene (12–17 Ma), and the Pleistocene is condensed and discontinuous.

Nevertheless, this site, in conjunction with others cored on the plateau, will be quite valuable for paleoceanographic studies. Taking the Neogene together with the Paleogene and Cretaceous sequences, we have an essentially complete record of the events that highlight the evolution of the Raggatt Basin on the Southern Kerguelen Plateau.

BACKGROUND AND OBJECTIVES

The Kerguelen Plateau extends between 46°S and 64°S and can be divided into two distinct domains: the Kerguelen-Heard Plateau to the north and the Southern Kerguelen Plateau to the south (Schlich, 1975, 1982; Houtz et al., 1977). Site 748 (58°26.45′S, 78°58.89′E) is located on the Southern Kerguelen Plateau in the western part of the Raggatt Basin, east of the Banzare Bank, approximately 900 km south of the present-day Antarctic Convergence at a water depth of 1290 m (see "Introduction" chapter, this volume).

Three northeast-trending multichannel seismic reflection lines (RS02-24, RS02-27, and RS02-29 extended to the east by RS02-33), separated by approximately 50 km, and one northwest-trending line (MD47-05) in the central part of the Raggatt Basin provide good regional control of the area close to Site 748 (Fig. 1). To the west the Raggatt Basin ends abruptly against faults associated with the 77°E Graben, or farther to the south against the basement outcrop of Banzare Bank. The eastern edge of the Raggatt Basin is a scarp or slope merging into the deep Labuan Basin. To the north and to the south, the sedimentary section thins gradually, but a lack of seismic reflection data prevents precise delineation of the basin.

The sediment cover in the central part of the Raggatt Basin reaches 2500–3000 m and rests upon a weakly defined basement

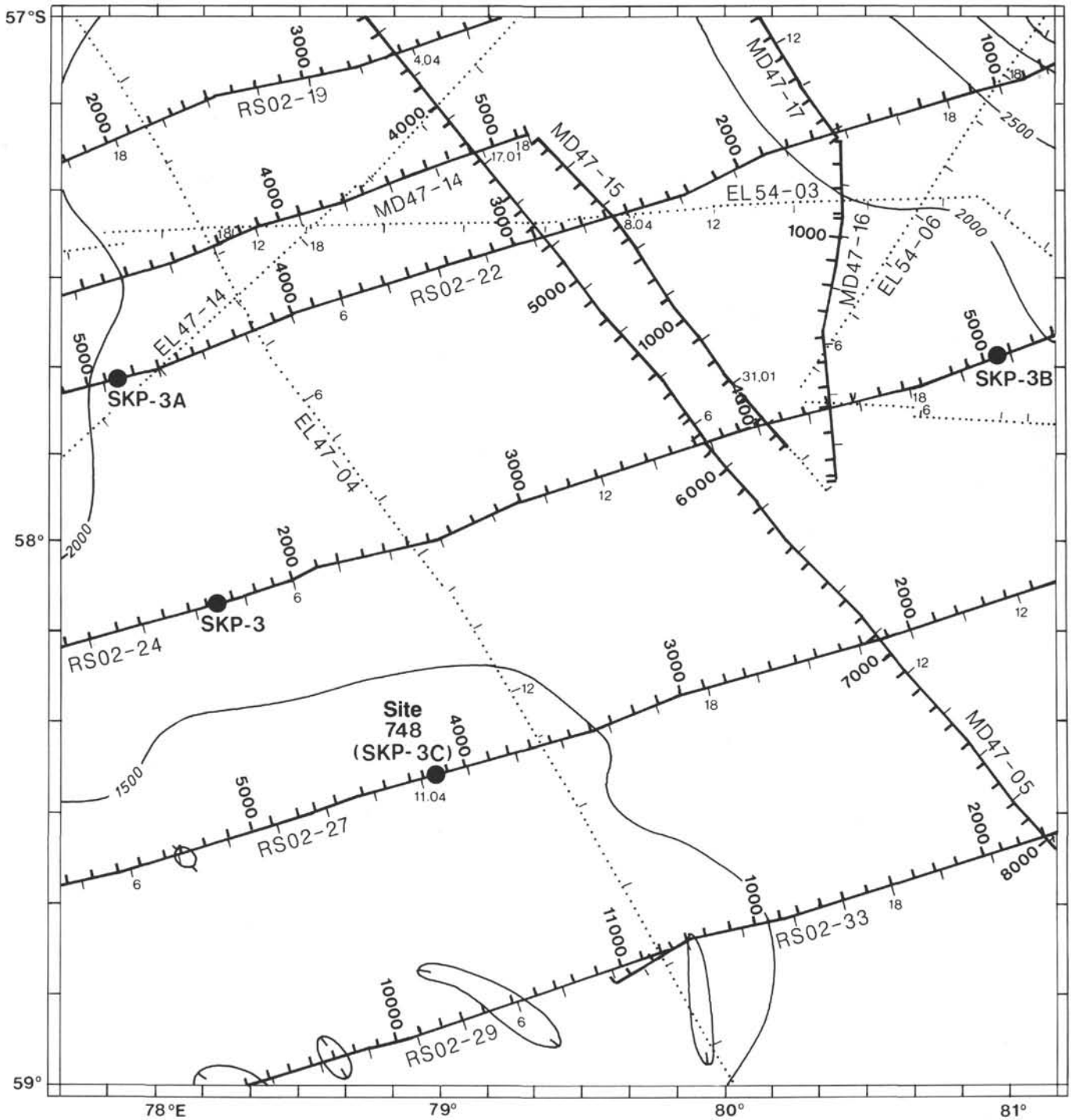

Figure 1. Track lines in the vicinity of Site 748. Bold lines denote *Rig Seismic* (RS02) and *Marion Dufresne* (MD47) multichannel seismic reflection profiles. The bathymetry is from Schlich et al. (1987) and is shown in meters.

reflector. Schlich et al. (1988) and Colwell et al. (1988) independently identified six seismic sequences in the basin. Joint interpretation of Australian and French multichannel seismic reflection data (Coffin et al., unpubl. data) distinguished seven seismic sequences that can be grouped into two megasequences. The upper megasequence is divided into three sequences (NQ1, PN1, and P2) and the lower megasequence into four sequences (P1, K3, K2, and K1). Leclaire et al. (1987a, 1987b) recovered the first significant assemblage of basement rocks along the 77°E Graben north of the site. The samples are basaltic and were dated at 114 Ma, and the lowermost exposed sediments are of Late Cretaceous age.

Site 748 (target site SKP-3C) is on Australian multichannel seismic reflection line RS02-27 (100.2340, shot point 4150) trending northeast across the Raggatt Basin, where the basement lies within 1100 and 1300 m and where an almost complete sedimentary section, ranging from Cretaceous to Holocene, is present. The location of the site is given along with seismic line RS02-27 in Figure 2.

Objectives

The prime objective of drilling Site 748 was to recover an expanded section of Paleogene and Cretaceous sediments reflecting the early tectonic history of the Southern Kerguelen Plateau

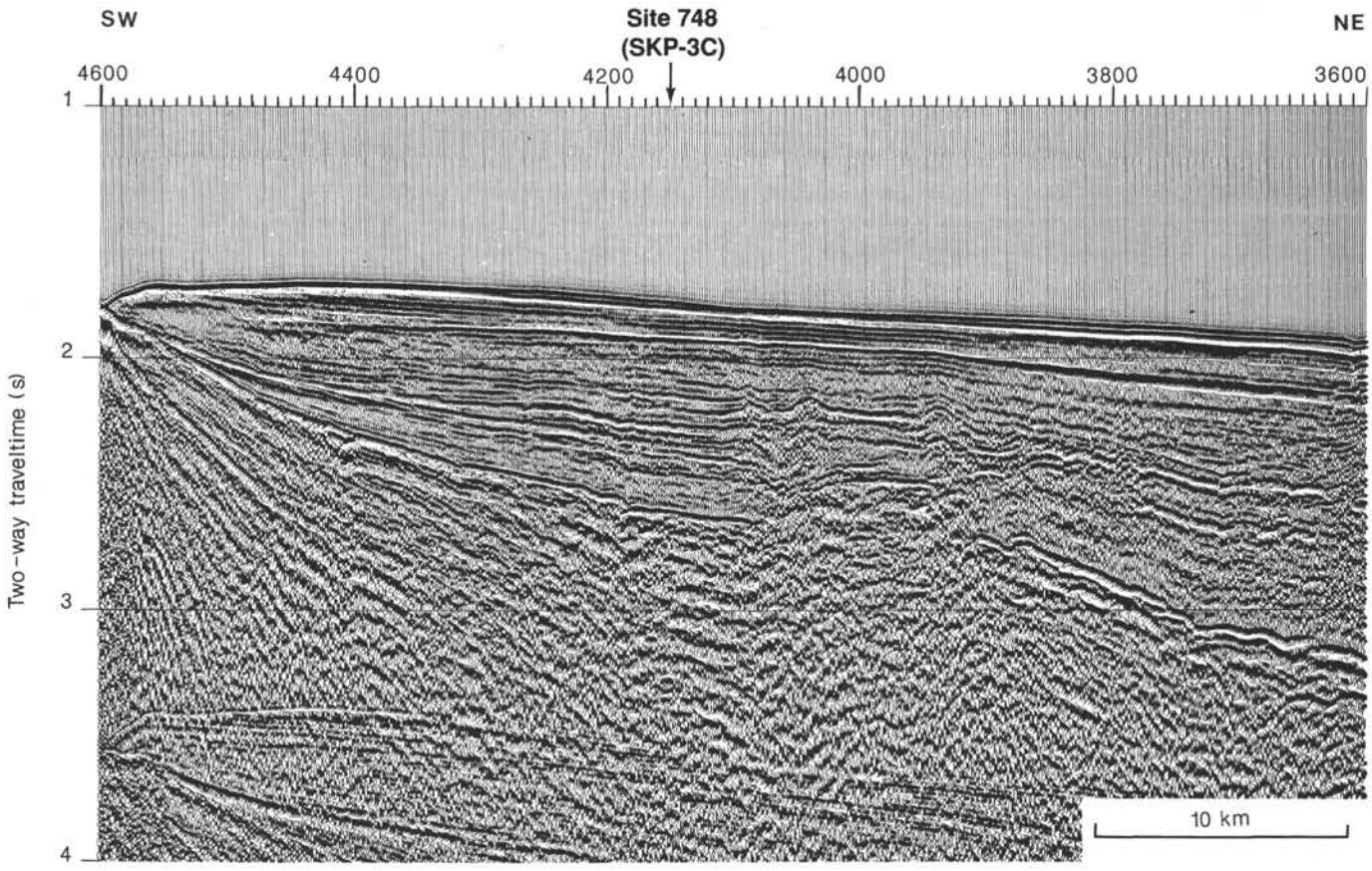

Figure 2. Seismic section RS02-27 (shot point 3600 to 4600) and SKP-3C site location (Site 748).

(i.e., the ages of the different sedimentary sequences, unconformities, rifting episodes, and vertical movements) and the evolution of Cretaceous and Paleogene climates. We planned to compare the results with the data obtained at Site 737 (KHP-3), the northern Paleogene-Mesozoic stratigraphic site drilled on Leg 119.

A second objective of drilling this site was to recover basement samples from the Raggatt Basin and to compare these rocks with those obtained at other Kerguelen Plateau basement sites (i.e., Site 738 in the southernmost part of the Kerguelen Plateau drilled on Leg 119, and Site 747 in the transition zone between the northern and southern parts of the Kerguelen Plateau and Site 749 on the Banzare Bank, both of which were drilled on Leg 120).

Several sites dealing with these objectives were considered by the different JOIDES panels. The original site SKP-3 on seismic line RS02-24 (97.0415) was approved only to 800 m to avoid penetrating a sequence of reflections forming a pinch-out at depth. Site SKP-3A on seismic line RS02-22 (96.1049) was eliminated because the basement and the lowermost sediments were probably out of reach. Site SKP-3B on seismic line RS02-24 (97.1950) and site SKP-3C on seismic line RS02-27 (100.2340, shot point 4150) were approved without restriction by the JOIDES panels.

Basement at site SKP-3B appears to be at about 1000 m, and at site SKP-3C at about 1200 m. At site SKP-3B most of the Neogene is missing and the lowermost Cretaceous sequence (K1) may also be missing. At site SKP-3C the sedimentary column was expected to be complete, but basement was considered out of reach. Considering the merits and disadvantages of both sites, priority was given on board to site SKP-3C (Site 748), which apparently contains a complete Cretaceous sedimentary sequence.

Drilling Strategy

Drilling strategy at Site 748 was to use the APC followed by the XCB until refusal. Then we planned to use the RCB with reentry to core the deeper part of the sedimentary section and eventually to sample the basement, thus achieving the stratigraphic and tectonic objectives.

SITE GEOPHYSICS

JOIDES Resolution departed Site 747 on 12 March 1988 in the late afternoon (1730 hr L). The magnetometer was towed immediately after departure, and continuous bathymetric and magnetic recording started at 0930 hr (UTC) along a line almost due south. At 1545 hr the ship changed course to 145° and headed toward Site 748 (proposed site SKP-3C).

Site 748, the first site to be drilled in the Raggatt Basin on the Southern Kerguelen Plateau, lies about 230 nmi south of Site 747 on *Rig Seismic* line RS02-27 (shot point 4150; Fig. 1). *JOIDES Resolution* intersected the Australian survey profile (RS02-27) at about 0830 hr (UTC) on 13 March 1988. At this point the ship changed course, our speed was reduced to 6 kt, and the seismic profiling gear was deployed. The final site approach was made with global positioning system (GPS) satellite navigation along a course of about 253°, following the *Rig Seismic* survey line (RS02-27) over a distance of about 28 mi.

A beacon was dropped on the initial crossing of the proposed site (SKP-3C). The *JOIDES Resolution* seismic data recorded over the site show good correlation with the *Rig Seismic* multichannel seismic reflection profile shot in 1985, and identi-

fication of the site location was unambiguous. The gear was retrieved at 1320 hr (UTC) on 13 March 1988 as soon as the site was passed, and the ship proceeded back to the beacon to commence drilling (Fig. 3). The final coordinates of Site 748 are 58°26.45′S and 78°58.89′E; the water depth (from sea level) as measured from the drill pipe (DPM) and corrected for the height of the rig floor above sea level at the three holes (748A, 748B, and 748C) ranges between 1287.5 and 1290.9 m.

Sediment cover in the Raggatt Basin reaches 2500–3000 m and rests upon a weakly defined basement reflector. Interpretation of the Australian and French multichannel seismic reflection data collected in the Raggatt Basin in 1985 and 1986 identified seven distinct seismic sequences, which can be grouped into two megasequences. The upper megasequence is divided into three sequences (NQ1, PN1, and P2). Sequences NQ1 and PN1 are only observed in the central part of the Raggatt Basin and are truncated in all directions by toplap. Sequence P2 filled the relief of the lower megasequence by onlap.

The lower megasequence is divided into the remaining four sequences (P1, K3, K2, and K1). Sequences P1 and K3 are characterized by mounds that appear either as isolated features or in association with normal faults. The thickness of Sequence P1 remains fairly uniform in the basin while Sequence K3 shows significant variations in thickness. Sequences K2 and K1 filled up the center of the basin and disappear in all directions by onlap. A major tectonic episode corresponding to normal faulting, occurred at the boundary between Sequences K3 and P1; this event is related to the shift of the depocenter, which moves from west (K1, K2, and K3) to east (P1, P2, PN1, and NQ1; see "Introduction" chapter, this volume).

Using all the available seismic data, an isochron map of the top of the acoustic basement (Fig. 4) and two isopach maps—one for the total sedimentary cover (Fig. 5) and one for the upper sequences NQ1 and PN1 (Fig. 6)—have been drawn for the area close to the drill site. Site 748 is located on the western flank of the Raggatt Basin where basement trends almost in a northwest direction and where the Neogene sedimentary sequences become extremely thin, thus offering the opportunity to sample the Paleogene and the Cretaceous. West of Site 748, at about 20 km, the Raggatt Basin is bounded by a series of northwest-trending normal faults that are probably related to an uplift episode.

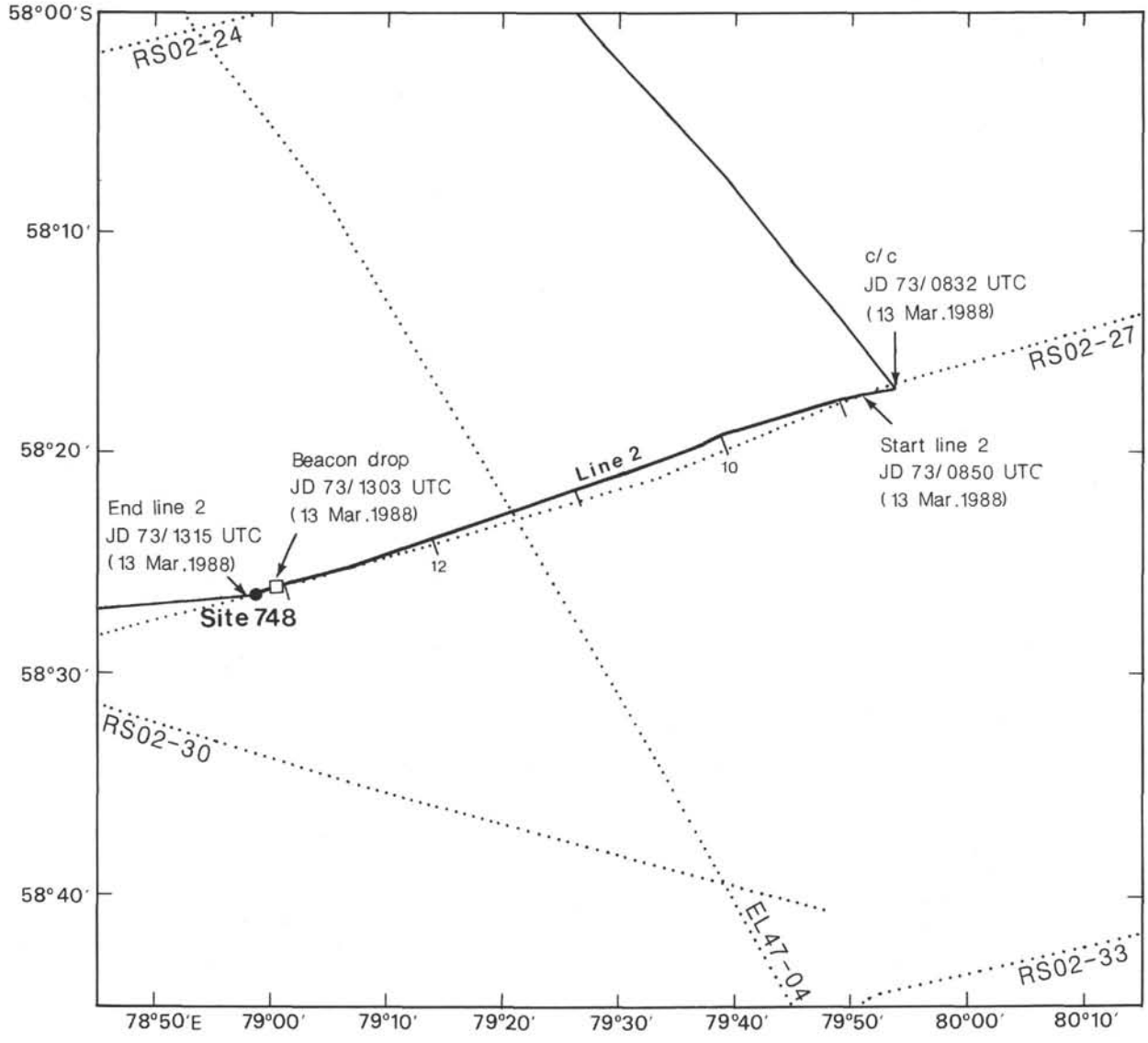

Figure 3. *JOIDES Resolution* site approach and Site 748 location.

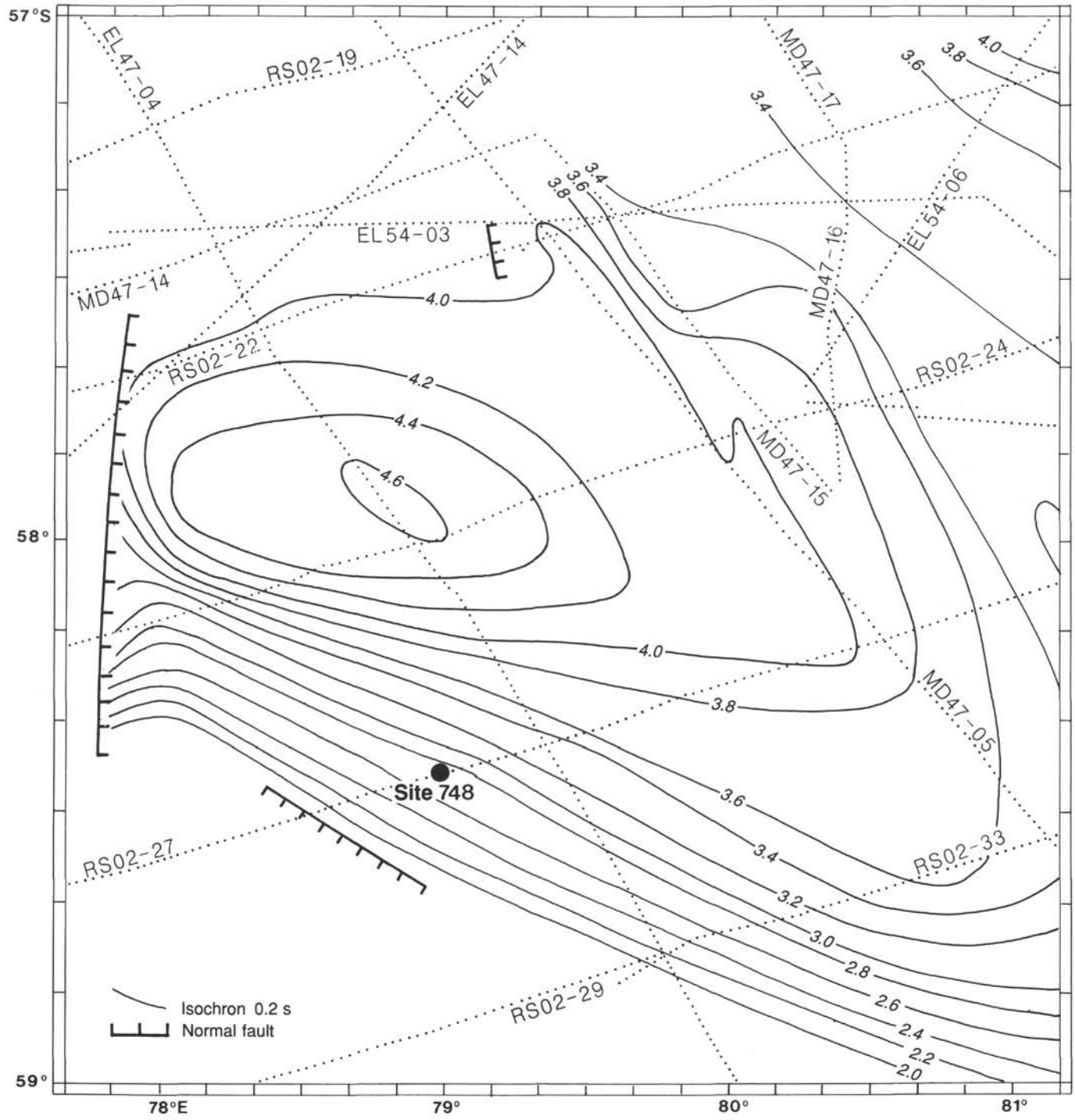

Figure 4. Isochron map of the top of the acoustic basement contoured in seconds (TWT).

The *JOIDES Resolution* survey line, shot with two 80-in^3 water guns and recorded with a 100-m hydrophone streamer, is shown on Figure 7. The similitude of this single channel seismic record with the Australian multichannel seismic reflection profile used to locate Site 748 is obvious (Fig. 2). However, all the reflectors observed on the multichannel line are not identifiable on the *JOIDES Resolution* survey line.

At Site 748 the basement reflector lies at about 0.92 s TWT below seafloor, and we can trace a major reflector corresponding to the boundary between K3 and P1 at 0.41 s TWT below seafloor. From seismic stratigraphic analyses, it is possible to scale several other reflectors at 0.83, 0.61, 0.29, 0.16, and 0.09 s TWT below seafloor at Site 748. The reflectors at 0.92, 0.83, and 0.41 s TWT below seafloor are visible on the *JOIDES Resolution* survey line. It is almost impossible, however, to scale the minor reflectors observed on the multichannel seismic line; these reflectors are masked by the noise level and the bubble pulse of the source. The correlation of *Rig Seismic* and *JOIDES Resolution* seismic sections at Site 748 is shown on Figure 8.

The vertical velocity distribution has been estimated from sonobuoy experiments carried out in the Raggatt Basin during *Marion Dufresne* cruise 47 (1986). Considering these results, we

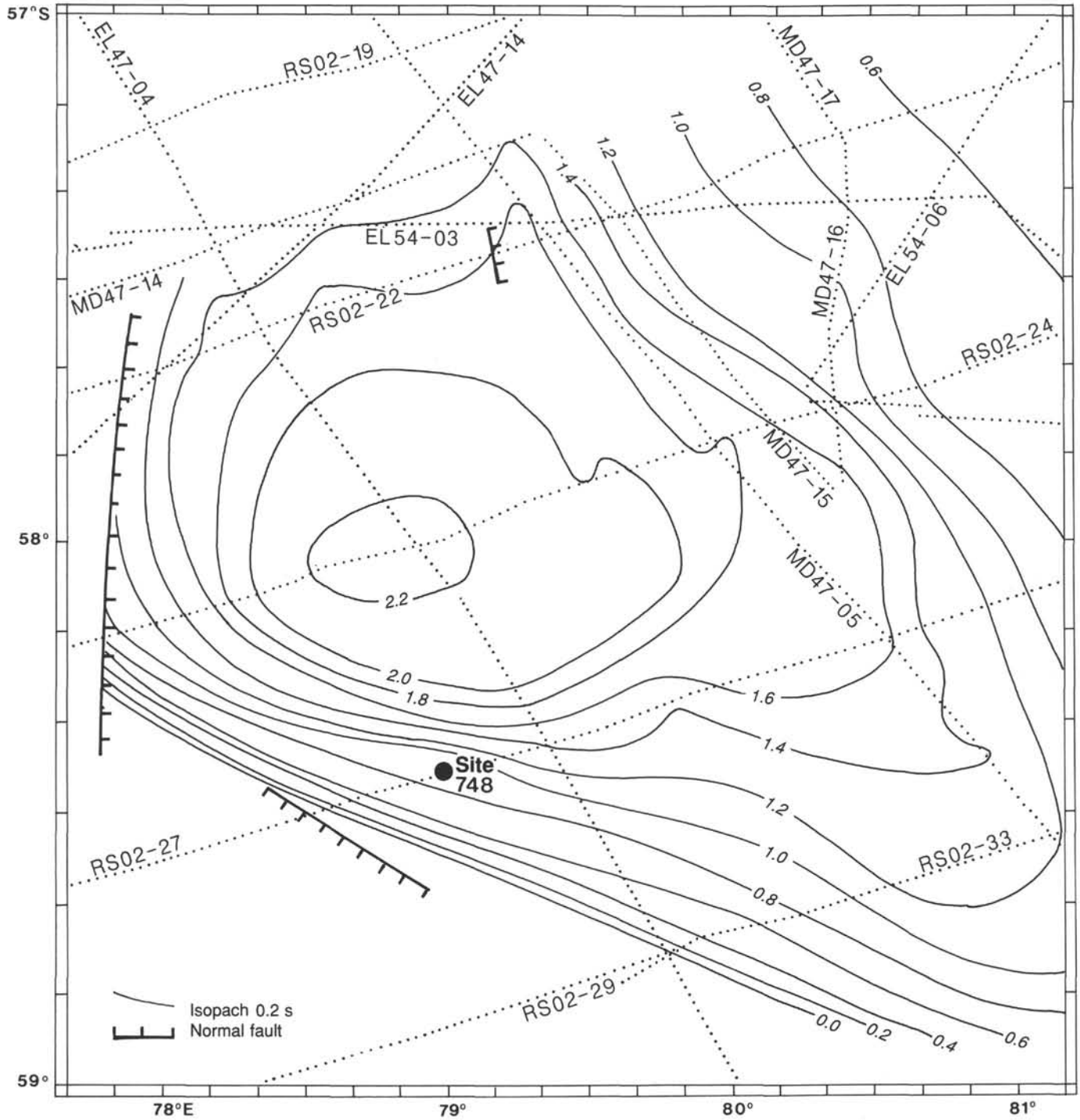

Figure 5. Total sediment isopach map contoured in seconds of reflection time.

expected basement at 1290 mbsf and the main reflector (the K3/P1 boundary) at 450 mbsf. Readjustment of the vertical velocity distribution made before drilling and based on drilling results at Site 747 suggested a basement depth of about 1130 mbsf (0.92 s TWT) and the K3/P1 boundary at about 370–390 mbsf (0.41 s TWT). A sonobuoy experiment planned on our departure from Site 748 was canceled to allow for our arrival at the next site in a GPS navigation window.

OPERATIONS

Site 747 to Site 748

The transit to Site 748 began at 1730 hr (L), 12 March 1988, on a southeasterly course with 16-ft swells running in the same direction. The 195-nmi run required 28¼ hr, including 15 nmi of preliminary surveying. The beacon was dropped at 2115 hr (L; 1303 hr UTC), 13 March 1988, and the survey gear was re-

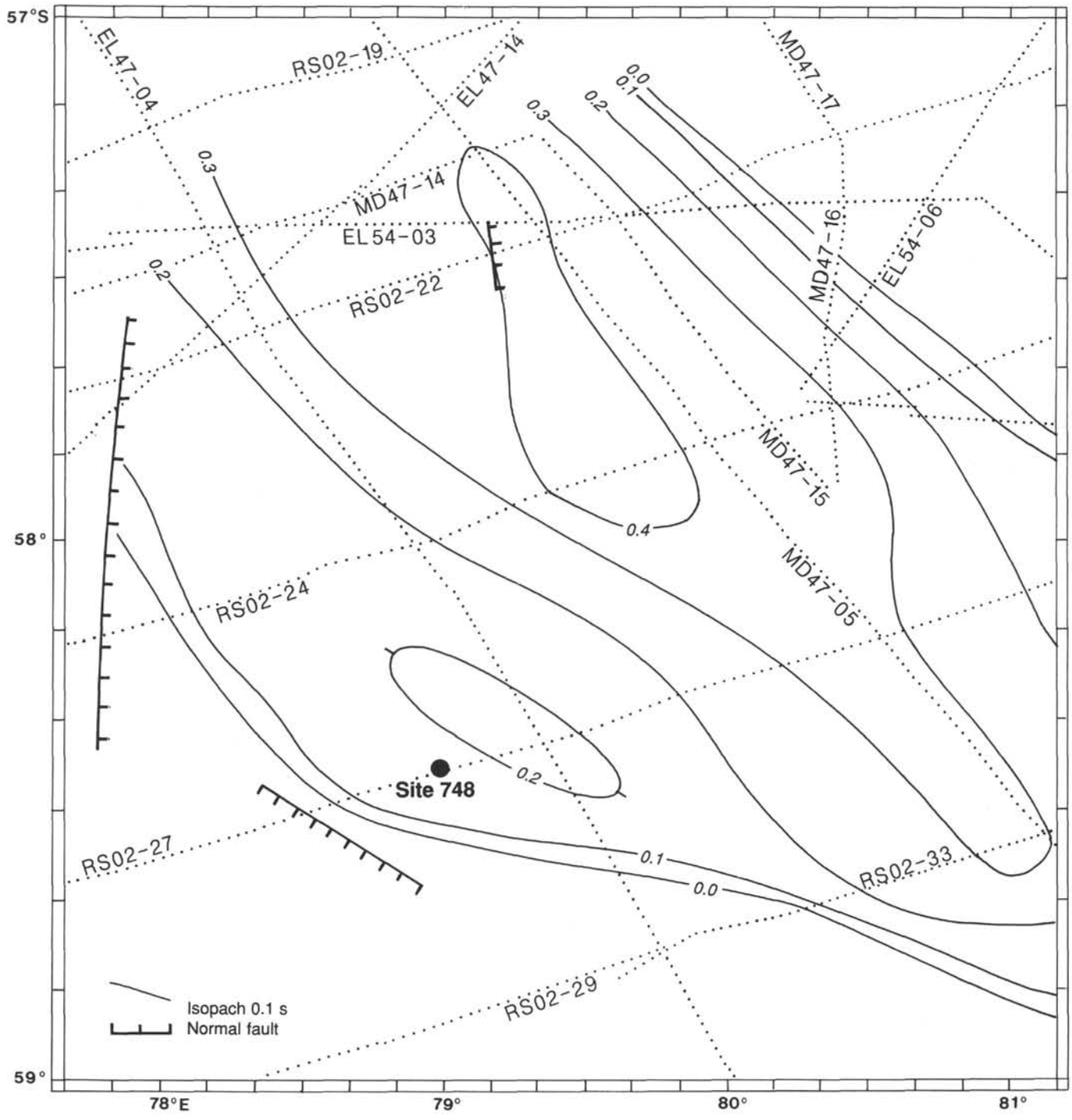

Figure 6. NQ1 and PN1 isopach map contoured in seconds of reflection time.

trieved quickly. Normally, the ship would have turned and headed back to the beacon, but the 16-ft swells would have caused a bad roll condition during the turn. To eliminate the roll problem, the ship maintained a heading into the wind and swell while backing down onto the beacon. This maneuver required only 1 hr to take station over the beacon.

Site 748 (SKP-3C)

Hole 748A

An XCB bit equipped with 1/2-in. angle jets and modified for a Polypak bit seal was made up to a nine-drill-collar APC/XCB BHA and run to the seafloor. The bit was positioned at 1300 m to shoot the mud line at 1304 m (as measured by precision depth recorder [PDR]). Almost a full core barrel was recovered for Core 120-748A-1H, and some doubt remained about the seafloor depth. After we had retrieved Core 120-748A-2H, the bit was pulled clear of the seafloor to respud and establish the correct depth.

Hole 748B

The bit was positioned at 1292 m, and the interface was recovered by the next APC core, at 1301.4 m. Continuous APC coring then proceeded in nannofossil ooze and chalk to 181

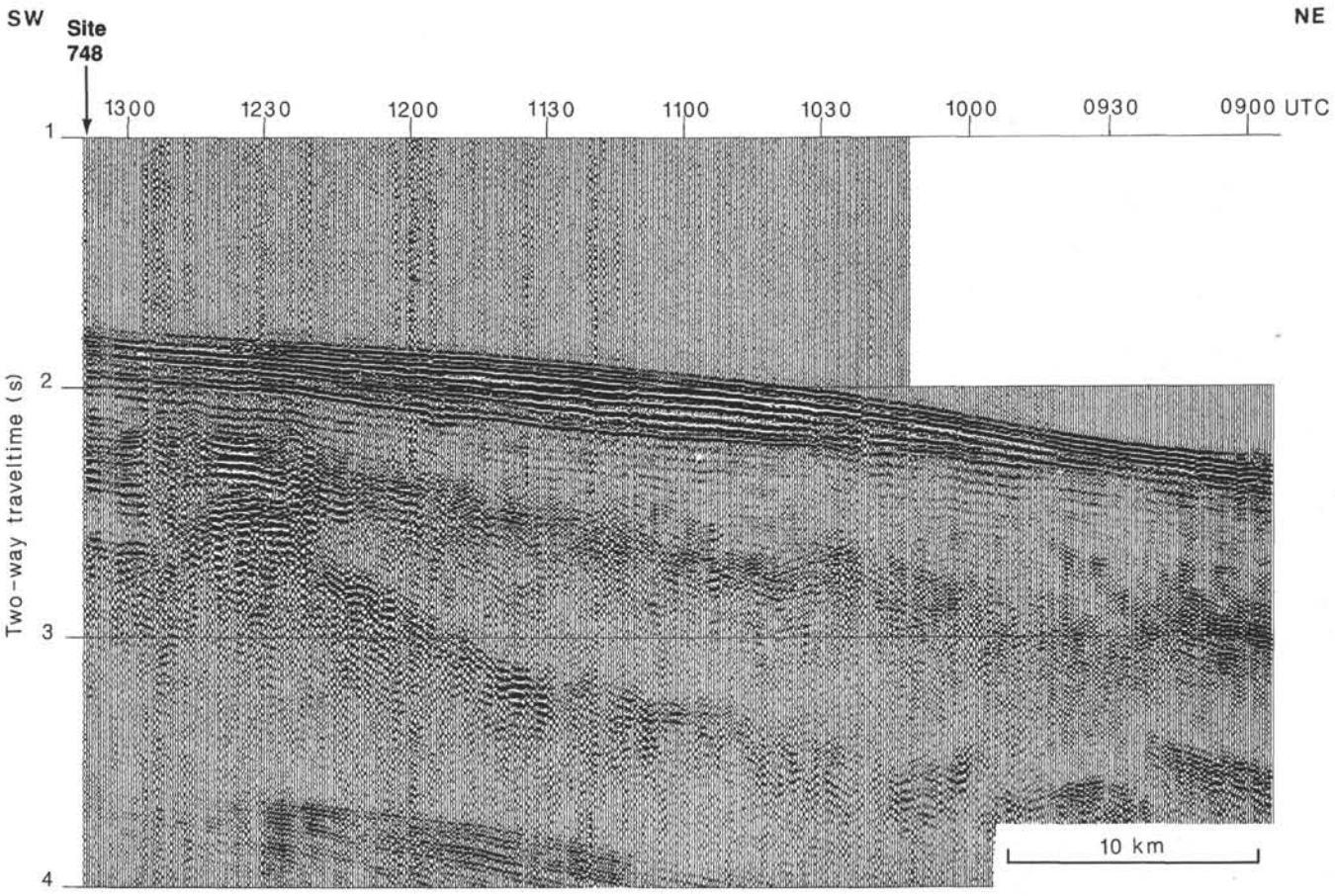

Figure 7. *JOIDES Resolution* single channel reflection profile on approach to Site 748.

mbsf, where overpull reached 50,000 lb. Core recovery was 100%. Temperature probe runs were made after Cores 120-748B-10H and -15H.

We then continued XCB coring in chalk with chert stringers to 216 m with average core recovery of only 15%. When the chert began to destroy the XCB shoes, further XCB penetration was abandoned in favor of the RCB system. The hole was filled with weighted mud, and the drill string was tripped for a RCB bit and BHA.

Hole 748C

A full-sized reentry cone installation had originally been planned for Site 748C. However, this time-expensive operation would have been extremely difficult or impossible to carry out under the prevailing weather conditions, and a minicone reentry was planned instead. Hole 748C was spudded at 1615 hr (L), 15 March 1988, and washed without rotation to 40 mbsf. At that point the sediment became too firm for jetting, and the hole was drilled to 172 mbsf. A temperature probe measurement was then taken before continuous RCB coring commenced.

Core recovery started out no better than with the XCB and soon became worse. Only hard siliceous streaks were recovered, and the soft chalk interbeds were lost. Recovery was further hampered by deteriorating weather conditions as winds gusted to 50 kt and vessel heave reached 8 ft.

At 435 mbsf, coring was interrupted for 2 hr for a wireline fishing job to recover a core barrel pulling tool that had backed off at the connection to the sinker bars. The nature of the fish was not suited to the commercial overshot-type fishing tools on hand, but a satisfactory substitute was devised through modification of an ODP core catcher.

With more severe weather forecasted, operations were again interrupted at 531 mbsf. A total of 5 1/2 hr was required to short-trip the pipe and deploy the minicone or free-fall reentry funnel (FFF). The funnel was emplaced at this point to maintain our ability to deepen the hole in case weather forced a hasty withdrawal.

Core recovery improved somewhat with depth, and upon reaching 742 mbsf, we decided to attempt to extend the hole with a second bit. Coring was therefore ended short of bit failure, the hole was conditioned with mud, and a drill string round-trip was made.

With marginal visibility at the seafloor, 1 1/2 hr of scanning and maneuvering were required before televised reentry was made. The bit encountered a bridge or restriction in the hole at about 388 mbsf (the approximate depth of the Cretaceous/Tertiary boundary) and became stuck. The pipe came free after it had been "worked" for 1 1/4 hr, but it was necessary to clean out several additional bridges or tight spots on the way to total depth (TD). Before coring could begin, another 1 1/2 hr were spent in clearing plastic coating that had fouled the upper drilling line guide.

The hole had been deepened by just 56 m when a delay of 22 hr was occasioned by an electrical fault in the main cable to the top drive. When coring resumed, core recovery began to improve dramatically with depth in glauconitic siltstone, but hole conditions had degenerated. A basalt flow was reached at about 900 mbsf. Very little core was recovered in the next 35 m, and

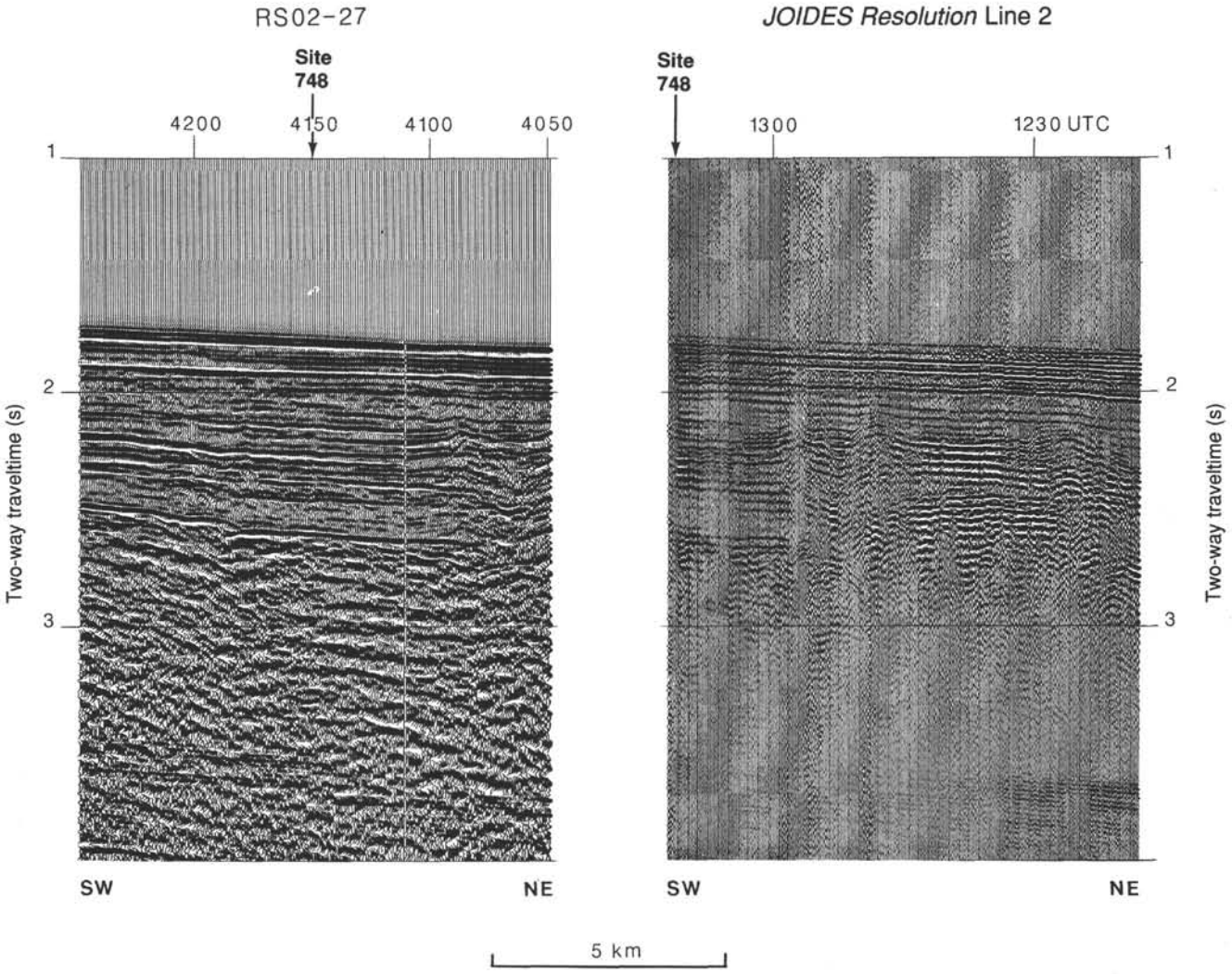

Figure 8. Comparison of *Rig Seismic* multichannel seismic reflection profile RS02-27 and *JOIDES Resolution* single channel survey Line 2 in the vicinity of Site 748.

the hole became increasingly unstable, with several meters of hole fill between cores and increasing circulating pressure.

Coring operations were terminated because of hole conditions, and efforts to condition the hole for logging were in progress when a failed float valve permitted suspended cuttings to "U-tube" from the annulus into the drill string and plug the BHA. Attempts to circulate the cuttings from the pipe were unsuccessful, resulting only in a burst kelly hose, and it was necessary to recover the drill string.

Because we had already met many of our scientific objectives and because of the adverse hole conditions, there was no attempt to clean out, log, or plug Hole 748C. After the lower 60 m of the BHA had been emptied of fine black drill cuttings, the vessel departed Site 748 at 2245 hr (L), 23 March 1988.

The coring summary for Site 748 appears in Table 1.

LITHOSTRATIGRAPHY AND SEDIMENTOLOGY

Introduction

Site 748 is located in the western part of the Raggatt Basin, Southern Kerguelen Plateau, in ~1290 m of water. The objective of drilling at this site was to recover a thick Paleogene and Cretaceous section in order to document the early sedimentation and tectonic history of the Southern Kerguelen Plateau. Three holes were drilled at this site, and the sequence divided into four lithologic units (Table 2 and Figs. 9 and 10).

Unit I consists of 13.3 m (Hole 748A) of diatom ooze with ice-rafted debris (IRD). The IRD consists of sand- to pebble-size clasts of igneous, metamorphic, and sedimentary origin (Table 3).

Unit II consists of nannofossil ooze, porcellanite, and chert and extends from 13.3 (Hole 748A) to 389.1 (Hole 748B) mbsf. It differs from the overlying unit by having fewer diatoms, and from the underlying unit by having no glauconite. This unit is subdivided at 180.6 mbsf into the overlying nannofossil ooze and the underlying nannofossil ooze and chalk with chert and porcellanite. After chert was encountered at 180.6 mbsf, drilling recovery decreased to less than 20%, compared with 100% in the above unit.

Unit III consists of 509.7 m of glauconitic rudstones, grainstones, packstones, wackestones, sandstones, siltstones, claystones, and a basal conglomerate. It is divided into three subunits. The uppermost subunit is bioclastic; the middle subunit is composed of glauconite, zeolites, and altered grains; the lower subunit is a basal basalt-cobble conglomerate.

Subunit IIIA was recovered at depths of 389.1–692.0 mbsf. It consists of rudstones, grainstones, packstones, and wackestones that, intermittently, are partly cemented by silica. The dominant

Table 1. Coring summary, Site 748.

Core no.	Date (March 1988)	Time (local)	Depth (mbsf)	Cored (%)	Recovered (%)	Recovery (%)
120-748A-						
1H	14	0700	0.0–9.5	9.5	10.10	106.3
2H	14	0735	9.5–19.0	9.5	9.15	96.3
Coring totals				19.0	19.25	101.3
120-748B-						
1H	14	0800	0.0–0.1	0.1	0.10	100.0
2H	14	0830	0.1–9.6	9.5	9.85	103.0
3H	14	0910	9.6–19.1	9.5	10.00	105.2
4H	14	0945	19.1–28.6	9.5	9.71	102.0
5H	14	1015	28.6–38.1	9.5	9.84	103.0
6H	14	1045	38.1–47.6	9.5	9.92	104.0
7H	14	1125	47.6–57.1	9.5	9.46	99.6
8H	14	1200	57.1–66.6	9.5	10.10	106.3
9H	14	1230	66.6–76.1	9.5	9.71	102.0
10H	14	1300	76.1–85.6	9.5	8.21	86.4
11H	14	1620	85.6–95.1	9.5	10.08	106.1
12H	14	1650	95.1–104.6	9.5	9.84	103.0
13H	14	1720	104.6–114.1	9.5	9.99	105.0
14H	14	1800	114.1–123.6	9.5	9.35	98.4
15H	14	1830	123.6–133.1	9.5	9.81	103.0
16H	14	2140	133.1–142.6	9.5	9.17	96.5
17H	14	2200	142.6–152.1	9.5	9.89	104.0
18H	14	2230	152.1–161.6	9.5	10.00	105.2
19H	14	2300	161.6–171.1	9.5	9.64	101.0
20H	14	2330	171.1–180.6	9.5	10.18	107.1
21X	15	0120	180.6–187.1	6.5	0.70	10.7
22X	15	0240	187.1–196.6	9.5	0.25	2.6
23X	15	0340	196.6–206.1	9.5	4.32	45.5
24X	15	0450	206.1–215.6	9.5	0.03	0.3
25X	15	0615	215.6–225.1	9.5	0.00	0.0
Coring totals				225.1	190.15	84.5
120-748C-						
1R	15	2320	173.0–182.5	9.5	2.94	30.9
2R	15	2350	182.5–192.0	9.5	0.14	1.5
3R	16	0020	192.0–201.5	9.5	0.04	0.4
4R	16	0050	201.5–211.0	9.5	0.00	0.0
5R	16	0115	211.0–220.5	9.5	0.00	0.0
6R	16	0140	220.5–230.0	9.5	0.17	1.8
7R	16	0200	230.0–239.5	9.5	0.08	0.8
8R	16	0225	239.5–249.0	9.5	0.01	0.1
9R	16	0255	249.0–258.5	9.5	0.01	0.1
10R	16	0345	258.5–268.0	9.5	3.86	40.6
11R	16	0420	268.0–277.5	9.5	0.20	2.1
12R	16	0455	277.5–287.0	9.5	0.89	9.4
13R	16	0520	287.0–296.5	9.5	0.02	0.2
14R	16	0600	296.5–306.0	9.5	1.64	17.2
15R	16	0625	306.0–315.5	9.5	0.17	1.8
16R	16	0720	315.5–320.5	5.0	0.10	2.0
17R	16	0740	320.5–330.0	9.5	0.09	1.0
18R	16	0830	330.0–331.0	1.0	0.00	0.0
19R	16	0900	331.0–340.5	9.5	0.51	5.4
20R	16	0940	340.5–350.0	9.5	0.30	3.2
21R	16	1020	350.0–359.5	9.5	1.04	10.9
22R	16	1100	359.5–369.0	9.5	0.42	4.4
23R	16	1120	369.0–378.5	9.5	0.27	2.8
24R	16	1150	378.5–388.0	9.5	1.32	13.9
25R	16	1220	388.0–397.5	9.5	1.24	13.0
26R	16	1305	397.5–407.0	9.5	0.24	2.5
27R	16	1400	407.0–416.5	9.5	2.21	23.2
28R	16	1440	416.5–426.0	9.5	1.21	12.7
29R	16	1520	426.0–435.5	9.5	0.64	6.7
30R	16	1830	435.5–445.0	9.5	1.90	20.0
31R	16	1915	445.0–454.5	9.5	0.26	2.7
32R	16	2005	454.5–464.0	9.5	0.53	5.6
33R	16	2050	464.0–473.5	9.5	1.22	12.8
34R	16	2200	473.5–483.0	9.5	1.60	16.8
35R	16	2300	483.0–492.5	9.5	1.48	15.6
36R	17	0005	492.5–502.0	9.5	3.13	32.9
37R	17	0220	502.0–511.5	9.5	3.22	33.9
38R	17	0415	511.5–521.0	9.5	2.96	31.1
39R	17	0600	521.0–530.5	9.5	3.26	34.3
40R	17	0750	530.5–540.0	9.5	0.74	7.8

Table 1 (continued).

Core no.	Date (March 1988)	Time (local)	Depth (mbsf)	Cored (%)	Recovered (%)	Recovery (%)
120-748C- (Cont.)						
41R	17	0930	540.0–549.5	9.5	0.42	4.4
42R	17	1640	549.5–559.0	9.5	0.98	10.3
43R	17	1835	559.0–568.5	9.5	1.41	14.8
44R	17	1945	568.5–578.0	9.5	1.68	17.7
45R	17	2110	578.0–587.5	9.5	2.05	21.6
46R	17	2230	587.5–597.0	9.5	2.29	24.1
47R	18	0010	597.0–606.5	9.5	2.08	21.9
48R	18	0200	606.5–616.0	9.5	1.34	14.1
49R	18	0320	616.0–625.5	9.5	1.37	14.4
50R	18	0425	625.5–635.0	9.5	0.89	9.4
51R	18	0600	635.0–644.5	9.5	1.50	15.8
52R	18	0740	644.5–654.0	9.5	0.99	10.4
53R	18	0910	654.0–663.5	9.5	2.63	27.7
54R	18	1050	663.5–673.0	9.5	4.35	45.8
55R	18	1230	673.0–682.5	9.5	6.30	66.3
56R	18	1432	682.5–692.0	9.5	4.55	47.9
57R	18	1610	692.0–701.5	9.5	0.01	0.1
58R	18	1750	701.5–711.0	9.5	0.05	0.5
59R	18	2100	713.0–722.5	9.5	0.03	0.3
60R	18	2300	722.5–727.5	5.0	0.06	1.2
61R	19	0130	727.5–732.5	5.0	4.59	91.8
62R	19	0400	732.5–742.0	9.5	9.39	98.8
63R	20	0905	742.0–751.5	9.5	1.48	15.6
64R	20	1140	751.5–761.0	9.5	5.46	57.5
65R	20	1345	761.0–770.5	9.5	0.92	9.7
66R	20	1600	770.5–780.0	9.5	1.27	13.3
67R	20	1740	780.0–789.5	9.5	1.50	15.8
68R	20	1930	789.5–797.5	8.0	0.80	10.0
70R	21	2200	807.0–816.5	9.5	6.66	70.1
71R	21	2355	816.5–826.0	9.5	9.85	103.0
72R	22	0150	826.0–835.5	9.5	6.27	66.0
73R	22	0315	835.5–845.0	9.5	9.27	97.6
74R	22	0430	845.0–854.5	9.5	6.82	71.8
75R	22	0550	854.5–864.0	9.5	8.54	89.9
76R	22	0720	864.0–873.5	9.5	8.87	93.3
77R	22	0930	873.5–883.0	9.5	8.96	94.3
78R	22	1050	883.0–892.5	9.5	8.72	91.8
79R	22	1300	892.5–902.0	9.5	8.77	92.3
80R	22	1650	902.0–908.0	6.0	0.01	0.2
81R	22	2200	908.0–914.5	6.5	0.00	0.0
82R	22	2359	914.5–917.5	3.0	0.07	2.3
83R	23	0145	917.5–921.5	4.0	0.00	0.0
84R	23	0345	921.5–924.5	3.0	0.02	0.7
85R	23	0510	924.5–927.5	3.0	0.01	0.3
86R	23	1015	927.5–934.0	6.5	0.08	1.2
87R	23	1345	934.0–935.0	1.0	0.11	11.0
Coring totals				760.0	185.88	24.5

bioclasts consist of abundant bryozoan debris in some zones, abundant inoceramid prisms and debris in others, and a mix of these in intervening spans. There is a gradual decrease in mean grain size downcore.

Subunit IIIB consists of glauconitic sand-, silt-, and claystones with rare, silicified bioclastic debris or none at all. It extends from 692.0 to 897.6 mbsf. In the lower part, there are pyritized wood fragments and rare mollusc shells. Gray, clayey laminae and cross-laminae and sideritic/smectitic concretions occur from Core 120-748C-65R through -72R. An altered grain component (palagonite?, devitrified ash?) appears in Core 120-748C-61R-CC and becomes increasingly abundant downhole.

Subunit IIIC is a 1.2-m-thick, basal conglomerate composed of rounded, altered alkaline-basalt cobbles and unaltered, broken mollusc shells in a glauconitic siltstone matrix.

Unit IV, the basal unit, is divided into two subunits. Subunit IVA is a 3.4-m-thick basalt flow. Subunit IVB consists of claystone chips known only from fragments recovered in the core-catcher socks of Cores 120-748C-80R through -87R and in the BHA. These are considered as a separate subunit because they

Table 2. Summary of dominant lithologic units, Site 748, Southern Kerguelen Plateau.

Unit and subunit	Lithology	Features	Depth (mbsf)	Core intervals	Thickness (m)	Age
I	Diatom ooze	Dropstones, ice-rafted debris	0–13.3 (A) 0–10.2 (B)	120-748A-1H (top) to 120-748A-2H-3, 80 cm, and 120-748B-1H (top) to 120-748B-3H-1, 60 cm	13.3 (A) 10.2 (B)	late Pleistocene to early Pliocene
IIA	Nannofossil ooze	White	13.3–18.5 (A) 10.2–180.6 (B)	120-748A-2H-3, 80 cm, to 120-748A-6H, 150 cm (TD) and 120-748B-3H-1, 60 cm, to 120-748B-20H-CC	167.3 (comp.) 170.4 (B)	late Miocene to middle Eocene
IIB	Nannofossil chalk, chert, and porcellanite		180.6–206.1 (B) 173.0–389.1 (C)	120-748B-21X to 120-748B-23X-CC and 120-748C-1R to 120-748B-25R-1, 110 cm	25.5 (B) 216.1 (C) 208.5 (comp.)	middle Eocene to late Paleocene
IIIA	Rudstones, grainstones packstones, and wackestones	Bioclastic, intermittently silica cemented	389.1–692.0	120-748C-25R-CC to 120-748C-56R-CC	302.9	late Paleocene to late Campanian
IIIB	Glauconitic sandstones, siltstones, and claystones	Siderite nodules, wood, altered grains	692.0–897.6	120-748C-57R (top) to 120-748C-79R-4, 58 cm	205.6	late Albian–Turonian
IIIC	Basalt cobble conglomerate	Glauconitic and bioclastic calcareous matrix	897.6–898.8	120-748C-79R-4, 58 cm, to 120-748C-79R-5, 25 cm	1.2	
IVA	Basalt	Altered flow	898.8–902.2	120-748C-79R-5, 25 cm, to 120-748C-79R-7, 110 cm	3.4	
IVB	Claystones and altered basalt	Only traces recovered	902.2–935.0 (TD)	120-748C-80R, 0 cm, to 120-748C-87R-CC and BHA	32.8(?)	

are unlike any previously recovered lithologic unit. They may belong to sedimentary units from below the basalt or may be downhole cavings from sections of poor recovery. They include (1) a brown to black claystone with thin, reticulate calcite/siderite veins; (2) a brick red and bright green claystone; and (3) a pink, highly altered basalt with alteration mineral-filled vesicles, as well as other assorted highly altered basalt or basalt-derived clasts. All of these lithotypes are dominantly smectitic and appear to be derived from the weathering of basalt. We stopped drilling after Core 120-748C-87R as a result of deteriorating hole conditions.

Lithologic Units

Unit I: Diatom Ooze

Interval: Cores 120-748A-1H, 0 cm, to 120-748A-2H-3, 80 cm, and Cores 120-748B-1H, 0 cm, to 120-748B-3H-1, 60 cm.
Depth: 0–13.3 mbsf (Hole 748A) and 0–10.2 mbsf (Hole 748B).
Thickness: 13.3 m (Hole 748A) and 10.2 m (Hole 748B).
Composite thickness: 13.3 m.
Age: late Pleistocene to early Pliocene.

Unit I was recovered at Holes 748A and 748B. It consists mainly of soft, white diatom ooze, with rare ice-rafted debris and dropstones. Some intervals are enriched in radiolarians and/or foraminifers. The actual thickness of the unit is uncertain because of difficulty in finding the mud line at both holes. At Hole 748A, two overfilled cores, with a total of 13.3 m of Unit I, were recovered. At Hole 748B, the base of Unit I was recovered near the top of Core 120-748B-3H at 10.2 mbsf. The discrepancy between the two thicknesses for this unit, 13.3 m for Hole 748A and 10.2 m for Hole 748B, may be drilling induced, produced by excessive ship heave as well as the result of some local topographic relief.

The diatom ooze is white to light gray and quite soft, with a high water content that gives it a gelatinous consistency. Diatom content ranges from 97% to 8% in the foraminifer-enriched intervals. Most of the unit has between 80% and 90% diatoms. Radiolarian-enriched intervals are 2 and 3 m thick and have 15%–20% radiolarians (Interval 120-748A-1H-2, 0 cm, to 120-748A-1H-3, 0–135 cm, and Interval 120-748B-2H-5, 95–100 cm, to 120-748B-2H-7, 60 cm). Foraminifer-enriched intervals, where foraminifer content reaches 15% of the sediment, occur in Intervals 120-748A-1H-1, 0–150 cm, and 120-748B-1H-CC, 0–6 cm.

Ice-rafted debris occurs as fine to coarse sand-size dark specks scattered throughout with dropstones up to 5 cm in diameter. The occurrence of abundant IRD in diatom ooze is clearly indicated by an increase in magnetic susceptibility of the sediment (Fig. 11). In Hole 748A, trace amounts of fine to coarse sand-size IRD occur throughout Cores 120-748A-1H and -2H and include mica, clear and frosted quartz, vesicular ash, obsidian, and basalt with small vesicles. Three intervals with abundant IRD and dropstones occur in Holes 748A and 748B, but they do not occur at the same depths in each hole, further indicating the possibly drilling-induced discrepancies between these two holes (Fig. 11).

In Hole 748A, at 4.1–4.2, 9.5–9.8, and 12.9–13.3 mbsf, dropstones include pebbles of quartz arenite, subangular to subrounded frosted pink quartz, granite, granitic biotite gneiss, and clear quartz with conchoidal fractures (Table 3). In Hole 748B, at 0.1–0.3, 1.7–3.1, and 9.6–10.4 mbsf, small pebbles and coarse sand are composed of clear and frosted quartz, feldspars, amphiboles, biotite gneiss, and subangular to subrounded basalt fragments (Table 3). No dropstones or IRD were found below Unit I except for a lower Oligocene occurrence in Core 120-748B-14H-1 and 120-748B-14H-2 (see next section, Subunit IIA).

Unit II: Nannofossil Ooze, Nannofossil Chalk, Chert, and Porcellanite

Interval: Cores 120-748A-2H-3, 80 cm, to 120-748A-6H, 150 cm (TD), Cores 120-748B-3H-1, 60 cm, to 120-748B-23X-CC, and Cores 120-748C-1R to 120-748C-25R-1, 110 cm.
Depth: 10.2–206.1 mbsf (Hole 748B; although TD = 225.1, there was no recovery below 206.1 mbsf) and 173.0–389.1 mbsf (Hole 748C).

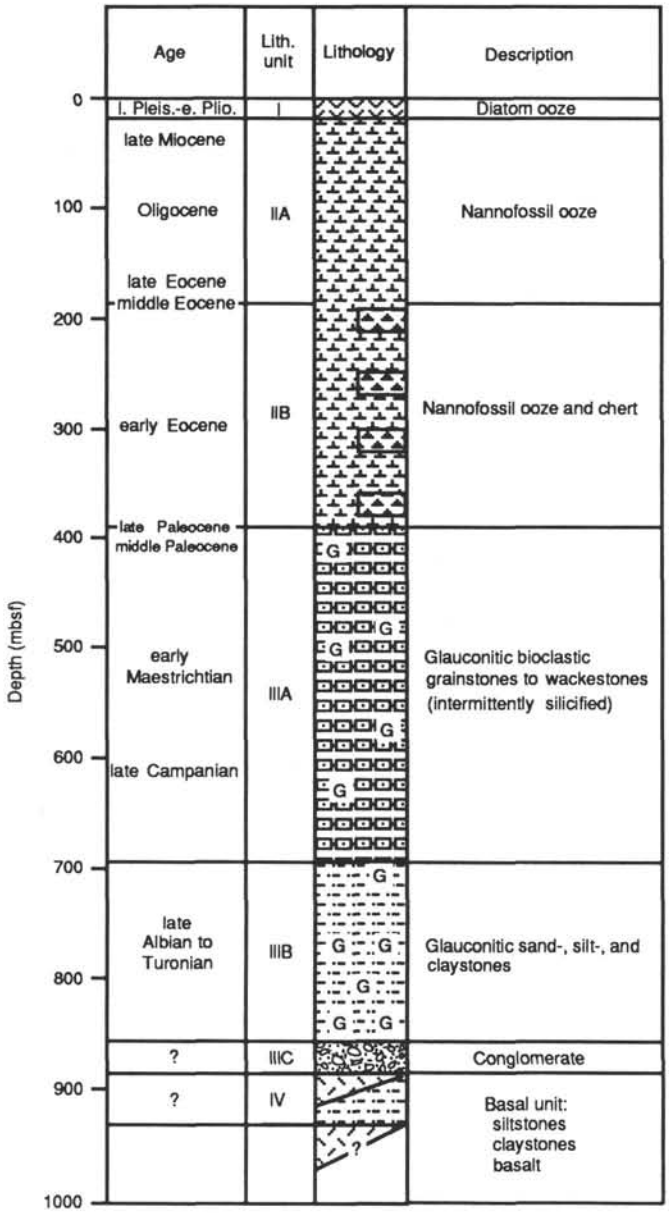

Figure 9. Summary of lithologic units, Site 748, western Raggatt Basin.

Thickness: 195.9 m (Hole 748B) and 216.1 m (Hole 748C).
Composite thickness: 375.8 m.
Age: late Miocene to late Paleocene.

This unit is composed of nannofossil ooze, chalk, chert, and porcellanite. The overlying Subunit IIA is nannofossil ooze. The underlying Subunit IIB has nannofossil ooze, chalk, chert, and porcellanite.

Subunit IIA: Nannofossil Ooze

Interval: Cores 120-748A-2H-3, 80 cm, to 120-748A-6H, 150 cm (TD), Cores 120-748B-3H-1, 60 cm, to 120-748B-20H-CC.
Depth: 10.2–180.6 mbsf (Hole 748B).
Thickness: 170.4 m.
Composite thickness: 167.3 m.
Age: late Miocene to middle Eocene.

Subunit IIA is composed predominantly of nannofossil ooze with occasional influxes of diatoms or siliceous debris composed of diatoms, radiolarians, sponge spicules, and silicoflagellates. It has no porcellanite or chert (Fig. 12). The nannofossil ooze is brilliant white and commonly laminated or mottled with tan, light greenish gray, or purple colors. The purple is caused by pyrite enrichment. Tan zones are enriched in foraminifers and the greenish gray areas are enriched in siliceous components. In greenish gray mottles and laminae, calcareous nannofossils show the effects of incipient dissolution. These and the tan intervals have mean grain sizes in excess of 15 μm as a result of the larger biogenic components (Fig. 12 and Table 4).

Greenish gray laminations are mostly very thin, up to 5 mm, but thicken up to 1 cm and become regularly spaced in Core 120-748B-9H. Burrows are often faint and indistinct (Fig. 13). The purple, pyrite-enriched burrows attain sizes up to 7.5 cm in diameter (Fig. 14). Several types were observed, including *Chondrites, Zoophycos, Planolites,* and possible *Skolithos.* Often these are crosscutting, with more than one generation of small *Chondrites* burrows. Glassy brown ash, sometimes with vesicles, occurs in four intervals where it makes up 1%–10% of the sediment (Fig. 12).

Lower Oligocene Ice-Rafted Debris

Intervals 120-748B-14H-1, 137–150 cm, and 120-748B-14H-2, 0–24 cm, contain an interval of ice-rafted debris that is earliest Oligocene in age (see "Biostratigraphy" section, this chapter). This material is not considered a lag deposit because there is no increase in grain size of the matrix. Scattered specks of the debris are visible in Figure 13 between 5 and 10 cm. Bioturbation has worked some of the IRD further downcore (Fig. 13, 24–45 cm). The IRD is dominantly fine to coarse sand size and is composed of altered feldspars, yellowish to brown feldspars, glauconite, and three kinds of quartz: (1) gray, translucent, (2) milky, and (3) clear with inclusions.

Shore-based investigation with the scanning electron microscope (SEM) and energy-dispersive X-ray analysis identified a suite of heavy minerals composed of garnet, hornblende, and ilmenite as well as textural surface features on quartz grains that are highly angular, with fresh conchoidal fractures characteristic of glacially derived material (Breza et al., 1988). Volcanic ash was not identified in this interval. For correlation with other lower Oligocene ice-rafted debris along the Antarctic continental margin and Ross Sea, see the "Summary and Conclusions" section, this chapter.

Subunit IIB: Nannofossil Chalk, Chert, and Porcellanite

Interval: Cores 120-748B-21X-1, 0 cm, to 120-748B-23X-CC and Cores 120-748C-1R-1, 0 cm, to 120-748C-25R-1, 110 cm.
Depth: 180.6–206.1 mbsf (Hole 748B) and 173.0–389.1 mbsf (Hole 748C).
Thickness: 25.5 m (Hole 748B) and 216.1 m (Hole 748C).
Composite thickness: 208.5.
Age: middle Eocene to late Paleocene.

Subunit IIB is distinguished from the overlying subunit by the presence of porcellanite and chert. The porcellanite is the same color as the interbedded chalk, but it has a hardness approaching that of chert. Details of the overlying nannofossil ooze, such as purple and tan burrows, foraminifer ghosts, and fine laminae, are preserved in the porcellanite (Fig. 15, Core 120-748B-22X-CC, 12–20 cm) that occurs as single pieces or as rims around olive brown chert (Fig. 15, Core 120-748B-22X-CC and 120-748C-2R-CC, 4–8 cm). The lighter-colored chert sometimes retains burrows or laminae (e.g., Fig. 15, Core 120-748B-22X-CC, 5–8 cm, Core 120-748C-2R-CC, and Core 120-748C-6R-CC). Most of the chert is brown, vitreous, and quite hard, and it also contains white pockmarks that are filled with a noncalcareous, white powder. Radiolarian ghosts, olive-colored burrows, and chalk(?) inclusions are visible in some pieces.

Recovery was characteristically poor in this subunit once the chert was reached, as it has been continually since this middle Eo-

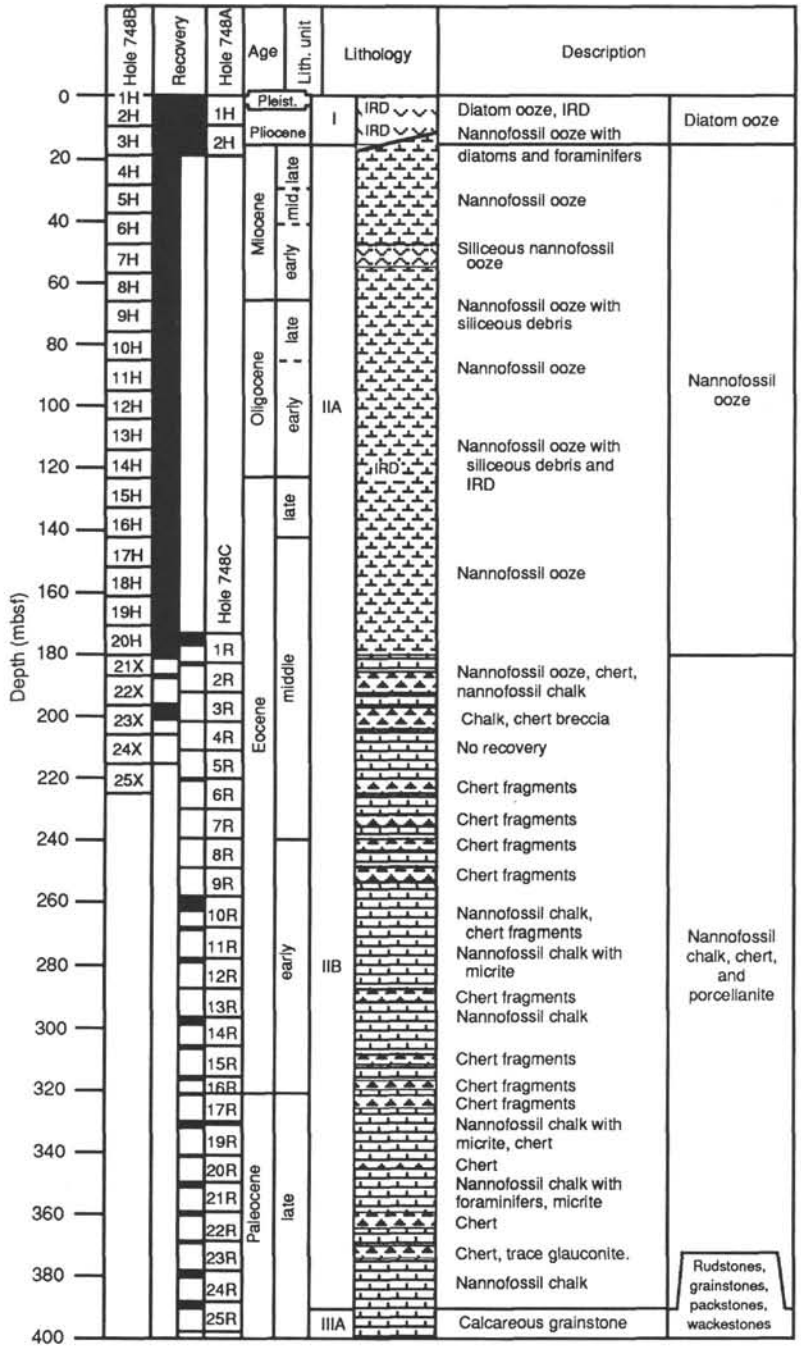

Figure 10. Detailed lithostratigraphic summary, Site 748, western Raggatt Basin. Note key to symbols used in the lithology column; see also "Explanatory Notes" chapter (this volume).

cene chert was first encountered during Leg 1 of the Deep Sea Drilling Program (DSDP). This subunit corresponds to chert of similar age throughout the North and South Atlantic oceans and much of the Pacific. Less than 1-m lengths of nannofossil chalk, similar to that described for Subunit IIA but firmer, were recovered between Cores 120-748C-21R to -23R and Cores 120-748B-1R through 120-749C-25R-1. Cores 120-748C-1R, -10R to -12R, -14R, and -19R to -25R have white nannofossil chalk with purple pyritic burrows and mottles.

There are intermittent increases in foraminifer abundance but not in siliceous components (Fig. 12). Nannofossils often are etched and partly dissolved; where this occurs, micrite is present. This subunit has an increase in *P*-wave velocity and bulk density, and a decrease in porosity and water content compared with the overlying nannofossil ooze (Fig. 16; see also "Physical Properties" section, this chapter). Glauconite was first observed in Core 120-748C-23R, where it composes 3% of the sediment.

Unit III: Glauconitic Sediment

Interval: Cores 120-748C-25R-CC to 120-748C-79R-5, 25 cm.
Depth: 389.1–898.8 mbsf.

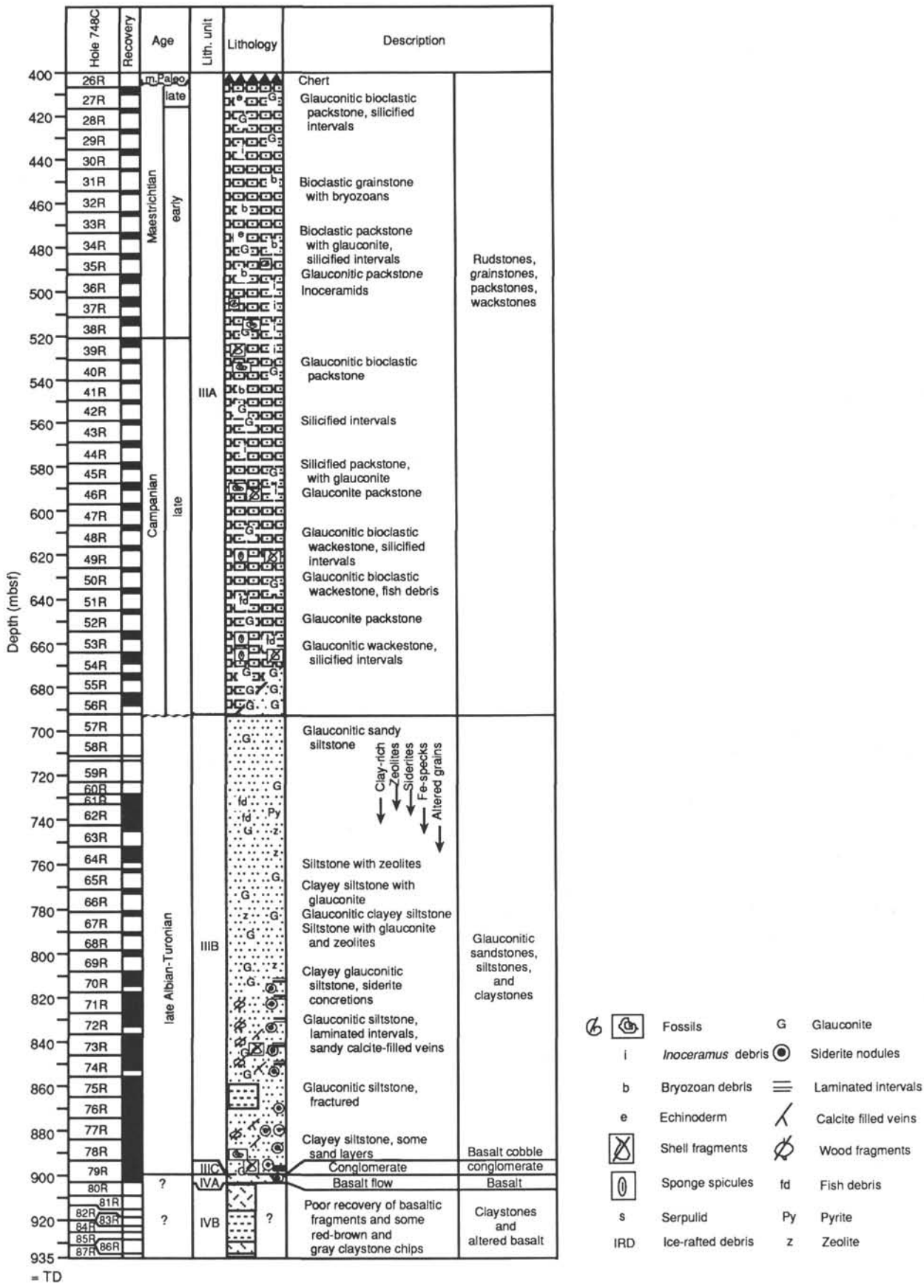

Figure 10 (continued).

Table 3. Intervals of abundant ice-rafted debris and their mineralogic composition, Holes 748A and 748B.

Depth (mbsf)	QF	QC	GR	FE	BG	BI	AM	BT	OB	AS	PX
120-748A-											
0.10	X	X	X					X	X	X	
9.50	X	X	X		X			X			
12.9	X	X		X	X	X					X
120-748B-											
0.10	X	X		X			X				
1.73	X	X		X	X	X	X				

Note: QF = frosted quartz, QC = clear quartz, GR = granite, FE = feldspar, BG = biotite gneiss, BI = biotite, AM = amphibole, BT = basalt, OB = obsidian, AS = ash, and PX = pyroxene.

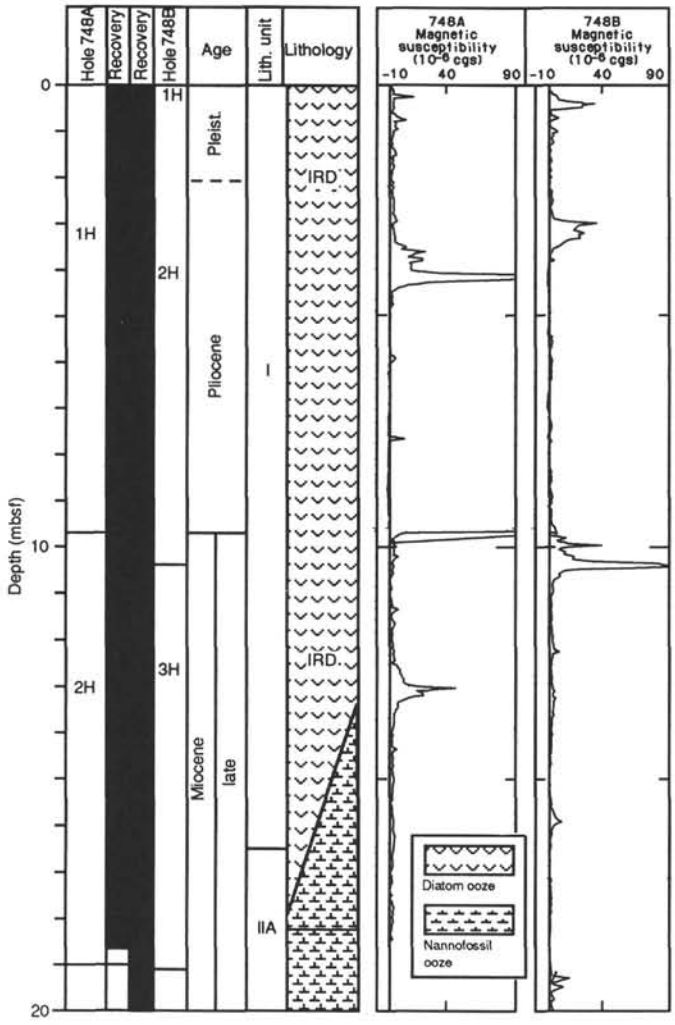

Figure 11. Magnetic susceptibility plot of Unit I from Holes 748A and 748B, showing intervals of abundant ice-rafted debris (IRD). Columns at left represent recovery for Cores 120-748A-1H to -2H and Cores 120-748B-1H to -3H.

Thickness: 509.7 m.
Age: late Paleocene to late Albian–Turonian.

Unit III consists of all glauconitic sediment and is divided into three subunits that differ in the type of dominant clast. Subunit IIIA consists of glauconitic rudstones, grainstones, packstones, and wackestones that are intermittently cemented by silica. Subunit IIIB consists of glauconitic sand- and siltstones with a few claystones that are indurated and sporadically cemented by carbonate. The bioclastic component diminishes gradually above the contact between Subunits IIIA and IIIB. The top of Subunit IIIB was chosen where carbonate bioclasts disappear downhole, near 692 mbsf. At this level, $CaCO_3$ content reaches a minimum (Fig. 16), and natural remnant magnetism (NRM) a maximum (Fig. 17). Subunit IIIC is a basal basalt cobble conglomerate with a glauconitic matrix.

As noted in the "Explanatory Notes" of this volume, we adopt the terminology of McRae (1972) and use the term *glauconite* to refer to sand-size green pellets of undetermined mineralogy.

Subunit IIIA: Intermittently Silica-Cemented, Glauconitic Rudstones, Grainstones, and Packstones

Interval: Cores 120-748C-25R-CC to 120-748C-56R-CC.
Depth: 389.1–692.0 mbsf.
Thickness: 302.9 m.
Age: late Paleocene to late Campanian.

Subunit IIIA has rudstones, grainstones, packstones, and wackestones that contain from 5% to 65% glauconite grains (Fig. 18). The glauconite is various shades of green or may be blackened by a coating of pyrite. Other grains are partly or wholly oxidized, as indicated by their red color. The glauconite is rounded, peloidal, or angular and often occurs as foraminifer and sponge spicule steinkerns that are sometimes coated by pyrite.

In thin section, three forms were observed: (1) green grains with pyrite filling, (2) small yellow-green peloids, and (3) armored (pyrite-coated), botryoidal grains. In X-ray diffraction of bulk samples, no 10-Å mica peak was observed, but smectite and other minerals are always present (see later discussion). The mineralogy of the glauconite is thus mixed or possibly highly interlayered, but it is not the "mineralogical glauconite" of McRae (1972).

The sediment is bioclastic, composed of fine sand- to granule-size debris (Fig. 19) consisting of bryozoans (Plate 1, Figs. 1 and 2), inoceramids, benthic foraminifers, echinoids (Plate 1, Fig. 3), sponge spicules, molluscs, radiolarians, crinoids, red algae (Plate 1, Fig. 4), and brachiopods. The coarser packstone intervals are enriched in either bryozoan or inoceramid debris, or a mix of these (Fig. 20). Bryozoan-enriched intervals range from Cores 120-748C-32R to -35R and Cores 120-748C-42R to -43R (Fig. 10). The bryozoans are broken and not in life position, but an entire irregular echinoid was found in place at the top of Core 120-748C-51R.

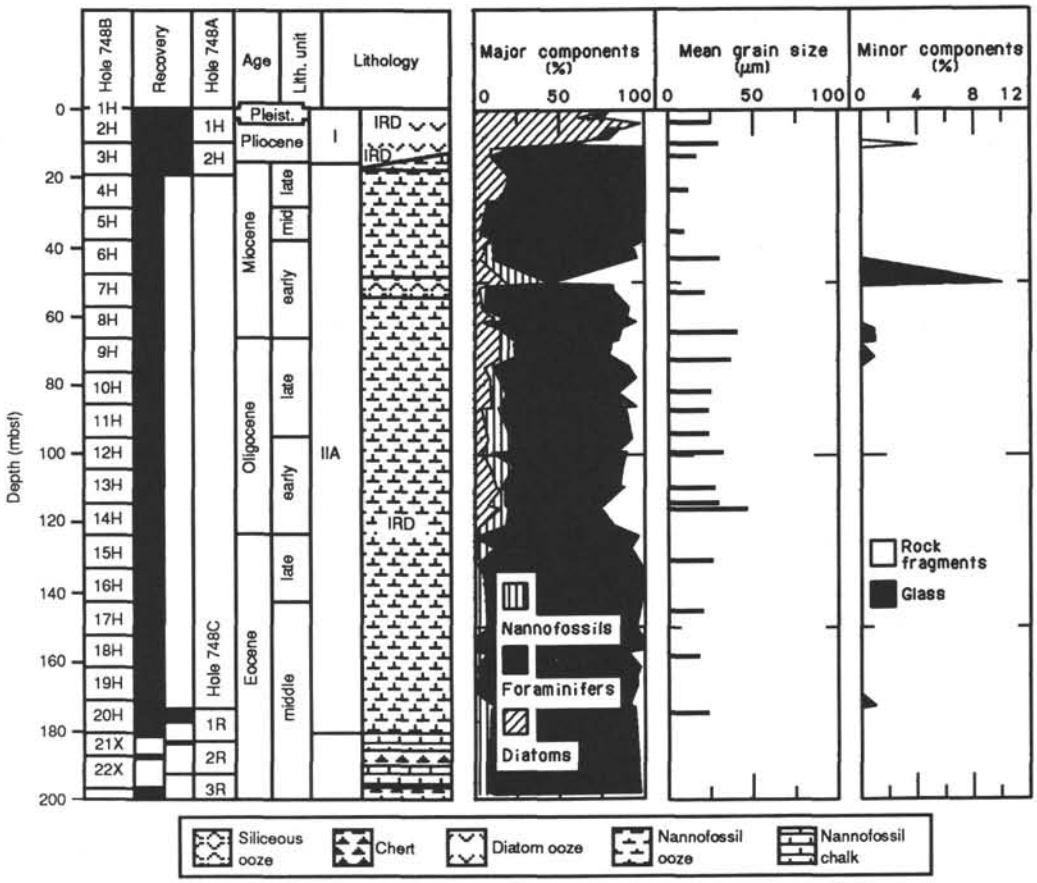

Figure 12. Lithologic summary of Unit I and Subunit IIA, Site 748, including major components (from smear slide data), grain size (data from Table 4), and occurrence of quartz and glass.

Inoceramid debris composes 20%–85% of the sediment in the interval from Cores 120-748C-35R to -40R (Fig. 10). Crinoid columnals are most abundant in Cores 120-748C-34R and -44R. Phosphatic vertebrate debris in the form of teeth, scales, and bones occurs sporadically. Sand-size basalt clasts were found in Core 120-748C-31R. Pyrite is pervasive, but never more than 5% of the sediment. It occurs as black sand-size grains, lines foraminifer chambers, and coats glauconite-filled spines, spicules, and foraminifer tests.

Angular, clear quartz and clear, untwinned feldspar are rare components. The quartz is angular to subrounded and sand size. The feldspar is clear to light yellow. Clay is not a common component of this subunit and is found concentrated only in flaser-bedded intervals (Fig. 20) and in clay-filled burrows (Fig. 21). The filling of the mollusc (brachiopod?) shell in Figure 21 is micrite, pyrite, and glauconite.

Rudstone and grainstone intervals include Cores 120-748C-32R to -34R, -37R, -38R, -41R, and -46R to -49R (Fig. 19). The remaining spans are packstones and wackestones that are well to moderately well sorted. Overall clay content increases downcore, with more wackestone in Cores 120-748C-54R through -56R. Clay-size sediment is largely composed of micrite in the upper part of Subunit IIIA. Micrite decreases downcore while clay mineral content increases. The clay-enriched areas are dark gray to grayish brown and have less glauconite than the surrounding sediment.

The grainstones may be massive or show faint, centimeter-scale beds, few of which appear graded. In Cores 120-748C-38R to -44R, bedding is outlined by thin, clay-enriched flasers (Fig. 20). Faint cross-beds (lenticular?) occur in Core 120-748C-55R. Clay rip-up clasts are present in Core 120-748C-50R. Bioturbation may be absent, moderate, or high, with *Chondrites, Planolites,* and *Thalassinoides*-type burrows. Commonly these burrows crosscut one another, particularly with more than one generation of *Chondrites* burrowing.

In thin section, silica-cemented intervals have from 50% to 60% micritic matrix with fronts of microcrystalline silica cement, mostly intergranular. The X-ray diffractograms of ground, silicified samples indicate the presence of a silica mineral intermediate between opal-C and opal-CT (Fig. 22). Chalcedony commonly fills voids, and only rarely are fossils replaced. Where the sediment is not silicified, sparry calcite cement is observed, although the bioclasts do not appear to be highly altered by diagenesis. The skeletal microstructures of red algae and bryozoans are well preserved. A summary of thin section observations is given in Table 5. There is a carbonate-cemented interval in Core 120-748C-54R. Overall carbonate content decreases between 668 and 692 mbsf (Fig. 16).

Subunit IIIB: Glauconitic Sandstones, Siltstones, and Claystones

Interval: Cores 120-748C-57R, 0 cm, to 120-748C-79R-4, 58 cm.
Depth: 692.0–897.6 mbsf.
Thickness: 205.6 m.
Age: late Albian to Turonian.

Subunit IIIB is distinguished from that above it by the absence of carbonate bioclasts. It consists of glauconitic sandstones and clayey sandstones in the upper part, and siltstones, clayey siltstones, and claystones in the lower. The sandstones occur from Core 120-748C-58R through -61R. They are composed

Table 4. Mean grain size and sand/silt/clay percent, Site 748.

Core, section, interval (cm)	Depth (mbsf)	Mean grain size (μm)	Sand (%)	Silt (%)	Clay (%)
120-748A-					
2H-3, 50–52	3.52	24.8	17	80	3
120-748B-					
2H-7, 46–49	9.56	29.3	21	76	3
3H-3, 49–51	13.09	16.8	8	89	13
4H-3, 52–54	22.62	11.1	1	95	4
5H-5, 50–52	35.12	8.9	1	61	38
6H-4, 54–56	43.14	30.2	14	70	16
7H-4, 69–71	52.79	21.5	8	74	18
8H-5, 87–89	63.97	40.9	30	63	7
9H-4, 127–129	72.37	36.7	25	66	9
10H-4, 76–78	81.36	25.1	10	80	10
11H-1, 122–124	86.87	24.4	10	77	13
11H-6, 25–27	93.35	24.4	11	79	10
12H-3, 129–131	99.39	32.4	19	69	12
13H-4, 57–59	109.67	27.5	12	76	12
14H-1, 34–36	114.44	30.2	15	82	13
14H-2, 15–17	115.75	46.2	36	58	6
15H-4, 126–128	130.86	27.0	14	75	11
17H-2, 130–132	145.40	20.2	7	79	14
18H-4, 134–136	157.94	18.5	6	75	19
20H-3, 84–86	174.94	23.8	9	77	14
120-748C-					
10R-1, 72–74	259.22	15.6	1	83	16
11R-CC	268.00	36.6	22	68	10
14R-1, 126–128	297.76	23.7	11	74	15
19R-1, 22–24	331.22	59.9	49	47	4
21R-1, 24–26	350.24	42.6	28	64	8
23R-CC	369.00	36.5	15	74	11
24R-1, 35–37	378.85	25.4	12	75	13
24R-1, 62–64	379.12	61.1	49	47	4
25R-CC	388.00	51.3	39	52	9
26R-1, 10–11	397.60	17.5	8	64	28
64R-3, 140–141	791.90	29.6	19	65	11
70R-2, 105	809.52	20.0	8	85	7
71R-2, 70–71	818.70	26.7	16	80	4
72R-4, 12–13	830.62	33.7	24	72	4
73R-3, 53–55	838.03	32.5	23	73	4
77R-3, 114	877.64	16.2	4	86	10

Note: Measured with Labtec 100, laserscan automatic particle size analyzer.

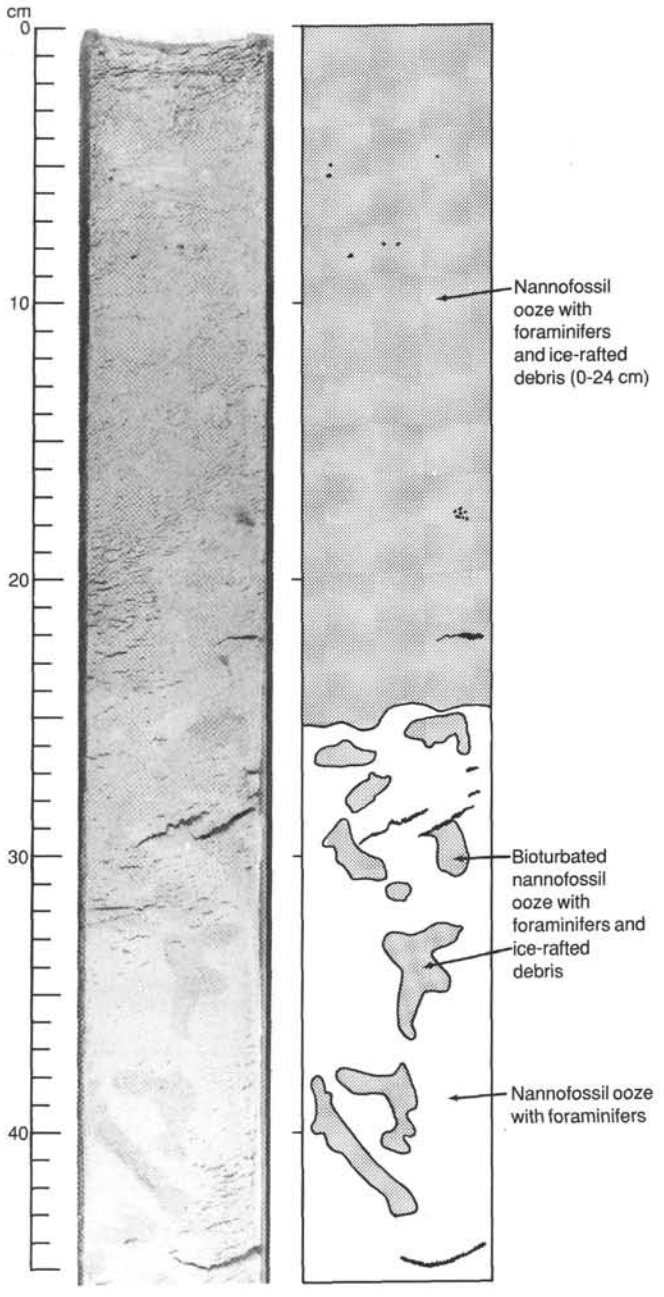

Figure 13. Sand-size ice-rafted debris of early Oligocene age in Core 120-748B-14H-2, 0–24 cm. This layer has been bioturbated into the underlying nannofossil ooze (Core 120-748B-14H-2, 24–45 cm).

predominantly of glauconite and silicified fossils. Many of these appear to be molds of radiolarians, foraminifers, and silicified sponge spicules (Plate 2, Figs. 1–5). In smear slides, the spicules have radial fibers in the center that are composed of chalcedony.

Other clastic components in this interval include rare foraminifers, pyrite, phosphatic vertebrate debris, and red (ferruginous?) opaque specks. Quartz continues to appear as a rare and sporadic component as does clear, untwinned feldspar. The most abundant component is glauconite, which occurs as light green chips and peloids (fecal pellets?) and as bulbous, dark grains. Many of the glauconite grains in this subunit have a black, pyritic coating. The bedding in this interval is faintly parallel. Several types of burrows crosscut one another, and many of these are filled with a brown to gray clay, which is not as glauconitic as the surrounding sediment.

Below Core 120-748C-61R (732.5 mbsf), there are no further sandstones. Siltstones and clayey siltstones with 5%–96% glauconite continue through Core 120-748C-79R. In some intervals, light- and dark-color laminae alternate on a millimeter scale (Fig. 23, Core 120-748C-65R-1, 9–11 cm). Often the laminae are disrupted by burrowing (Fig. 23, Core 120-748C-65R-1, 18–20 cm). Flaser-type, clay-enriched laminae and massive bedding due to bioturbation are visible in Figure 23 (Core 120-748C-65R-1, 11–18 cm). Cross-laminae are illustrated in Figure 24 (Core 120-748C-72R-3, 101–103 cm). These and inclined laminae (Fig. 25) indicate deposition by currents.

There are occasional centimeter-thick clay beds of a dark gray color (Fig. 26, 82–87 cm) that may be interrupted by bioturbation. Scattered throughout Subunit IIIB are small burrows filled with siderite and smectite (Figs. 27 and 28). Some of these have small spheres of siderite-smectite within them (Fig. 27); others have no internal structure (Fig. 28). They first appear in Core 120-748C-68R and become larger and more abundant downhole. The larger ones are sideritic concretions. One of these has formed across cross-laminae in Figure 25 (73–78 cm).

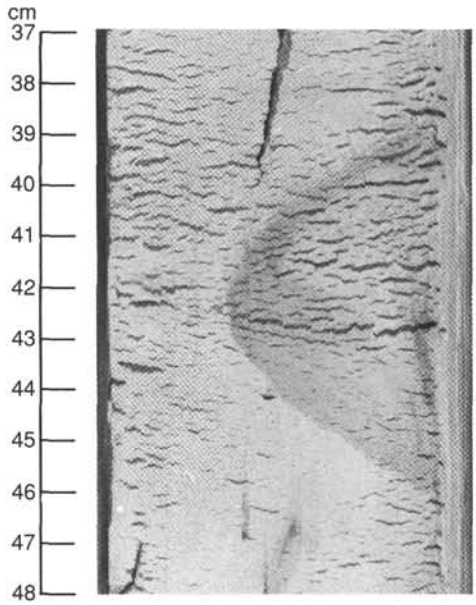

Figure 14. Pyrite enrichment in nannofossil ooze in Core 120-748B-16H-6, 37–48 cm.

They are ovoid in cross section (Fig. 28, 33–35 cm) or irregular (Fig. 28, 22–24 cm) and often are internally bioturbated (Fig. 24, 107–117 cm, and Fig. 28, 33–35 cm).

Slickensided fractures filled with green sparry calcite, from a few millimeters to 1 cm thick, occur in Cores 120-748C-73R, -74R, and -78R. In Core 120-748C-78R, they occur as conjugates.

In Core 120-748C-63R (742.0 mbsf) through to Core 120-748C-71R-2 (819.5 mbsf), zeolites are an important component of the sediment, up to 30% in Core 120-748C-64R (Fig. 29). X-ray diffraction indicates that the major zeolite is clinoptilolite, which survived heating to 400°C overnight (method of Alietti, 1972) (Fig. 30). Another component, first observed in Core 120-748C-61R-CC and increasingly important downhole, is an "altered grain," which may be devitrified ash or basaltic glass (palagonite). These grains are generally translucent and isotropic, with high relief, low refractive index, and low birefringence. These grains often have a more opaque center that is yellow and of low birefringence. X-ray diffraction indicates smectite, which is typical of devitrified ash or glass. It composes from 5% (Cores 120-748C-69R and 120-748C-77R-4) to 100% of the sediment (Core 120-748C-79R).

Pyritized wood fragments first appear downhole in Core 120-748C-71R. These are either disseminated in massively bedded intervals or concentrated along bedding planes (Figs. 25, 72–73 cm, and Fig. 28, 26–29 cm). Several larger pieces were found in the core catcher of Core 120-748C-71R. Quartz and clear, untwinned feldspar may compose up to 10% of the sediment in Sections 120-748C-60R-CC to 120-748C-71R-2. Glauconite is absent from brown-colored sediment, which occurs interbedded with green glauconitic sediment in Cores 120-748C-76R through -79R.

Subunit IIIC: Basalt Cobble Conglomerate

Interval: Cores 120-748C-79R-4, 58 cm, to 120-748C-79R-5, 25 cm.
Depth: 897.6–898.8 mbsf.
Thickness: 1.2 m.
Age: ?

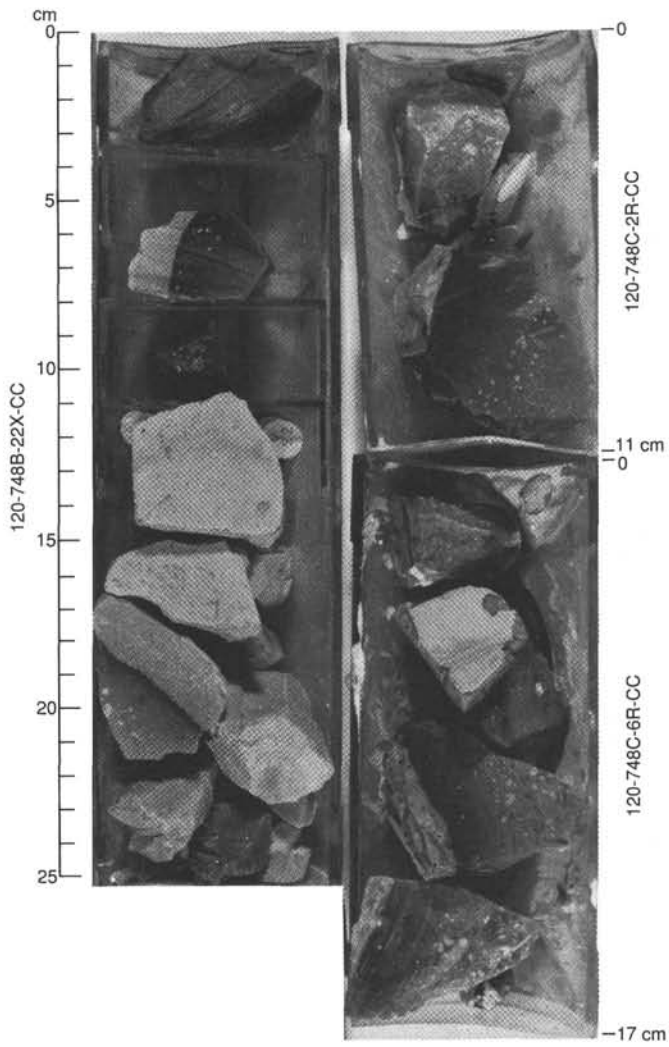

Figure 15. Chert and porcellanite of Subunit IIB, Sections 120-748B-22X-CC (upper left), 120-748C-11R-CC (lower left), 120-748C-2R-CC (upper right), and 120-748C-6R-CC (lower right). Porcellanite is light gray and preserves burrows (e.g., 11–17 cm, left) and laminae (e.g., 17–20 cm, right); sometimes it also rims chert (e.g., 5–8 cm, left). Chert is olive brown and vitreous, with burrows and fossil ghosts.

A conglomerate composed of rounded, altered basalt cobbles and boulders, unaltered but broken mollusc (and brachiopod?) shells, and a matrix of glauconitic, calcareous siltstone with altered volcanic debris sprinkled throughout was recovered in Sections 120-748C-79R-4 to 120-748C-79R-5, 0–25 cm, which are illustrated in Figures 31 and 32. The cobbles are wholly to partially rimmed with sparry calcite. Small, sparry calcite veins less than 1 mm thick pervade the sediment (Fig. 32). There is a 40-cm-thick altered basalt layer or boulder in Section 120-748C-79R-4 that has an 8-mm-wide vein of zeolite and siderite through its middle. The conglomerate above and below it is similar and shows no baked contact. The conglomerate continues below this for several decimeters until, at 898.8 mbsf, the top of an altered basalt unit is reached.

Unit IV: Basalt and Underlying (?) Claystones

Interval: Cores 120-748C-79R-5, 25 cm, to 120-748C-87R-CC.
Depth: 898.8–935.0 mbsf (TD).
Thickness: ?
Age: ?

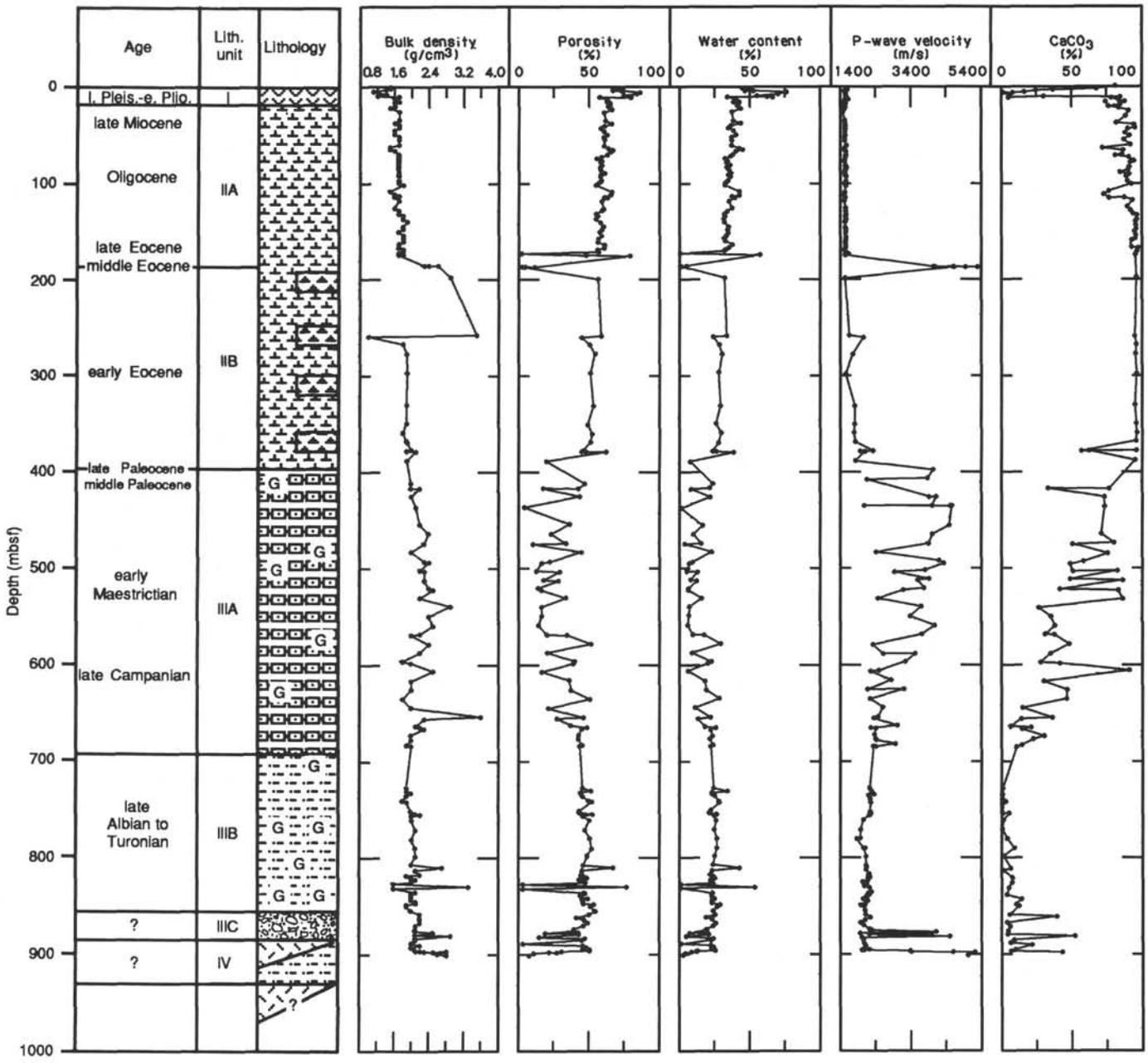

Figure 16. Downhole variation of wet-bulk density, porosity, water content, *P*-wave velocity, and carbonate content, Site 748. Increases in the measurements for wet-bulk density, *P*-wave velocity, water content, and porosity near 200 mbsf correspond to chert and porcellanite, and between 400 and 700 mbsf, to silicified glauconitic rudstones, grainstones, packstones, and wackestones. The gradual decrease in carbonate content between 400 and 700 mbsf corresponds to a decrease in the bioclastic component of glauconitic sediment.

Subunit IVA: Basalt Flow

Interval: Cores 120-748C-79R-5, 25 cm, to 120-748C-79R-7, 110 cm.
Depth: 898.8–902.2 mbsf.
Thickness: 3.4 m.
Age: ?

Subunit IVA is composed of a basalt flow that is 3.4 m thick. The contact of the overlying conglomerate with the basalt does not appear altered or baked because the molluscs are not recrystallized, glauconite grains remain unaltered, and there is no drastic color change from the base to the top of the conglomerate. There is no evidence of even a thin, chilled margin in the sediment. For a detailed description of the basalt, see "Igneous Petrology" section, this chapter.

Subunit IVB: Sub-Basalt (?) Claystones

Interval: Core-catcher socks 120-748C-80R, 0 cm, to 120-748C-87R-CC and BHA.
Depth: 902.2–935.0 mbsf (TD).
Thickness: ?
Age: ?

Recovery was almost nil following Core 120-748C-79R except for some debris trapped by the core-catcher socks and BHA. Much of this sediment appears to be the product of downhole

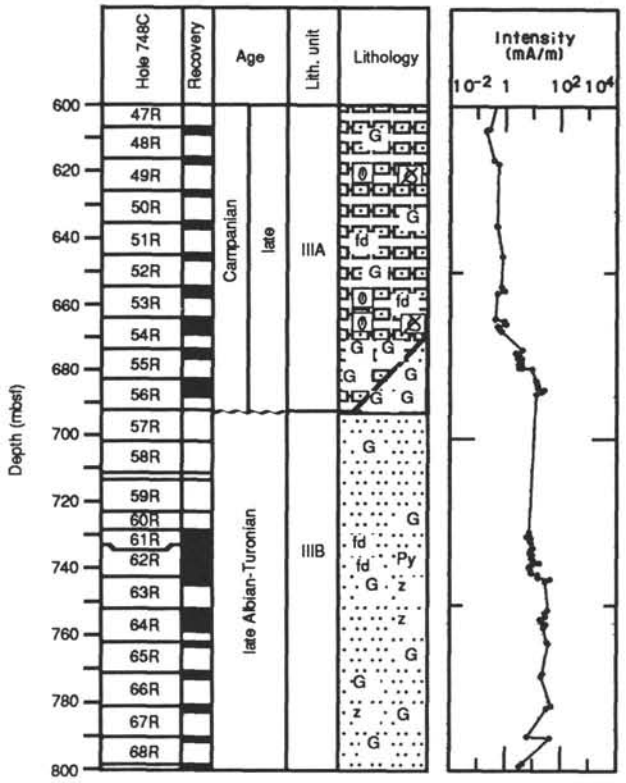

Figure 17. Downhole variation in natural remnant magnetism (NRM), Site 748, for Unit III. The increase between 650 and 700 mbsf corresponds to a decrease in bioclastic component of glauconitic sediment. Lithology and age units are from Figure 10.

caving, but there are some chips of material that differ from previously described lithologic units. The inference that these represent sub-basalt-flow sediments is an important one, as it indicates that the basalt recovered in Core 120-748C-79R is not the top of basement. These chips include two types of claystones and highly altered basalt.

The claystone chips are all composed of highly crystalline smectite and interlayered glauconite (Fig. 30). The two types are (1) a brick red and bright green smectitic/glauconitic clay, with the two colors in laminae or splotches; and (2) a brown to black smectitic/glauconitic clay with tiny (< 1 mm thick) calcite-plus-siderite veins that run vertically, diagonally, and horizontally through the chips. The red color of the smectitic/glauconitic clay comes from goethite and hematite (Fig. 30), as neither pyrite nor siderite were detected in X-ray diffraction. The presence of highly altered basalt is documented by pinkish red chips with vesicles filled with alteration minerals. Thus, at least three new and distinct lithotypes occur that may be derived from sediments below the lava flow.

Summary

Unit I from Site 748 consists of the uppermost 13.3 m of white, soft, Pliocene-Pleistocene diatom ooze. Diatoms are occasionally diluted by large influxes of radiolarians or foraminifers. Magnetic susceptibility measurements helped to identify intervals that are enriched in dropstones and ice-rafted debris (Fig. 11). These are related to the growth of sea ice over this site. The IRD is derived from a variety of igneous, metamorphic, and sedimentary rocks that will be identified in greater detail through shore-based studies with the aim of linking them to sources in Antarctica.

Unit II consists of 375.8 m of nannofossil ooze, nannofossil chalk, chert, and porcellanite. This unit was divided into two subunits. The composite upper subunit extends from 13.3 to 180.6 mbsf and has only nannofossil ooze. The lower subunit extends from 180.6 to 389.1 mbsf and includes chert and porcellanite interbedded with nannofossil chalk. Both chalk and porcellanite from the lower subunit resemble the ooze of Subunit IIA but are more indurated.

Unit III consists of 509.7 m of glauconitic sediment divided into three subunits. The upper subunit has bioclasts of broken but unaltered bryozoans and inoceramids as the dominant components. Less abundant components include the debris of red algae, crinoids, molluscs, and brachiopods. Subunit IIIA is intermittently partly cemented by silica, which has not replaced bioclasts but fills pore space as chalcedony. Mud content increases downhole through the entire unit and changes from micrite to clay minerals in the lower part of Subunit IIIA. Accompanying the decrease in micrite is the decrease in bioclastic components. A calcium carbonate minimum is reached in Core 120-748C-56R, below which, at 692.0–897.5 mbsf, Subunit IIIB has no or only silicified bioclasts and is composed dominantly of glauconite, zeolites, and clay minerals.

Beginning in Core 120-748C-61R (730 mbsf) and increasing downhole, altered grains, probably the alteration product of glass or ash, become the dominant component. Sideritic concretions appear in this core and become more abundant downhole, along with increasing abundance of quartz and feldspar. Glauconite is absent from thin intervals from Core 120-748C-71R downward. Pyritized wood fragments first appear in Core 120-748C-71R and persist to the base of Subunit IIIB. Subunit IIIC is a 1.2-m-thick basalt cobble conglomerate with unaltered, broken mollusc shells and glauconitic siltstone as matrix.

Unit IV contains basalt and possible underlying claystones. A 3.4-m-thick basalt flow, Subunit IVA, is below the conglomerate, and there is no evidence of any sort of altered or baked contact. Although recovery was very poor below the basalt (902.2 mbsf), two types of smectitic/glauconitic claystones that had not been observed in uphole cores were recovered as small chips in core-catcher socks and the BHA. In addition to these, at least one type of highly altered basalt with alteration mineral-filled vesicles was identified. All of these make up Subunit IVB, and all appear to be the products of basalt alteration.

BIOSTRATIGRAPHY

Introduction

Drilling at Site 748 revealed the presence of a thick sequence of Upper Cretaceous and Cenozoic sediments with a stratigraphic record spanning at least the last 75 m.y. Initial estimates indicate that slightly less than 80% of the total geologic history is represented by sediment; the rest is represented by unconformities. Approximately 407 m of Cenozoic and 492 m of Upper Cretaceous sediments were penetrated before reaching a basalt flow. Evidence of additional sediment below the basalt indicates that basement was not reached. Four lithologic units were recognized (see "Lithostratigraphy and Sedimentology" section, this chapter).

Unit I consists of a thin (13.3 m) diatom ooze unit of upper Miocene to lower Pleistocene. Unit II consists of a 375.8-m sequence spanning the lower upper Paleocene to upper Miocene. It is divided into two subunits based on the presence of chert: Subunit IIA (nannofossil ooze devoid of chert) is middle Eocene to upper Miocene, whereas the chert-bearing Subunit IIB is lower upper Paleocene to middle Eocene. Unit III is a thick (509.7 m) sequence of glauconitic sediments spanning the upper Albian through upper Paleocene, and Unit IV consists of a basalt flow and possible underlying claystones.

Biostratigraphic subdivision and paleoecologic interpretation of this sequence is based on investigations of planktonic fora-

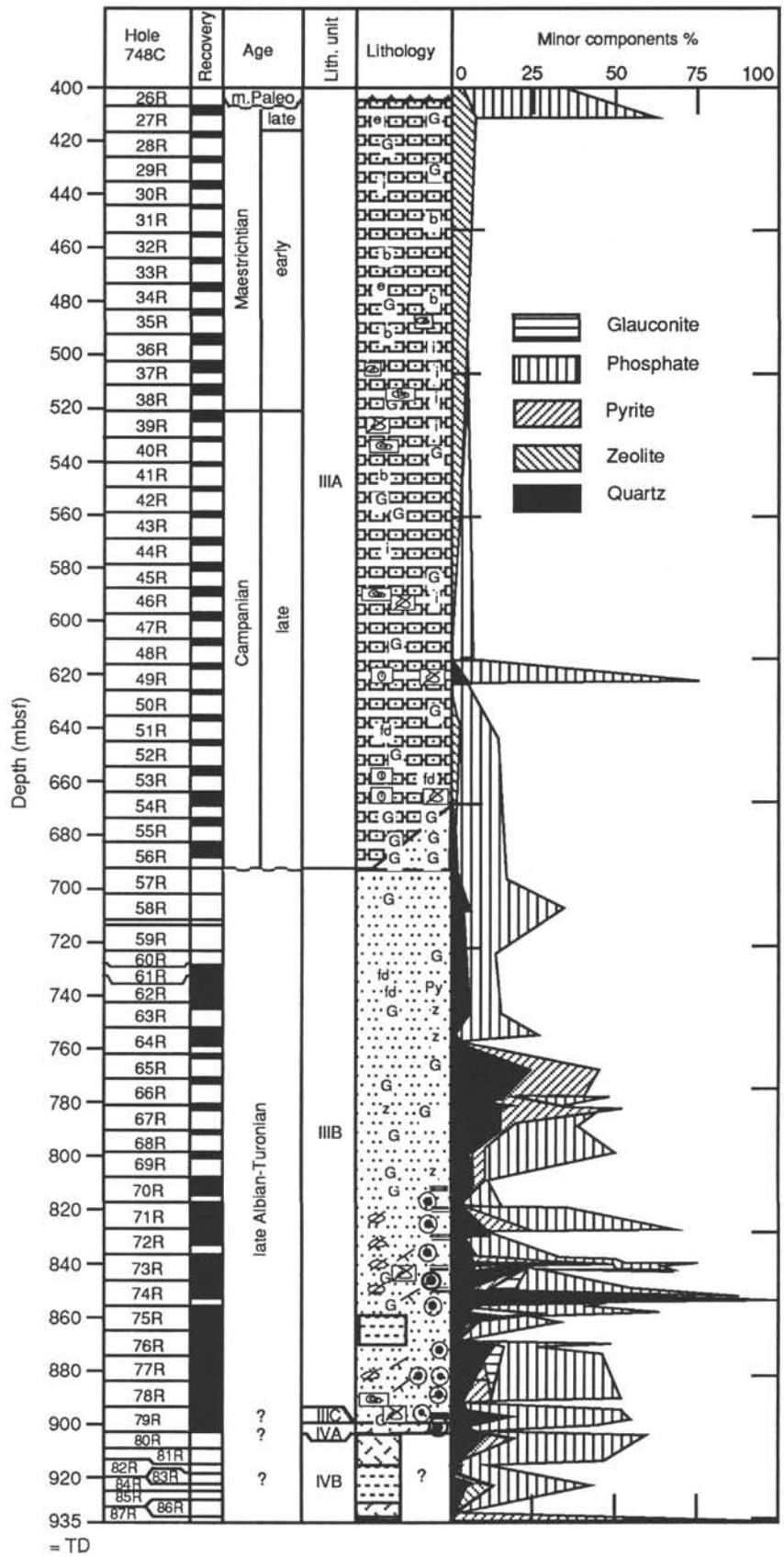

Figure 18. Downhole variation in minor sediment components, Site 748, for Units III and IV. Note the presence of quartz between 600 and 900 mbsf, and zeolites between 730 and 850 mbsf. Lithology, age units, and key to symbols as in Figure 10.

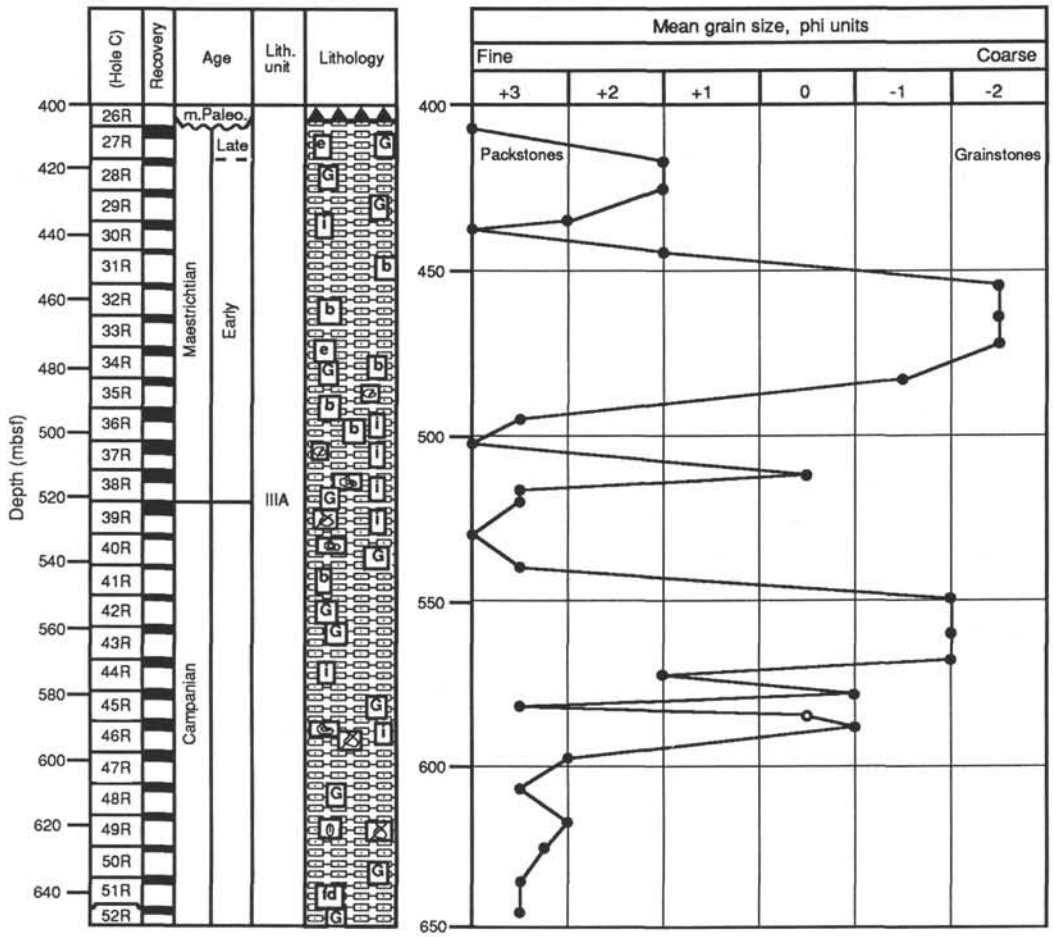

Figure 19. Downhole variation in mean grain size for Unit III, Site 748. Grainstones have higher mean grain size; packstones have lower. Lithology and age units from Figure 10.

minifers, benthic foraminifers, calcareous nannofossils, radiolarians, diatoms, silicoflagellates, and ebridians. The results of these initial investigations are summarized in Figures 33 and 34 and discussed below.

Cenozoic

Planktonic Foraminifers

The Cenozoic stratigraphic record of Site 748 is represented by about 407 m and spans the middle Paleocene (around 61 Ma) to the present. The middle Paleocene to Pleistocene (including present-day) sequence contains at least one unconformity detectable by planktonic foraminifer biostratigraphy: it occurs at about 39.5 mbsf (Core 120-748B-6H between Sections 1 and 2) and separates uppermost middle Miocene from upper lower Miocene sediments. The hiatus associated with this unconformity is estimated at approximately 6 m.y. The Oligocene/Miocene boundary occurs at or near the base of Core 120-748B-8H (around 66 mbsf) and the Eocene/Oligocene boundary lies between Cores 120-748B-14H and -15H at 123.6 mbsf.

The Eocene is about 200 m thick (top of Core 120-748B-15H to within Core 120-748C-17R; 123.6–325 mbsf). The Paleocene extends from the middle of Core 120-748C-17R to the base of Core 120-748C-26R (325–407 mbsf), where it lies unconformably upon the upper Maestrichtian.

Core-catcher samples have been examined from Cores 120-748A-1H and -2H, Cores 120-748B-1H to -24H, and Cores 120-748C-6R to -26R. Chert beds were encountered between 170 and 180 mbsf, at which point recovery diminished, and biostratigraphy below this level is often based upon examination of scraps of carbonate attached to chert fragments or isolated pieces of soft calcilutite. Only Core 120-748C-10R recovered a substantial amount of sediment (3.86 m), which upon closer study has yielded a detailed lower Eocene stratigraphy.

Neogene

Low-diversity late Neogene planktonic foraminifer assemblages dominated by *Neogloboquadrina pachyderma* characterize Samples 120-748A-1H-CC, 120-748B-1H-CC, and 120-748B-2H-CC. *Globorotalia scitula* and *Globigerina bulloides* characterize Samples 120-748A-2H-CC and 120-748B-3H-CC, which is suggestive of the late Miocene if compared with results at Site 747. The presence of *Neogloboquadrina nympha, N. continuosa,* and large *Globigerina bulloides* in Samples 120-748B-4H-CC and 120-748B-5H-CC suggests a late Miocene (equivalent to Zone N15) age. Sample 120-748B-6H-CC yielded a late middle to early late Miocene fauna characterized by *Globorotalia zealandica, Paragloborotalia incognita,* and *P. semivera,* which belongs to Zone M3 of Berggren et al. (1983).

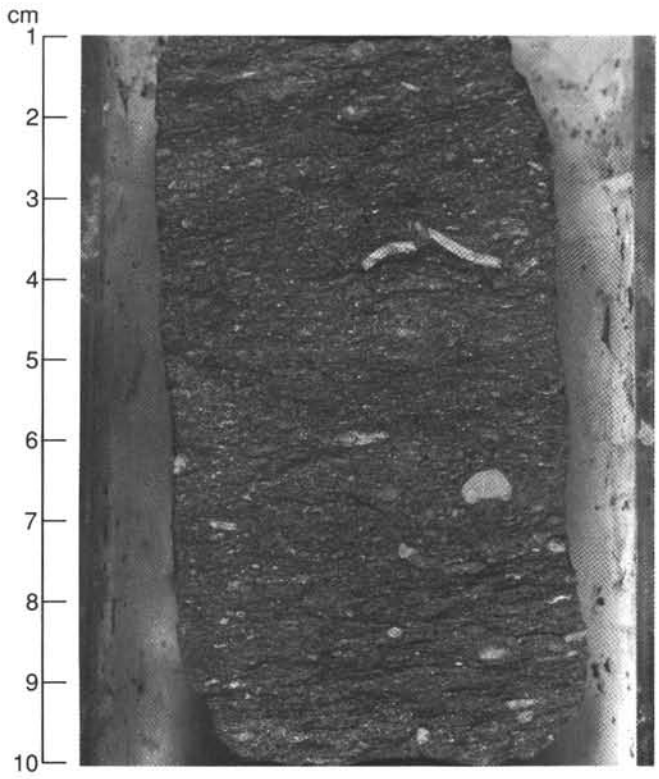

Figure 20. Glauconitic packstone from Subunit IIIA, Site 748, Section 120-748C-45R-CC. Inoceramid debris at 3 cm; bryozoan debris between 7 and 10 cm. Dark brown, thin, clay-rich flaser beds are especially abundant between 7 and 10 cm.

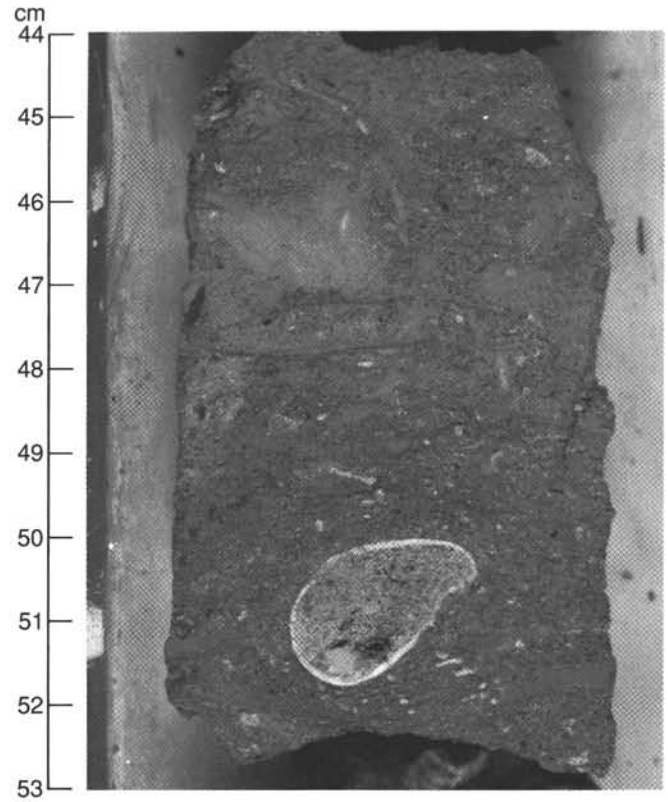

Figure 21. Light to dark clay-filled burrows in glauconitic packstone, Subunit IIIA, Site 748, Section 120-748C-46R-1. The mollusc between 50 and 52 cm is filled with glauconite, micrite, and pyrite.

These two ages (middle Miocene, $< \sim 12.1$ Ma, for Sample 120-748B-5H-CC, based on the first appearance datum [FAD] of *N. nympha* in Core 120-747A-7H-7 [around 65–66 mbsf] at a level equivalent to the base of Anomaly Correlative 5A, and late early Miocene, >16.8 Ma, for Sample 120-748B-6H-CC), less than 10 m apart, suggest the presence of a hiatus, or an extremely condensed section within Core 120-748B-6H. A detailed study of this core indicates the following sequence of biostratigraphic events: the *G. zealandica* assemblage ends in Sample 120-748B-6H-2, 40–44 cm; *Catapsydrax dissimilis* in Sample 120-748B-6H-3, 40–44 cm; and *P. incognita* in Sample 120-748B-6H-4, 40–44 cm. All three groups characterize the sequence below (Sections 5, 6, 7, and CC). Thus, it would appear that an unconformity is situated at or about a level between Sections 1 and 2 of Core 120-748B-6H (= 39.6 mbsf).

Samples 120-748B-7H-CC and 120-748B-8H-CC contain early Miocene faunas with *Paragloborotalia nana, Catapsydrax dissimilis, Globigerina brazieri,* and *Globigerina woodi connecta.* The latter form has its initial appearance in Sample 120-748B-8H-CC and is used here to denote the position of the Oligocene/Miocene boundary (cf. Kennett and Srinivasan, 1983).

Paleogene

Late Oligocene faunas (*Subbotina euapertura, Catapsydrax unicavus, Tenuitella gemma,* among others) occur in Samples 120-748B-9H-CC and 120-748B-10H-CC. The sequential downhole last appearance datums (LADs) of *Chiloguembelina* (Sample 120-748B-10H-CC) and *Subbotina angiporoides* (Sample 120-748B-11H-CC) serve as useful middle Oligocene biostratigraphic reference points. *Subbotina angiporoides* dominates early Oligocene faunas in Samples 120-748B-12H-CC, 120-748B-13H-CC, and 120-748B-14H-CC. *Chiloguembelina* is abundant in Sample 120-748B-13H-CC (earliest Oligocene) and occurs only sporadically in 120-748B-10H-CC to 120-748B-12H-CC above. This is in contrast to its continued common occurrence into younger levels at Site 747.

The Eocene/Oligocene boundary is situated between Cores 120-748B-14H and -15H based on the LADs of *Globigerapsis index* and *Subbotina linaperta* in Sample 120-748B-15H, 24 cm, and their absence in Sample 120-748B-14H-CC. Faunas containing these two taxa, together with *Subbotina galavisi* and chiloguembelinids, characterize Samples 120-748B-16H-CC and 120-748B-17H-CC. The LAD of *Acarinina* sp. in Sample 120-748B-17H-CC suggests that the middle/upper Eocene contact lies within Core 120-748B-17H.

Middle Eocene faunas characterize samples from Cores 120-748B-18H through -24H, at which level APC coring ended because indurated cherts were present. The LAD of *Acarinina primitiva* in Sample 120-748B-18H-CC and the lowest occurrence of *Globigerapsis index* in Sample 120-748B-20H-CC suggest a correlation with levels within Zone P13 and P11, respectively, of the "standard" low-latitude, tropical zonation schemes. The common occurrence of *Acarinina densa* in Cores 120-748B-21X, -23X, and -24X, in the absence of definitive evidence of an early Eocene age, suggests an early middle Eocene age (Lutetian) approximately correlative with Zone P10 of the low-latitude zonation.

Rotary coring (Hole 748C) began at about 173 mbsf, and the first core overlapped with Core 120-748B-20H. The fauna of *Globigerapsis index, Subbotina linaperta, Acarinina primitiva, Pseudohastigerina micra,* among others, in Sample 120-748C-1R-CC is middle Eocene in age and correlates well with Sample

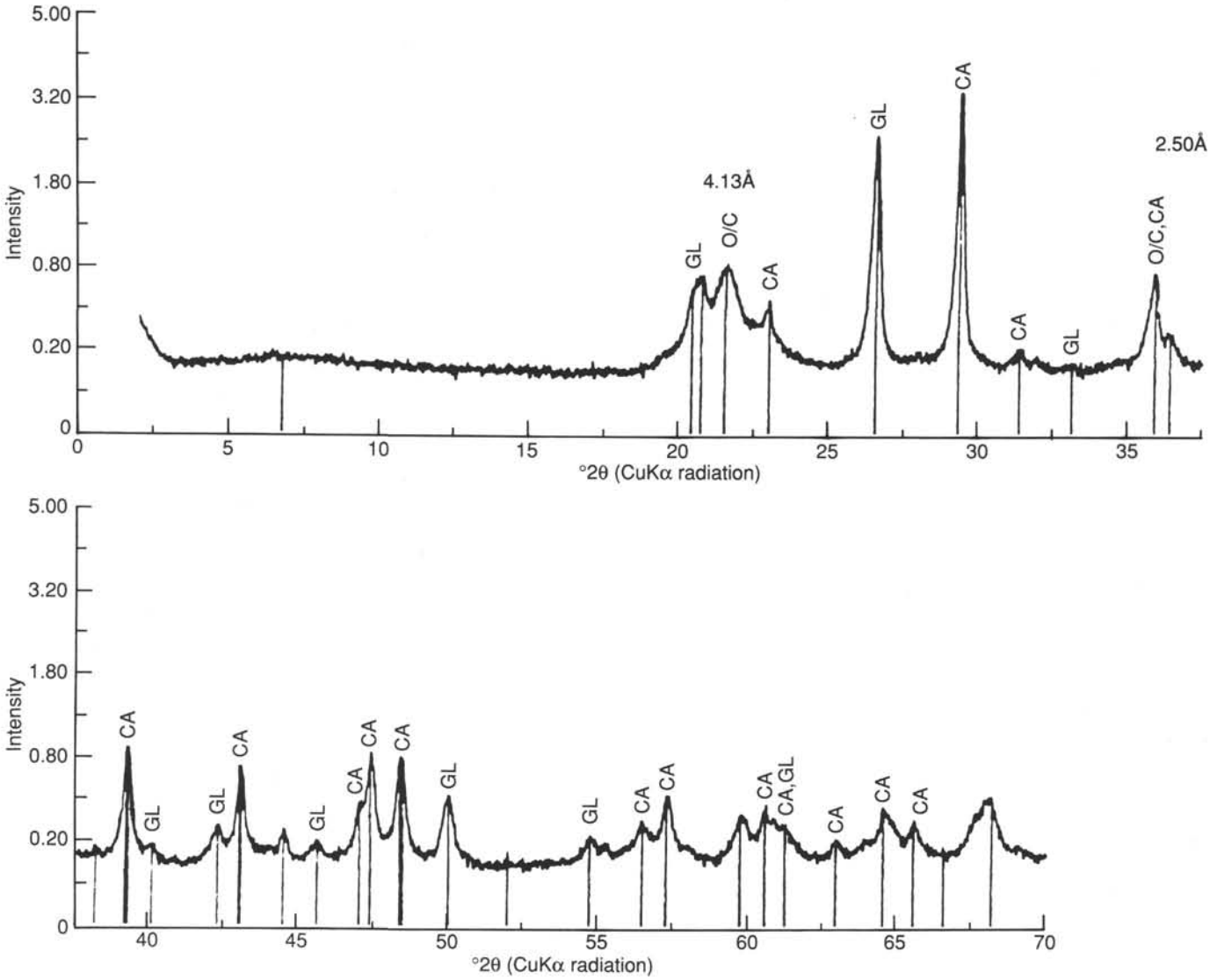

Figure 22. The X-ray diffractogram from Sample 120-748C-27X-1, 1–3 cm (ground bulk sample). A mineral between opal-C and opal-CT is indicated by peaks at 4.13 and 2.50 Å. Calcite (CA) and glauconite (GL) are the other abundant minerals. O/C = opal-C/opal-CT.

120-748B-20H-CC. This suggests that the occurrence of *G. index* at this level is, indeed, close to its FAD. There was basically no recovery in Cores 120-748C-2R through -5R.

Sample 120-748C-6R-CC yielded an early middle Eocene fauna (below the FAD of *G. index*) characterized by *Subbotina linaperta, Acarinina primitiva, A. angulosa, A. pentacamerata, Pseudohastigerina micra, P. wilcoxensis,* and *Globigerapsis senni.* This fauna is biostratigraphically equivalent to Zone P10, although the index forms of that zone are not present at Site 748. There was essentially no core recovery in Cores 120-748C-7R through -9R.

Approximately 3.86 m of sediment was recovered in Core 120-748C-10R, and a sample has been examined from each of the three sections obtained in addition to the core catcher. Core 120-748C-10R spans the P8–P9 zonal interval and at its base (CC) may be equivalent to Zone P7. Sample 120-748C-10R-1, 19–21 cm, yielded a late Ypresian (P9) fauna with *Subbotina patagonica, S. linaperta, S. frontosa, Acarinina bullbrooki–A. densa* group, *A. angulosa, Pseudohastigerina wilcoxensis, Planorotalites australiformis, P. elongata,* and abundant chiloguembelinids.

Sample 120-748C-10R-2, 97–99 cm, contains a similar fauna but also present are *Acarinina pseudotopilensis, Igorina broedermanni,* and (rare) individuals morphologically transitional between *Morozovella aragonensis* and *M. caucasica* (supportive of a P8 or base P9 assignment; see Berggren and Miller, 1988; Toumarkine and Luterbacher, 1985). The FAD of the benthic form *Cibicidoides subspiratus* occurs in this sample, also supporting the P9 age determination (Tjalsma and Lohmann, 1983; Van Morkhoven et al., 1986; see the report on benthic foraminifers below).

Sample 120-748C-10R-3, 23–35 cm, contains a fauna with *A. pentacamerata, A. primitiva, A. soldadoensis, A. angulosa,* and *Subbotina patagonica. Acarinina densa* is notably absent, suggesting a Zone P8 age assignment. Sample 120-748C-10R-CC has an early Eocene fauna of Zone P7–P8 (undifferentiated) age with *S. patagonica, Pseudohastigerina wilcoxensis, Igorina convexa,* and *Planorotalites australiformis,* but no morozovellids, the presence of which might make a more definitive age assignment possible.

Samples 120-748C-11R-CC and 120-748C-12R-CC contain nondiagnostic early Eocene subbotinid-acarininid faunas. The

Table 5. Summary of observations of thin sections from Subunit IIIA, Site 748.

Thin section	Description
1) 120-748B-21X-1, 3–7 cm	White, foraminifer micritic limestone, partially silicified
2) 120-748C-25R-1, 1–3 cm	Silicified, foraminifer micritic limestone
3) 120-748C-25R-CC, 0–5 cm	White, partially silicified foraminifer limestone, with glauconite
4) 120-748C-27R-1, 12–13 cm	Bioclastic packstone, with foraminifers and some glauconite
5) 120-748C-27R-1, 27–32 cm	Micritic silicified chalk with foraminifers and glauconite
6) 120-748C-29R-1, 14–17 cm	Silicified bioclastic grainstone with glauconite
7) 120-748C-31R-CC	Silicified bioclastic grainstone
8) 120-748C-32R-1, 36–38 cm	Bioclastic grainstone to rudstone; algal, echinoid, bryozoan fragments
9) 120-748C-32R-1, 49–50 cm	Silicified bioclastic grainstone, medium sand size, inoceramid fragments
10) 120-748C-33R-1, 15–16 cm	Calcareous bioclastic grainstone; rudstone with large bryozoans
11) 120-748C-33R-1, 55–57 cm	Bioclastic grainstone, large bryozoans, red algae, echinoid fragments
12) 120-748C-34R-1, 59–62 cm	Silicified bioclastic grainstone to rudstone; bryozoan fragments
13) 120-748C-34R-1, 116–119 cm	Bioclastic grainstone; echinoid, bryozoa, and inoceramid fragments
14) 120-748C-37R-1, 136–140 cm	Bioclastic grainstone; with inoceramid hash
15) 120-748C-37R-2, 45–46 cm	Silicified bioclastic packstone, inoceramid fragments
16) 120-748C-37R-2, 96–100 cm	Bioclastic packstone; inoceramid debris, silicified
17) 120-748C-39R-2, 49–53 cm	Bioclastic packstone; large inoceramid shell and prisms
18) 120-748C-46R-2, 48–49 cm	Bioclastic packstone; bivalve fragments, sterraster polyaxon
19) 120-748C-49R-1, 53–60 cm	Bioclastic wackestone with glauconite; sterraster polyaxon
20) 120-748C-56R-2, 27–30 cm	Glauconitic, silicified limestone with (phosphate?)
21) 120-748C-58R-CC	Glauconitic, silicified packstone; pyrite, sterraster polyaxon
22) 120-748C-78R-1, 8–11 cm	Sideritic nodule with glauconite
23) 120-748C-79R-5, 8–10 cm	Basalt cobble limestone matrix with glauconite and mollusc fragments
24) 120-748C-79R-5, 17–20 cm	Basalt cobble matrix; bioclastic wackestone, mollusc fragments

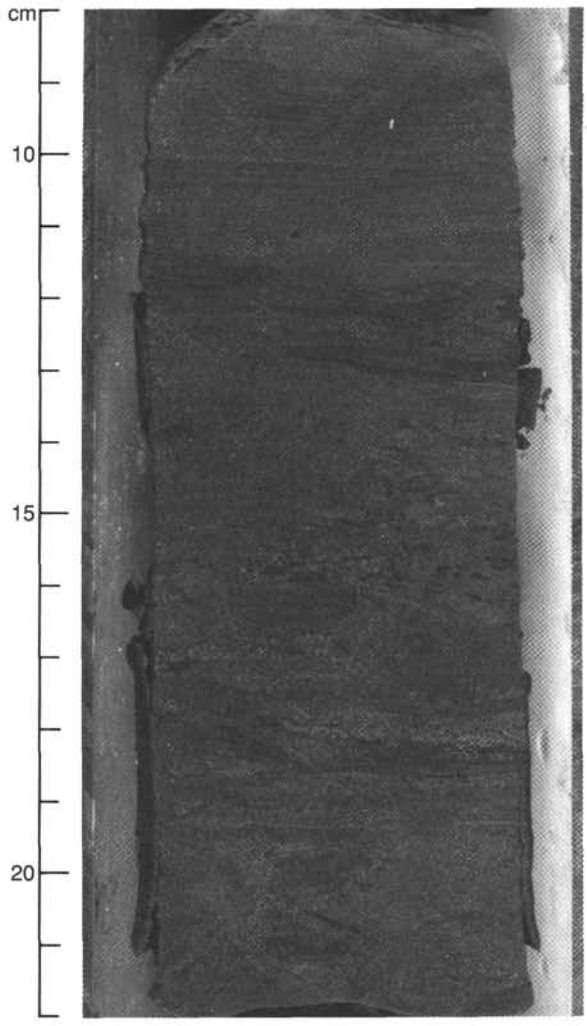

Figure 23. Clayey glauconitic siltstone within Subunit IIIB in Section 120-748C-65R-1. Alternate dark and light laminae are 1 mm thick or less (9–11 cm); clay-enriched flasers indicate deposition by currents (11–13 cm). Massive bedding, some of which is caused by extensive bioturbation, occurs between 13 and 17 cm; faint laminae disrupted by bioturbation occur between 17.5 and 19.5 cm.

presence of *Pseudohastigerina wilcoxensis* indicates correlation of this interval with the *P. wilcoxensis* Zone of Jenkins (1985). Sample 120-748C-14R-CC contains *Morozovella formosa gracilis* (rare), *Acarinina soldadoensis,* and *Planorotalites chapmani,* but no pseudohastigerinids, and is assignable to Zone P6b of Berggren and Miller (1988). Sample 120-748C-15R-CC contains a fauna dominated by *Acarinina soldadoensis* and *Subbotina* sp. cf. *S. triangularis* and is of basal early Eocene age. This is supported by the presence of an early Eocene assemblage of benthic foraminifers.

Sample 120-748C-16R-CC contains a subbotinid-acarininid fauna characterized in particular by *Acarinina primitiva, A. coalingensis, A. pseudotopilensis,* and *A. soldadoensis,* but no morozovellids. The occurrence of *Tappanina selmensis* (LAD) in this sample suggests a latest Paleocene (P6a) age based on the extinction of this taxon in Zone P6a in Hole 747C and elsewhere (Van Morkhoven et al, 1986; see also the discussion of benthic foraminifers, below).

Sample 120-748C-17R-CC contains abundant *Acarinina soldadoensis* and subbotinids of the *Subbotina velascoensis* and *S. triangularis* groups, which suggests a late Paleocene age (equivalent to Zone P5). Sample 120-748C-19R-CC contains a biostratigraphically undiagnostic late Paleocene fauna of subbotinids, acarininids, planorotaliids, and chiloguembelinids of small size. The benthic fauna supports a late Paleocene age determination. The presence of *Igorina tadjikistaensis, I. albeari = laevigata,* and *Subbotina velascoensis* in Sample 120-748C-20R-CC suggests a biostratigraphic level equivalent to Zone P4 of Berggren and Miller (1988).

Samples 120-748C-21R-CC and 120-748C-22R-CC contain an indeterminate fauna of small acarininids and subbotinids. The presence of the benthic form *Bulimina bradburyi* suggests an age no older than Zone P4 (by correlation; Tjalsma and Lohmann, 1983; Van Morkhoven et al., 1986). Sample 120-748C-23R-CC contains the LAD of *Subbotina triloculinoides* (s.s.), common *Acarinina mckannai,* and the FAD of *Bulimina bradburyi,* which suggests a level correlative with Zone P4. Non-age-diagnostic acarininids and subbotinids characterize Samples 120-748C-24R-CC and 120-748C-25R-1, 122–124 cm, although the presence of *Igorina pusilla* in Sample 120-748C-24R-CC suggests an age correlative with Zone P4 (Berggren and Miller, in press).

The oldest Cenozoic (Paleocene) sample (120-748C-26R-CC) contains *Subbotina triloculinoides, S. varianta, Acarinina mc-*

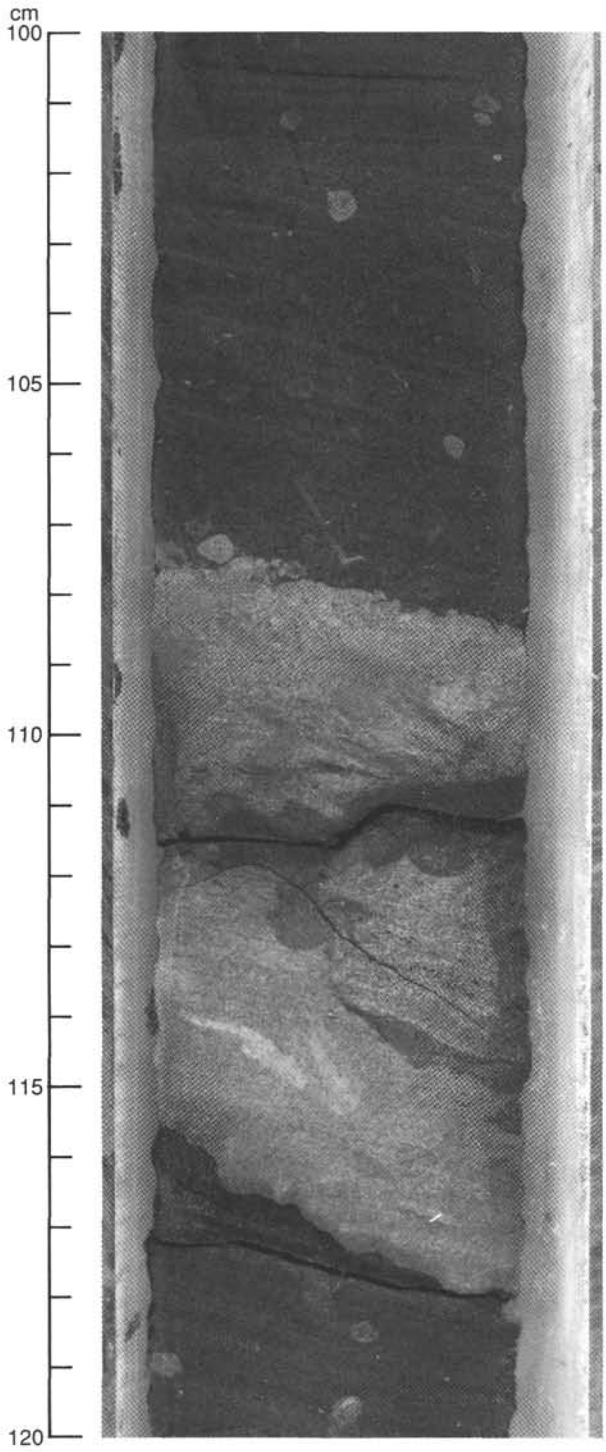

Figure 24. Glauconitic siltstone within Subunit IIIB in Section 120-748C-72R-3. Cross laminae are visible between 101 and 103 cm; small siderite/smectite-filled burrows are scattered throughout; a large siderite concretion, with laminae and burrows preserved inside, occurs from 107 to 117 cm.

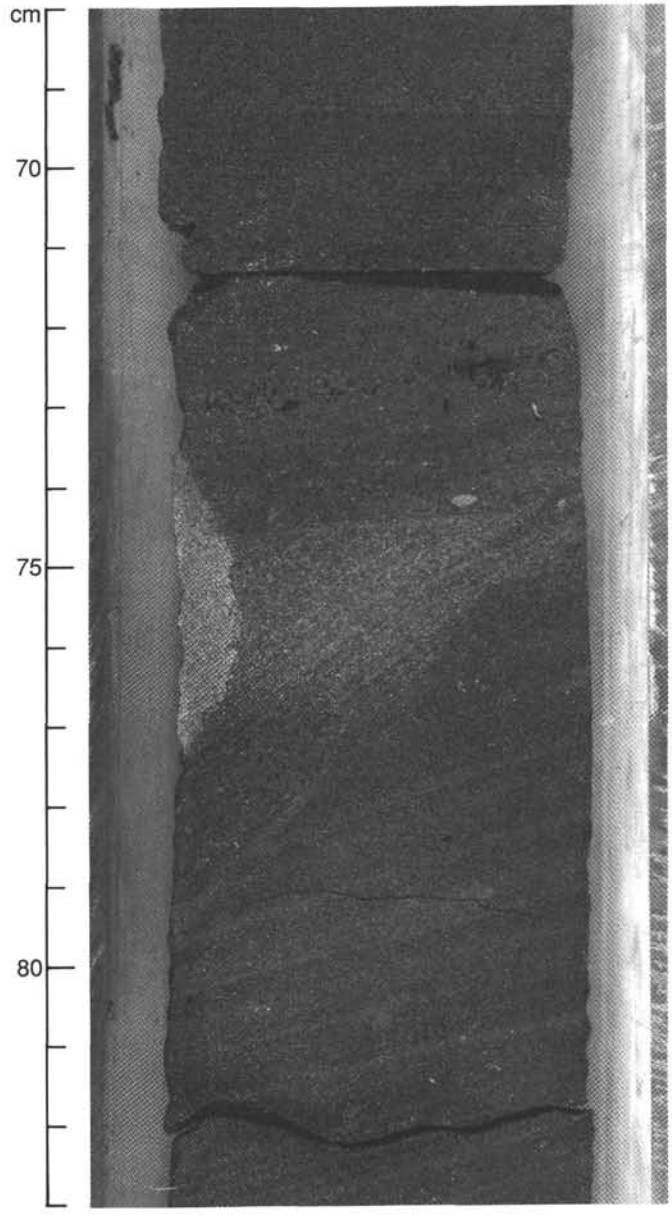

Figure 25. Glauconitic siltstone within Subunit IIIB in Section 120-748C-72R-4. Cross beds between 74 and 83 cm indicate deposition by currents. Pyritized wood is concentrated along bedding planes at 73 cm. A sideritic concretion has formed across cross and plane beds, 73–77 cm.

kannai, Chiloguembelina morsei, and *C. midwayensis* and appears to be correlative with Zone P3b. An older age is unlikely based on the assemblage of acarininids present.

In summary, the main features of the Cenozoic planktonic foraminifer record include the following:

1. Recovery of a virtually complete, well-preserved upper Paleocene to lower Pleistocene succession; a hiatus within Core 120-748B-6H separates uppermost middle Miocene from upper lower Miocene sediments.
2. The faunal succession contains a temperate, high-latitude fauna throughout with evidence of incursion by tropical elements only near the Paleocene/Eocene boundary.
3. The good Paleogene to lower Neogene recovery should enable us to obtain an integrated biostratigraphic and stable isotopic (temperature) record for this part of the Cenozoic record and, in particular, across the Eocene/Oligocene boundary interval.
4. A nearly complete magnetostratigraphic record was obtained from the Pliocene-Pleistocene to the upper Eocene, which,

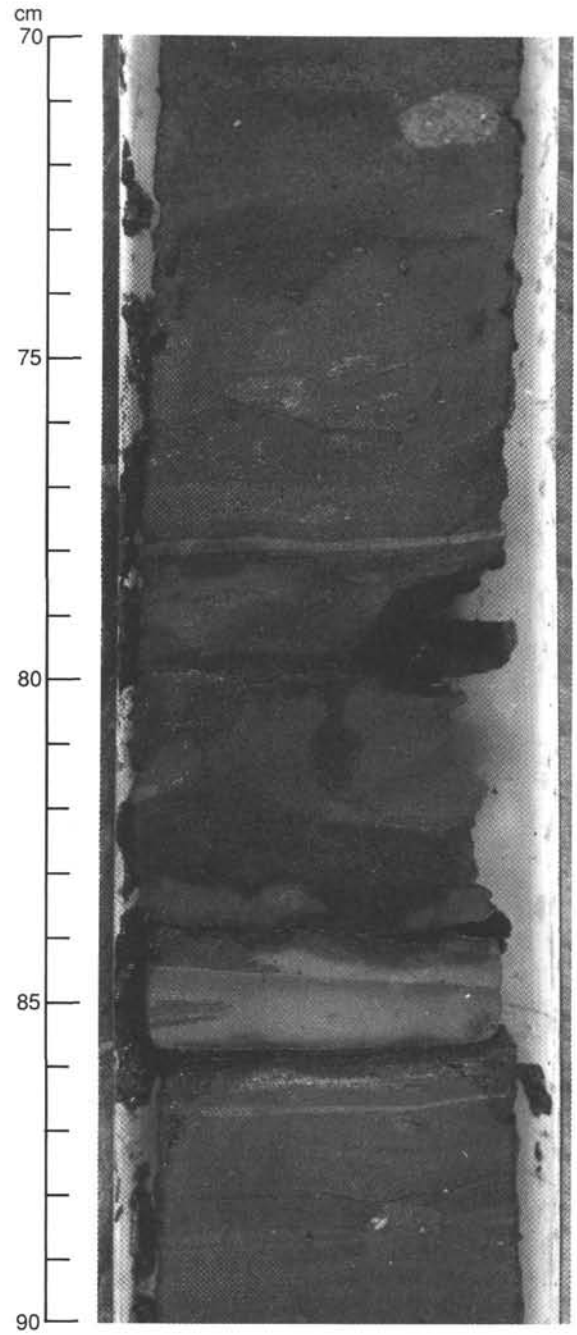

Figure 26. Glauconitic siltstone with clay within Subunit IIIB in Section 120-748C-71R-6. Dark gray clay beds are up to 1 cm thick between 83 and 88 cm.

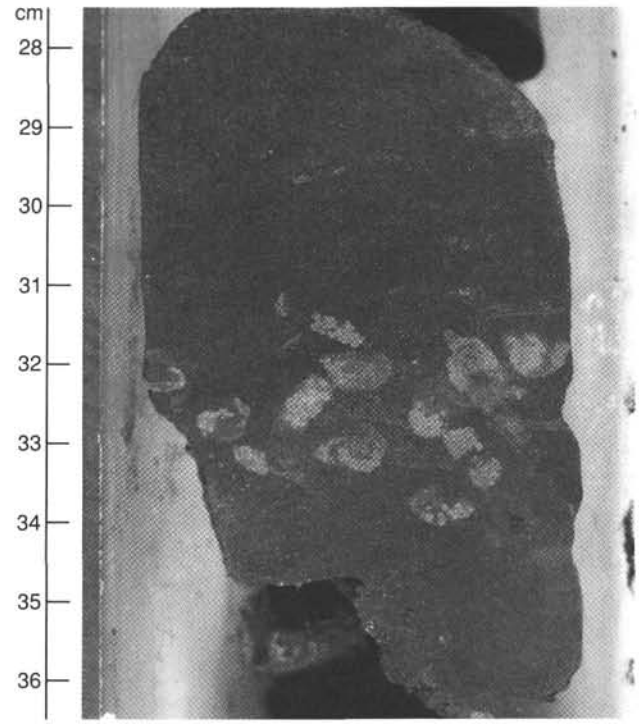

Figure 27. Clayey siltstone with glauconite within Subunit IIIB in Section 120-748C-68R-1. Burrows with internal structure are filled with siderite and smectite.

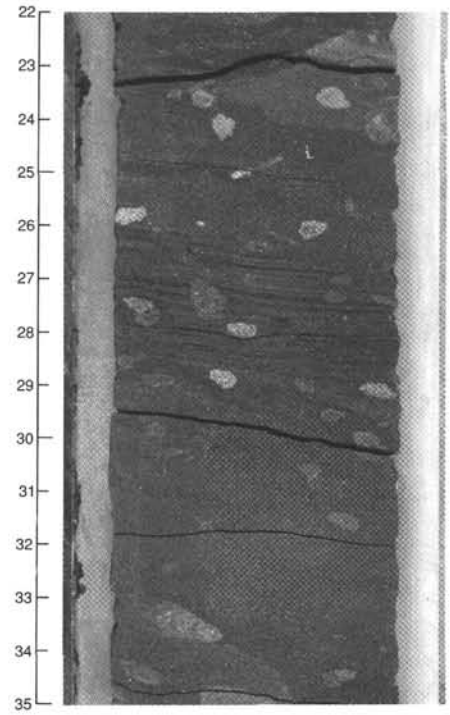

Figure 28. Glauconitic siltstone within Subunit IIIB in Section 120-748C-72R-4. Burrows with no internal structure are filled with siderite and smectite. Some of these disrupt laminae between 26 and 29 cm. The black color of these laminae is caused by concentration of pyritized wood along bedding planes. Sideritic concretions occur at 22–24 cm and 33–35 cm.

together with results from Site 747, should provide us with the opportunity to obtain an integrated calcareous and siliceous high-latitude magnetobiostratigraphy for the last 40 m.y. (see "Sedimentation Rates" section, this chapter).

Benthic Foraminifers

All Cenozoic core-catcher samples from Holes 748B and 748C were analyzed for their benthic foraminifer content as far as they were disaggregatable. Additional samples were investigated when major changes in the benthic fauna occurred or the core catcher yielded an incomplete or badly preserved fauna. Between 100 and 400 specimens of each sample were picked and

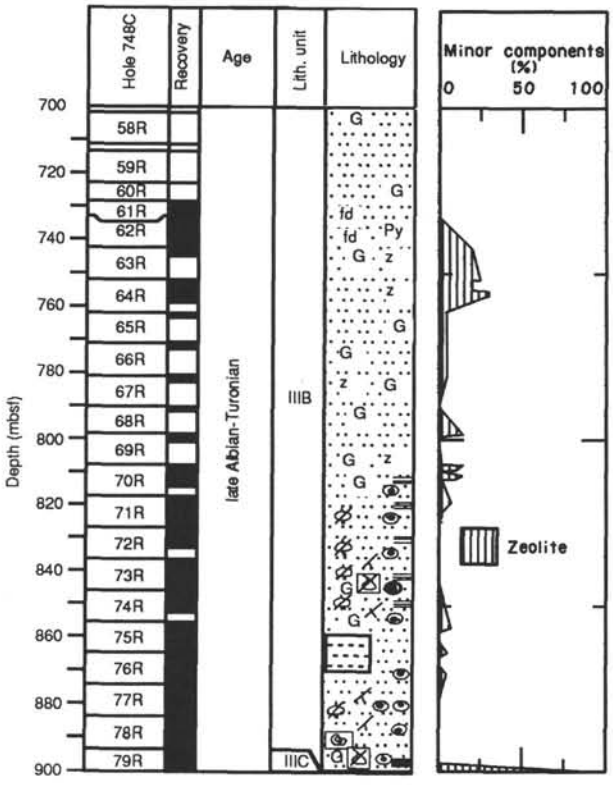

Figure 29. Downhole variation in zeolite abundance, Units III and IV, Site 748. Lithology, age units, and key to symbols as in Figure 10.

mounted from the >125-μm fraction. Benthic foraminifers are generally well preserved and abundant in all Paleogene core-catcher samples, although they are rare in comparison with planktonic foraminifers. Some of the Neogene faunas are poorly preserved.

The following benthic foraminifer assemblages were recognized in the Cenozoic sequence of Holes 748B and 748C (the subdivision of benthic foraminifer assemblages into "a" and "b" categories is preliminary and is used only for consistency and convenience in comparing them with the faunas described in Site 747).

Assemblage 1a: Pleistocene

This assemblage is represented by Sample 120-748B-1H-CC (0.20 mbsf). The fauna is dominated by *Trifarina earlandi* and *Bulimina aculeata. Globocassidulina subglobosa* and *Cibicidoides* cf. *wuellerstorfi* are frequent constituents. Rare, but characteristic components of this fauna are *Stilostomella* spp., *Oridorsalis umbonatus, Pullenia bulloides, Pyrgo murrhina, Fissurina* spp., *Eggerella bradyi,* and *Karreriella* sp.

A similar fauna dominated by *B. aculeata* is found living on the eastern continental slope of the Weddell Sea between 1700 and 2100 m water depth. Today, in the eastern Weddell Sea in this water depth interval, a water mass boundary occurs between the warmer Weddell Deep Water and the Antarctic Bottom Water. The surface sediments there are characterized by relatively high organic carbon and very low carbonate contents (Mackensen, unpubl. data). More detailed studies of the Pliocene-Pleistocene foraminifer fauna of Site 748 may show a possible use of this assemblage as an indicator for changes in paleoproductivity and, eventually, for the identification of ancient water mass boundaries.

Assemblage 1b: Pliocene

This assemblage is chosen to represent an independent fauna (Sample 120-748B-2H-CC) due to the absence of *Bulimina aculeata,* one of the dominant species of the Pleistocene assemblage described above. Benthic foraminifers are very rare. The assemblage is characterized by *Laticarinina pauperata, Oridorsalis umbonatus, Martinottiella nodulosa, Pullenia subcarinata,* and *P. bulloides. Trifarina earlandi* is still present, but rare. *Lagena* spp., *Gyroidina* spp., *Uvigerina* sp., *Stilostomella* spp., *Psammosphaera fusca,* and *Cibicidoides* sp. are accessory components. The lower boundary was chosen below the FO of *Trifarina earlandi.*

Assemblage 2: Late Miocene

Epistominella exigua is the characteristic component of this fauna, although in other respects this assemblage is similar to the previous one. It is represented by Samples 120-748B-3H-CC through 120-748B-5H-CC. Both the diversity and the number of specimens are low. *Astrononion pusillum, Cibicidoides mundulus, Cibicidoides* spp., *Karreriella bradyi, Pyrgo* spp., *Gyroidina* spp., *Pleurostomella* spp., *Fursenkoina* sp., *Pullenia bulloides, Bulimina* sp., *Stilostomella* spp., *Uvigerina* spp., *Uvigerina proboscidea, Fissurina* spp., *Quinqueloculina* sp., and *Bolivina* spp. are common constituents of this benthic assemblage. The lower boundary is a middle Miocene unconformity that coincides at this site with the FO of *Epistominella exigua* and the last occurrence (LO) of *Nuttallides umbonifera.*

Assemblage 3: Early Miocene–Late Eocene

The upper boundary of this assemblage is defined by the LO of *Nuttallides umbonifera.* It comprises Samples 120-748B-6H-CC through 120-748B-15H-CC. The fauna is variable, but throughout this section *Stilostomella* spp., *Cibicidoides* spp., *Uvigerina hispidocostata, Nuttallides umbonifera, Gyroidina* spp., and *Astrononion pusillum* are characteristically the most abundant species. *Laticarinina pauperata* is common down to its FO in Sample 120-748B-12H-CC.

Common accessory species are *Uvigerina* spp., *Pullenia bulloides, Bulimina* spp., *Pleurostomella* sp., *Globocassidulina subglobosa, Karreriella* spp., *Oridorsalis umbonatus, Fissurina* spp., *Bolivina* spp., *Cassidulina* sp., and *Lagena* spp. *Anomalina spissiformis* and *Turrilina alsatica* are common in the lower Oligocene samples (LO in Sample 120-748B-13H-CC). Agglutinated taxa such as *Reophax* spp., *Eggerella* spp., *Cyclammina*? sp., *Tritaxia* sp., and *Textularia* spp. are rare.

This fauna closely resembles a coeval assemblage that is described by E. Thomas (Barker, Kennett, et al., 1988) from the Maud Rise at a somewhat deeper present water depth. The common occurrence of *Nuttallides umbonifera* might indicate a water mass highly corrosive to $CaCO_3$. The lower boundary of this assemblage was chosen above the LO of *Bulimina elongata.*

Assemblage 4a: Late to Middle Eocene

The upper boundary of this assemblage (Samples 120-748B-16H-CC through 120-748B-18H-CC) was chosen at the LO of *Nuttallides truempyi* and *Bulimina elongata. Bulimina elongata* is abundant and dominates the diverse fauna, whereas *N. truempyi* is rare in Samples 120-748B-16H-CC and 120-748B-17H-CC and is not found in Sample 120-748B-18H-CC. *Stilostomella* spp. and *Cibicidoides praemundulus* are frequent. *Pleurostomella* spp., *Cibicidoides eocaena, Nodosaria* sp., *Oridorsalis umbonatus, Fissurina* spp., *Lagena* spp., *Plectofrondicularia* sp., *Lenticulina* spp., *Pullenia subcarinata, P. bulloides, Anomalina spissiformis,* and *Karreriella* spp. are accessory components.

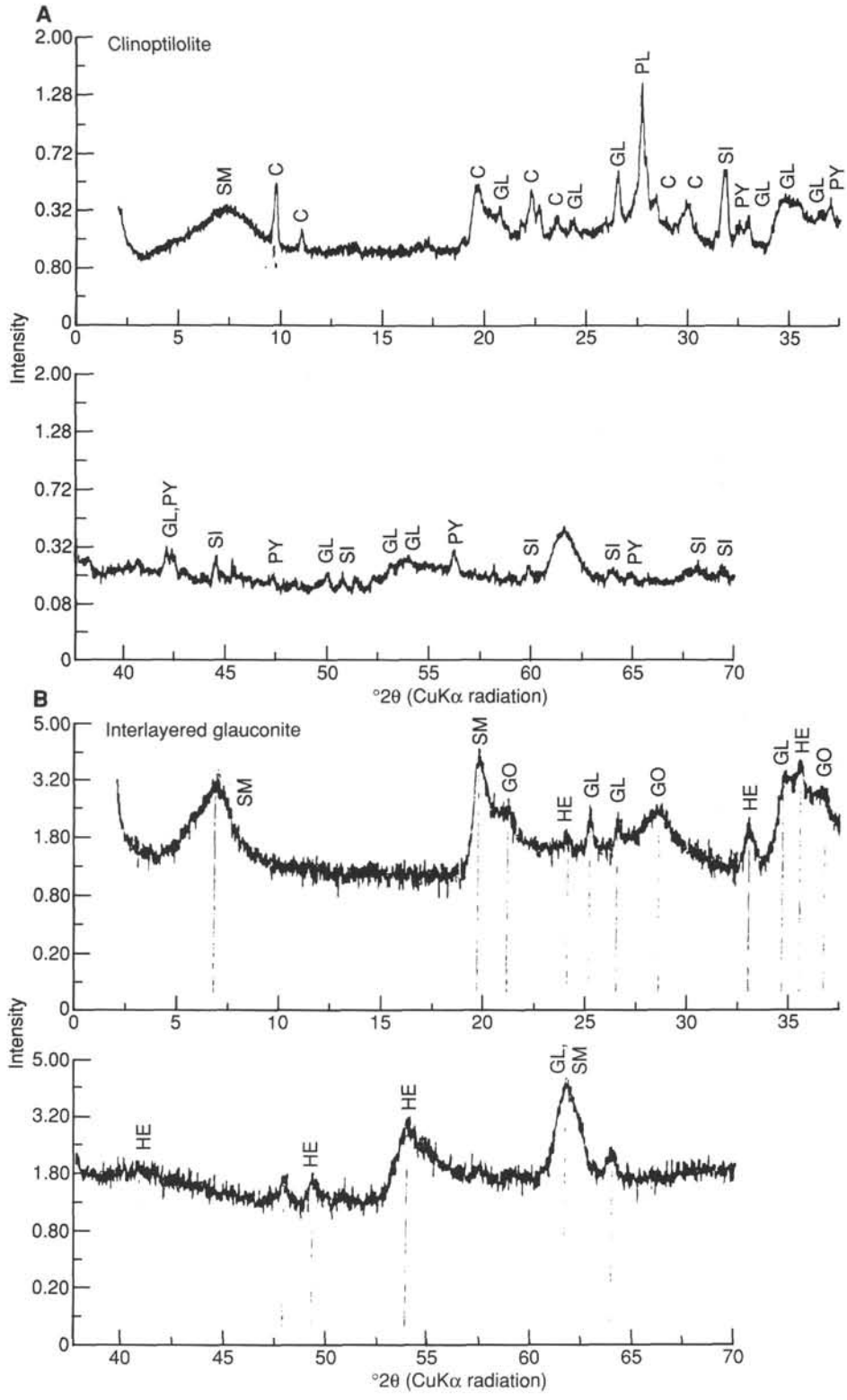

Figure 30. X-ray diffractograms of samples from Units III and IV, Site 748. **A.** Sample 120-748C-66R-1, 27–30 cm, from a zeolite-enriched interval. Sample is unoriented, ground, bulk. The zeolite is clinoptilolite. **B.** Section 120-748C-BHA, a chip of red claystone, with well-crystallized smectite, hematite, and glauconite. C = clinoptilolite; GL = glauconite; GO = goethite; HE = hematite; PL = plagioclase; PY = pyrite; SI = siderite; SM = smectite.

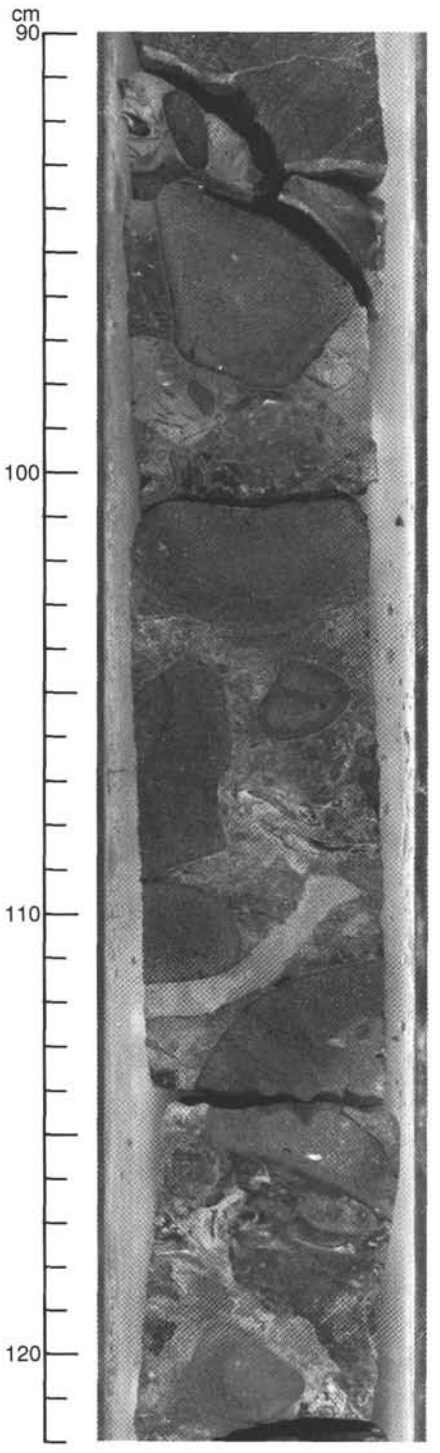

Figure 31. Upper part of conglomerate, Subunit IIIC, Section 120-748C-79R-4. Dark gray, rounded basalt cobbles are mixed with unaltered, broken mollusc fragments in glauconitic siltstone. Post-depositional bioturbation is evidenced by a large burrow, 109–113 cm.

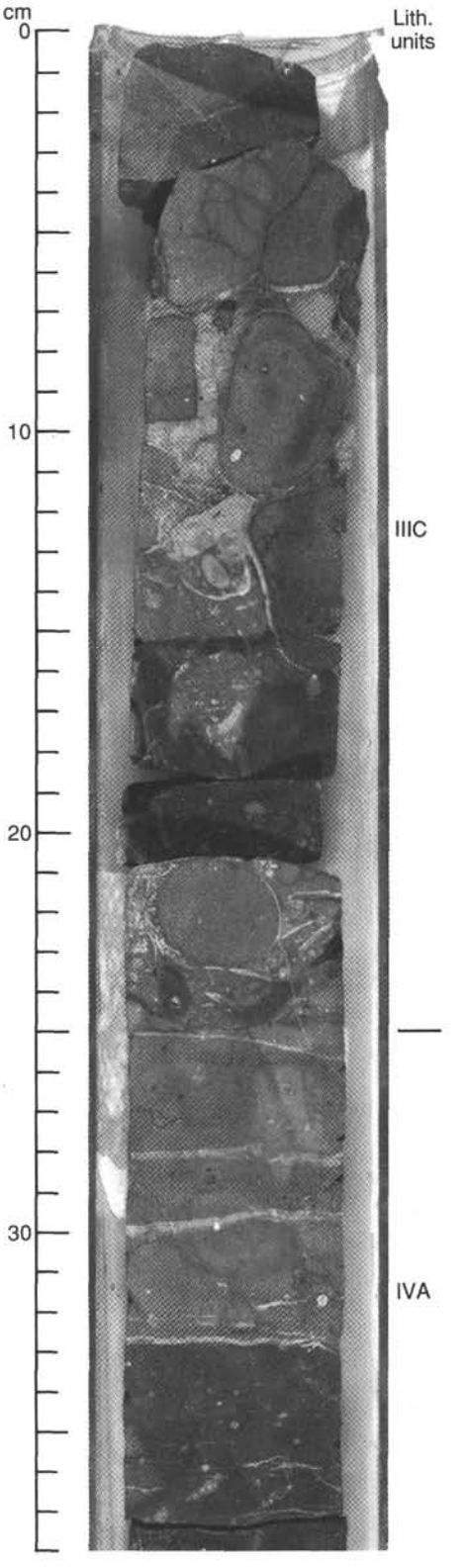

Figure 32. Lower part of conglomerate, Subunit IIIC, Section 120-748C-79R-5, showing contact with Subunit IVA, the basalt flow. Many basalt cobbles are rimmed with sparry calcite, at 6–7, 11–16, and 21–23 cm. Small, sparry calcite-filled vein extends from the upper, highly altered part of the basalt (25 cm) to the conglomerate (22 cm). Unaltered mollusc shells, 23–25 cm, indicate that the basalt was cool before sediment was deposited. The light gray interval from 24 to 33 cm is highly altered basalt.

In Sample 120-748B-16H-CC, transitional forms between *Nuttallides truempyi* and *N. umbonifera* as well as specimens of *N. umbonifera* (s.s.) are present. This confirms the range of *N. truempyi* as given by Van Morkhoven et al. (1986), who suggest a worldwide LAD of *N. truempyi* at the top of the Eocene. In the Maud Rise sites of Leg 113, *N. truempyi* was only found in considerably older sediments. This was explained by the rela-

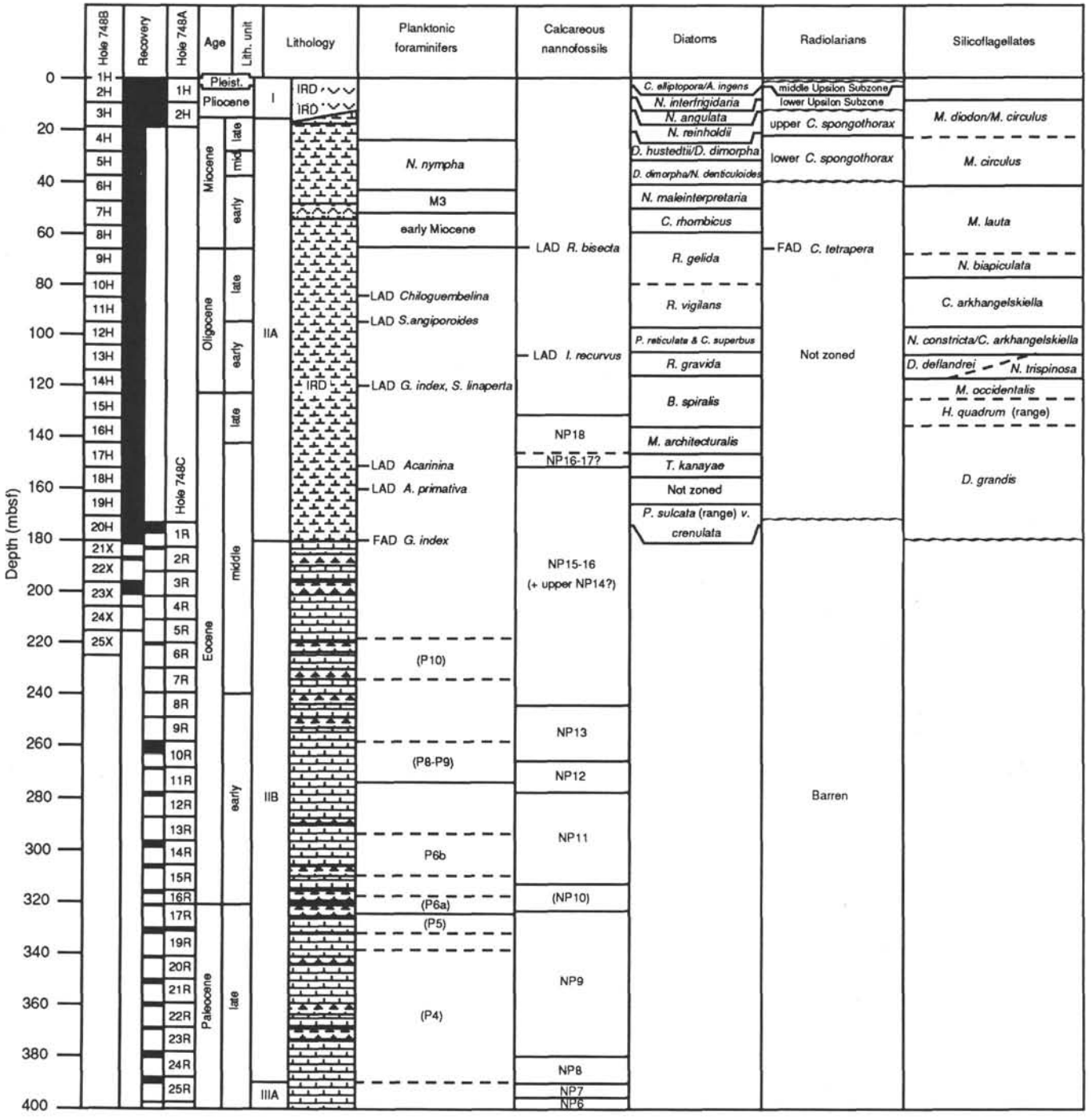

Figure 33. Summary of biostratigraphic age assignments for the Cenozoic sediments recovered at Site 748. Parentheses enclosing zonal assignments indicate zonal equivalents for sediments lacking the primary index taxa for the zone, as described in the text. Lithology, age units, and key to symbols as in Figure 10.

tively shallow paleowater depth (about 2000 m) of Site 689 (Barker, Kennett, et al., 1988).

The LO of *Bulimina alazanensis* occurs in Sample 120-748B-18H-CC. This sample contains *Hanzawaia cushmani, Cibicidoides subspiratus, Uvigerina* sp., *Pullenia eocaenica, Spiroplectammina spectabilis,* and pieces of *Saccorhiza ramosa,* in addition to the previously mentioned components of Assemblage 4a.

Assemblage 4b: Middle Eocene

The upper boundary of Assemblage 4b at this site is defined by the LO of *Bulimina bradburyi.* The fauna is characterized by the common occurrence of *Lenticulina* sp. *Bulimina alazanensis* is the abundant *Bulimina* species, whereas *Bulimina elongata* is only a minor constituent in the uppermost Sample 120-748B-19H-CC. *Bulimina macilenta* and *Plectina elongata* are found

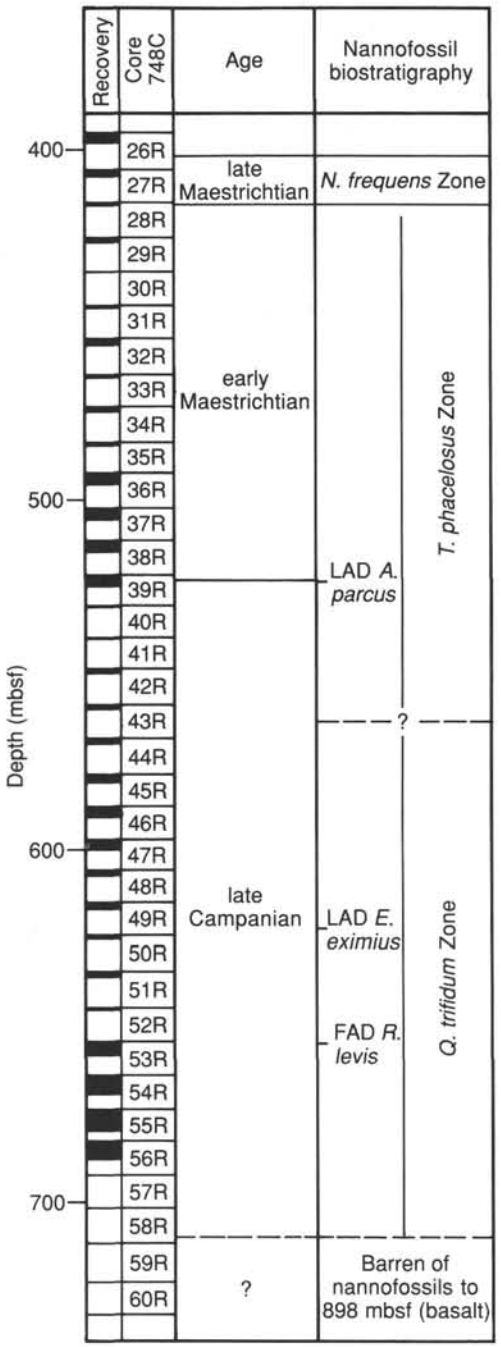

Figure 34. Summary of nannofossil age assignments for the Cretaceous sediments recovered from Hole 748C.

exclusively in this assemblage. *Anomalinoides capitatus, A. semicribatus, Vulvulina spinosa, Pullenia eocaenica, P. bulloides, Globocassidulina subglobosa, Cibicidoides eocaena* and *Cibicidoides* spp., *Uvigerina* spp., *Gyroidina* spp., *Hanzawaia cushmani, Oridorsalis umbonatus, Anomalina spissiformis, Stilostomella* spp., *Pleurostomella* spp., *Nodosaria* sp., *Spiroplectammina spectabilis, Karreriella subglabra,* and *Textularia* spp. are accessory components of this middle Eocene benthic foraminifer assemblage. This benthic fauna is found in the recovered sediment from Samples 120-748B-19H-CC through 120-748B-24H-CC and 120-748C-6R-CC.

In the middle Eocene of the Atlantic Ocean, a very similar *Lenticulina* fauna is indicative of bathyal water depths between 1000 and 2000 m (Tjalsma and Lohmann, 1983).

Assemblage 4c: Early Eocene

The main constituents of the middle Eocene benthic fauna (Samples 120-748C-10R-CC through 120-748C-12R-CC and 120-748C-14R-CC) remain the same in the early Eocene, but *Bulimina alazanensis* and *B. macilenta* are not found. Their early Eocene predecessor is *B. trinitatensis.* Consequently, the LO of *B. trinitatensis* was chosen as the upper boundary for this assemblage. The lower boundary is defined by the FO of *Anomalinoides capitatus,* which agrees well with the FAD of this species at the Paleocene/Eocene boundary in the Atlantic (Tjalsma and Lohmann, 1983).

Lenticulina sp., *Bulimina bradburyi, Oridorsalis umbonatus, Nuttallides truempyi,* and *Anomalinoides capitatus* are common constituents of this fauna in addition to the abundant *Stilostomella* spp. Less common are *Hanzawaia cushmani, Vulvulina spinosa, Aragonia aragonensis, Abyssamina quadrata,* and *A. poagi* (very rare), *Pullenia eocaenica, Lagena apiopleura, Cibicidoides eocaena,* and *Nonion havanensis.* A few *Tappanina selmensis* occur in the basal Eocene (Zone P6, Sample 120-748C-14R-CC).

Assemblage 5a: Late Paleocene–Earliest Eocene

This assemblage comprises samples examined from Section 120-748C-16R-CC through 120-748C-26R-CC. They are dated by means of planktonic foraminifers and calcareous nannofossils as earliest Eocene to late Paleocene. Only samples from Cores 120-748C-19R to -26R yielded well-preserved benthic foraminifer faunas for quantitative treatment. The upper part of this sequence (through Sample 120-748C-24R-CC) is grouped into Assemblage 5a. The upper boundary is chosen above the FO of *Stensioina beccariiformis* and the lower boundary is below the FO of *Bulimina trinitatensis.*

This fauna is composed of *Bulimina bradburyi, B. thanetensis, Tappanina selmensis, Stensioina beccariiformis, Aragonia* sp., *Stilostomella* spp., *Turrilina brevispira, Anomalina praeacuta, Hanzawaia* sp., *Oridorsalis umbonatus, Pullenia coryelli, Vulvulina spinosa, Bulimina trinitatensis, Lenticulina whitei* and *Lenticulina* spp., *Lagena* spp., *Fissurina* spp., *Alabamina creta,* and *Nodosaria* spp.

Assemblage 5b: Early Late Paleocene

The upper boundary of the lower Paleocene assemblage is chosen above the LO of *Coryphostoma midwayensis* (i.e., above Sample 120-748C-25R-1, 122–124 cm). This assemblage is characterized by a high relative abundance of *Stensioina beccariiformis* and the presence of *Bolivinoides delicatulus. Bulimina navarroensis*? (dominant in Sample 120-748C-26R-CC), *Pullenia coryelli,* and *Tappanina selmensis* are common constituents of the benthic foraminifer fauna. Accessory species are *Aragonia* spp., *Lenticulina* spp., *Vulvulina spinosa, Alabamina creta, Turrilina brevispira, Anomalina praeacuta,* and *Spiroplectammina subhaeringensis.*

In contrast to the early Paleocene fauna at Site 747, *Nuttallides truempyi* is found only rarely at this site. This species is reported abundant only from lower bathyal and abyssal water depth, whereas *Cibicidoides midwayensis* is known as an inhabitant of neritic to upper bathyal paleoenvironments.

In summary, the Cenozoic benthic foraminifer succession from Site 748 can be divided into nine distinct assemblages based on taxonomic composition and the ranges of selected taxa. The compositions of these assemblages indicate that the water depth of the site has remained similar to that of the

present day (lower bathyal) throughout the Cenozoic. It is suggested that the site may have had bottom waters corrosive to $CaCO_3$ during the late Eocene to early Miocene.

Calcareous Nannofossils

We recovered 400 m of Pleistocene through upper Paleocene sediments consisting primarily of nannofossil ooze at Site 748. Recovery was excellent in the upper part of the section (Cores 120-748B-1H through -20H, 0–180 mbsf) but decreased considerably below as chert was encountered in the middle Eocene. Recovery was often limited to a few chert fragments between Cores 120-748B-21X and 120-748C-26R. Scraping of the nannofossil ooze encrusted on the cherts allowed biostratigraphic control down to the base of the Cenozoic section (Core 120-748C-26R, 407 mbsf).

Calcareous nannofossils were abundant at all levels except in the upper 9 m of the section (Core 120-748B-1H), and their preservation was generally excellent. Neogene calcareous nannofossil assemblages are of very low diversity, but their diversity increases steadily downward, reaching a maximum in lower Eocene and upper Paleocene sediments. It is noteworthy that a 3° latitudinal move southward between Sites 747 and 748 resulted in the loss of some of the temperate (and even "tropical") species encountered at Site 747. This is particularly true for the Neogene, but it applies as well to the Paleogene.

Major differences are evident in the composition of correlative assemblages from Sites 747 and 748. For example, the lower Eocene assemblages at Site 747 consist mostly of various species of *Toweius*, whereas at Site 748 they consist mainly of different species of *Chiasmolithus*. Onshore quantitative study of the geographic distribution of some "biogeographic markers" will be of prime importance for paleobiogeographic reconstructions.

The biostratigraphic subdivisions presented below result from an analysis of core-catcher samples and, when necessary, from toothpick samples taken in cores.

Neogene

Calcareous nannofossil assemblages are of extremely low diversity in Neogene sediments recovered at Site 748 and do not provide any biostratigraphic control. Reworking of late Eocene to early Oligocene taxa (e.g., *Reticulofenestra umbilica, R. hillae, R. abisecta, Chiasmolithus altus, C. oamaruensis,* and *Zyrghablithus bijugatus*) into the lower middle and lower Miocene (see radiolarian and diatom stratigraphies) is common in Cores 120-748B-6H through -8H.

Paleogene

The Oligocene/Miocene boundary, as indicated by the LO of *Reticulofenestra bisecta,* is placed between Samples 120-748B-8H-CC and 120-748B-9H-CC (between 66.6 and 76.1 mbsf). Biostratigraphic subdivision of Oligocene sediments is difficult at Site 748 because of the absence of upper Oligocene biozonal markers and reworking of early Oligocene species up to the Oligocene/Miocene boundary (as defined by planktonic foraminifer biostratigraphy) and into the Miocene.

The LO of *Isthmolithus recurvus* in Core 120-748B-13H is used to characterize lower Oligocene sediments until onshore studies allow a definitive placement of the lower/upper Oligocene contact. According to planktonic foraminifer biostratigraphy, the Eocene/Oligocene boundary occurs between Cores 120-748B-14H and -15H (at about 123.6 mbsf). Because of the scarcity of discoasters in lower Oligocene–upper Eocene assemblages recovered at this site, biostratigraphic subdivision of the lower Oligocene–upper upper Eocene interval will be established more precisely onshore.

It is uncertain at this time whether the sedimentary section is continuous from the upper through middle Eocene. The interval between Samples 120-748B-15H-CC and 120-748B-16H-CC is assigned to the lower upper Eocene Zone NP18. The LO of *Chiasmolithus solitus,* which defines the top of Zone NP16, is observed in Sample 120-748B-17H-CC. Nannofossil Zone NP17 may be represented within Core 120-748C-17H, although onshore studies will be necessary to verify its presence.

The interval between Samples 120-748B-17H-CC and 120-748C-7R-CC is of middle Eocene age and corresponds to Zones NP16, NP15, and possibly Zone NP14 (upper part). The common occurrence of species of *Nannotetrina* in Sample 120-748B-23-CC probably indicates Zone NP15. It appears that a subdivision of the middle Eocene interval can be established based on the occurrence of *Reticulofenestra hillae, R. umbilica,* and *R. samodurovii.* However, the validity of this subdivision needs to be checked by comparison with planktonic foraminifer biostratigraphy and magnetostratigraphy from other sites. It is unfortunate that poor recovery through the middle Eocene may well jeopardize good biostratigraphic resolution.

The interval between Samples 120-748C-8R-CC and 120-748C-26R-CC represents an apparently continuous section from the lower Eocene through lower upper Paleocene. Biostratigraphic subdivision is straightforward because all zonal index species are present except *Tribrachiatus contortus* and *Tribrachiatus bramlettei.* Despite the absence of these taxa, it is possible to designate the interval equivalent to NP10 based on the ranges of other fossils and the stratigraphic position of the samples. The biostratigraphic sequence within this interval is as follows:

Zone NP13 = from Samples 120-748C-8R-CC to 120-748C-10R-CC;
Zone NP12 = in Sample 120-748C-11R-CC;
Zone NP11 = from Samples 120-748C-12R-CC to 120-748C-15R-CC;
Zone NP10 (equivalent) = in Sample 120-748C-16R-CC;
Zone NP9 = from Samples 120-748C-17R-CC to 120-748C-23R-CC;
Zone NP8 = in Sample 120-748C-24R-CC;
Zone NP7 = in Sample 120-748C-25R-CC; and
Zone NP6 = in Sample 120-748C-26R-CC.

The Paleocene/Eocene boundary occurs within Core 120-748C-17R.

In summary, calcareous nannofossil biostratigraphy indicates the following at Site 748:

1. An apparently continuous section was recovered from the upper Oligocene through lower upper Paleocene.
2. An unconformity is present between lower upper Paleocene sediments and underlying Cretaceous (Maestrichtian) deposits. This unconformity represents a hiatus with a minimum duration of 6 m.y.
3. Cherts are developed throughout the middle and lower Eocene, and also possibly in the upper Paleocene.

Like Site 747, Site 748 is of critical importance for calcareous nannofossil biostratigraphic and paleobiogeographic studies. It provides complementary data to those obtained at Site 747. For instance, the magnetobiostratigraphic correlations that are drawn for the Neogene section at Site 747 can be extended through the Oligocene section recovered at Site 748. Despite poor recovery, it is clear from the glimpses given by drilling at Site 748 that the Paleogene sections of the South Kerguelen Plateau are of great potential for biostratigraphic and paleobiogeographic studies.

Radiolarians

Sediments from Site 748 yielded moderately well-preserved radiolarians from the middle Eocene to the Holocene. Below

middle Eocene Sample 120-748B-19H-CC, radiolarians are absent in the underlying Cenozoic sediment. The Cenozoic assemblages are very similar to those seen at Site 747, but they differ in being somewhat better preserved in the Paleogene at Site 748 than at Site 747. The Paleogene sequence from Site 748 will be particularly useful for developing and calibrating Paleogene radiolarian zonations. By contrast, hiatuses have removed some of the Neogene record at Site 748, reducing the usefulness of this site for Neogene radiolarian studies.

All Neogene assemblages recovered are of an Antarctic aspect, suggesting that Site 748, like Site 747, has been south of the Antarctic Convergence throughout the Neogene. Although Paleogene assemblages also appear to be dominated by endemic high-latitude forms, too little is known about Paleogene radiolarian biogeography to draw any conclusions about Paleogene water-mass distributions.

Hole 748A

Only two cores were recovered from this hole. Radiolarians are abundant and well preserved in the samples examined and are typical of Antarctic assemblages. Sample 120-748A-1H-3, 45–47 cm (Psi? Zone), contains abundant to common *Cycladophora davisiana* and *Antarctissa cylindrica* and rare to few reworked lower Pliocene and upper Miocene specimens. Sample 120-748A-1H-CC is in the lower Upsilon Subzone (middle Pliocene), while Samples 120-748A-2H-5, 45–47 cm, and 120-748A-2H-CC are both late Miocene in age (upper *Cycladophora spongothorax* Subzone).

Hole 748B

Neogene. Sample 120-748B-1H-CC contains *Cycladophora davisiana,* but not *Cycladophora pliocenica,* and is thus <1.9 Ma in age. No specimens of other upper Pliocene–Holocene stratigraphic indicators were seen (i.e., *Stylatractus universus, Phormostichoartus pitomorphus,* or *Pterocanium charybdeum trilobum*); thus, a precise zonal assignment is not possible. A sample taken from the base of Section 120-748B-2H-3 (i.e., 120-748B-2H-3, "Bottom") is assigned to the middle Upsilon Subzone, while 120-748B-2H-CC is within the lower Upsilon Subzone.

A sample from the top of Section 120-748B-2H-3 (i.e., 120-748B-2H-3, "Top") shows evidence of strong reworking and contains a mixture of middle Pliocene, lower Pliocene, and upper Miocene radiolarians, including *Desmospyris spongiosa, C. pliocenica, Antarctissa denticulata, Antarctissa cylindrica, Lychnocanium grande, Prunopyle titan, Prunopyle hayesi, Antarctissa deflandrei,* and *Cycladophora spongothorax.* Diatom stratigraphy (see discussion of diatoms below) indicates the presence of an unconformity at this level.

Sample 120-748B-3H-1, 45–47 cm, is assigned to the upper Tau Subzone. Samples 120-748B-3H-2, 45–47 cm, 120-748B-3H-3, 45–47 cm, 120-748B-3H-CC, and 120-748B-4H-2, 45–47 cm, are assigned to the upper *C. spongothorax* Subzone, while samples from 120-748B-4H-4, 45–47 cm, through 120-748B-5H-CC are within the lower *C. spongothorax* Subzone. The absence of the Tau Zone, the relatively short upper *C. spongothorax* Subzone, and the presence of reworked lower Pliocene and upper Miocene radiolarians in the overlying Pliocene (Sample 120-748B-2H-3, "Top") all suggest the presence of a hiatus in Core 120-748B-3H between the base of the Pliocene sequence (Sample 120-748B-3H-2, 45–47 cm) and the top of the Miocene (Sample 120-748B-3H-3, 45–47 cm).

Sample 120-748B-6H-1, 45–47 cm, cannot be zoned at present, although the radiolarian assemblage indicates that this sample is of early Miocene age. Lower Miocene indicators such as *Cycladophora golli* (both subspecies *C. g. golli* and *C. g. regipileus*) are common, while middle Miocene or younger indicators are absent (*Actinomma golownini, Eucyrtidium punctatum, Thyrsocyrtis clausa,* etc). Thus, the entire remaining part of the middle Miocene, as well as the uppermost part of the lower Miocene, appears to have been removed by a hiatus between Sections 120-748B-5-CC and 120-748B-6H-1, spanning the interval approximately 12–17 Ma.

Although changes are seen within the radiolarian assemblages in Samples 120-748B-6H-4, 45–47 cm, through 120-748B-8H-2, 45–47 cm, no zonal assignments are possible. The base of the range of *Cyrtocapsella tetrapera* occurs between Samples 120-748B-8H-2, 45–47 cm, and 120-748B-8H-4, 45–47 cm, and is taken as marking the base of the Miocene. The age of this datum is given by Nigrini (1985) as approximately 22 Ma. Her age estimate, however, is based on a different time scale (Barron et al., 1985) than the one used for Leg 120 (Berggren et al., 1985a). This datum is estimated to be at approximately 23 Ma, based on the original biostratigraphic data from DSDP Leg 85 radiolarians (Nigrini, 1985), calcareous nannofossils (Pujos, 1985), and planktonic foraminifers (Saito, 1985), and on the correlation of calcareous microfossil zones to the chronologic scale by Berggren et al. (1985a).

Paleogene. Samples 120-748B-8H-4, 45–47 cm, through 120-748B-19H-CC contain common to abundant Paleogene radiolarians, which are usually moderately to well preserved. Miocene species such as *C. tetrapera* and *C. golli* are not observed in this interval. Samples 120-748B-8H-CC through 120-748B-10H-CC contain *Cyrtocapsella*(?) aff. *longithorax, Lychnocanium* sp. (*Lynchnocanella conica* of Petrushevskaya, 1975) and many undescribed forms. Samples 120-748B-11H-CC through 120-748B-13H-CC include *Cyrtocapsella semipolita, Cyclampterium milowi*(?), *Lychnocanoma amphitrite,* and *Eucyrtidium* sp. of Chen (1975). This assemblage is similar to the assemblage described from the lower Oligocene of Site 274 by Chen (1975).

Samples 120-748B-15H-CC through 120-748B-18H-CC contain *C. milowi*(?), *L. amphitrite,* and *Stylacontarium* sp. with robust spines. Sample 120-748B-19H-CC includes *C. milowi*(?), *L. amphitrite, Lophoconus titanothericeraos, Dictyoprora amphora,* and *Lophocyrtis biaurita,* which indicate an Eocene age.

In summary, the Cenozoic radiolarians from Site 748 indicate a discontinuous Neogene section with at least two, and perhaps three, unconformities punctuating the sequence. Although most of the Neogene sequence could easily be placed in existing zonation schemes, two intervals (upper Pliocene to Holocene and lower Miocene) could not be zoned due to the lack of characteristic taxa. Zonation of the Paleogene could not be accomplished during the cruise because of the lack of formally proposed Antarctic zonations for this time interval. All of the Neogene assemblages are of an Antarctic aspect, and the Paleogene assemblages appear to contain many endemic high-latitude forms.

Diatoms

Cenozoic sediments recovered from Site 748 yielded rich lower Oligocene to lower Pleistocene diatom assemblages. Poorly preserved middle and upper Eocene diatoms were recovered from Hole 748B. Most Neogene diatoms from Site 748 are characteristic of Southern Ocean assemblages, and standard biostratigraphic zonal schemes were applied with minor revision in some cases. Diatom biostratigraphic zonal assignments are outlined below and summarized in Figure 33.

Many diatom species that dominate upper Paleogene Southern Ocean diatom assemblages are absent or very poorly represented at Site 748. These include *Pterotheca* spp., *Pyxilla* spp., *Hemiaulus pacificus, H. caracteristicus, Thalassiosira hydra,* and the archaeomonads, *Archaeosphaeridium* spp. Their absence suggests that a major biogeographic barrier, perhaps similar to the modern Polar Front, was present to the south of Site 748 during the Oligocene, and these species were restricted to

waters south of the Polar Front. Gombos and Ciesielski (1983) note a similar biogeographic distinction between DSDP Sites 511 and 513 in the Oligocene South Atlantic Ocean.

Hole 748A

The lower Pleistocene *Coscinodiscus elliptipora/Actinocyclus ingens* Zone occurs at the top of Hole 748A with the highest occurrence of *A. ingens* in Sample 120-748A-1H, 0–1 cm. The base of this zone was not recognized because of the absence of *Rhizosolenia barboi.* The highest occurrence of *Coscinodiscus kolbei* in Sample 120-748A-1H-1, 90–91 cm, defines the top of the *C. kolbei/Rhizosolenia barboi* Zone. The base of this zone is most likely bounded by an unconformity that removed the upper Pliocene *Coscinodiscus vulnificus, Cosmiodiscus insignis, Nitzschia weaveri,* and *N. interfrigidaria/C. vulnificus* Zones. This unconformity represents approximately 1 m.y. from 2.2 to 3.1 Ma and is identified by the highest occurrences of *C. vulnificus, C. insignis,* and *N. interfrigidaria* and the lowest occurrence of *N. kerguelensis* in Sample 120-748A-1H-3, 90–91 cm.

Below this unconformity, the *N. interfrigidaria* Zone is identified in Samples 120-748A-1H-4, 90–91 cm, and 120-748A-1H-CC by the presence of *N. interfrigidaria* in the absence of *C. vulnificus* and *N. weaveri.* The lower Pliocene *N. "angulata"* Zone is identified below the lowest occurrence of *N. interfrigidaria* in Sample 120-748A-1H-CC down to the lowest *N. "angulata,"* which occurs in Sample 120-748A-2H-2, 90–91 cm. The highest *Denticulopsis hustedtii* in Sample 120-748A-2H-3, 0–1 cm, marks the boundary between the *N. reinholdii* Zone and the underlying *D. hustedtii* Zone.

The bottom of Hole 748A ends in the upper Miocene *D. hustedtii/D. dimorpha* Zone, the top of which is placed within the interval between Samples 120-748A-2H-5, 0–1 cm, and 120-748A-2H-CC, as indicated by the highest occurrence of *D. dimorpha.* Note that zonal boundaries identified on Figure 33 are for Hole 748B, not 748A.

Hole 748B

Diatom biostratigraphy in the upper three cores of Hole 748B largely duplicates the above stratigraphic division of Hole 748A. The upper Pliocene unconformity occurs between Samples 120-748B-2H-2, 83–84 cm, and 120-748B-2H-3, 12–13 cm, and appears to represent a slightly greater amount of time than in Hole 748A. This is indicated by the fact that the highest occurrence of *Coscinodiscus kolbei* occurs at the unconformity in Hole 748B rather than above (as in Hole 748A), suggesting that the interval from approximately 1.9 to 3.1 Ma is missing.

The following datums are noted within the top three cores of Hole 748B; zonal assignments based on these datums are presented in Figure 33:

1. Highest *A. ingens* at the top of Hole 748B defines a position within the *Coscinodiscus elliptipora–Actinocyclus ingens* Zone;
2. Highest *C. kolbei, C. vulnificus, C. insignis, Thalassiosira torokina,* and *N. interfrigidaria* between Samples 120-748B-2H-2, 83–84 cm, and 120-748B-2H-3, 12–13 cm;
3. Lowest *N. kerguelensis* and highest *N. praeinterfrigidaria* between Samples 120-748B-2H-3, 149–150 cm, and 120-748B-2H-4, 83–84 cm;
4. Lowest *Thalassiosira lentiginosa* between Samples 120-748B-2H-4, 83–84 cm, and 120-748B-2H-6, 81–82 cm;
5. Highest *T. umbonatus* and lowest *N. interfrigidaria* between Samples 120-748B-2H-6, 81–82 cm, and 120-748B-2H-CC;
6. Lowest *N. "angulata"* between Samples 120-748B-2H-CC and 120-748B-3H-1, 40–41 cm;
7. Highest *D. hustedtii* and lowest *N. praeinterfrigidaria* and *T. umbonatus* between Samples 120-748B-3H-1, 129–130 cm, and 120-748B-3H-1, 140–141 cm; and
8. Highest consistent *D. dimorpha* between Samples 120-748B-3H-4, 0–1 cm, and 120-748B-3H-CC.

Diatom biostratigraphic datums within Core 120-748B-3H are deemed unreliable at this time because of the high degree of bioturbation noted in this core (see "Lithostratigraphy and Sedimentology" section, this chapter, and the core descriptions for Site 748 at the end of this book), which resulted in a mixing of upper Miocene and lower Pliocene diatoms and silicoflagellates throughout. This highly bioturbated interval disrupts what appears to be a conformable Miocene/Pliocene transition. Future detailed sampling will resolve the nature of this boundary and the true age of Core 120-748B-3H.

The top of the *Denticulopsis dimorpha–Nitzschia denticuloides* Zone occurs between Samples 120-748B-4H-CC and 120-748B-5H-6, 100–101 cm, and is identified by the highest occurrence of *Nitzschia denticuloides* in the presence of *D. dimorpha.* An unconformity representing the lower portion of the *D. dimorpha–N. denticuloides* Zone down to the upper portion of the *Nitzschia maleinterpretaria* Zone is identified between Samples 120-748B-5H-CC and 120-748B-6H-2, 40–41 cm. The time interval from approximately 12 to 16 Ma is represented by this unconformity.

The base of the underlying lower Miocene *Nitzschia maleinterpretaria* Zone and the top of the *Coscinodiscus rhombicus* Zone is identified in Sample 120-748B-6H-CC by the highest occurrence of *C. rhombicus. Azpetia oligocenicus* v. *nodus* and *Asteromphalus oligocenicus* dominate the *C. rhombicus* Zone of Sample 120-748B-6H-CC, where the highest occurrence of *Rocella gelida, Hemiaulus rectus* v. *twista, Thalassiosira fraga, Stictodiscus* sp. Gombos and Ciesielski, and *Asteromphalus symmetricus* are noted. The boundary between the *C. rhombicus* and *R. gelida* Zones was not recognized because of the apparent absence of *Rossiella symmetrica* from Site 748. The highest *Synedra jouseana* and *Hemiaulus incisus* and the lowest *Thalassiosira fraga* and *Nitzschia maleinterpretaria* occur in Sample 120-748B-7H-CC.

Sample 120-748B-8H-CC contains the only occurrence of *Bogorovia veniamini* and the lowest occurrence of *Rocella schraderi.* This sample lies within the acme horizon of *Rocella gelida,* indicating a level just below the Oligocene/Miocene contact. This acme and that of *R. vigilans* in Sample 120-748B-9H-CC led to an increase in the siliceous biogenic sediment component in the upper Oligocene. Sample 120-748B-9H-CC contains the lowest *C. rhombicus,* the highest *Rocella vigilans* (within an acme of this species), and the only occurrence of *Lisitzinia ornata. Actinocyclus ehrenbergii* v. *tenella* first appears as a common element in the upper Oligocene in Sample 120-748B-10H-CC.

The base of the *Rocella gelida* Zone is placed somewhere in Core 120-748B-10H. The base of the *Rocella vigilans* Zone occurs within Core 120-748B-12H, as indicated by the lowest occurrence of *R. vigilans* and *Synedra jouseana* in Sample 120-748B-11H-CC. A hiatus is tentatively suggested between Samples 120-748B-11H-CC and 120-748B-12H-CC by the highest occurrence of numerous lower Oligocene diatom taxa including *Asterolampra schmidtii, A. punctifera, Cestodiscus antarcticus, Coscinodiscus hajosae, C. superbus,* and *Pyxilla reticulata* in Sample 120-748B-12H-CC.

The highest occurrence of *Rhizosolenia gravida* in Sample 120-478B-13H-CC identifies the top of the *R. gravida* Zone. The top of the *Brightwellia spiralis* Zone is approximated within Core 120-748B-13H-CC based on the highest occurrence of *B.*

spiralis, Triceratium macroporum (concave) sensu Gombos and Ciesielski, *Asterolampra gradiata,* and *Coscinodiscus mutabilis* in this sample. The lowest *Asteromphalus oligocenicus,* the marker datum for the top of the *B. spiralis* Zone, occurs only down to Sample 120-748B-12H-CC.

The top of the *Melosira architecturalis* Zone is noted in Sample 120-748B-15H-CC by the highest occurrence of *M. architecturalis* and *Skeletonema barbadiense. Triceratium pulvinar* (*T. unguicuilatum* of Gombos and Ciesielski), and *Triceratium inconspicuum* v. *trilobum* first occur in Sample 120-748B-16H-CC. The range of the latter species approximates the middle Eocene *Triceratium kanayae* Zone. The interval including Cores 120-748B-17H and -18H contains poorly preserved diatom assemblages in low abundance. *Brightwellia corona* and *Paralia sulcata* v. *crenulata* occur in Samples 120-748B-19H-CC and 120-748B-20H-CC and suggest a middle Eocene age at this level.

Numerous fragments of chert from the above two samples contain well-preserved and abundant diatom assemblages within the siliceous chert matrix. These occurrences lead to two observations: (1) a study of these middle Eocene diatom assemblages through thin sections of selected chert samples is feasible; and (2) increased diatom productivity, indicated by the rich assemblages identified in the chert fragments, may have played a role in the deposition of siliceous horizons associated with lower Eocene cherts.

In summary, diatoms are abundant and well preserved from the upper Oligocene through Pleistocene, allowing recognition of standard Southern Ocean zones throughout. Abundance and preservation deteriorates in the middle Eocene through lower Oligocene, although assemblage quality is still good enough to permit standard zonal recognition. At least two, and perhaps three, disconformities were identified by diatom biostratigraphy (Table 6).

Silicoflagellates, Ebridians, and Endoskeletal Dinoflagellates

Silicoflagellates are well represented in the Pliocene to middle Eocene sediments of Hole 748B by diverse assemblages, including 3 taxa in the Pliocene, 18 taxa each in the Miocene and Oligocene, and 15 taxa in the Eocene. Ebridians are less well represented with 6 species in the Pliocene to Eocene sequence. Two species of endoskeletal dinoflagellates, *Actiniscus pentasterias* and *Carduifolia gracilis,* are noted from the Pliocene to upper Oligocene and upper Oligocene to upper Eocene intervals, respectively. *Macrora stella,* of unknown affinity, was noted in Sample 120-748B-12H-CC. This report is based on the study of core-catcher samples and several additional samples chosen to shorten sample spacing in key intervals.

Table 6. Unconformities identified by shipboard paleontology.

Position	Depth (mbsf)	Hiatus (m.y.)	Age (Ma)	Fossil group(s)
120-748A-1H-3	3.0–4.5	0.9	2.2–3.1	Diatoms
120-748B-2H-2 to 120-748B-2H-3	3.1–4.6	2.0	1.2–3.2	Diatoms, radiolarians
120-748B-3H-1 to 120-748B-3H-2	10.05–11.55	4.0	~4.3–~8.5	Radiolarians
120-748B-6H-1 to 120-748B-6H-2	39.0–40.0	5.0	12–17	Planktonic foraminifers, diatoms, radiolarians
120-748B-11H to 120-748B-12H	95.0–104.0	Minimal	middle Oligocene	Diatoms
120-748B-15H	Uncertain	Uncertain	late Eocene	Calcareous nannofossils
120-748C-26R to 120-748C-27R	407.0–408.0	6.0	61–67	Calcareous nannofossils
120-748C-CC	416.0–418.0	2.0	67–69	Calcareous nannofossils

Note: Estimations for age and hiatus are based on available biogeochronologic calibrations (see "Explanatory Notes," this volume).

Silicoflagellates

Silicoflagellate biostratigraphy for Hole 748B uses the zonal scheme of Shaw and Ciesielski (1983) for Pliocene through middle Eocene sediments. The silicoflagellate biostratigraphic division of Hole 748B is outlined below, with the approximate position of zonal boundaries presented in Figure 33.

Pliocene and uppermost Miocene intervals are dominated by the silicoflagellate *Distephanus speculum* with minor *D. quinquangellus* in all samples from Samples 120-748B-1H, 2–3 cm, to 120-748B-3H, 0–1 cm. In Sample 120-748B-2H-6, 81–82 cm, *Dictyocha* spp. first appears, with abundances roughly two times that of *Distephanus* spp. Samples 120-748B-2H-4, 83–84 cm, and 120-748B-3H-1, 40–41 cm (above and below the *Dictyocha*-rich sample), contain only *Distephanus.* The increase in *Dictyocha* suggests an early Pliocene warming of surface waters over Site 748 by approximately 7°C, based on the *Dictyocha/Distephanus* ratio temperature calibration of Ciesielski and Weaver (1974). These workers also noted an early Pliocene warming in the Southern Ocean.

A similar warming is indicated for the middle late Miocene by near-equal numbers of *Dictyocha* and *Distephanus* in Sample 120-748B-3H-CC. Samples 120-748B-3H-4, 0–1 cm, and 120-748B-4H-1, 43–44 cm, are dominated by *Distephanus,* indicating the stratigraphic extent of these warm-water events. In the present ocean, *Dictyocha* spp. is not found south of the Polar Front (Pichon et al., 1987), suggesting that the Polar Front may have migrated south of Site 748 when sediments of Samples 120-748B-2H-6, 81–82 cm, and 120-748B-3H-CC were deposited during the early Pliocene and late Miocene, respectively.

Silicoflagellates *Mesocena diodon* and *M. circulus* are noted in Sample 120-748B-3H-1, 129–130 cm, suggesting the upper Miocene *M. diodon/M. circulus* Zone as applied by Shaw and Ciesielski (1983). However, because Core 120-748B-3H is highly bioturbated and numerous upper Miocene diatoms and radiolarians occur with lower Pliocene diatom assemblages in this core, the co-occurrence of *Mesocena diodon* and *M. circulus* may be a result of this mixing and not a natural occurrence.

Silicoflagellates are absent from Sample 120-748B-4H-CC and are poorly represented in Sample 120-748B-5H-CC by rare specimens of upper Miocene *Distephanus speculum* v. *giganteus, Paradictyocha apiculata,* and *Mesocena circulus.* The presence of *M. circulus* in the absence of *M. diodon* in Sample 120-748B-5H-CC indicates the middle to upper Miocene *M. circulus* Zone as applied by Shaw and Ciesielski (1983).

Diverse silicoflagellate assemblages first appear in lower Miocene Sample 120-748B-6H-CC, with nine taxa represented; *Mesocena apiculata, Corbisema apiculata,* and *Distephanus speculum* dominate this sample. Other species include *Corbisema hastata globulata, Distephanus crux, D. boliviensis* v. *hemisphaericus, Mesocena oamaruensis, M. pappii,* and *Naviculopsis lata.* Sample 120-748B-7H-CC contains the above assemblage and the highest occurrence of *Mesocena apiculata curvata* and *Naviculopsis trispinosa; D. boliviensis hemisphaericus, D. crux,* and *D. speculum* dominate. Diversity decreases and preservation is poor in Sample 120-748B-8H-CC, where *D. quinquangellus* dominates and the highest *Naviculopsis biapiculata* is noted. This latter datum marks the top of the *N. biapiculata* Zone in the lowest Miocene.

The occurrence of *Corbisema archangelskiana* in Sample 120-748B-10H-CC identifies the top of the upper Oligocene *C.*

archangelskiana Zone; the highest occurrence of *Dictyocha pentagona* and *Mesocena apiculata glabra* are noted in this sample.

The highest occurrences of *Dictyocha deflandrei* and *Mesocena occidentalis* in Sample 120-748B-12H-CC indicate a position within the lower Oligocene *Naviculopsis constricta/Corbisema archangelskiana* Interval Zone, as noted by Shaw and Ciesielski (1983) in DSDP Hole 513A. The base of this zone is noted in Sample 120-748B-13H-CC by the highest occurrence of *N. constricta,* which also defines the top of the underlying *N. constricta/D. deflandrei* Zone. The base of this zone could not be recognized due to the inconsistent occurrence of *D. deflandrei* throughout this hole. The base of the underlying *Naviculopsis trispinosa* Zone, however, was noted in Sample 120-748B-13H-CC by the lowest common occurrence of *N. trispinosa.*

The presence of *Hannaites quadria* in Sample 120-748B-15H-CC suggests the presence of upper Eocene sediments at this level. Silicoflagellates are poorly represented in Cores 120-748B-16H through -18H due to poor preservation, but the robust silicoflagellate *Dictyocha grandis* is noted as identifiable fragments in Samples 120-748B-17H-CC and 120-748B-18H-CC, identifying the middle Eocene *Dictyocha grandis* Zone. Samples 120-748B-19H-CC and 120-748B-20H-CC contain rich assemblages of silicoflagellates, including the following elements of the *D. grandis* Zone: *Dictyocha fibula, Mesocena oamaruensis, Naviculopsis biapiculata, N. constricta,* and *Mesocena apiculata,* the presence of which suggests a level within the *M. apiculata* Subzone of the *D. grandis* Zone. Silicoflagellates are absent below Core 120-748B-20-CC.

Ebridians

Ebridians are present throughout the upper Miocene to middle Eocene of Hole 748B from Samples 120-748B-3H-CC to 120-748B-20H-CC, except for the interval of poor siliceous microfossil preservation within Cores 120-748B-16H to -18H. The following ebridians are listed in descending order of highest occurrence:

1. *Ammodochium rectangulare,* which occurs sporadically from the upper Miocene to middle Eocene in Samples 120-748B-3H-CC to 120-748B-15H-CC;
2. *Pseudammodochium sphericum,* which occurs sporadically in the middle Miocene to middle Eocene in Samples 120-748B-7H-CC to 120-748B-20H-CC;
3. *Hovasserbia brevispinosa,* which occurs consistently from the upper Oligocene to upper Eocene in Samples 120-748B-10H-CC to 120-748B-15H-CC;
4. *Ebriopsis crenulata* (frequently with lorica stage attached), which occurs consistently, and *Ammodochium ampulla,* which occurs sporadically from the lower Oligocene to middle Eocene in Samples 120-748B-13H-CC to 120-748B-20H-CC; and
5. *Micromarsupium anceps,* which occurs in the upper to middle Eocene in Samples 120-748B-15H-CC to 120-748B-20H-CC.

Cretaceous

Foraminifers

The quality and composition of the foraminifer assemblages recovered from the Cretaceous section at Site 748 were disappointing in comparison with those from Site 747, especially as Site 748 was to be a Cretaceous hole with a thick section including the K1, K2, and K3 seismic sequences (see "Site Geophysics" section, this chapter). Our goals for this site were to recover the oldest sediments on the Southern Kerguelen Plateau and to date the onset of sedimentation following the formation of the plateau. As it happens, much of the recovered section is barren of foraminiferal faunas, particularly the entire interval below Sample 120-748C-60R-CC (727.5 mbsf).

The faunas recovered are dominantly of benthic forms similar in species composition and faunal structure to those from western Australia documented by Belford (1960). Only one good planktonic fauna (Sample 120-748C-27R-1, 90–92 cm) was encountered. The faunas below this core are neither as diverse nor as well preserved and appear to have accumulated in a much shallower regime. Planktonic faunas do exist in sediments below this core, but they are of very small species and their study will be an important component of onshore research. Biostratigraphic results from the Cretaceous of Site 748 are summarized in Figure 34.

Planktonic Foraminifers

In Section 120-748C-27R-1, 90–92 cm, planktonic forms make up a considerable proportion (35%) of the fauna in the fraction coarser than 125 μm and include larger species such as *Rugoglobigerina rugosa* (Plummer) as well as the important smaller forms such as *Guembelitria cretacea* Cushman and *Globigerinelloides ultramicrus* (Subbotina). *Bolivinoides* sp. aff. *B. decoratus* (Jones) (sensu Barr, 1970) is present and with the planktonic component suggests an age of early Maestrichtian. Allocation to zones defined in warm-water sections is not possible. This is the only sample in which planktonic species make up a significant portion of the fauna retained on a 125-μm sieve.

Other samples down to Sample 120-748C-31R-CC contain *G. cretacea* sporadically, but that is the oldest sample so far studied to contain a diagnostic planktonic form. The 63- to 125-μm fraction of some samples contains planktonic species, but a detailed study has not been carried out on board ship.

Benthic Foraminifers

Benthic forms occur between Samples 120-748C-27R-1, 90–92 cm, and 120-748C-58R-CC, inclusive. Below that depth all samples studied were barren. Further onshore studies will test this generalization. The fossiliferous section consists of two subintervals:

1. Sample 120-748C-27R-1, 90–92 cm, consists of chalk with abundant foraminifers including a significant planktonic component (see above). The benthic component includes *Bolivinoides* sp. aff. *B. decoratus.* Otherwise, the benthic element is dominated by *Bulimina-Bolivina* (s.l.)-*Gavelinella* plus a minor component of many other species. This would seem to be an outer continental shelf fauna. A greater depth is probably ruled out because of the relatively low planktonic percentage.
2. Samples 120-748C-28R-CC to 120-748C-58R-CC contain benthic foraminifers in significant numbers and diverse enough to allow realistic estimates to be made of the relative proportions of the various species and species groups. In all these samples, foraminifers are a minor part volumetrically of the fossil material, being completely overshadowed by bryozoan, echinoid, and crinoid debris. Preservation is moderate to good, but there are a few samples in which preservation is poor and some that are barren. Cores 120-748C-32R, -33R, -39R to -45R, and -53R were not sampled either because recovery was too low or nonexistent, or because the recovered samples were too indurated to warrant study (silicified in the cases of Cores 120-748C-42R and -43R).

Although the assemblage proportions vary from sample to sample, foraminifer faunas are dominated by *Gyroidina* and *Gavelinella* (several species of each) with minor amounts of other species. The foraminifers (and other biota) in a few samples are physically abraded, attesting to vigorous water move-

ment. These features and the low diversity and high dominance point to shallow-water deposition for much of this part of the section, probably in inner-continental-shelf depths.

Calcareous Nannofossils

Preliminary investigation indicates that Cretaceous nannofossils occur from Cores 120-748C-27R through -58R (407–711 mbsf). Biostratigraphic assignments of sediments within this 26-core interval are based on core-catcher samples unless otherwise noted. The 26-core interval can be subdivided into the three formal zones of Sissingh (1977). In general, calcareous nannofossils make up only a small proportion of the sediment and were concentrated by gravitational settling for study.

Core 120-748C-27R (407–416.4 mbsf) contains nannofossils that indicate the late Maestrichtian *Nephrolithus frequens* Zone, including *Nephrolithus frequens, Nephrolithus corystus, Cribrosphaerella daniae,* and *Arkhangelskiella cymbiformis.* The co-occurrence of *N. frequens* and *N. corystus* indicates the lower portion of the *N. frequens* Zone. The presence of *Nephrolithus corystus* indicates the austral nature of this assemblage. Preservation is variable within the core and seems largely dependent on the degree of cementation. Poorly indurated sediment (such as Sample 120-748C-27R-1, 68–69 cm) contains well-preserved material, whereas well-indurated sediment (such as Sample 120-748C-27R-CC) is essentially barren of nannofossils. This upper Maestrichtian sediment is unconformably separated from the overlying Paleocene and the underlying lower Maestrichtian.

The sequence from Core 120-748C-28R through -58R contains a relatively continuous sequence that spans much of the upper Campanian through lower Maestrichtian. One interval from Core 120-748C-40R to -45R (530.5–587.5 mbsf) is apparently barren of all planktonic microfossils. Preservation varies from moderate to good throughout the sequence (where nannofossils are present). This sequence is divisible into the two formal zones of Sissingh (1977). In addition, five informal intervals can be recognized based on taxon ranges.

The sequence from Core 120-748C-28R through -39R (416.5–530.5 mbsf) contains nannofossil assemblages of the *Tranolithus phacelosus* Zone of late Campanian through early Maestrichtian age. The persistent presence of *Monomarginatus quaternarius* indicates the austral nature of these assemblages. The presence of *Aspidolithus parcus* in Sample 120-748C-39R-CC and its absence in the overlying sequence (Cores 120-748C-28R through -37R) indicates that the Campanian/Maestrichtian boundary lies somewhere between Samples 120-748C-37R-CC and 120-748C-39R-CC. Poor preservation in Core 120-748C-38R prevents more exact placement of the boundary. Further shore-based sampling may refine biostratigraphic relationships in this interval.

The boundary between the overlying *T. phacelosus* Zone and the underlying *Quadrum trifidum* Zone, marked by the LO of *Reinhardtites anthophorus,* probably occurs within the interval from Cores 120-748C-40R through -45R (530.5–587.5 mbsf). Unfortunately, this stratigraphic interval consists of glauconitic, bryozoan grainstones and packstones that are apparently barren of *in-situ* age-diagnostic nannofossils. *Reinhardtites anthophorus* does occur in the first nannofossil-bearing sediment below these grainstones (Sample 120-748C-46R-CC; 597 mbsf). This sample contains *A. parcus, R. anthophorus,* and *Reinhardtites levis,* whose concurrent range defines a short zone in the late (but not latest) Campanian.

Both species of *Reinhardtites* are present downhole through Sample 120-748C-52R-CC (654 mbsf), where *R. levis* has its FAD. *Eiffellithus eximius* has its LO in Sample 120-748C-49R-CC (625.5 mbsf). The LAD of *E. eximius* has been used as a proxy indicator for the top of the *Q. trifidum* Zone by Perch-Nielsen (1979, 1985). At this site, however, its last appearance occurs at least 30 m below the defining datum for the top of the *Q. trifidum* Zone (LAD of *R. anthophorus*). *Reinhardtites levis* has its first appearance near Sample 120-748C-52R-CC (654 mbsf), indicating a late Campanian age for this horizon. The absence of such temperate-tropical forms as *Quadrum gothicum, Quadrum trifidum,* and *Quadrum sissinghi* indicates the austral nature of these assemblages.

The sequence from Cores 120-748C-53R through -58R (654–711 mbsf) contains sparse nannofossil assemblages similar to those in the overlying sequence, but it lacks *R. levis.* The lack of the *Quadrum* spp. makes it impossible to assign this sequence to the *Q. trifidum* Biozone. Several factors, however, suggest placement of this sequence in the upper Campanian:

1. The lack of any specimens of *Marthasterites furcatus* suggests the interval is above the top of the lower Campanian last appearance of this taxon.
2. With the exception of the lack of *R. levis,* there are no apparent differences between the nannofossil assemblages above and below the FAD of *R. levis.* This argues for a continuity in sedimentation, as it is probable that a detectable change in assemblage composition would be evident across any disconformity with a significant hiatus.
3. There is no abrupt lithologic change associated with this sequence, again arguing for a continuity of sedimentation and, therefore, the lack of a significant hiatus.

The sequence from Cores 120-748C-59R to 120-748C-79R-5, 35 cm, consists of glauconitic siltstone, which is barren of calcareous planktonic fossils.

Diatoms

Siliceous microfossil-bearing horizons are noted in the Campanian of Cores 120-748C-46R through -48R. The interval around Sample 120-748C-47R-CC yielded the best diatom assemblages including *Gladius speciosus, Benetorus* sp., *Hemiaulus asymmetricus, H. polymorphus* v. *morsianus, Triceratium indefinita, Rhizosolenia cretacea, Stellarima morenoensis, Stephanopyxis ornata,* and *Thalassiosiropsis wittianus.*

Radiolarians

Sediments from Hole 748C contain a few sporadic occurrences of poorly preserved Upper Cretaceous radiolarians. Sample 120-748C-27R-1, 89–91 cm, contains *Amphipyndax stocki* and *Dictyomitra* sp. Samples 120-748B-47R-CC through 120-748B-49R-CC and 120-748B-51R-CC contain few to very rare, moderate to poorly preserved radiolarians. Identifiable radiolarians are observed only in Sample 120-748B-47R-CC, which includes *Amphipyndax stocki, Stichomitra asymbatos*?, and *Dictyomitra* sp. Few to abundant ellipsoid-shaped sponge spicules were observed in Samples 120-748C-45R-CC through 120-748C-53R-CC.

Macrofossils

Sample 120-748C-73R-5, 128–131 cm, contains a macrofauna consisting of the serpulid worm *Rotularia* (or perhaps *Serpula* itself) and current-aligned, convex-upward valves of a bivalve, including specimens showing very well the dentition of both valves (Fig. 35). Sample 120-748C-51R, 1–2 cm, contains an irregular echinoid (probably typical of forms producing the spines so prevalent in the surrounding sediment); and Sample 120-748C-54R-CC, a bivalve akin to *Camptonectes.*

In addition to the above macrofossils that are represented by individual, more-or-less complete specimens, there are parts of the section where macrofossil fragments are a significant component of the rock. The most important in this context is the

Figure 35. Serpulid worm tube and accompanying current-oriented, convex-upward molluscan valves in Sample 120-748C-73R-6, 128–131 cm. Arrow indicates stratigraphic top of sample.

large bivalve *Inoceramus* (s.l.). The disaggregated prisms, or clasts made up of clusters of such prisms of this shell, are present in noteworthy proportions from Section 120-748C-29R-CC through Core 120-748C-58R. Between Sections 120-748C-35R-1 and 120-748C-38R-CC, *Inoceramus* is a dominant component of the rock. The species of *Inoceramus* responsible is not known, but it is very similar in rock-forming occurrence as *Inoceramus* is in the Santonian-Campanian of western Australia. All these macrofossils will be documented in the Leg 120 *Scientific Results* volume.

Major portions of the Upper Cretaceous section are composed of bryozoan, echinoid, and crinoid debris. The bryozoans are worthy of detailed study. Ostracods and sponges (especially noteworthy are ovoid and discoid chalcedonic bodies of sponge origin) are present in many Cretaceous samples. Wood (represented by small carbonized fragments) is a consistent component below Section 120-748C-71R-CC. Fragments of bone are present throughout the Cretaceous section, reaching a peak in Core 120-748C-63R where they are a significant rock-forming component.

Palynology

Preliminary palynology studies were conducted at two shore-based laboratories in order to provide age determinations for Subunit IIIB. Toward the base of the unit in Cores 120-748C-77R and -70R, B. Mohr (written comm., 1989) observed trilete spores, bisaccate pollen grains, primitive angiosperm pollen, and dinoflagellate cysts. The dinocysts include common *Cribroperidinium muderongensis* and *Cyclonephelium* sp. in addition to *Odontochitina operculata, Odontochitina circulodinium, Odontochitina deflandrei, Cleistosphaeridium* sp., *Prolixiosphaeridium* sp., *Oligosphaeridium* sp., and *Spiniferites* sp. An age determination for this assemblage is difficult, however, because of the lack of zonal markers.

The presence of the pollen *Clavatipollenites hughesii* suggests an Albian to Cenomanian age, and the absence of advanced (tricolpate) angiosperm pollen may infer a late Albian age. In close agreement, D.P.C. Hos (telex comm., 28 April 1988) assigned Core 120-748C-78R to the dinoflagellate *Palaeohystrichophora infusorioides* Zone, which Helby et al. (1987) place in the Cenomanian. We, therefore, adopt here a late Albian to Cenomanian age for these cores.

Mohr reported common *Cyclonephelium membraniphorum* in Core 120-748C-62R. This dinocyst is common in the lower Cenomanian of the Perth Basin, and is common in the Cenomanian and Turonian of Europe. Hos assigns this core to the *Conosphaeridium striatoconus* Zone, which Helby et al. (1987) place in the Turonian. We adopt an age of Cenomanian to Turonian for this interval.

Mohr (written comm., 1988) also reports that most of the organic matter in Unit IIIB has a thermal alteration index (TAI) of more than 3.0 and seems to be reworked from highly coalified older strata. The remaining particles, including all of the sporomorphs and dinocysts are quite mature with a TAI between 2.6 and 2.8.

Paleontological Summary of Site 748

Drilling at Site 748 yielded a composite sedimentary section of approximately 900 m overlying the youngest basalt encountered. Paleontologic reconnaissance of this material indicates a relatively complex geologic history that spans at least 75 m.y. and includes depositional environments from nearshore shelf to deep marine. Unfortunately, only somewhat less than 80% of this geologic history has been preserved in the sedimentary record. However, the preserved rock record yields abundant evidence of the later Cretaceous and Cenozoic development of this part of the Southern Kerguelen Plateau. This paleontologic evidence, and our preliminary deductions based on that evidence, are summarized in Figures 33 and 34 and below.

Neogene and Quaternary

The record of the late Cenozoic at Site 748 is contained in the sediments of Hole 748A (Cores 120-748A-1H and -2H) and Hole 748B (Cores 120-748B-1H through -8H). The approximate thickness of the upper Cenozoic at this site is 66 m. Core recovery was excellent throughout this sequence.

Pliocene-Pleistocene calcareous microplankton fossil assemblages are generally of low diversity and provide little or no biostratigraphic resolution. Planktonic foraminifer diversity increases in the Miocene, improving their biostratigraphic resolution so that a disconformity separating the lower Miocene from the middle Miocene (in Core 120-748B-6H) can be recognized and its hiatus estimated (Table 6). Calcareous nannofossil assemblages, however, do not improve appreciably in the Miocene. In addition, the nannofossil record is further degraded by common reworking of upper Eocene to lower Oligocene taxa into the lower to lower middle Miocene sediments.

Siliceous microfossils are abundant and diverse throughout most of the upper Cenozoic and provide most of the biostratigraphic control for this interval. The radiolarians are all of an Antarctic aspect. They provide good age control throughout most of the sequence, although some intervals (e.g., upper Pliocene to Pleistocene, lower Miocene) could not be placed into formal zones because of the lack of characteristic taxa. The increased biostratigraphic resolution available with radiolarians allows identification and hiatus estimation of at least two, and possibly three, unconformities within the upper Cenozoic sequence (Table 6). Radiolarian biostratigraphy clearly identifies a disconformity spanning the upper Pliocene and lower Pleistocene within Core 120-748B-2H as well as the Miocene disconformity discussed above. A third disconformity, within Core

120-748B-3H, may exist although it is not recognized by other fossil groups. Additional onshore work will be necessary to verify the presence of this stratigraphic break.

Diatoms yield the greatest biostratigraphic resolution in the upper Cenozoic of Site 748. Diatom assemblages are abundant and diverse throughout the upper Cenozoic. Characteristic Southern Ocean assemblages occur throughout, allowing the use of standard zonations. At least two, and perhaps three, disconformities are recognizable based on diatom biostratigraphy. Both the middle Miocene (Core 120-748B-6H) and upper Pliocene–lower Pleistocene (Core 120-748B-2H) disconformities are evident in the diatom record. In addition, a disconformity of similar stratigraphic position and hiatus to the latter (Table 6) was recognized in Core 120-748A-1H-3, allowing a firm point for correlation of the sections recovered in Holes 748A and 748B.

Silicoflagellate assemblages are diverse throughout most of the upper Cenozoic, although they degrade notably in the lower Miocene. Silicoflagellate biostratigraphy, although lacking the resolution of the diatoms, confirms the results of the other fossil groups. Assemblage compositions suggest two periods of significant warming of the surface waters: during the early Pliocene and during the middle late Miocene.

Benthic foraminifers are divided into four distinctive assemblages based on assemblage compositions and taxon ranges: Pleistocene, Pliocene, upper Miocene, and lower Miocene (continuing downward into the upper Eocene). The Pleistocene assemblage is very similar to those occurring on the eastern continental slope of the present-day Weddell Sea at a deeper water depth. These assemblages may represent high surface-water productivities and/or water-mass boundary conditions. The lower Miocene (to upper Eocene) assemblage may be indicative of early Miocene bottom waters that were corrosive to $CaCO_3$.

Paleogene

The Paleogene record from Site 748 is contained in Cores 120-748B-9H through 120-748C-26R, yielding a composite section with a thickness of approximately 341 m. Sediment recovery was good in the Oligocene and upper Eocene, but it deteriorated significantly in the lower Paleogene when chert was encountered.

Calcareous planktonic fossil assemblages provide most of the biostratigraphic control for the Paleogene, especially in the Paleocene and Eocene (Fig. 33). This increase in resolution is the result of higher assemblage diversities (relative to the Neogene). Planktonic foraminifer assemblages lack many of the tropical-temperate index taxa necessary for precise correlation, although zonal equivalents often can be reliably identified based on other taxon ranges. Planktonic foraminifers are used to determine the top and base of the Oligocene as well as to provide a biostratigraphic framework, albeit of a low resolution, for the Oligocene.

Calcareous nannofossil biostratigraphy for the Oligocene of Site 748 is plagued by the paucity of index taxa and some reworking. Both planktonic foraminifers and calcareous nannofossils identify a short (<20 m) section of upper Eocene. We speculate that the upper Eocene is either largely missing or condensed at this site. Further shore-based work should resolve this problem.

Subdivision of the middle Eocene is difficult because of the lack of tropical-temperate index taxa. Both groups of calcareous planktonic fossils indicate a relatively complete lower upper Paleocene to lower Eocene sequence in Hole 748B (Cores 120-748C-8R through -26R). All nannofossil index taxa, with the exception of *Tribrachiatus bramlettei* and *T. contortus,* are present within the sequence.

Although some planktonic foraminifer index taxa are apparently absent from the assemblages, most zonal equivalents can be recognized by the use of other taxon ranges. The base of the Cenozoic section is dated as early late Paleocene (around 61 Ma).

Siliceous planktonic fossils are generally common through the upper Paleogene but are absent or only sparsely represented in the lower Paleogene. Radiolarians are common to abundant in the middle Eocene through Oligocene, although zonal determinations were not made on board. Diatoms are common and well preserved in the upper Oligocene, but assemblage quality degrades in the lower Oligocene and middle Eocene. Despite this degradation in assemblage quality, biostratigraphic zonation is possible from the Oligocene through the middle Eocene (Fig. 33).

The truncation of several diatom taxon ranges between Cores 120-748B-11H and -12H suggests the presence of a further disconformity within the middle Oligocene. More detailed work is necessary to verify its presence. Silicoflagellates are sporadic in abundance and preservation from the Oligocene through the middle Eocene, although some samples provide assemblages of sufficient quality to allow zonal assignment.

Benthic foraminifers of the Paleogene have been divided into six distinct assemblages based on taxonomic composition and assemblage structure: (early Miocene) Oligocene to late Eocene, late to middle Eocene, middle Eocene, early Eocene, late Paleocene, and early late Paleocene. The early Miocene to late Eocene assemblage may be indicative of bottom waters that were corrosive to $CaCO_3$. The middle Eocene assemblage is similar to an Atlantic *Lenticulina* assemblage indicative of 1000–2000-m paleowater depth.

Cretaceous

Approximately 510 m of Upper Cretaceous glauconitic sediment was recovered from above the basalt flow in Hole 748C. The Cretaceous sequence is separated from the overlying Cenozoic (lower upper Paleocene) by a disconformity with an estimated hiatus of 6 m.y. The paleontology of the Upper Cretaceous sediments indicates a complex history of deposition that differs markedly from the overlying deep marine sediments of the Cenozoic.

Core 120-748C-27R consists of intermittently silicified, glauconitic, bioclastic grainstones and packstones containing planktonic microfossil assemblages of middle Maestrichtian age. The planktonic foraminifer and calcareous nannofossil assemblages are oceanic and austral in character, and the character of the microplanktonic and microbenthic fossil assemblages suggests deposition of the unit in outer shelf depths. This middle Maestrichtian material is separated from the underlying sequence by a disconformity with an estimated hiatus of 2 m.y. (Table 6).

The 482-m sequence between the Maestrichtian disconformity and the top of the basalt flow can be divided paleontologically into two distinct intervals: (1) an upper biounit (Cores 120-748C-28R through -58R, 416–711 mbsf) that contains calcareous planktonic fossils and benthic foraminifers, and (2) a lower biounit (Core 120-748C-59R through Section 120-748C-79R-5, 711–898 mbsf) that is barren of calcareous planktonic fossils and benthic foraminifers. The upper biounit roughly corresponds to Subunits IIIA and IIIB; the lower biounit roughly corresponds to Subunit IIIC.

Biostratigraphic control within the upper biounit is based on the calcareous nannofossil zonation: two formal zones and five taxon range intervals have been identified (Fig. 34). The sequence of nannofossils indicates that the upper biounit is late Campanian through early Maestrichtian in age, with the Cam-

panian-Maestrichtian boundary in Cores 120-748C-38R or -39R. The nannofossil assemblages are of low diversity, with a composition and structure suggestive of restricted paleoecologic conditions. Planktonic foraminifers within the upper biounit are sparse, consisting mainly of small forms.

Benthic foraminifers are common within the upper biounit. They consist mainly of low-diversity *Gyroidina/Gavelinella*-dominated assemblages that suggest inner-shelf deposition. Both nannofossils and planktonic foraminifers are absent from Cores 120-748C-40R through -45R, an interval containing coarse-grained bioclastic grainstones with abundant bryozoans as well as echinoderm, molluscan, and calcareous red algal debris. We interpret this interval as one deposited under very shallow shelf conditions, perhaps indicative of a short-term, sea-level drop.

The lower biounit is distinguished by its lack of calcareous planktonic and benthic foraminifer fossils. Preliminary dinoflagellate palynology indicates a late Albian to Cenomanian age for this biounit. Other biogenic components from this biounit include terrestrial plant spores, carbonized wood, and fish debris. Carbonized and/or pyritized wood are common throughout the biounit, but especially so in the lower part (Cores 120-748C-71R through -79R). Fish debris is more common near the base of the unit, especially in Sample 120-748C-63R-CC where it is a major rock-forming component.

Preliminary results from Site 748 indicate that it will serve as an important source for information on the paleontologic and geologic history of the southern Indian Ocean. The presence of diverse assemblages of calcareous and siliceous microfossils, when integrated with the nearly complete magnetostratigraphic record spanning the late Eocene to the early Pleistocene, will permit calibration of numerous important biostratigraphic datum levels. The well-preserved calcareous assemblages in the upper Paleocene and lower Eocene should yield important paleoceanographic and paleobiogeographic data about a crucial period of the breakup of southern Gondwanaland. Finally, the paleontology of the Upper Cretaceous section promises a wealth of information on southern high-latitude foraminifers, calcareous nannofossils, and diatoms, as well as insight on the foundering of the Kerguelen Plateau.

PALEOMAGNETICS

At Site 748 located in the western part of the Raggatt Basin on the Southern Kerguelen Plateau (58°26.45′S, 78°58.89′E), we obtained a good magnetostratigraphic record from the Pleistocene to the middle Eocene and a long normal sequence in the Upper Cretaceous. The polarity reversal series from Site 748 continues the magnetostratigraphic record beyond Anomaly Correlative 10, where it stopped at Site 747, by 12 m.y. to Anomaly Correlative 18. The inclinations of samples from the basalt layer seem to indicate that no significant tilting or displacement in the direction of the magnetic meridian have taken place since the acquisition of remanent magnetization.

Sediments

We measured natural remanent magnetization (NRM) on archive halves of Cores 120-748A-2H, 120-748B-2H through -20H, and 120-748C-70R through -79R using the cryogenic magnetometer. A 10-cm spacing between measurements was chosen for all archive halves at Site 748. After measuring the NRM, each core was demagnetized with a decreasing alternating field (AF) of 9-mT peak value and subsequently remeasured. The two cores from Hole 748A were disturbed and did not show a clear magnetic reversal sequence.

The first 20 cores from Hole 748B were recovered with the APC and were well suited for paleomagnetic investigation. Cores 120-748B-21X through -25X had a low recovery rate and were too disturbed for whole-core cryogenic (WCC) measurements. Cores 120-748C-1R through -69R had low recovery and were not preserved well enough for WCC measurements because of the rotary drilling. Cores 120-748C-70R through -79R consisted of glauconitic siltstones and could be measured with the pass-through magnetometer because of the high recovery rate and the well-preserved state of the core.

The NRMs of discrete cylindrical samples from Cores 120-748C-27R through -70R and from Core 120-748C-79R were measured with the spinner magnetometer. The spinner proved to be more sensitive than the cryogenic magnetometer for single sample measurements. The sample holder for single specimens on the pass-through cryogenic instrument had a magnetization (0.25 mA/m) similar to the magnetic intensity of some discrete samples. Sample 120-748C-64R-1, 101–103 cm, was stepwise AF demagnetized with the Schonstedt demagnetizer to examine the remanent magnetization for its stability.

The results from the NRM measurements of Hole 748B are shown in Figure 36. The inclinations of the NRMs show an indication of a polarity reversal sequence, although it has a significant normal overprint. A bias of the inclinations toward negative values (normal polarity) is evident especially in the section from 50–100 mbsf. This normal polarity overprint could be either a viscous remanent magnetization (VRM) or a drilling-induced magnetization.

As at Site 747 (see "Paleomagnetics" section, "Site 747" chapter), we find occasional clustering of the declinations between 0° and 90°. These declinations, sometimes constant as a function of depth, can be interpreted as caused by a normal component of magnetization in cores that seem to be roughly oriented with respect to azimuth (i.e., declination). Because of relatively calm seas, the noise level of the cryogenic magnetometer was below 0.1 mA/m, which is an improvement by a factor of 2 compared with Site 747.

In general, the NRM intensities of the archive halves were sufficiently strong to be measured with the shipboard superconducting quantum interference detector (SQUID) magnetometer. Parts of the downhole magnetostratigraphic record have data gaps, resulting from core disturbance. These data gaps are indicated by the long vertical lines in the intensity plots.

An AF demagnetization at 9 mT removed some of the bias that the inclinations had toward normal polarity and revealed a more detailed magnetic field reversal pattern, which is shown in Figure 37. This improvement of reversal stratigraphy upon AF demagnetization becomes especially evident when one compares the section from 50 to 100 mbsf before and after AF treatment (Figs. 36 and 37). Despite the improvement in the magnetostratigraphic record, some of the normal chrons appear slightly longer than what is expected from a comparison with the seafloor anomaly record, as discussed in the following section. This difficulty with achieving a complete removal of secondary overprints shows the urgent need for higher AF demagnetization levels (>10 mT) on the cryogenic magnetometer.

Even after AF demagnetization, the transitions between two different polarities are still diffuse, that is, much slower than the $<10^4$ yr usually found for reversals (e.g., Clement et al., 1982). These apparent long polarity transitions, as for example at 63 and 68 mbsf in Figure 37, may be caused by different physical processes during the acquisition of magnetic remanence in the sediment. The black stars in Figure 37 represent inclinations obtained from stepwise AF demagnetization of discrete samples on the shore. We show only inclinations from discrete samples that complement or contradict the whole-core cryogenic record.

An interpretation of the inclination record in terms of normal (black) and reversed (white) chrons is shown in Figure 37. Uninterpretable data are shown by a diagonal line pattern. Inclination data that could not be interpreted with certainty are indicated by one half of the tentative polarity chron and with diago-

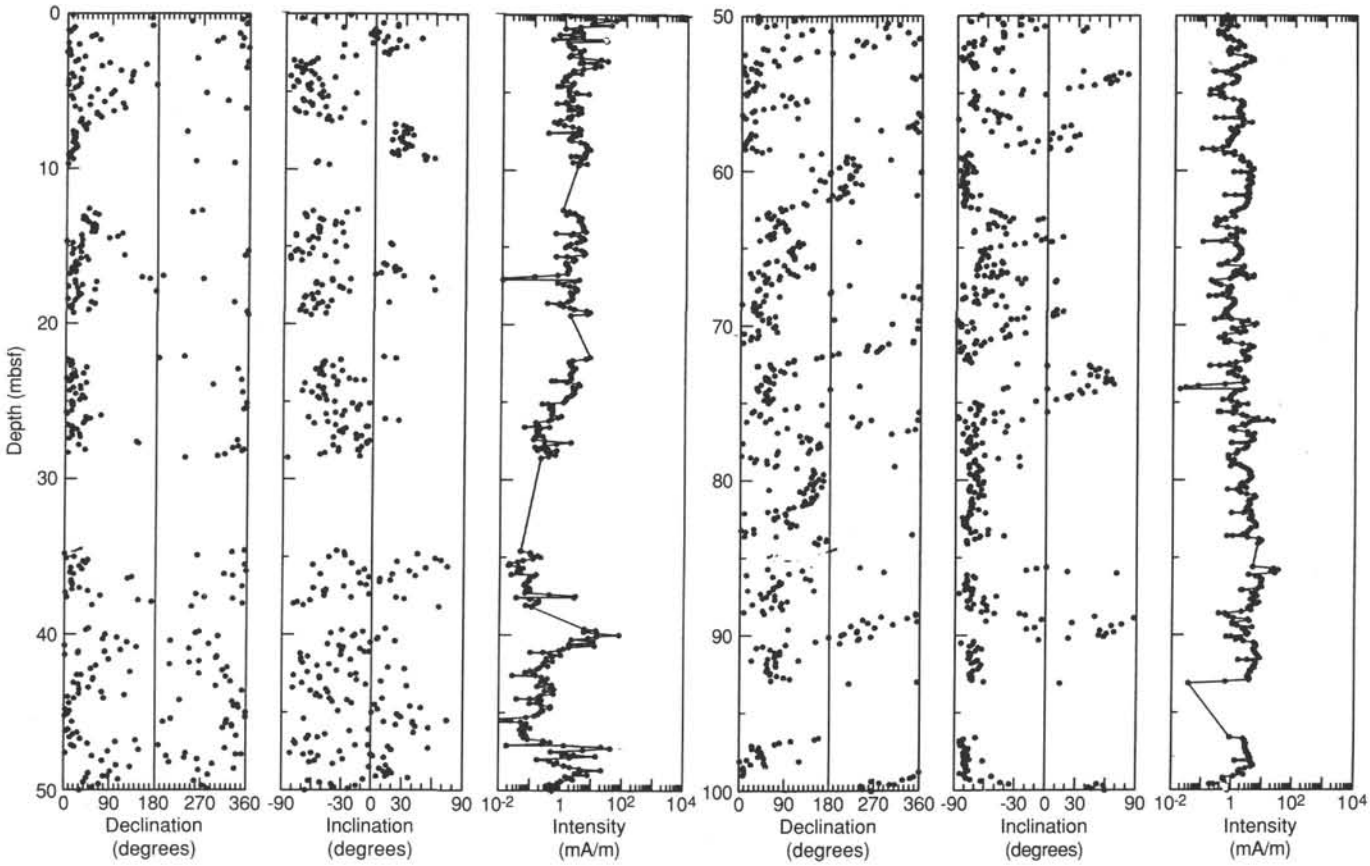

Figure 36. Declination, inclination, and intensity of NRM of archive halves as a function of depth (mbsf) measured with the pass-through SQUID magnetometer for Hole 748B. Negative inclinations represent normal magnetic polarity and positive inclinations represent reversed polarity. The NRMs seem to be overprinted by a normal component of magnetization. Normal intervals prevail in this polarity sequence, especially in the section from 50 to 100 mbsf.

nal lines in the second half (Fig. 37). A first rough identification of the polarity chrons could be obtained by comparison with the marine magnetic anomaly record. An improved identification of the polarity chrons was achieved in collaboration with the paleontologists of Leg 120 by cross-calibrating the magnetic reversal sequence with biostratigraphic events using the Berggren et al. (1985b) time scale. For details on the integration of magneto- and biostratigraphy, the reader is referred to the "Sedimentation Rates" section (this chapter).

The normal period from 3.3 to 6.9 mbsf (Fig. 37) is identified as the Gauss normal polarity chron, that is, Anomaly Correlative 2A. Below the Gauss, we find evidence for the Gilbert reversed polarity chron, which is followed by either Anomaly Correlative 4 or 4A. The short normal period at the very top of this record (Section 120-747B-2H-1) may represent the Olduvai Subchron. The normal chrons (14–25 mbsf) with their short reversed subchrons can tentatively be correlated to Anomalies 4 and/or 4A. Below 26 mbsf the intensity of magnetization approaches the lower limit of resolution for the cryogenic magnetometer, and the scattered inclination values do not permit any interpretation. The anomaly interpretation presented so far agrees with a constant sedimentation rate and with diatom and radiolarian data (see "Sedimentation Rates," this chapter).

At approximately 38 mbsf, the sedimentation rate curve requires a hiatus of about 5 m.y. Also at 38 mbsf, a 5000-fold increase in the magnetic intensity occurs, which might be an additional argument for a hiatus at that depth. Unfortunately, this increase in magnetization occurs exactly at the boundary between cores and could also be related to a contamination with drilling mud at the top of the core. The identification of anomaly correlatives between 38 and 65 mbsf is less certain at the moment, requiring stronger constraints from micropaleontologic markers. A possible order of normal chrons between 5D and 6B is shown in Figure 37. The difficulties in reaching a more definite identification result partly from the low intensity of magnetization (0.1 mA/m), which leads to less interpretable data between 41 and 47 mbsf.

The three normal subchrons of 6C at the boundary between the Miocene and Oligocene can be easily recognized between 65 and 68 mbsf. The sedimentation rate curve ("Sedimentation Rates," this chapter) requires a hiatus of approximately 2 m.y. at 69.5 mbsf. This hiatus might be expressed also by the abrupt drop in inclination at 69.6 mbsf. The short normal period at 70 mbsf could be the lower part of Anomaly Correlative 7, followed by 7A and 8 at 72 and 76 mbsf, respectively. The correlation of Anomalies 9–11 to our reversal pattern (Fig. 37) should be regarded as preliminary until better data are available from the shore-based measurements on discrete samples.

With some certainty one can identify Anomaly Correlatives 12 and 13 (Fig. 37), if one disregards the few short normal events in between 12 and 13 as spurious data. Below 120 mbsf (Fig. 37), the intensities of the sediments become too low to draw any reliable conclusions, except for the possible occurrences of parts of Anomaly Correlatives 16, 17, and 18 at 130, 144, and 156 mbsf, respectively. Evidence from calcareous microfossil biostratigraphy in Section 120-748C-17R-CC supports

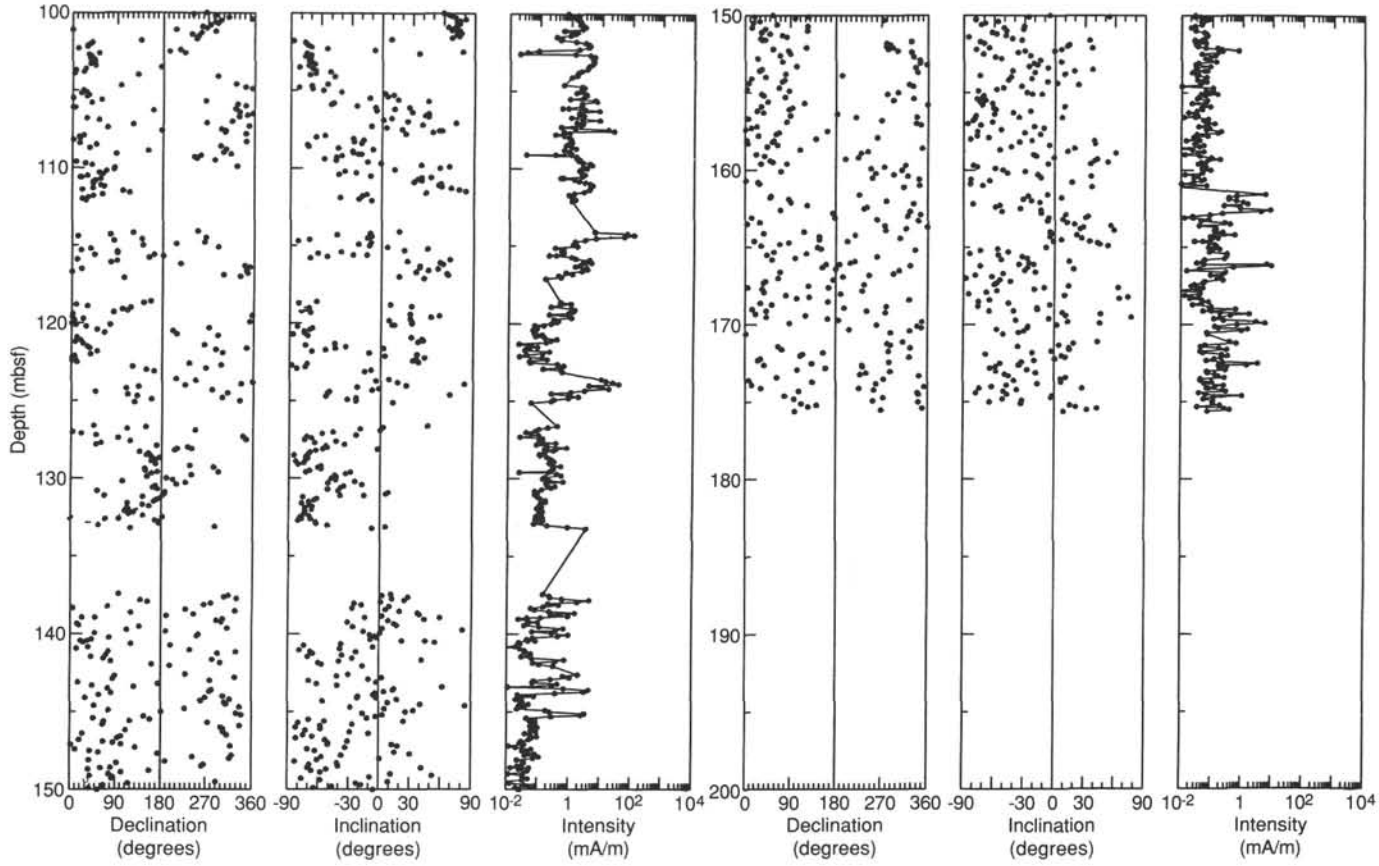

Figure 36 (continued).

the presence of Anomaly Correlative 18 ("Sedimentation Rates," this chapter). The magnetic moments of sediments between 160 and 176 mbsf were too low and the inclinations too scattered for any reasonable interpretation of the data.

Good paleomagnetic data could be obtained from Subunits IIIA and IIIB (389–897 mbsf) (see "Lithostratigraphy and Sedimentology" section, this chapter). The NRMs of discrete samples from Cores 120-748C-27R through -70R (400–800 mbsf in Fig. 38) were measured with the spinner magnetometer. All NRMs of the discrete sample spinner (DSS) measurements had normal polarity. The results after AF demagnetization of the archive halves of Cores 120-748C-70R through -79R (807–897 mbsf) are shown in Figure 39. The large majority of the measurements between 400 and 897 mbsf indicate normal magnetic polarity. The few reversed inclinations in Figure 39 coincide with very low intensities or the top of sections, which are sometimes disturbed.

Paleontologic evidence suggests that the normal polarity sequence in Figures 38 and 39 contains nannofossils from the Maestrichtian and Campanian (see "Biostratigraphy" section, this chapter). This places our long normal interval tentatively in the time interval of Anomalies 32 and/or 33 (time scale of Kent and Gradstein, 1985). So far there is no indication for a reversed polarity interval, which is required between Anomaly Correlatives 32 and 33. The existence of a reversed period cannot be excluded because of the possibility of magnetic overprinting and data gaps in the record (Fig. 38). The spinner and cryogenic magnetometer measurements overlapped at Section 120-748C-70R-1. Results from both instruments show negative inclinations, giving an independent verification for the two methods of measurement.

Progressive AF demagnetization of a single specimen (Sample 120-748C-64R-1, 101–103 cm) up to 50 mT shows a nearly single-component magnetization on the orthogonal vector projection (Fig. 40). A viscous component is removed at approximately 10-mT peak AF. The result from a single sample suggests that this type of sedimentary rock might give good paleomagnetic data during the planned shore-based investigations. The increase in intensity by nearly a factor of 2 at 680 mbsf (Fig. 38) coincides with the lithologic boundary between Subunits IIIA and IIIB ("Lithostratigraphy and Sedimentology" section, this chapter).

In conclusion, the magnetostratigraphic record presented above contains major parts of the magnetic reversal sequence from the present to the middle Eocene. A long normal magnetic interval is tentatively identified as Anomaly Correlatives 32 and/or 33 in the Late Cretaceous. Further refinements to the magnetic polarity record (Fig. 37) are expected from the demagnetization of discrete samples from these cores. The magnetostratigraphy of Site 748 should complement the magnetic reversal sequence obtained at Site 747, which was established down to the upper Oligocene. A cross-correlation of the biostratigraphy and the magnetic polarity records from both Sites 747 and 748 has the potential to establish an integrated magnetobiostratigraphy for high southern latitudes.

Igneous Rocks

Two samples from the basalt layer (Sections 120-748C-79R-6 and 120-748C-79R-7) were stepwise demagnetized by alternating fields up to 40 mT. Both samples possess stable single-component magnetizations as shown by the Zijderveld diagrams and stereographic projections in Figure 41. Samples 120-748C-79R-

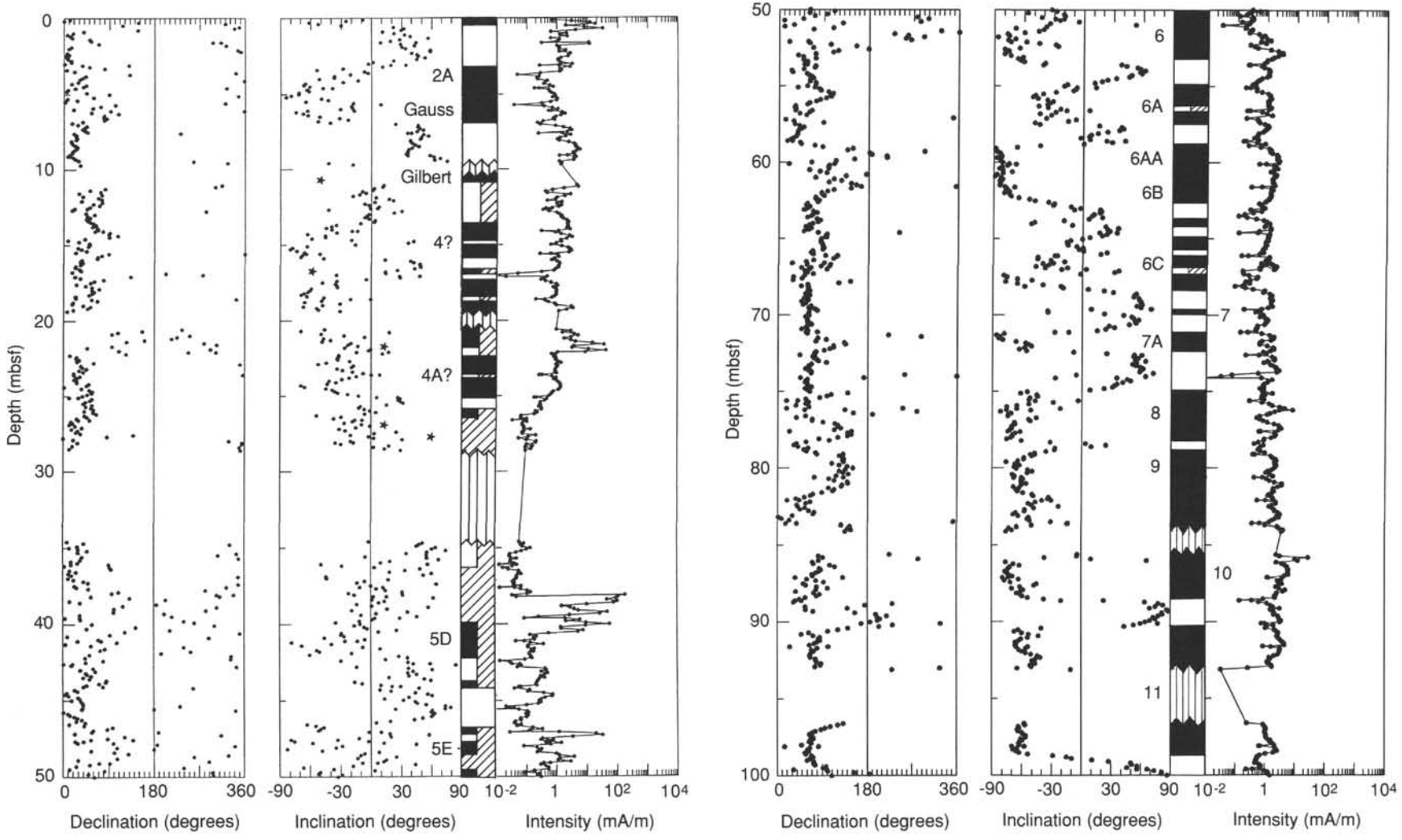

Figure 37. Declination, inclination, and intensity of archive halves of Hole 748B after AF demagnetization at 9-mT peak alternating field. Results from measurements with the cryogenic magnetometer are shown by black dots. Black stars represent results from AF demagnetization of discrete samples. A preliminary identification of normal polarity chrons (in black) is shown to the right of the inclination record. Data gaps are shown by vertical lines and uninterpretable data by diagonal lines. Polarity chrons, which are based on less reliable data, are indicated by one half appearing as diagonal lines.

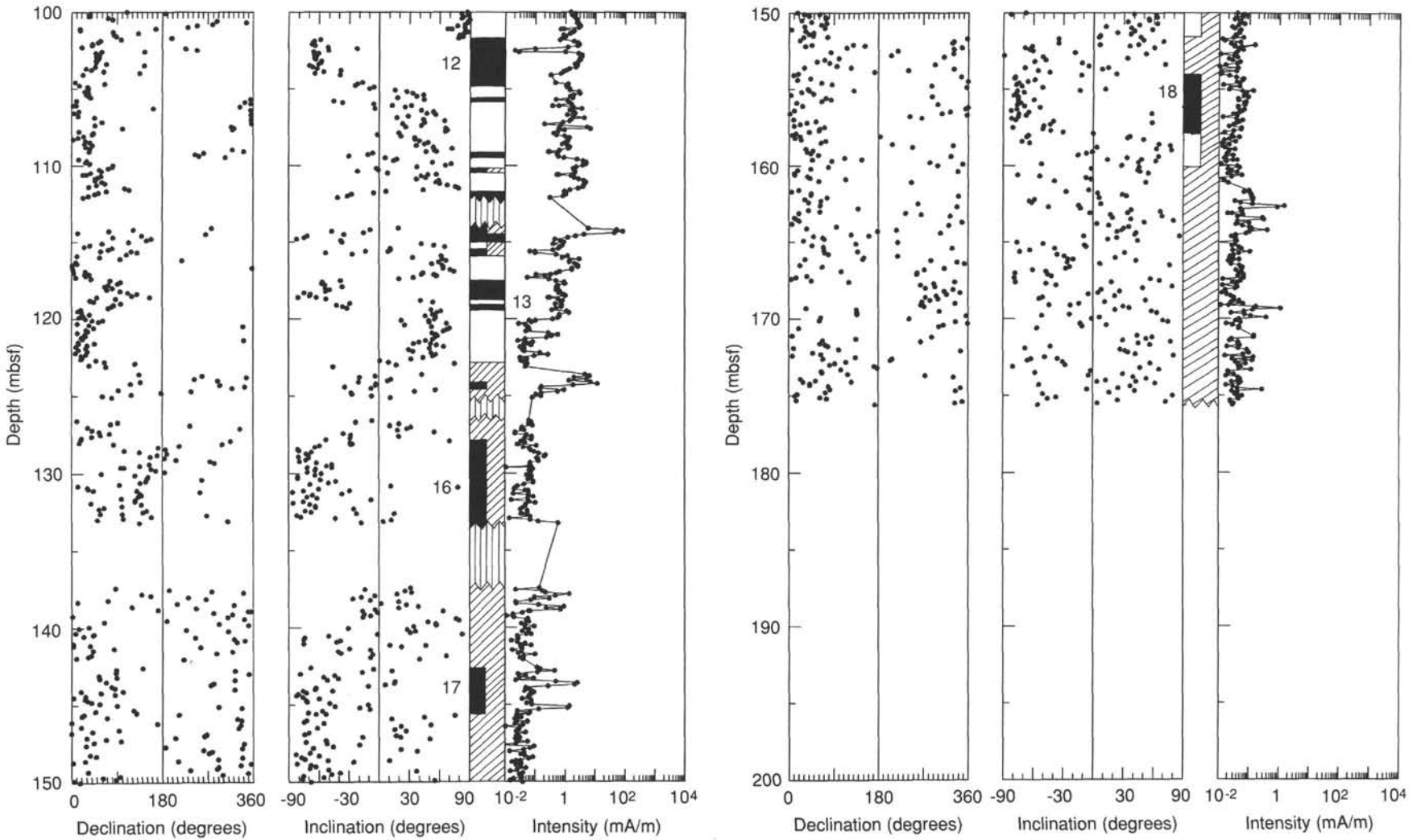

Figure 37 (continued).

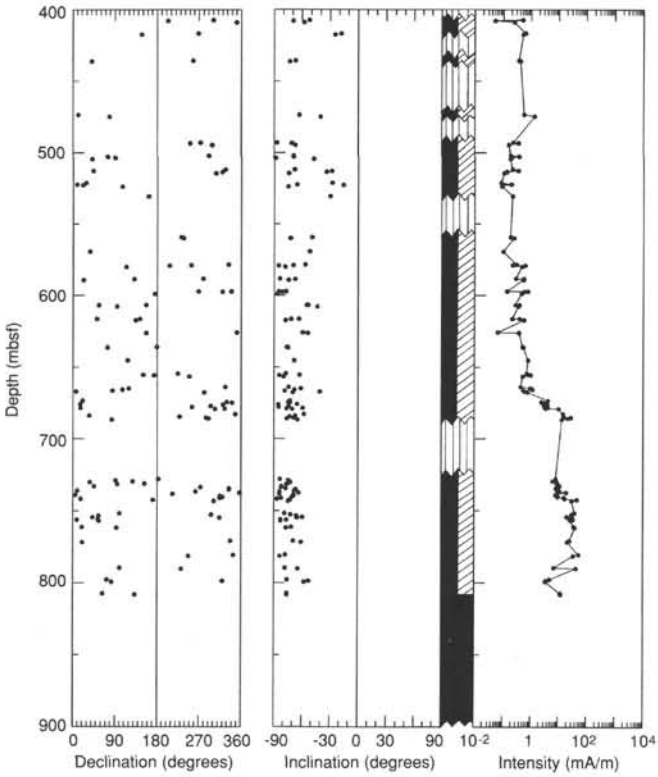

Figure 38. Declination, inclination, and intensity of NRM of discrete samples measured with the spinner magnetometer. All samples have normal polarity. This long normal interval corresponds possibly to Anomalies 32 and/or 33. The long normal period between 800 and 900 mbsf is based on data from Figure 39.

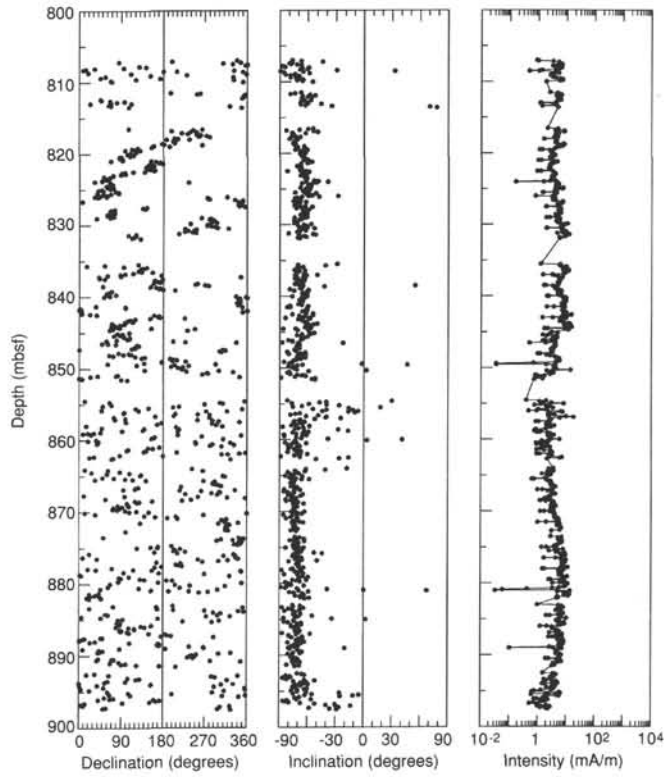

Figure 39. Measurements of declination, inclination, and intensity on glauconitic siltstone halves with the cryogenic magnetometer after AF demagnetization at 9 mT. These samples had exclusively normal polarity, and the few reversed measurements could be identified as unreliable measurements from the tops or bottoms of core sections.

6, 121–123 cm, and 120-748C-79R-7, 45–47 cm, had median destructive fields of 8 and 13 mT and inclinations of −70° and −68°, respectively. Sample 120-748C-79R-6, 50–52 cm, was stepwise thermally demagnetized up to 530°C. Thermal demagnetization shows a single-component remanence, which becomes shallow at 530°C (Fig. 42). The decrease in intensity during the thermal demagnetization suggests the presence of two magnetic phases. The inclination of −68°, which was obtained from thermal demagnetization, agrees well with the average of −69° from AF demagnetization.

There are two possible interpretations for these characteristic directions (Figs. 41 and 42). The first possibility is that the characteristic direction (inclination = −69°) is a chemical remanent magnetization (CRM). The chemical origin of remanence is supported by the highly altered nature of the basalt ("Igneous Petrology" section, this chapter) and the indication of a shallower component with high blocking temperatures. The second possibility is that the characteristic direction is a primary magnetization from the time when the basalt cooled through the Curie point. In both cases, the magnetic remanence was acquired in a magnetic field similar to the present-day field (inclination equals −73°, assuming a geocentric axial dipole field) or in a position slightly north of the present latitude.

The basalt layer dips 1.6° in a southwest-trending direction. This angle has been calculated from the seismic survey lines shot across the Raggatt Basin ("Site Geophysics" section, this chapter). Our inclinations are not corrected for this small angle, since it falls within the error of the measurements. A comparison of the inclinations of basalt samples from Sites 747 through 749 (see "Paleomagnetics" section, "Site 749" chapter) will

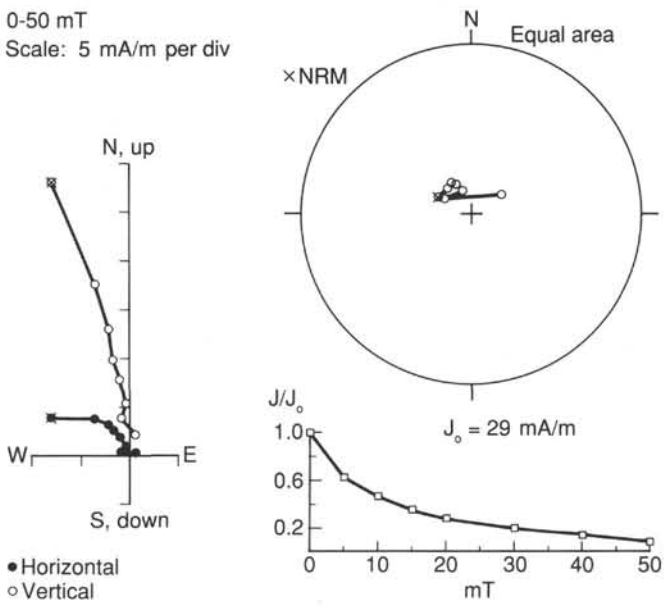

Figure 40. Progressive AF demagnetization of Sample 120-748C-64R-1, 101–103 cm. The orthogonal vector projection shows a single-component magnetization, with a soft overprint that is removed after 10-mT AF demagnetization. The average inclination is −73°. The stereographic equal area projection shows little scatter of the magnetization vector during demagnetization. The NRM is a soft magnetization, because the median destructive field is only 9 mT.

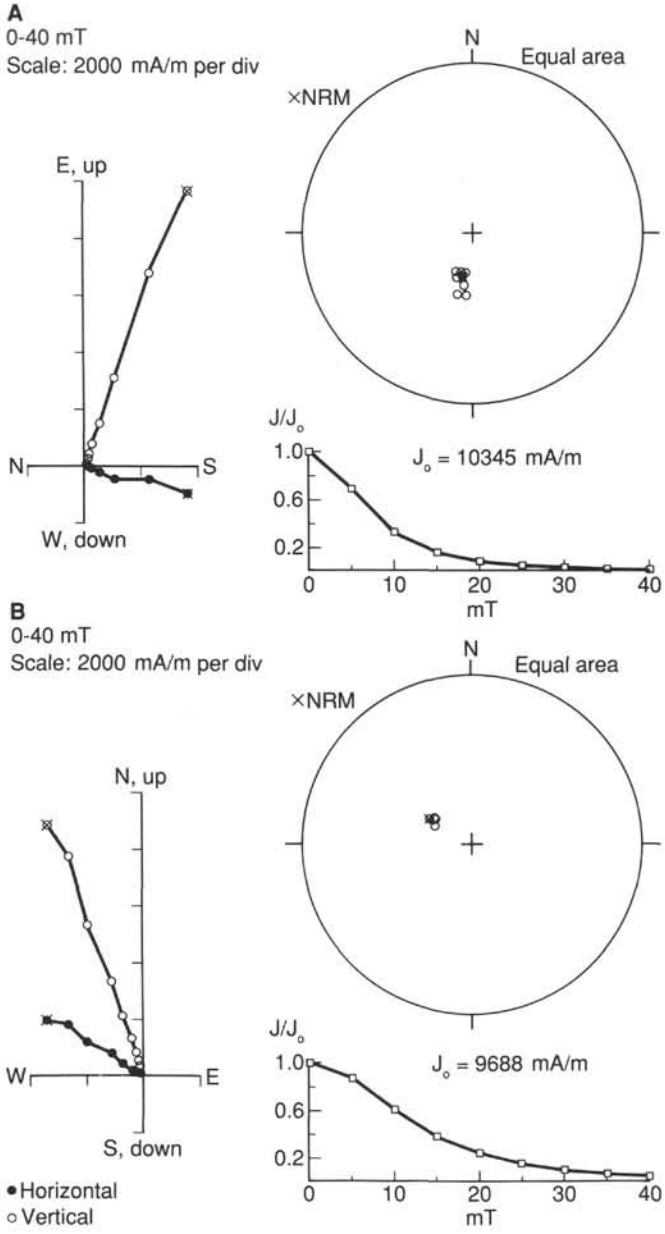

Figure 41. AF demagnetization characteristics of samples from the basalt layer. **A.** Sample 120-748C-79R-6, 121–123 cm. **B.** Sample 120-748C-79R-7, 45–47 cm. Both samples illustrated have single-component magnetizations as is evident from the straight lines in the orthogonal vector projections and the close grouping of directions on the stereographic projection. There is a small viscous overprint that is easily removed by a 5-mT peak alternating field. The two samples illustrated have inclinations of −70° and −68°, respectively. The declinations are arbitrary since the cores were unoriented.

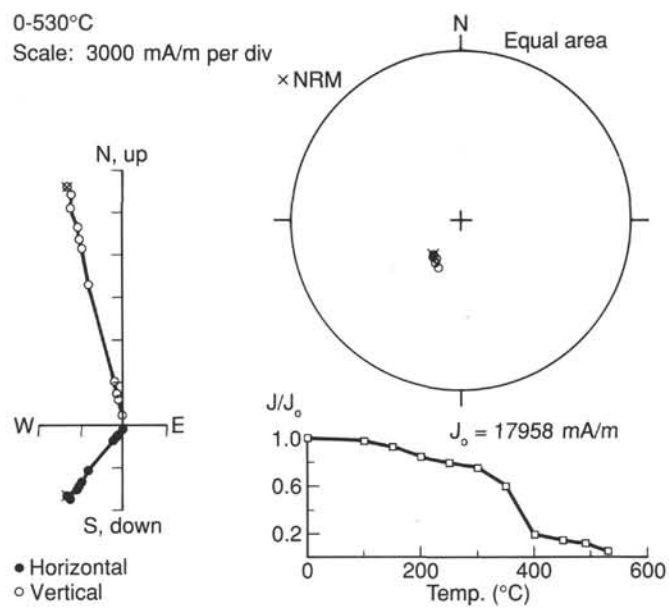

Figure 42. Stepwise thermal demagnetization of Sample 120-748C-79R-6, 50–52 cm, from the basalt layer. Zijderveld plot and stereographic projection show a single-component magnetization. The intensity decay curve suggests two magnetic phases.

help us to determine a paleolatitude for the Kerguelen Plateau. These results are rather preliminary, and detailed paleomagnetic and rock-magnetic studies are planned to resolve the question whether the NRM is a CRM or a primary magnetization.

SEDIMENTATION RATES

Data

Both biostratigraphic and paleomagnetic data were used to construct an age-depth curve for Site 748 (Fig. 43). Biostratigraphic data are listed in Table 7. Detailed paleomagnetic data can be found in the "Paleomagnetics" section of this chapter with an interpretation of the magnetic reversal sequence. This sequence is duplicated in the left column of Figure 43.

Biostratigraphic data are available from calcareous microfossils throughout Hole 748B and in Hole 748C down to Core 120-748C-58R. Siliceous microfossils provide age control for Hole 748B down to Core 120-748B-20H, coinciding with available paleomagnetic data for the Cenozoic. Paleomagnetic data are also available for the Upper Cretaceous in Hole 748C from Cores 120-748C-27R to -79R.

Methods

Biostratigraphic data from calcareous and siliceous microfossils were first used to estimate the approximate age of sediments from Site 748 and to construct a generalized sedimentation rate curve. This curve provided a means of comparing the paleomagnetic data from each depth interval to the age-equivalent portion of the paleomagnetic reversal scale (Berggren et al., 1985a; Kent and Gradstein, 1985). This contributed to the identification of polarity reversal events recognized in the "Paleomagnetics" section of this chapter and in Figure 43.

Initial biostratigraphic control points are presented in Figure 43 as vertical bars and boxes and identified in Table 7. Paleomagnetic reversal boundaries are plotted as solid and stippled circles, depending on the reliability of the data. In order to reduce clutter on the figure, not all polarity boundaries are plotted. Linearity produced by the arrangement of circles represents the sedimentation rate curve for Site 748 in the intervals where paleomagnetic data are available. In intervals where only biostratigraphic data are available, a line is drawn as a best-fit through control points.

Several biostratigraphic datums identified in Site 748 sediments were used to identify specific magnetic anomaly correlatives, since these datums in other sections consistently occur in association with particular anomaly correlatives. These include the following datums in descending order and their respective anomaly correlatives: D3 (Anomaly Correlative 2A); D4 and D5 (Anomaly Correlative 3); D6 (Anomaly Correlative 5); F3 (Anomaly Correlative 5D); D10 (Anomaly Correlative 6B); N1 (Anom-

Table 7. Biostratigraphic data used in constructing Figure 43.

#	Depth (mbsf)	Age (Ma)		Name
Foraminifers				
F1	38.1–38.6	<12.1	B	*N. nympha*
F2	38.1–40.0	>16.8	T	*G. zealandica*
F3	40.0–42.0	17.6	T	*C. dissimilis*
F4	66.6–76.1	23.7	B	*G. woodi connecta*
F5	76.1–85.6	30.0	T	*C. cubensis*
F6	85.6–104.6	32.0	T	*S. angiporoides*
F7	123.6–123.8	36.6	T	*S. linaperta* and *G. index*
F8	142.6–152.1	40.0	T	*Acarinina*
F9	161.6–171.1	42.6	T	*A. primitiva*
F10	180.6–187.1	47.0	B	*G. index*
F11	258.5–265	53.5	B	*A. densa*
F12	306–315.5	57.5	B	*G. formosa gracilis*
Calcareous nannoplanktons				
N1	66.6–76.1	23.6	T	*R. bisecta*
N2	104.6–114.1	34.9	T	*I. recurvus*
N3	123.6–133.1	37.8	B	*I. recurvus*
N4	142.6–152.1	39.8	B	*C. oamaruensis*
N5	152.1–161.6	42.3	T	*C. solitus*
N6	206.1–215.6	46.0	B	*R. umbilica*
N7	268.0–277.5	53.7	T	*T. orthostylus*
N8	277.5–287.0	55.3	B	*D. lodoensis*
N9	315.5–320.5	56.6	B	*T. orthostylus*
N10	320.5–330.0	57.6	T	*F. tympaniformis*
N11	378.5–388.0	59.2	B	*D. multiradiatus*
N12	397.5–407.0	60.4	B	*D. mohleri*
N13	407	61.6	B	*H. kleinpelli*
N14	416.5 hiatus	67.3	B	*N. frequens*
N15	416.5 hiatus	69.0–72	T	*T. phacelosus*
N16	511.5–530.5	74.5–73.5	T	*A. parcus*
N17	530.5–597.0	75.5–74.5	T	*R. anthophorus*
N18	616.0–625.5	75.0–76.0	T	*E. eximius*
N19	654.0–663.5	76.5–75.5	B	*R. levis*
Radiolarians				
R1	0.1	<2.5		*C. davisiana* range
R2	4.6–9.6	3.2	T	*P. titan*
R3	19.1	>5.4		*C. spongothorax* range
R4	21.1–24.1	10+/0.5	T	*A. golownini*
			B	*E. pseudoinflatum*

Table 7 (Continued).

#	Depth (mbsf)	Age (Ma)		Name
Radiolarians (continued)				
R5	38.1–40.1	11–13	B	*C. spongothorax*
R6	40.1	>17	early Miocene assemblage	
R7	59.1–62.1	~23	B	*C. tetrapera*
Diatoms				
D1	0.1	>0.62	T	*A. ingens*
D2	0.1–2.35	1.9–2.64	T	*C. kolbei, N. weaveri*
D3	4.6–9.6	3.1–3.3	T	*N. praeinterfrigidaria*
			B	*N. weaveri, N. kerguelensis, N. interfrigidaria*
D4	9.6–11.0	3.8–4.1	B	*C. kolbei* to
			B	*N. "angulata"*
D5	9.6–11.0	4.5	T	*D. hustedtii*
D6	19.1–28.6	10–11	T	*D. dimorpha* common occurrence
D7	28.6–38.1	11.4	T	*D. denticuloides*
D8	42.6–47.6	16.7	B	*N.* sp. 17 Schrader and *D. maccollumii*
D9	42.6–47.6	17.8–18.5	B	*D. nicobarica*
			T	*C. rhombicus*
D10	57.1–66.6	23	B	*N. maleinterpretaria*
D11	38.1–47.6	20.8	T	*C. oligocenicus, R. gelida*
D12	38.1–47.6	21.2	T	*A. symmetricus*
D13	66–76	25–26	Acme of *R. gelida*	
D14	66.6–76.1	24.0	T	*L. ornata*
D15	76.1–85.6	29.0	B	*C. rhombicus*
D16	95.1–104.6	32.0	B	*R. gelida*
D17	95.1–104.6	31.0	B	*R. vigilans, S. jouseana*
D18	95.1–104.6	32.5–33.5	T	*P. reticulata, C. superbus, A. punctifera, C. reticulatus*
D19	104.6–114	35.0	T	*R. gravida*
D20	104.6–114	36–37	T	*B. spiralis*
D21	123.6–133.1	38	T	*M. architecturalis, M. barbadense*
D22	133.1–142.6	40–41	T	*T. inconspicum* var. *triloba*
D23	171.1–171.6	43–46	L	*B. corona, P. sulcata* var. *crenulata*

Note: Biostratigraphic datums are numbered in descending order and identified by prefix. D = diatom, F = planktonic foraminifer, N = calcareous nannofossil, and R = radiolarian. See "Explanatory Notes" chapter (this volume) and "Biostratigraphy" section (this chapter) for age and depth information. "B" and "T" preceding microfossil names refer to the base and top of a species' stratigraphic range.

aly Correlative 6C); D13 (Anomaly Correlatives 6C-R and 7); D17 and F6 (Anomaly Correlative 11); N2 (Anomaly Correlative 13); N3, F7, and F10 (Anomaly Correlative 15); N4 (Anomaly Correlative 17); and F8 and N5 (Anomaly Correlative 18). The relationship of these datums and anomaly correlatives is evident in Figure 43.

Nannofossil datum N6, the first occurrence of *Reticulofenestra umbilica,* in the middle Eocene is shown on Figure 43 away from the sedimentation rate calibration line to indicate the unreliability of this datum at Site 748 (see calcareous nannofossil discussion in "Biostratigraphy" section, this chapter).

Hiatuses

There are apparently several hiatuses in Holes 748B and 748C based on biostratigraphic evidence (see "Biostratigraphy" section, "Paleontological Summary of Site 748," this chapter). Only one of these is noted on the sedimentation rate curve, represented by a time interval of ~5 m.y. between the middle and early Miocene from ~12 to 17 Ma. One additional hiatus within the middle of Core 120-748B-9H is indicated in the paleomagnetic data by the absence of the interval including the upper part of Anomaly Correlative 7 and the lower portion of the long-reversed interval beneath Anomaly Correlative 6C. The horizontal spread of biostratigraphic datums between Cores 120-748B-9H and -10H supports the existence of this hiatus.

Other hiatuses suggested on paleontological criteria within Cores 120-748B-2H, -3H, -11H, and -14H are not recognized in Figure 43, suggesting that they represent a short interval of time or that some of the paleomagnetic reversals are not correctly identified in Hole 748B. Other hiatuses are suggested by biostratigraphic data for intervals where no magnetostratigraphic data are available to verify their presence and help estimate their duration. These are suggested within Cores 120-748C-26R and -27R (see "Biostratigraphy" section, this chapter).

Rates of Sedimentation

Sedimentation rates at Site 748 show a progressive increase with depth. Rates of approximately 4 m/m.y. are suggested for the lower Pleistocene through middle Miocene. This rate is probably greater in the Pliocene but is decreased due to the presence of a short (1 m.y.) hiatus that is not apparent in Figure 43. Sedimentation rates for the early Miocene to latest Oligocene are approximately 4.3 m/m.y; late Oligocene rates approach 5 m/m.y; and early Oligocene through middle middle Eocene sedimentation rates are approximately 6.3 m/m.y. Sedimentation rates increase to ~18.5 m/m.y. for the early Eocene and Paleocene; the exact point of increase occurs within an interval in the early middle to early Eocene where biostratigraphic data are lacking.

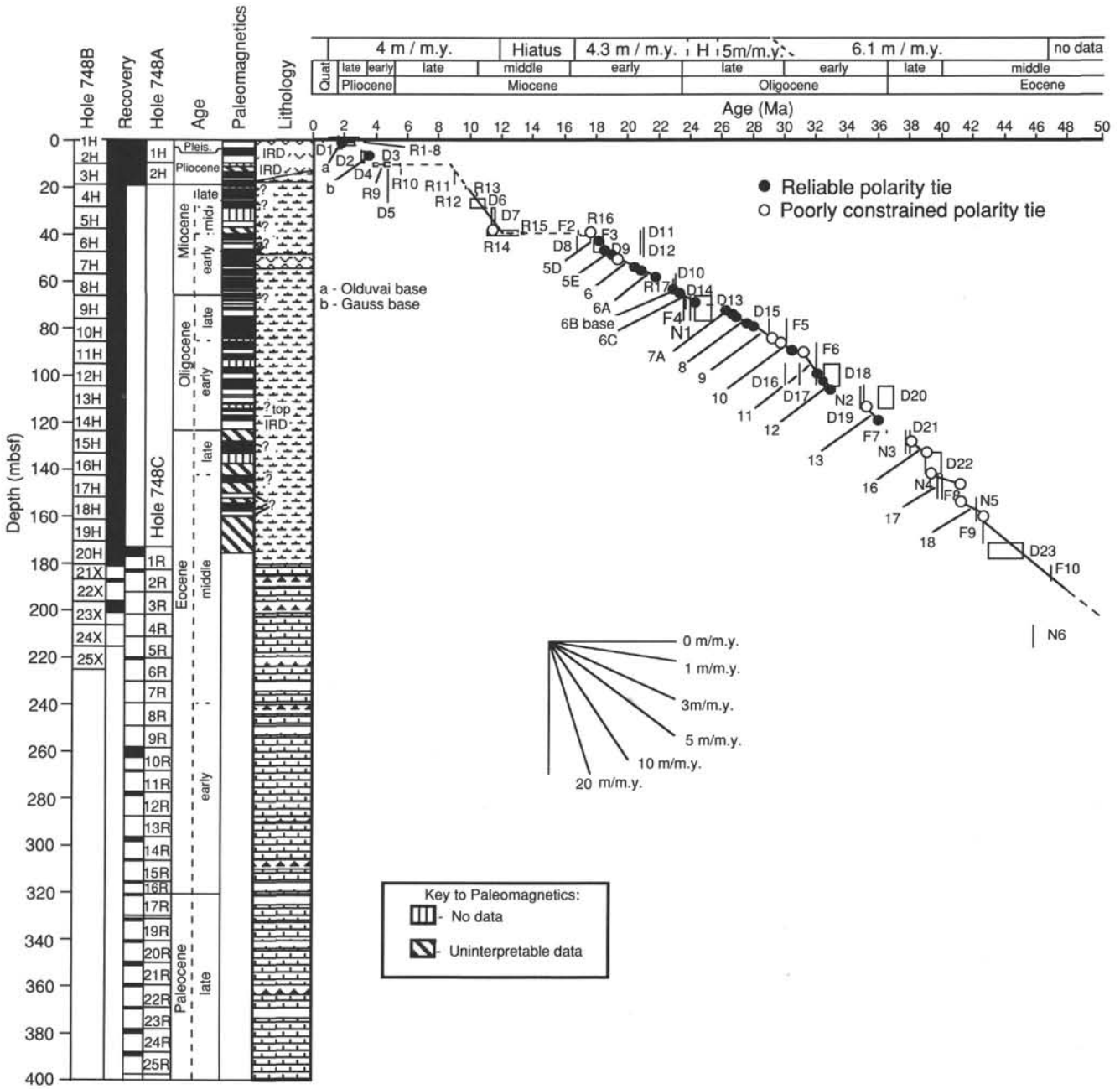

Figure 43. Age vs. depth curve for Site 748 showing sedimentation rates for Cenozoic intervals in Holes 748B and 748C based on biostratigraphic data and interpreted magnetostratigraphy. Lithology, age units, and key to symbols as in Figure 10. Time scale is from Berggren et al. (1985a, 1985b, 1985c) and Kent and Gradstein (1985). Biostratigraphic datum levels are from Table 7; vertical lines reflect depth uncertainty of datum level due to sample spacing, and horizontal lines reflect uncertainty in age calibration. Magnetostratigraphic control points (tops and bottoms of magnetic anomalies) are illustrated as solid circles if polarity reversals are reliable and as open circles if paleomagnetic signal is weak or data are absent. Solid lines represent sedimentation rates based on biostratigraphic control points in the absence of paleomagnetic control. Dashed horizontal lines denote the position and duration of hiatuses. Average rates of sedimentation are presented at the top of the figure.

Extrapolation of sedimentation rate curves from above and below this interval of no data suggests the increase began in the interval of overlap for Holes 748B and 748C and is marked by the first occurrence of chert within Core 120-748B-21X.

Sedimentation rates for the Upper Cretaceous are based on age constraints provided by calcareous microfossil biostratigraphy (Table 7) and the identification of long normal polarity intervals that are most likely correlative with magnetic Anomalies 32 and/or 33 (see "Paleomagnetics" section, this chapter). Calcareous nannofossil biostratigraphy indicates a middle Maestrichtian age (~69 Ma) for Core 120-748C-27R down to a middle Campanian age for Core 120-748C-58R, below which no calcareous microfossils were encountered. This age control suggests that the broad interval of normal polarity between Cores 120-748C-36R to -78R correspond to Anomalies 32 and/or 33. Sediment accumulation rates for the upper, calcareous interval are 35–45 m/m.y. The lower, noncalcareous Subunit IIIB has only minimal age control at present. Based on this preliminary data, possible sedimentation accumulation rates range from 19 to 47 m/m.y.

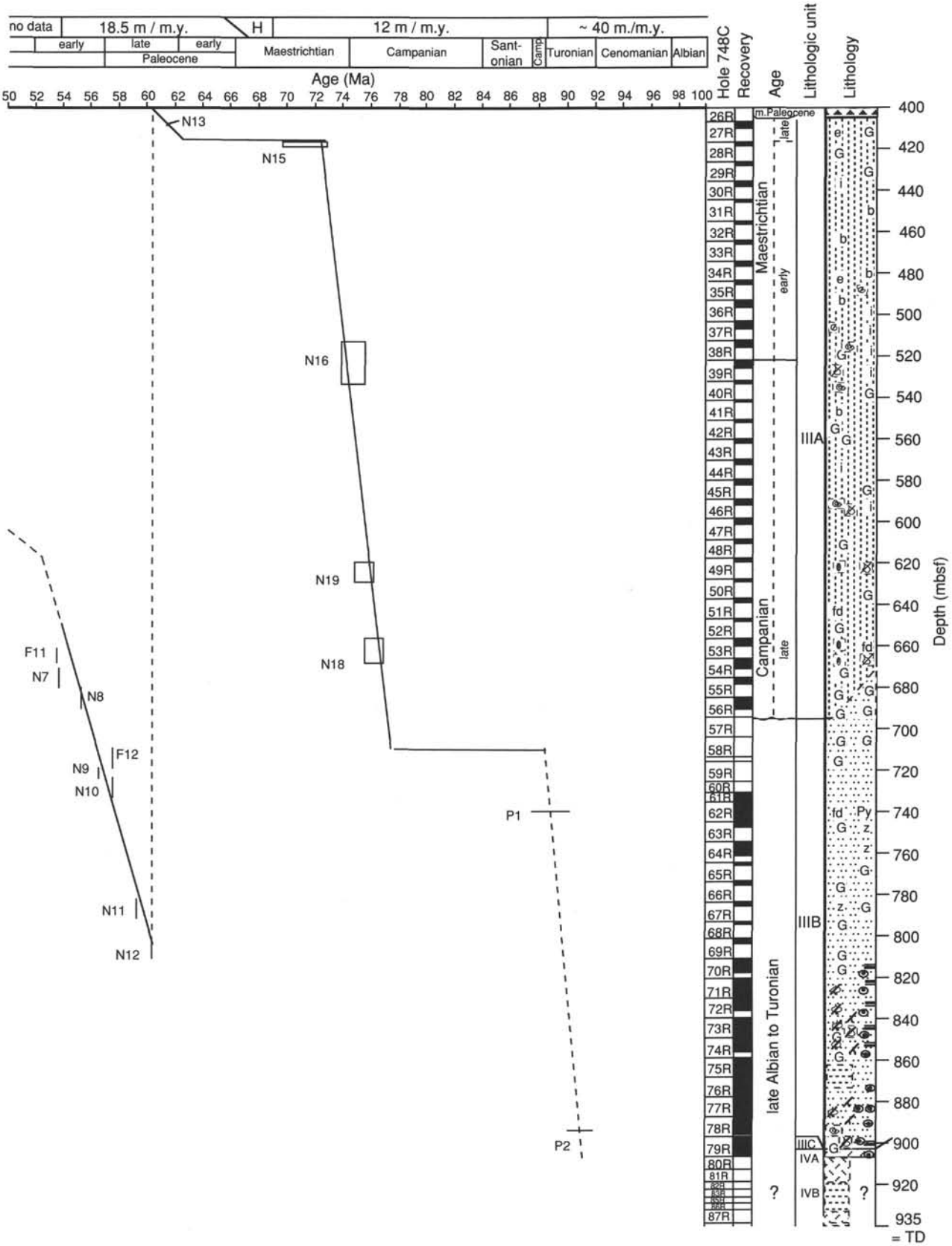

Figure 43 (continued).

INORGANIC GEOCHEMISTRY

Introduction

At Site 748, located on the Southern Kerguelen Plateau about 230 nmi south of Site 747, three holes were drilled into Upper Cretaceous to Holocene sediments and underlying basaltic basement. Only Paleogene to Quaternary soft sediments (siliceous and calcareous ooze and chalk) provided sufficient interstitial water (IW), whereas at deeper levels abundant chert layers, poor core recovery, and disturbed lithologic units precluded thorough sampling. Neither did the lithified glauconitic, green silt sediment at depths greater than 397.4 mbsf provide IW. Estimated sedimentation rates are low (around 0.4 cm/1000 yr) throughout the entire Neogene. For the Paleogene sequence sedimentation rate estimates are higher (see "Sedimentation Rates" section, this chapter). Compared with Site 747, the Cenozoic sequence of Site 748 has lower sedimentation rates for the Neogene.

A total of ten samples from depths between 7 and 296 mbsf were obtained, and squeezed fluids from each sample amounted to between 25 and 82 cm^3. Shipboard analysis of pH, alkalinity, salinity, sulfate, chlorine, magnesium, calcium, and silica were conducted according to the methods described by Gieskes and Peretsman (1986; see also "Explanatory Notes," this volume). Results of IW analysis are reported in Table 8 and Figure 44. Concentrations are reported in millimoles per liter (mM), except for silica (μM).

Results

Salinity and Chlorinity

Salinity values range from 35.6 to 36.3 g/kg (average = 36.0 g/kg) and show little variation except for a low initial value (35.8 g/kg) reflecting proximity to the bottom seawater, and a low value at 297.95 mbsf (35.6 g/kg) that most probably reflects seawater influx through rotary drilling. The average contents of total dissolved solids (36.0 g/kg) is well above standard seawater (35.2 g/kg), but nevertheless demonstrates the overall seawater derivation of the IW.

Chlorine concentrations are above 559 mM (standard seawater) except for low values for the uppermost sample (120-748B-2H-5 = 553 mM and the lowermost sample (120-748C-14R-1 = 559 mM). The Cl concentrations reflect the elevated salinity to some degree. The decrease in Cl concentrations from 572 to 559 mM within the lowermost samples is attributed to seawater contamination and processes not yet understood.

Alkalinity and pH

Alkalinity values display a regular decrease from 2.553 at the top to 1.503 mM at 159.55 mbsf downhole. Both carbonate and silica precipitation can lower alkalinity as well as lower the slightly alkaline pH (>7) by withdrawal of cations other than H^+. It is assumed that depth-controlled changes in the carbonate system (and CO_2^- and sulfate system) are responsible for the decrease in alkalinity and pH. The observed increase in alkalinity and pH from 159.55 mbsf downhole reflects mixing processes with seawater introduced by drilling techniques.

In most natural waters, total alkalinity equals carbonate alkalinity and is controlled by HCO_3^- concentration at pH greater than 7 (Drever, 1982). Withdrawal of HCO_3^- by carbonate precipitation (and to a far lesser degree, silicate precipitation) effectively lowers alkalinity. Therefore, small-scale carbonate precipitation is thought to be responsible for the decrease in alkalinity.

The pH value decreases from 7.87 at the top to a low of 7.16 at 102.55 mbsf and then stays around 7.2. The carbonate system buffers the pH at this value.

Sulfate

Sulfate concentrations display a decrease from 27.88 mM at the top to 22.70 at the bottom of the drill hole. The high value at 199.55 mbsf (24.24 mM) is related to seawater input (about 30%) through drilling. The entire sulfate reduction is very low due to the absence of reducing agencies such as organic material (see "Organic Geochemistry" section, this chapter). A possible effect lowering sulfate is Mg cation exchange with Fe in clay minerals and formation of pyrite due to local sulfate reduction. Fine pyrite is occasionally observed as grey streaks in the white oozes (see "Lithostratigraphy and Sedimentology" section, this chapter). This effect, however, is very limited. The high sulfate concentrations, which seem to asymptotically approach a value around 22 mM, reflect the overall oxidizing environment.

Magnesium and Calcium

Magnesium shows a steady decrease with depth from 52.44 mM (Sample 120-748B-2H-5) at 7.55 mbsf to 37.05 mM (Sample 120-748B-18H-5) at 159.55 mbsf. This decrease is correlated with a steady increase in calcium from 12.75 to 25.16 mM. Increasing depth and thus increasing calcium undersaturation of IW are compensated by cation exchange where Mg replaces Ca in the carbonates and Ca therefore goes into solution. A slight but significant surplus in magnesium loss may be due to magnesium incorporation into alteration minerals or due to calcium carbonate precipitation, which would then explain the decrease in alkalinity and pH.

Slightly irregular Mg and Ca behavior at 199.55 mbsf again reflects disturbance of the IW by drill water, but calcium concentrations are still twice as high as in normal seawater. A 7:3 mixture of IW (extrapolated 26 mM Ca) with seawater (10.55 mM Ca) creates the observed calcium concentrations. The same

Table 8. Interstitial water chemical data, Site 748.

Core, section, interval (cm)	Depth (mbsf)	Vol. (cm^3)	pH	Alk. (mM)	Sal. (g/kg)	Mg^{2+} (mM)	Ca^{2+} (mM)	Cl^- (mM)	SO_4^{2-} (mM)	Si (μM)	Mg^{2+}/Ca^{2+}
120-748B-											
2H-5, 145–150	7.55	82	7.87	2.553	35.8	52.44	12.75	553.00	27.88	762	4.11
3H-5, 145–150	17.05	41	7.55	2.579	36.1	49.04	14.88	563.00	27.18	743	3.30
6H-5, 145–150	45.55	54	7.54	2.312	36.0	44.70	19.64	561.00	25.28	792	2.28
9H-5, 145–150	74.05	45	7.28	2.032	36.0	41.58	22.33	577.00	24.70	814	1.86
12H-5, 145–150	102.55	30	7.16	1.839	35.8	39.28	23.99	565.00	23.61	803	1.64
15H-5, 145–150	131.05	35	7.21	1.779	36.0	37.78	24.65	576.00	23.28	779	1.53
18H-5, 145–150	159.55	25	7.20	1.503	36.0	37.05	25.16	574.00	22.83	779	1.47
23X-2, 145–150	199.55	32	7.28	1.762	36.1	40.99	21.44	572.00	24.24	442	1.91
120-748C-											
10R-2, 145–150	261.45	27	7.21	2.310	36.3	38.11	24.74	564.00	22.68	133	1.54
14R-1, 145–150	297.95	40	7.37	1.810	35.6	37.97	24.46	559.00	22.70	139	1.55

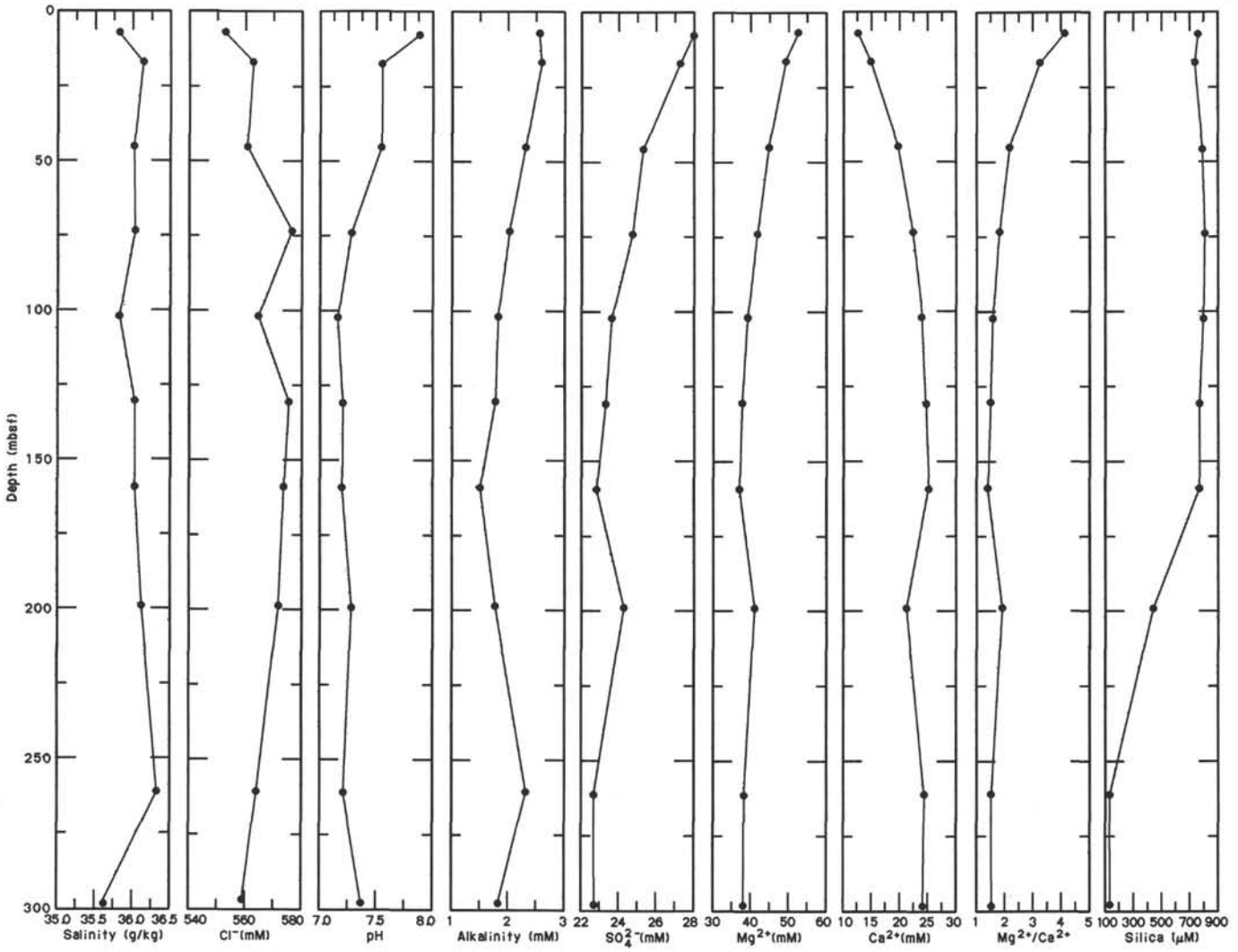

Figure 44. Summary of interstitial water analyses, Site 748, as a function of depth.

calculation done for Mg (36 mM Mg in IW, 54 mM Mg in seawater) gives 41.4 mM; the observed value is 40.99 mM Mg.

The Mg^{2+}/Ca^{2+} ratios drop systematically from 4.11 to 1.55 at the bottom of the sediment pile and again reflect the magnesium depletion of IW due to cation exchange with calcium. A Mg^{2+} vs. Ca^{2+} plot demonstrates the linear relationship between the two elements (Fig. 45). From the linear relationship between calcium and magnesium and the depth-dependent calcium undersaturation of seawater, a conservative behavior (i.e., cation exchange) between the two elements is assumed.

Silica

Silica concentrations are high (743–814 μM) within the upper 160 m of the IW column. This tenfold increase of dissolved silica in IW compared with standard seawater is explained by the overall presence of opaline siliceous microfossils such as diatoms (see "Biostratigraphy" section, this chapter). Below about 160 mbsf, silica concentrations decrease to 442 μM, which is a result of seawater contamination and reduced abundance of soluble opaline material due to initial chert formation.

Another explanation is the absence of appropriate soluble siliceous material because of less favorable living conditions for diatoms (see "Biostratigraphy" section, this chapter). Further downhole (261.45 and 297.95 mbsf) silica concentrations drop to 133 and 139 μM, respectively. The low values are due to the onset of chert formation by recrystallization of soluble opaline silica and the precipitation of dissolved silica, which accounts only for a few percent of total chert volume.

Summary

Salinity and chlorinity reflect the overall seawater nature of the IW. Calcium and magnesium dissolution and precipitation are due to cation exchange between these two elements as a function of increased calcium undersaturation of IW with depth.

The slightly alkaline character of the IW is reflected by pH values greater than 7; buffering of pH around 7.2 at depth is due to the carbonate system. High sulfate concentrations and low alkalinity values point to highly oxidizing environmental conditions. Some carbonate, and perhaps silicate, precipitation accounts for a continuous drop in alkalinity, whereas the onset of chert formation and the disappearance of opaline diatom skeletons terminated high silica concentrations in the IW.

The IW column can be regarded as an open system within the upper 160 m. Chert formation, calcium saturation, and admixing of seawater by drilling techniques delimit continuous gradients at depths >160 mbsf.

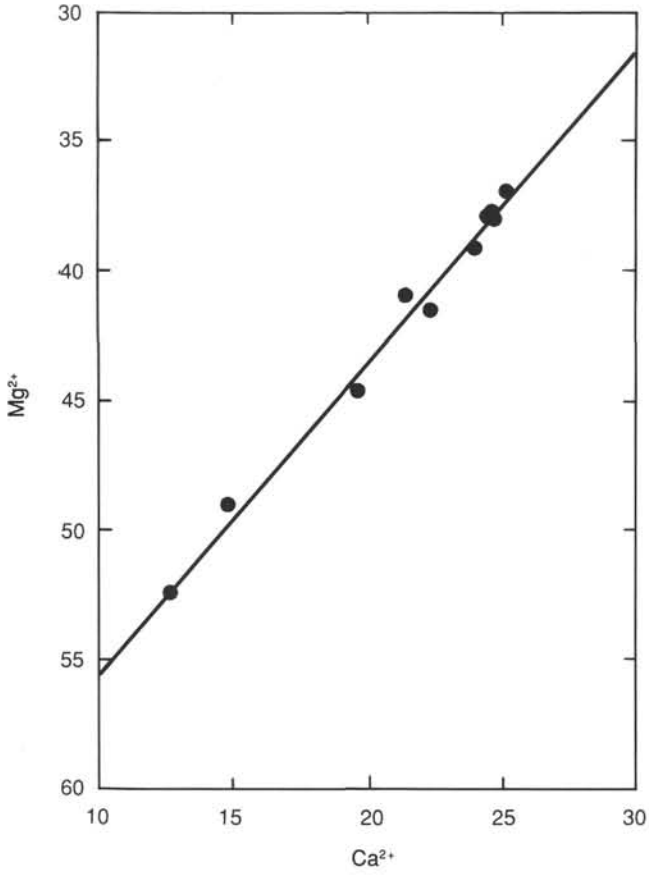

Figure 45. Mg^{2+} vs. Ca^{2+} plot of interstitial water samples from Site 748.

ORGANIC GEOCHEMISTRY

Inorganic and Organic Carbon

Inorganic carbon analyses were conducted on a total of 172 samples from Holes 748A, 748B, and 748C. The majority of samples analyzed were physical properties samples taken at 2–3 per core intervals. Total organic carbon content (TOC) was determined by the difference in total carbon and inorganic carbon. All inorganic and organic carbon results are reported in Table 9 and Figure 46. Analytical methods are outlined in the "Explanatory Notes" chapter (this volume).

The inorganic carbon content or percent carbonate shows considerable variability with depth at Site 748. Values range from 1.4% to 95.8%. Most of the significant changes in percent carbonate correspond with major stratigraphic and lithologic boundaries. Over the upper several meters of Site 748, there is a rapid decrease in carbonate content from 80.1% to 1.4%, reflecting the high concentration of siliceous microfossils in the Pliocene-Pleistocene sediments. Carbonate contents increase from 30% to 80% at 11 mbsf. This change occurs at the Miocene/Pliocene contact (see "Biostratigraphy" section, this chapter) and corresponds with the transition from a diatom-rich to a more coccolith-rich sediment assemblage (see "Sedimentology," this chapter). From 10 to 109 mbsf, carbonate values vary from 80% to 95% with occasional intervals falling below 70%. One such low interval occurs near the position of the Oligocene/Miocene contact at 64.0 mbsf.

Much of the more minor variability is associated with changes in the relative percentages of siliceous and calcareous microfossils and, less commonly, glacial debris. The base of this se-

Table 9. Total carbon, inorganic and organic carbon, and carbonate conter of samples from Holes 748A, 748B, and 748C.

Core, section, interval (cm)	Depth (mbsf)	Total carbon (%)	Inorganic carbon (%)	Organic carbon (%)	Carbonate (%)
120-748B-2H-1, 50–52	0.60	9.61	9.61	0.00	80.1
120-748A-1H-2, 104–106	2.54	8.11	8.05	0.06	67.1
120-748B-2H-3, 16–18	3.26	4.54	4.40	0.14	36.7
120-748B-2H-3, 50–52	3.60		1.96		16.3
120-748A-1H-3, 136–138	4.36		3.00		25.0
120-748A-1H-4, 134–136	5.84	0.27	0.17	0.10	1.4
120-748B-2H-5, 55–57	6.65	0.98	0.98	0.00	8.2
120-748B-2H-7, 46–49	9.56		3.59		29.9
120-748A-1H-7, 80–82	9.80		0.72		6.0
120-748A-2H-1, 100–102	10.50	0.61	0.59	0.02	4.9
120-748B-3H-1, 121–123	10.81	10.02	10.03	0.00	83.6
120-748B-3H-3, 49–51	13.09		9.29		77.4
120-748B-3H-5, 47–49	16.07	10.46	10.47	0.00	87.2
120-748A-2H-5, 100–102	16.50		8.74		72.8
120-748B-3H-7, 46–48	19.06		10.00		83.3
120-748B-4H-1, 133–135	20.43	8.99	9.03	0.00	75.2
120-748B-4H-3, 52–54	22.62		9.90		82.5
120-748B-4H-5, 132–134	26.42	10.81	10.81	0.00	90.1
120-748B-5H-3, 50–52	32.10		10.56		88.0
120-748B-5H-7, 43–45	38.03	9.70	9.70	0.00	80.8
120-748B-6H-2, 124–126	40.84		11.29		94.1
120-748B-6H-4, 54–56	43.14	11.33	11.33	0.00	94.4
120-748B-6H-5, 54–56	44.64		10.72		89.3
120-748B-7H-2, 100–102	50.10		10.49		87.4
120-748B-7H-4, 69–71	52.79	10.92	10.93	0.00	91.1
120-748B-7H-6, 77–79	55.87	10.40	10.41	0.00	86.7
120-748B-8H-3, 83–85	60.93		10.99		91.6
120-748B-8H-5, 87–89	63.97	8.76	8.57	0.19	71.4
120-748B-8H-6, 81–83	65.41		8.50		70.8
120-748B-9H-1, 61–63	67.21	10.48	10.38	0.10	86.5
120-748B-9H-3, 116–118	70.76		10.29		85.7
120-748B-9H-4, 127–129	72.37	9.72	9.72	0.00	81.0
120-748B-9H-6, 22–24	74.32		10.97		91.4
120-748B-10H-1, 125–127	77.35	10.87	10.87	0.00	90.6
120-748B-10H-2, 81–82	78.41		11.31		94.2
120-748B-10H-4, 76–78	81.36		10.99		91.6
120-748B-10H-6, 41–43	84.01	10.83	10.83	0.00	90.2
120-748B-11H-1, 122–124	86.82		10.78		89.8
120-748B-11H-3, 126–128	89.86	10.00	10.03	0.00	83.6
120-748B-11H-5, 44–46	92.04		10.93		91.1
120-748B-11H-6, 25–27	93.35	10.55	10.55	0.00	87.9
120-748B-12H-2, 119–121	97.79		10.67		88.9
120-748B-12H-3, 129–131	99.39		10.74		89.5
120-748B-12H-4, 136–138	100.96	11.07	11.07	0.00	92.2
120-748B-12H-6, 36–38	102.96		11.08		92.3
120-748B-13H-4, 57–59	109.67	9.16	9.09	0.07	75.7
120-748B-13H-6, 59–61	112.69		8.70		72.5
120-748B-14H-1, 134–136	115.44	10.45	10.45	0.00	87.1
120-748B-14H-2, 15–17	115.75		9.10		75.8
120-748B-14H-4, 68–70	119.28	11.10	11.26	0.00	93.8
120-748B-15H-2, 127–129	126.37		10.78		89.8
120-748B-15H-4, 126–128	129.36		10.98		91.5
120-748B-15H-6, 126–128	132.36		11.18		93.1
120-748B-16H-2, 30–32	134.73	11.55	11.56	0.00	96.3
120-748B-16H-4, 20–22	137.63		11.56		96.3
120-748B-16H-6, 20–22	140.63		11.46		95.5
120-748B-17H-2, 130–132	145.40	11.43	11.48	0.00	95.6
120-748B-17H-4, 130–132	148.40		11.47		95.6
120-748B-17H-6, 130–132	151.40	11.36	11.34	0.02	94.5
120-748B-18H-2, 130–132	154.90		11.47		95.6
120-748B-18H-4, 134–136	157.94	11.47	11.40	0.07	95.0
120-748B-18H-6, 132–134	160.92		11.12		92.6
120-748B-19H-2, 132–134	164.42	10.93	10.99	0.00	91.6
120-748B-19H-4, 132–134	167.42		11.11		92.6
120-748B-19H-6, 52–54	169.62		11.63		96.9
120-748B-20H-1, 59–61	171.69		11.45		95.4
120-748C-1R-1, 77–79	173.77	11.63	11.50	0.13	95.8
120-748B-20H-3, 84–86	174.94	11.53	11.46	0.07	95.5
120-748C-1R-2, 99–101	175.49		11.45		95.4
120-748B-23X-2, 106–108	199.16	11.51	11.54	0.00	96.1
120-748C-10R-1, 72–74	259.22	11.38	11.39	0.00	94.9
120-748C-10R-2, 35–37	260.35		11.44		95.3
120-748C-11R-CC, 1–2	268.01		11.53		96.0
120-748C-12R-1, 48–50	277.98	11.47	11.47	0.00	95.6
120-748C-14R-1, 126–128	297.76	11.49	11.54	0.00	96.1
120-748C-19R-1, 22–24	331.22	11.52	11.45	0.07	95.4
120-748C-21R-1, 24–26	350.24	11.55	11.55	0.00	96.2
120-748C-22R-1, 30–32	359.80	11.57	11.57	0.00	96.4
120-748C-23R-CC, 20–22	369.20		11.47		95.6
120-748C-24R-1, 1–3	378.51		7.45		62.1
120-748C-24R-1, 35–37	378.85	11.47	11.49	0.00	95.7

Table 9 (continued)

Core, section, interval (cm)	Depth (mbsf)	Total carbon (%)	Inorganic carbon (%)	Organic carbon (%)	Carbonate (%)
120-748C-24R-1, 62-64	379.12		6.76		56.3
120-748C-25R-CC, 1-3	389.10		11.39		94.9
120-748C-27R-2, 146-148	-999.99	9.04	8.64	0.40	72.0
120-748C-28R-1, 97-98	417.47		9.11		75.9
120-748C-28R-1, 98-99	417.48	4.28	4.06	0.22	33.8
120-748C-29R-1, 28-30	426.28	8.89	8.68	0.21	72.3
120-748C-30R-1, 131-133	436.81	8.98	8.73	0.25	72.7
120-748C-33R-1, 43-45	464.43	8.71	8.45	0.26	70.4
120-748C-34R-1, 81-83	474.31	9.82	9.63	0.19	80.2
120-748C-34R-1, 112-114	474.62		6.02		50.2
120-748C-35R-1, 87-89	483.87	9.13	8.99	0.14	74.9
120-748C-36R-1, 121-123	493.71		6.95		57.9
120-748C-36R-2, 70-71	494.70	6.00	5.81	0.19	48.4
120-748C-37R-1, 77-78	502.77		6.08		50.7
120-748C-37R-2, 67-69	504.17	10.26	9.89	0.37	82.4
120-748C-38R-1, 75-77	512.25	6.10	5.82	0.28	48.5
120-748C-38R-2, 8-10	513.08	10.58	10.26	0.32	85.5
120-748C-39R-1, 23-26	521.23	5.25	5.02	0.23	41.8
120-748C-39R-2, 55-56	523.05	10.82	9.97	0.85	83.1
120-748C-40R-1, 45-47	530.95	10.92	10.38	0.54	86.5
120-748C-41R-1, 18-20	540.18	3.59	3.18	0.41	26.5
120-748C-42R-1, 77-79	550.27	4.66	4.26	0.40	35.5
120-748C-43R-1, 96-98	559.96	4.88	4.58	0.30	38.2
120-748C-44R-1, 49-51	568.99	4.23	3.77	0.46	31.4
120-748C-44R-1, 107-109	569.57	4.88	4.51	0.37	37.6
120-748C-45R-1, 93-95	578.93	6.17	5.76	0.41	48.0
120-748C-46R-1, 5-7	587.55	4.42	4.20	0.22	35.0
120-748C-47R-1, 23-25	597.23	3.87	3.40	0.47	28.3
120-748C-47R-2, 44-46	598.94	6.02	4.98	1.04	41.5
120-748C-48R-1, 39-41	606.89	11.09	10.94	0.15	91.1
120-748C-49R-1, 115-117	617.15	4.09	3.67	0.42	30.6
120-748C-50R-1, 79-81	626.29	6.19	5.54	0.65	46.2
120-748C-51R-1, 52-54	635.52	6.23	5.50	0.73	45.8
120-748C-52R-1, 34-36	644.84	2.06	1.82	0.24	15.2
120-748C-53R-1, 63-66	654.63	5.06	4.37	0.69	36.4
120-748C-53R-2, 60-62	656.10	2.20	1.77	0.43	14.7
120-748C-54R-1, 26-28	663.76	1.41	0.87	0.54	7.3
120-748C-54R-2, 58-60	665.58		2.52		21.0
120-748C-54R-3, 22-24	666.72		1.78		14.8
120-748C-55R-1, 14-16	673.14	3.98	3.62	0.36	30.2
120-748C-55R-4, 29-31	677.51		2.71		22.6
120-748C-56R-1, 95-97	683.45	1.99	1.78	0.21	14.8
120-748C-56R-2, 107-109	685.07	1.70	1.31	0.39	10.9
120-748C-61R-1, 57-59	728.07	0.61	0.12	0.49	1.0
120-748C-61R-3, 57-59	731.07	0.63	0.11	0.52	0.9
120-748C-62R-1, 26-28	732.76	0.63	0.06	0.57	0.5
120-748C-62R-2, 27-29	734.27		0.05		0.4
120-748C-62R-3, 29-31	735.79		0.07		0.6
120-748C-62R-6, 108-110	741.08	0.39	0.08	0.31	0.7
120-748C-63R-1, 55-57	742.55	0.39	0.17	0.22	1.4
120-748C-63R-1, 78-79	742.78	0.66	0.35	0.31	2.9
120-748C-64R-1, 47-49	751.97	0.32	0.15	0.17	1.3
120-748C-64R-1, 56-59	752.06		0.13		1.1
120-748C-64R-2, 90-92	753.90		0.68		5.7
120-748C-64R-3, 94-96	755.44		0.35		2.9
120-748C-64R-4, 69-72	756.69	0.47	0.25	0.22	2.1
120-748C-65R-1, 10-12	761.10	0.45	0.22	0.23	1.8
120-748C-65R-1, 21-23	761.21		0.11		0.9
120-748C-66R-1, 57-59	771.07	0.51	0.10	0.41	0.8
120-748C-67R-1, 12-14	780.12	0.93	0.54	0.39	4.5
120-748C-68R-1, 55-57	790.05	1.22	1.17	0.05	9.8
120-748C-69R-1, 70-72	798.20	0.44	0.28	0.16	2.3
120-748C-70R-3, 63-65	810.63	1.00	0.86	0.14	7.2
120-748C-70R-5, 16-18	813.16		0.19		1.6
120-748C-71R-3, 115-117	820.65	1.32	0.99	0.33	8.3
120-748C-71R-7, 48-50	825.98		0.86		7.2
120-748C-72R-1, 79-80	826.79		0.90		7.5
120-748C-72R-4, 126-128	831.76	0.86	0.62	0.24	5.2
120-748C-73R-3, 35-37	838.85	0.57	0.42	0.15	3.5
120-748C-73R-6, 57-59	843.57	2.16	1.69	0.47	14.1
120-748C-74R-2, 69-71	847.19	1.61	1.30	0.31	10.8
120-748C-74R-4, 96-99	850.46		1.48		12.3
120-748C-75R-4, 8-11	859.08	0.90	0.69	0.21	5.8
120-748C-75R-6, 27-30	862.27		4.67		38.9
120-748C-76R-3, 30-32	867.30	1.04	0.52	0.52	4.3
120-748C-76R-5, 91-93	870.91	1.06	0.76	0.30	6.3

Table 9 (continued)

Core, section, interval (cm)	Depth (mbsf)	Total carbon (%)	Inorganic carbon (%)	Organic carbon (%)	Carbonate (%)
120-748C-77R-2, 124-126	876.24	0.73	0.61	0.12	5.1
120-748C-77R-4, 62-64	878.62		0.60		5.0
120-748C-77R-6, 41-43	881.41	6.21	6.16	0.05	51.3
120-748C-78R-2, 67-69	885.17		1.10		9.2
120-748C-78R-4, 131-133	888.81		0.79		6.6
120-748C-78R-6, 25-27	890.75	3.09	2.60	0.49	21.7
120-748C-79R-2, 119-122	895.19	1.35	1.17	0.18	9.8
120-748C-79R-4, 29-31	896.40		0.83		6.9
120-748C-79R-5, 16-19	897.75	5.31	5.10	0.21	42.5

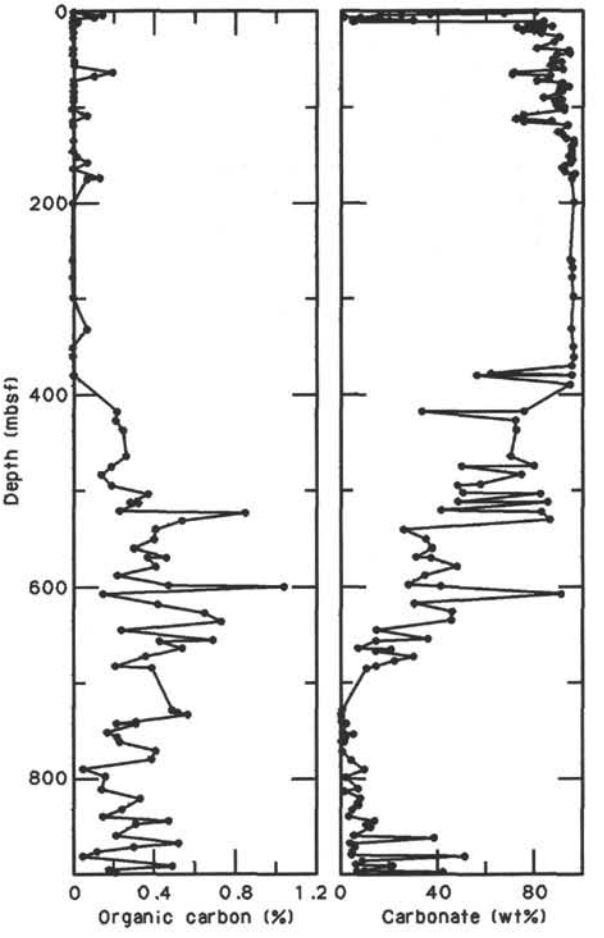

Figure 46. Total organic carbon and carbonate contents plotted vs. depth at Site 748.

quence correlates with another interval of relatively low carbonate content from 109 to 115 mbsf. In addition, the transition from the Eocene to the Oligocene as determined by planktonic foraminifer biostratigraphy occurs somewhere within this interval (see "Biostratigraphy" section, this chapter).

Below this interval to 370 mbsf, the carbonate contents are extremely high, averaging 95%. Unfortunately, several chert string-

ers were encountered during drilling of this interval, resulting in poor recovery and, consequently, a poor sampling resolution. Nonetheless, based on the few samples recovered, it appears that carbonate concentrations are consistently high throughout this portion of the sequence. From the base of this interval to the bottom of the hole (900 mbsf), carbonate contents show an overall decline.

Superimposed on the overall decline are numerous high-amplitude fluctuations. From 400 to 700 mbsf, these changes appear to be associated with alternating intervals of silica and carbonate-cemented grainstones. Below this, most of the variability in the carbonate record reflects alternating concentrations of biogenic and terrigenous components.

Overall, organic carbon contents are low at Site 748 (Fig. 46). Sediments from 0 to 400 mbsf contain essentially no organic carbon. In sharp contrast, the sediments from 400 to 900 mbsf contain from 0.2% to 1.0% organic carbon with the average near 0.45%. This trend is clearly reflected in color and mineral changes observed in split cores from this site. The upper 400 m of sediment consist mainly of white to white gray diatom and nannofossil oozes and chalk, while the lower 500 m of sediment are composed predominantly of dark green to black grainstones, siltstones, and claystones rich in fine-grained pyrite and glauconite (see "Sedimentology" section, this chapter).

The decrease in organic carbon content upsection may reflect changes in sedimentation rates, which decrease from the Late Cretaceous through the Cenozoic, as well as the source of organic matter, which is a mix of terrestrial and marine in the Cretaceous and mainly just marine above.

Rock-Eval

Rock-Eval analyses provide an estimate of the source and maturity of sedimentary organic matter. At Site 748 analyses were conducted on a small number of the organic-carbon-bearing samples from 417.48 to 876.24 mbsf; results are listed in Table 10. The number of analyses were limited due to instrument malfunction. Analytical techniques are outlined in the "Explanatory Notes" chapter (this volume).

Under normal operating procedures, the total organic carbon (TOC) is determined by the Rock-Eval and is used to calculate the hydrogen (HI) and oxygen (OI) index. However, an instrument malfunction prevented measurement of TOC, thereby making it necessary to substitute TOC values obtained from the coulometer to calculate the various indexes. The hydrogen indexes range from 0 to 227 mg/g. There is no clear trend in the distribution of values with depth, although the two highest HI values were recorded in adjacent Cores 120-748C-38R and -39R.

The oxygen indexes show considerable variability, with values ranging from 55 to 391 mg/g. Plotted on a van Krevelen diagram (Tissot and Welte, 1984), most of the sample values fall in the type III field with a few in the region between types II and III (Fig. 47). The results of the analyses are similar to those recorded for Upper Cretaceous South Atlantic green claystones with low organic carbon contents (Deroo et al., 1984) and indi-

Table 10. Results of Rock-Eval analyses of discrete samples from 500–900 mbsf at Hole 748C.

Core, section, interval (cm)	Depth (mbsf)	Wt. (mg)	T_{max} (°C)	S_1	S_2	S_3	PI	S_2/S_3	PC	TOC (%)	HI	OI
120-748C-												
28R-1, 98–99	417.48	93.2	356	0.03	0.00	0.74	1.00	0.00	0.00	0.22	0	336
30R-1, 131–133	436.81	19.0	415	0.00	0.07	0.75	0.00	0.09	0.00	0.25	28	300
33R-1, 43–45	464.43	97.9	314	0.05	0.00	0.54	1.00	0.00	0.00	0.26	0	207
34R-1, 81–83	474.31	9.0	330	0.03	0.03	0.45	0.50	0.06	0.00	0.19	15	236
35R-1, 87–89	483.87	5.6	239	0.04	0.00	0.52	1.00	0.00	0.00	0.14	0	371
36R-2, 70–71	494.70	95.3	325	0.18	0.01	0.56	1.00	0.01	0.01	0.19	5	294
37R-2, 67–69	504.17	3.4	429	0.05	0.10	0.53	0.36	0.18	0.01	0.37	27	143
38R-2, 8–10	513.08	0.9	421	0.02	0.49	0.54	0.04	0.90	0.04	0.32	153	168
39R-2, 55–57	523.05	97.9	443	0.09	1.93	0.62	0.04	3.11	0.16	0.85	227	72
40R-1, 45–47	530.95	97.3	435	0.02	0.31	0.51	0.06	0.60	0.02	0.54	57	94
41R-1, 18–20	540.18	98.8	426	0.05	0.17	0.48	0.23	0.35	0.01	0.41	41	117
42R-1, 77–79	550.27	97.1	426	0.10	0.18	0.46	0.36	0.39	0.02	0.40	45	115
43R-1, 96–98	559.96	6.8	415	0.21	0.20	0.70	0.52	0.28	0.03	0.30	66	233
44R-1, 49–51	568.99	3.2	419	0.06	0.27	0.73	0.19	0.36	0.02	0.46	58	158
45R-1, 93–95	578.93	92.6	423	0.08	0.29	0.75	0.22	0.38	0.03	0.41	70	182
46R-1, 5–7	587.55	14.3	374	0.07	0.09	0.79	0.44	0.11	0.01	0.22	40	359
47R-2, 44–46	598.94	3.9	434	0.08	1.49	0.73	0.05	2.04	0.13	1.04	143	70
48R-1, 39–41	606.89	106.4	431	0.00	0.03	0.18	0.00	0.16	0.00	0.15	20	120
49R-1, 115–117	617.15	101.3	428	0.08	0.42	0.60	0.16	0.70	0.04	0.42	100	142
50R-1, 79–81	626.29	100.2	430	0.09	0.54	0.52	0.15	1.03	0.05	0.65	83	80
51R-1, 52–54	635.52	98.2	434	0.08	0.62	0.59	0.11	1.05	0.05	0.73	84	80
52R-1, 34–36	644.84	98.4	434	0.14	0.27	0.61	0.35	0.44	0.03	0.24	112	254
53R-1, 63–65	654.63	100.0	428	0.13	0.49	0.83	0.21	0.59	0.05	0.69	71	120
53R-2, 60–62	656.10	107.6	462	0.13	0.29	0.64	0.31	0.45	0.03	0.43	67	148
54R-1, 26–28	663.76	100.3	432	0.16	0.36	0.56	0.31	0.64	0.04	0.54	66	103
55R-1, 14–16	673.14	100.1	418	0.08	0.20	0.90	0.29	0.22	0.02	0.36	55	250
56R-1, 95–97	683.45	101.7	364	0.08	0.10	0.59	0.44	0.16	0.01	0.21	47	280
56R-2, 107–109	685.07	104.2	428	0.03	0.12	0.58	0.21	0.20	0.01	0.39	30	148
61R-1, 57–59	728.07	105.4	486	0.05	0.23	0.28	0.18	0.82	0.02	0.49	46	57
61R-3, 57–59	731.07	106.5	431	0.07	0.19	0.29	0.27	0.65	0.02	0.52	36	55
62R-1, 26–28	732.76	111.7	430	0.04	0.17	0.42	0.20	0.40	0.01	0.57	29	73
62R-6, 108–109	741.08	106.7	370	0.05	0.05	0.42	0.50	0.11	0.00	0.31	16	135
63R-1, 78–79	742.78	106.9	311	0.02	0.03	0.52	0.50	0.05	0.00	0.31	9	167
64R-1, 47–49	751.97	110.1	311	0.00	0.00	0.27		0.00	0.00	0.17	0	158
65R-1, 10–12	761.10	112.7	272	0.04	0.00	0.22	1.00	0.00	0.00	0.23	0	95
71R-3, 115–117	820.65	106.0	369	0.00	0.06	1.03	0.00	0.05	0.00	0.42	14	245
77R-2, 124–126	876.24	112.7	250	0.00	0.00	0.47		0.00	0.00	0.12	0	391

Note: PI = production index; PC = pyrolized carbon; TOC = total organic carbon; HI = hydrogen index; and OI = oxygen index. TOC values were obtained from coulometric analyses.

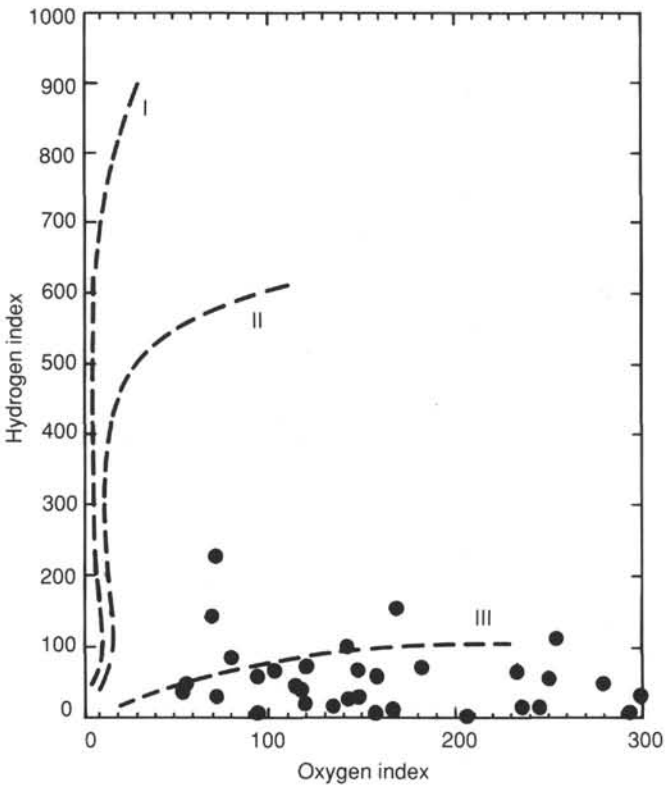

Figure 47. Van Krevelen plot of hydrogen (mg HC/g TOC) and oxygen (mg CO_2/g TOC) indexes of organic matter determined from Rock-Eval analyses of samples from Hole 748C.

cate that the organic matter (OM) from 500 to 900 mbsf at Site 748 is composed of terrestrial and/or highly oxidized marine OM. The presence of terrestrial organic matter is confirmed by visual observations of woody particles in cores from the lower portion of the sequence (see "Sedimentology" section, this chapter). The two samples with high hydrogen index values, 120-748C-38R-2, 8–10 cm and 55–57 cm, as well as all overlying samples, may contain mainly highly oxidized marine organic matter. This would be consistent with the separation and subsidence of land masses during the Late Cretaceous (Colwell et al., 1988) and the associated transition from a shallow to deeper shelf to a hemipelagic depositional environment.

Hydrocarbon Gases

Gases were extracted from gas pockets in the core barrel by vacutainer before splitting, and from sediment samples by headspace techniques. Headspace analyses were conducted on a routine basis with sampling of every third core. An outline of analytical procedures is provided in the "Explanatory Notes" chapter (this volume).

Hydrocarbon gas concentrations were extremely low in all samples analyzed at Site 748. The C_1 and C_2 gases were just above the detectable limit in both headspace and vacutainer extractions.

PHYSICAL PROPERTIES

Introduction

The objective of the physical properties program at Site 748 was to aid in the interpretation of stratigraphic and geophysical data from the Raggatt Basin, Southern Kerguelen Plateau. We cored three holes: 748A, 748B, and 748C. Two cores were recovered by the APC technique from Hole 748A; no mud line was recovered and the hole was abandoned at 19.0 mbsf. Hole 748B was completed by APC and XCB techniques to 225.1 mbsf. Hole 748C employed the RCB to a depth of 935.0 mbsf. Measurements were made at regular intervals in order to determine the physical properties of the sediment and rock comprising the lithologic column at Site 748. The results of the determinations are displayed in tabular and graphic form. In several of the summary figures the physical properties data from the three holes have been combined to form semicontinuous profiles for Site 748.

At Site 748 the physical properties were determined as follows: (1) index properties (grain density, water content, and porosity) in discrete samples, and wet-bulk density in discrete samples as well as with the continuous gamma ray attenuation (GRAPE) method (Figs. 48 and 49; Table 11); (2) compressional wave velocity, in discrete samples (Hamilton Frame [HF]) and through whole APC and XCB cores (*P*-wave logger [PWL]; Figs. 50–52; Table 12); (3) undrained shear strength (Fig. 53; Table 13); (4) thermal conductivity (Figs. 54 and 55; Table 14); and (5) temperature at the mud line and in the holes (Fig. 56; Table 15).

Geotechnical stratigraphy employs physical properties data to define distinctive geotechnical units within a sedimentary section (Taylor, 1984). The geotechnical properties of a particular unit are the result of both depositional and post-depositional processes. At Site 748 variations in index properties, compressional wave velocity, and carbonate content have been used to delineate five geotechnical units; these may be correlated with the lithologic units (see "Lithostratigraphy and Sedimentology" section, this chapter). Variations in the physical properties of sediment can commonly be correlated with the environmental and tectonic history of a region. The physical properties data provide a vital link between geophysical data from a site and the stratigraphic record determined from core material.

The methods employed in the measurement of physical properties during Leg 120 are described in the "Explanatory Notes" chapter (this volume). A more detailed discussion of these measurements can be found in Lambe and Whitman (1969) and Boyce (1976, 1977).

Index Properties

Values for index properties determined from Site 748 samples appear in Table 11 and are plotted in Figure 48. For discrete samples, a Scientec balance was employed for weight determinations, a Penta pycnometer for volume measurements, and a Labconco freeze-dry apparatus for drying. The GRAPE was used on APC and XCB cores for continuous determinations of wet-bulk density. Poor core recovery and disturbance caused by the RCB technique below ~180 mbsf did not allow closely spaced physical properties sampling, and biases toward recovered material may exist.

Downhole variations in index properties commonly correlate with changes in sediment lithology (see "Lithostratigraphy and Sedimentology" section, this chapter) and carbonate content (see "Organic Geochemistry" section, this chapter). Overall downhole trends in index properties indicate a general inverse relation between wet-bulk density and water content (Fig. 48). An inverse relation also appears between carbonate and porosity (Fig. 49).

From the seafloor to 10.5 mbsf wet-bulk density is low (< 1.65 g/cm^3); water content is high (> 40%); porosity is high (> 66%); and carbonate content is generally < 70% (Figs. 48 and 49). The uppermost 15.5 m of sediment at Site 748 consist primarily of diatom ooze.

Between 10.5 and ~400 mbsf index properties change very little, with the exception of sharp anomalies caused by chert ho-

Table 11. Index properties data from Site 748.

Core, section, interval (cm)	Depth (mbsf)	Water content (%)	Porosity (%)	Wet-bulk density (g/cm^3)	Dry-bulk density (g/cm^3)	Grain density (g/cm^3)
120-748B-2H-1, 50	0.60	44.04	66.81	1.59	0.89	2.59
120-748A-1H-2, 104	2.54	49.82	70.54	1.50	0.75	2.43
120-748B-2H-3, 16	3.26	45.66	66.47	1.49	0.81	2.38
120-748A-1H-3, 136	4.36	52.21	73.00	1.45	0.69	2.49
120-748A-1H-4, 134	5.84	75.61	85.42	1.16	0.28	1.86
120-748B-2H-5, 55	6.65	69.67	83.16	1.27	0.39	2.14
120-748B-2H-7, 46	9.56	54.81	74.31	1.44	0.65	2.40
120-748A-1H-7, 80	9.80	61.84	79.09	1.35	0.51	2.34
120-748A-2H-1, 100	10.50	65.68	78.66	1.29	0.44	1.92
120-748B-3H-1, 121	10.81	33.99	57.29	1.77	1.17	2.64
120-748B-3H-3, 49	13.09	39.65	62.79	1.67	1.01	2.60
120-748B-3H-5, 47	16.07	37.64	62.23	1.71	1.07	2.76
120-748A-2H-5, 100	16.50	42.03	64.72	1.60	0.93	2.56
120-748B-3H-7, 46	19.06	40.97	64.36	1.62	0.96	2.63
120-748B-4H-1, 133	20.43	40.34	63.12	1.65	0.99	2.56
120-748B-4H-3, 52	22.62	42.97	65.83	1.59	0.91	2.59
120-748B-4H-5, 132	26.42	36.60	60.09	1.73	1.10	2.64
120-748B-5H-5, 50	35.10	37.98	61.68	1.71	1.06	2.66
120-748B-5H-7, 43	38.03	42.71	65.66	1.61	0.92	2.59
120-748B-6H-2, 124	40.84	35.74	60.41	1.76	1.13	2.78
120-748B-6H-4, 54	43.14	34.10	58.07	1.75	1.16	2.71
120-748B-6H-6, 52	46.12	37.98	60.34	1.68	1.04	2.51
120-748B-7H-2, 100	50.10	40.10	62.57	1.64	0.98	2.53
120-748B-7H-4, 69	52.79	36.52	59.93	1.71	1.09	2.63
120-748B-7H-6, 77	55.87	37.06	60.66	1.72	1.08	2.65
120-748B-8H-3, 83	60.93	36.97	60.60	1.74	1.10	2.66
120-748B-8H-5, 87	63.97	42.16	63.62	1.59	0.92	2.42
120-748B-8H-6, 81	65.41	44.32	66.65	1.57	0.87	2.54
120-748B-9H-1, 61	67.21	39.75	65.15	1.69	1.02	2.87
120-748B-9H-3, 116	70.76	37.73	62.40	1.70	1.06	2.77
120-748B-9H-4, 127	72.37	36.01	58.53	1.70	1.09	2.54
120-748B-9H-6, 22	74.32	32.17	55.34	1.78	1.21	2.65
120-748B-10H-1, 125	77.35	34.23	58.58	1.78	1.17	2.75
120-748B-10H-2, 81	78.41	33.67	57.83	1.77	1.17	2.74
120-748B-10H-4, 76	81.36	36.15	59.07	1.72	1.10	2.58
120-748B-10H-6, 41	84.01	33.52	57.89	1.77	1.18	2.76
120-748B-11H-1, 122	86.82	35.27	58.42	1.72	1.12	2.61
120-748B-11H-3, 126	89.86	36.57	60.96	1.72	1.09	2.74
120-748B-11H-5, 44	92.04	34.46	58.08	1.76	1.16	2.67
120-748B-11H-6, 25	93.35	36.21	57.74	1.70	1.09	2.44
120-748B-12H-2, 119	97.79	34.04	58.35	1.78	1.17	2.75
120-748B-12H-3, 129	99.39	33.72	57.64	1.78	1.18	2.71
120-748B-12H-4, 136	100.96	32.30	55.83	1.79	1.21	2.68
120-748B-12H-6, 36	102.96	32.28	54.73	1.83	1.24	2.57
120-748B-13H-4, 57	109.67	42.45	66.11	1.59	0.92	2.67
120-748B-13H-6, 57	112.67	42.25	65.31	1.63	0.94	2.60
120-748B-14H-1, 34	114.44	37.13	60.87	1.73	1.09	2.67
120-748B-14H-2, 15	115.75	39.25	62.60	1.62	0.99	2.62
120-748B-14H-4, 68	119.28	34.85	58.90	1.76	1.15	2.72
120-748B-15H-2, 127	126.37	37.47	60.42	1.68	1.05	2.58
120-748B-15H-4, 126	129.36	34.16	58.75	1.79	1.18	2.78
120-748B-15H-6, 126	132.36	31.75	55.09	1.79	1.22	2.67
120-748B-16H-2, 20	134.63	32.49	56.10	1.81	1.22	2.69
120-748B-16H-4, 20	137.63	31.40	54.88	1.81	1.24	2.69
120-748B-16H-6, 20	140.63	32.17	58.01	1.91	1.30	2.95
120-748B-17H-2, 130	145.40	35.13	60.44	1.81	1.17	2.86
120-748B-17H-4, 130	148.40	34.36	59.27	1.80	1.18	2.82
120-748B-17H-6, 130	151.40	34.76	57.77	1.74	1.13	2.60
120-748B-18H-2, 130	154.90	33.39	58.55	1.84	1.22	2.86
120-748B-18H-4, 134	157.94	31.62	56.44	1.86	1.27	2.84
120-748B-18H-6, 132	160.92	32.49	56.10	1.80	1.21	2.69
120-748B-19H-2, 132	164.42	37.65	61.17	1.73	1.08	2.64
120-748B-19H-4, 132	167.42	34.84	60.71	1.79	1.17	2.93
120-748B-19H-6, 52	169.62	32.67	55.84	1.80	1.21	2.64
120-748B-20H-1, 59	171.69	31.47	56.38	1.86	1.28	2.85
120-748C-1R-1, 77	173.77	0.81	2.15	1.79	1.77	2.75
120-748B-20H-3, 84	174.94	26.44	47.72	1.88	1.38	2.57
120-748C-1R-2, 99	175.49	56.93	79.00	1.79	0.77	2.87
120-748B-22X-CC, 2	187.12	5.44	11.26	2.35	2.22	2.24
120-748B-22X-CC, 7	187.17	2.06	4.66	2.45	2.40	2.36
120-748B-22X-CC, 8	187.18	1.15	2.83	2.68	2.64	2.54
120-748B-23X-2, 106	199.16	32.37	56.63	2.99	2.03	2.77
120-748C-10R-1, 72	259.22	34.03	58.90	3.50	2.31	2.82
120-748C-10R-2, 35	260.35	24.16	44.88	1.06	0.81	2.59
120-748C-11R-CC, 4	268.04	28.67	50.65	1.89	1.35	2.59
120-748C-12R-1, 48	277.98	31.18	54.84	1.92	1.32	2.72
120-748C-14R-1, 126	297.76	28.03	51.17	1.91	1.37	2.73
120-748C-19R-1, 22	331.22	29.80	53.56	1.95	1.37	2.75
120-748C-21R-1, 24	350.24	26.37	49.12	1.97	1.45	2.73
120-748C-22R-1, 30	359.80	30.25	52.44	1.82	1.27	2.58
120-748C-23R-CC, 20	369.20	28.28	51.25	1.90	1.36	2.70
120-748C-24R-1, 1	378.51	23.75	45.14	2.03	1.55	2.68
120-748C-24R-1, 35	378.85	26.68	48.16	1.99	1.46	2.59
120-748C-24R-1, 62	379.12	38.59	62.39	2.14	1.32	2.67
120-748C-25R-C, 1	389.10	8.18	20.15	1.97	1.81	2.88
120-748C-27R-2, 148	412.00	24.23	47.27	2.05	1.56	2.85
120-748C-28R-1, 97	417.47	21.93	42.90	2.09	1.63	2.71
120-748C-28R-1, 99	417.49	8.70	18.27	2.21	2.02	2.38
120-748C-29R-1, 28	426.28	21.99	43.44	2.04	1.59	2.77

Table 11 (continued).

Core, section, interval (cm)	Depth (mbsf)	Water content (%)	Porosity (%)	Wet-bulk density (g/cm^3)	Dry-bulk density (g/cm^3)	Grain density (g/cm^3)
120-748C-30R-1, 131	436.81	2.02	4.28	2.12	2.07	2.20
120-748C-32R-1, 38	454.88	17.15	36.42	2.22	1.84	2.81
120-748C-33R-1, 43	464.43	10.72	23.41	2.48	2.21	2.59
120-748C-34R-1, 81	474.31	15.73	33.83	2.34	1.98	2.78
120-748C-34R-1, 112	474.62	4.98	10.93	2.39	2.27	2.38
120-748C-35R-1, 87	483.87	23.10	44.93	2.07	1.59	2.76
120-748C-36R-1, 121	493.71	9.67	22.33	2.33	2.11	2.73
120-748C-36R-2, 70	494.70	7.54	16.58	2.47	2.28	2.47
120-748C-37R-1, 77	502.77	5.81	12.78	2.27	2.14	2.42
120-748C-37R-2, 67	504.17	13.40	29.42	2.39	2.07	2.74
120-748C-38R-1, 75	512.25	8.53	18.27	2.34	2.14	2.43
120-748C-38R-2, 8	513.08	12.76	28.20	2.35	2.05	2.73
120-748C-39R-1, 23	521.23	6.73	14.13	2.48	2.31	2.32
120-748C-39R-2, 55	523.05	6.97	16.30	2.54	2.37	2.64
120-748C-40R-1, 45	530.95	16.19	33.70	2.23	1.87	2.67
120-748C-41R-1, 18	540.18	7.57	16.64	2.96	2.74	2.48
120-748C-42R-1, 77	550.27	7.48	16.89	2.46	2.27	2.55
120-748C-43R-1, 96	559.96	6.19	14.06	2.52	2.37	2.52
120-748C-44R-1, 49	568.99	10.23	20.17	2.20	1.97	2.25
120-748C-44R-1, 107	569.57	17.94	34.47	2.03	1.67	2.44
120-748C-45R-1, 93	578.93	29.83	51.72	2.43	1.70	2.55
120-748C-46R-1, 5	587.55	9.39	20.65	2.21	2.01	2.55
120-748C-47R-1, 23	597.23	23.01	40.02	1.83	1.41	2.26
120-748C-47R-2, 44	598.94	20.96	39.32	2.03	1.60	2.48
120-748C-48R-1, 39	606.89	6.81	16.60	2.57	2.40	2.77
120-748C-49R-1, 115	617.15	18.75	35.90	2.02	1.64	2.46
120-748C-50R-1, 79	626.29	19.50	37.51	2.04	1.64	2.51
120-748C-51R-1, 52	635.52	28.84	50.69	1.84	1.31	2.57
120-748C-52R-1, 34	644.84	11.33	21.54	2.07	1.84	2.18
120-748C-53R-1, 63	654.63	22.42	46.29	3.65	2.83	3.03
120-748C-53R-2, 60	656.10	13.77	27.53	2.30	1.98	2.42
120-748C-54R-1, 26	663.76	18.74	37.16	2.13	1.73	2.60
120-748C-54R-2, 58	665.58	26.18	49.04	2.27	1.68	2.75
120-748C-54R-3, 22	666.72	22.35	45.27	2.34	1.82	2.92
120-748C-55R-1, 14	673.14	24.15	43.21	2.08	1.58	2.42
120-748C-55R-4, 29	677.51	22.11	42.63	2.04	1.59	2.66
120-748C-56R-1, 96	683.46	24.20	45.67	1.96	1.48	2.67
120-748C-56R-2, 107	685.07	22.81	43.91	2.09	1.62	2.69
120-748C-61R-1, 57	728.07	24.69	45.98	1.97	1.48	2.63
120-748C-61R-3, 57	731.07	34.33	51.75	1.94	1.27	2.07
120-748C-62R-1, 27	732.77	23.51	44.42	2.04	1.56	2.64
120-748C-62R-2, 27	734.27	23.42	44.54	1.96	1.50	2.67
120-748C-62R-3, 29	735.79	25.50	45.60	1.91	1.43	2.48
120-748C-62R-6, 108	741.08	28.60	50.01	1.89	1.35	2.53
120-748C-63R-1, 55	742.55	28.71	52.44	1.99	1.42	2.78
120-748C-64R-1, 56	752.06	22.68	43.46	2.08	1.61	2.66
120-748C-64R-2, 90	753.90	21.72	43.37	2.17	1.70	2.80
120-748C-64R-3, 94	755.44	27.02	52.72	2.26	1.65	3.06
120-748C-64R-4, 69	756.69	24.81	45.65	2.00	1.50	2.58
120-748C-65R-1, 21	761.21	26.75	50.64	2.08	1.52	2.85
120-748C-66R-1, 57	771.07	24.70	47.49	2.11	1.59	2.80
120-748C-67R-1, 12	780.12	27.09	50.84	2.03	1.48	2.82
120-748C-68R-1, 55	790.05	26.89	52.19	2.11	1.54	3.01
120-748C-69R-1, 70	798.20	25.46	49.03	2.11	1.57	2.86
120-748C-70R-1, 46	807.46	24.43	46.12	2.03	1.53	2.69
120-748C-70R-3, 63	810.63	42.95	67.11	2.72	1.55	2.74
120-748C-70R-5, 16	813.16	23.43	45.39	2.12	1.62	2.76
120-748C-71R-1, 113	817.63	22.48	45.59	2.23	1.73	2.93
120-748C-71R-2, 94	818.94	24.75	44.69	1.94	1.46	2.49
120-748C-71R-3, 115	820.65	25.54	48.97	2.04	1.52	2.84
120-748C-71R-4, 111	822.11	24.43	46.10	2.07	1.57	2.68
120-748C-71R-5, 72	823.22	22.03	42.87	2.10	1.64	2.70
120-748C-71R-7, 48	825.98	24.28	47.98	2.09	1.59	2.92
120-748C-72R-1, 79	826.79	1.34	3.54	1.67	1.65	2.74
120-748C-72R-3, 123	830.23	53.82	76.90	3.31	1.53	2.88
120-748C-72R-4, 126	831.76	1.26	3.32	1.68	1.66	2.74
120-748C-73R-1, 93	836.43	23.74	46.33	2.14	1.63	2.81
120-748C-73R-2, 25	837.25	24.26	47.69	2.06	1.56	2.89
120-748C-73R-3, 35	838.85	22.63	44.26	2.06	1.59	2.76
120-748C-73R-4, 34	840.34	23.49	44.76	2.06	1.58	2.68
120-748C-73R-5, 128	842.78	25.62	49.69	2.04	1.52	2.91
120-748C-73R-6, 57	843.57	23.93	45.76	2.07	1.57	2.72
120-748C-74R-1, 62	845.62	23.46	46.17	2.13	1.63	2.84
120-748C-74R-2, 69	847.19	23.70	46.66	2.12	1.62	2.86
120-748C-74R-3, 69	848.69	29.42	53.77	1.98	1.40	2.83
120-748C-74R-4, 96	850.46	27.32	51.40	1.96	1.43	2.85
120-748C-75R-1, 52	855.02	24.48	54.99	2.09	1.58	3.83
120-748C-75R-4, 8	859.08	26.06	50.32	2.20	1.63	2.92
120-748C-75R-6, 27	862.27	19.51	41.54	2.21	1.78	2.98
120-748C-76R-1, 39	864.39	23.91	46.94	2.23	1.70	2.86
120-748C-76R-3, 30	867.30	26.32	49.75	2.20	1.62	2.81
120-748C-76R-5, 91	870.91	24.29	46.31	2.15	1.62	2.73
120-748C-77R-1, 90	874.40	19.63	39.58	2.15	1.73	2.72
120-748C-77R-2, 124	876.24	18.75	38.73	2.18	1.77	2.78
120-748C-77R-3, 138	877.88	8.18	19.68	2.51	2.31	2.80
120-748C-77R-4, 62	878.62	20.57	42.68	2.21	1.75	2.92
120-748C-77R-5, 58	880.08	21.33	43.22	2.19	1.73	2.85
120-748C-77R-6, 41	881.41	5.68	15.28	2.91	2.74	3.04
120-748C-78R-1, 64	883.64	24.45	47.25	2.13	1.61	2.81

Table 11 (continued).

Core, section, interval (cm)	Depth (mbsf)	Water content (%)	Porosity (%)	Wet-bulk density (g/cm^3)	Dry-bulk density (g/cm^3)	Grain density (g/cm^3)
120-748C-78R-2, 67	885.17	22.78	45.59	2.11	1.63	2.88
120-748C-78R-4, 131	888.81	1.90	3.81	2.05	2.01	2.07
120-748C-78R-6, 25	890.75	22.26	45.42	2.25	1.75	2.95
120-748C-79R-1, 24	892.74	24.78	48.42	2.09	1.57	2.89
120-748C-79R-2, 119	895.19	23.35	45.96	2.14	1.64	2.83
120-748C-79R-3, 50	896.00	25.57	51.14	2.12	1.58	3.09
120-748C-79R-4, 29	896.40	26.02	50.48	2.24	1.65	2.94
120-748C-79R-4, 78	896.89	13.68	30.84	2.38	2.06	2.86
120-748C-79R-4, 121	897.32	12.30	27.49	2.53	2.22	2.75
120-748C-79R-5, 16	897.75	9.10	22.10	2.81	2.56	2.88
120-748C-79R-5, 19	897.78	3.41	8.10	2.53	2.44	2.54
120-748C-79R-5, 88	898.47	4.29	10.77	2.62	2.51	2.74
120-748C-79R-5, 112	898.71	5.76	13.36	2.60	2.45	2.56
120-748C-79R-6, 15	899.14	4.54	10.87	2.65	2.53	2.60
120-748C-79R-6, 44	899.43	4.54	10.80	2.67	2.54	2.59
120-748C-79R-7, 66	900.98	3.28	7.92	2.82	2.73	2.57

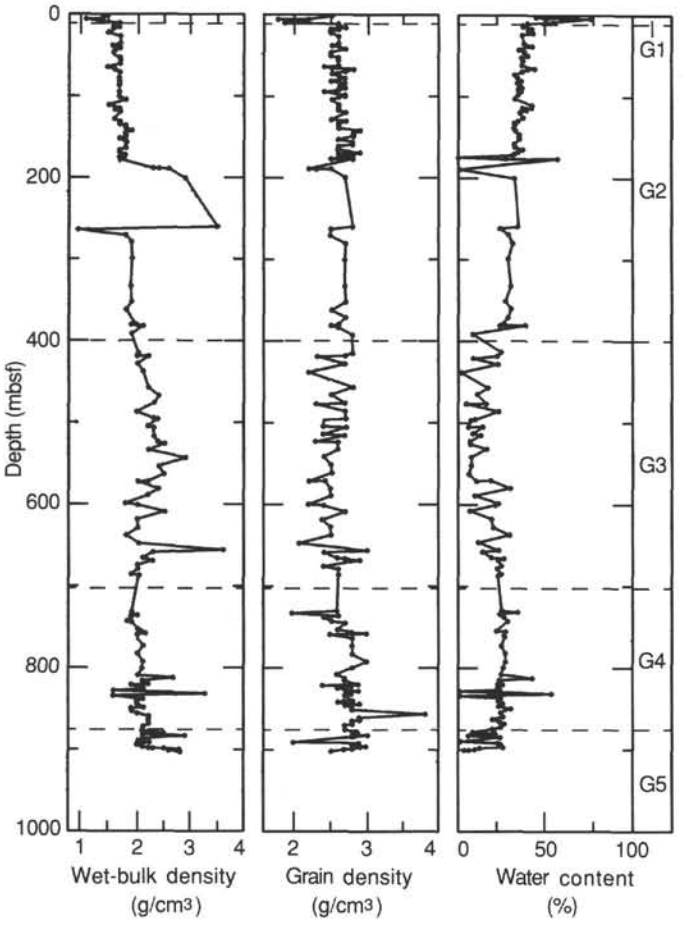

Figure 48. Overview of index properties (wet-bulk density, grain density, and water content) from 0–1000 mbsf, with the geotechnical units delineated as defined in the text, Site 748.

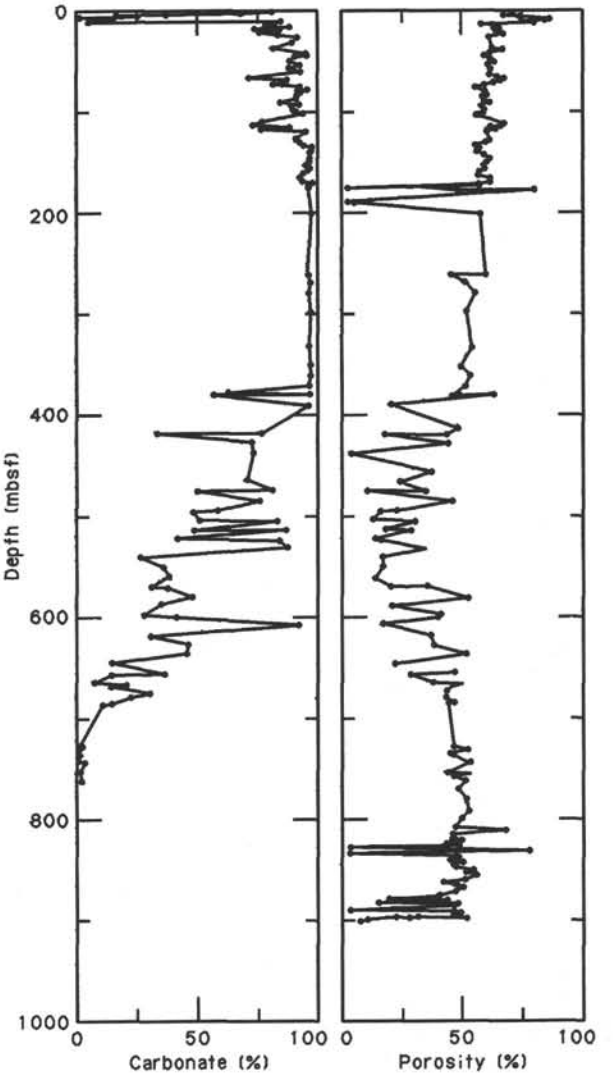

Figure 49. Downhole summary of carbonate content and porosity, Site 748.

rizons between ~185 and ~260 mbsf (Fig. 48). Downward through the entire interval, wet-bulk density gradually increases from ~1.60 to ~1.90 g/cm^3, water content gradually decreases from ~40% to ~25%, porosity gradually decreases from ~65% to ~50%, and carbonate content commonly ranges between ~70% and ~95% (Fig. 49). A downhole transition in lithology from dominantly siliceous (diatom ooze) to calcareous (nannofossil ooze) sediment occurs at 15.5 mbsf, and the section remains overwhelmingly calcareous to 397.4 mbsf. More scatter is observed in the data below ~350 mbsf.

A convex trend is observed in wet-bulk density values between ~400 and ~700 mbsf, corresponding to concave trends in water content and porosity (Fig. 48). Wet-bulk density commonly ranges from ~1.90 to ~2.60 g/cm^3, water content from ~30% to ~5%, and porosity from ~50% to ~10% in the interval. The dominant lithologies are glauconitic, bioclastic grainstone and wackestone. Carbonate content gradually decreases from >90% at ~400 mbsf to <10% at ~700 mbsf (Fig. 49).

Between ~700 and ~875 mbsf wet-bulk density, water content, porosity, and carbonate content values show little change, although a fair amount of scatter is observed (Figs. 48 and 49). Wet-bulk density ranges from ~1.90 to ~2.25 g/cm^3, water content from ~20% to ~30%, porosity from ~40% to ~55%, and carbonate content from 5% to 0%. Glauconitic sand-, silt-, and claystone were recovered from this interval.

Below ~875 mbsf index properties, especially porosity, show a large amount of scatter (Figs. 48 and 49). Between ~875 and ~900 mbsf, porosity varies from <5% to >50%, water content from ~2% to 26%, and wet-bulk density from 2.05 to 2.82

g/cm^3. Siltstone lacking any carbonate and basalt were recovered from the interval.

Compressional Wave Velocity

At Site 748 compressional wave velocities were calculated from both discrete (HF) and continuous (PWL) measurements (Table 12; Figs. 50–53). Discrete samples were measured downhole to 900.98 mbsf. Measurements were generally made parallel to bedding, although some samples were oriented perpendicular to bedding to investigate velocity anisotropy. The PWL was used for those APC and XCB cores that completely filled the core liners. Void spaces within the liner result in inaccurate values for compressional wave traveltimes and attenuate sonic signal strength. Thus, RCB cores are not suitable for PWL measurements.

The two techniques produce comparable velocity data. Neither technique, however, allows for velocity determination at *in-situ* pressure-temperature conditions, making correlation with logging and site survey multichannel seismic reflection (MCS) data difficult. The variations in compressional wave velocities downhole commonly correlate with changes in sediment lithology (see "Lithostratigraphy and Sedimentology" section, this chapter).

Sonic velocity is relatively uniform at ~1540 m/s between the seafloor and ~180 mbsf (Fig. 51). The lithology in this interval consists of 15.5 m of diatom ooze underlain by nannofossil ooze extending to 180.6 mbsf. Starting at ~180 mbsf, chert with a velocity between ~3700 and ~4800 m/s was encountered downhole, and recovery decreased severely in alternating nannofossil ooze and chert layers. The few samples between ~180 and ~400 mbsf for which compressional velocity could be determined show an increasing downhole trend, from ~1550 to ~2000 m/s.

At ~400 mbsf compressional wave velocity increases from 3600 to 3700 m/s as downhole lithology changes abruptly from nannofossil ooze and chert to glauconitic, bioclastic grainstone and wackestone. Two trends are observed downhole in the ~400 to ~700 mbsf interval: one of high velocity that decreases with depth, and one of low velocity that has a slightly convex shape (Fig. 51). The higher velocities, in the 2800 to 4800 m/s range, are characteristic of silicified intervals of grainstone and wackestone. The lower velocities, ranging from ~2100 to ~2400 m/s, are representative of the lithology where not silicified.

No samples were available for velocity determination between ~685 and ~728 mbsf; lithology changed downhole at 692.0 mbsf to glauconitic sand-, silt-, and claystone. Within this lithologic unit velocity generally decreases downhole, from ~2200 m/s near the top to ~1900 m/s at 883.0 mbsf (Fig. 51). Four data points between ~750 and ~800 mbsf produce a concave perturbation in the downhole decreasing velocity trend.

Beneath 883.0 mbsf velocity values show a great deal of scatter, from ~2000 m/s in the sediment to ~4700 m/s in basalt. Two velocity peaks occur in the velocity profile (Fig. 51): the upper at ~878 to ~881 mbsf corresponds to silicified intervals of the siltstone, and the lower represents a basaltic lava flow (see "Igneous Petrology" section, this chapter).

The overall shape of the compressional velocity curve beneath ~400 mbsf at Site 748 (Fig. 51) is not commonly observed in marine sediment. In general, compressional wave velocity increases with depth, because the bulk and rigidity moduli commonly increase at a greater rate than does the density with depth. The velocity inversion observed between ~400 mbsf and the top of the basalt unit near 900 mbsf was not predicted by sonobuoy wide-angle reflection and refraction experiments in the Raggatt Basin (see "Introduction" chapter, this volume). The inversion could be local if Cretaceous facies change toward deeper parts of the Raggatt Basin.

Table 12. Compressional wave velocity determined from Hamilton Frame data, Site 748.

Core, section, interval (cm)	Depth (mbsf)	DIR	Velocity (m/s)
120-748B-2H-1, 50	0.60	C	1575.1
120-748A-1H-2, 104	2.54	C	1597.0
120-748B-2H-3, 16	3.26	C	1568.1
120-748A-1H-3, 136	4.36	C	1510.6
120-748A-1H-4, 134	5.84	C	1532.6
120-748B-2H-5, 55	6.65	C	1545.5
120-748B-2H-7, 46	9.56	C	1560.4
120-748A-1H-7, 80	9.80	C	1526.8
120-748A-2H-1, 100	10.50	C	1552.7
120-748B-3H-1, 121	10.81	C	1563.0
120-748A-2H-3, 50	13.00	C	1610.1
120-748B-3H-3, 49	13.09	C	1542.9
120-748B-3H-5, 47	16.07	C	1478.6
120-748A-2H-5, 100	16.50	C	1544.5
120-748B-3H-7, 46	19.06	C	1451.6
120-748B-4H-1, 133	20.43	C	1530.3
120-748B-4H-3, 52	22.62	C	1512.9
120-748B-4H-5, 132	26.42	C	1465.4
120-748B-5H-5, 50	35.10	C	1520.0
120-748B-5H-7, 43	38.03	C	1532.9
120-748B-6H-2, 124	40.84	C	1528.6
120-748B-6H-4, 54	43.14	C	1532.4
120-748B-6H-6, 52	46.12	C	1531.9
120-748B-7H-2, 100	50.10	C	1524.3
120-748B-7H-4, 69	52.79	C	1517.7
120-748B-7H-6, 77	55.87	C	1522.9
120-748B-8H-3, 83	60.93	C	1562.0
120-748B-8H-5, 87	63.97	C	1521.8
120-748B-8H-6, 81	65.41	C	1519.4
120-748B-9H-1, 61	67.21	C	1542.6
120-748B-9H-3, 116	70.76	C	1560.9
120-748B-9H-4, 127	72.37	C	1537.8
120-748B-9H-6, 22	74.32	C	1534.9
120-748B-10H-1, 125	77.35	C	1493.0
120-748B-10H-2, 81	78.41	C	1525.9
120-748B-10H-4, 76	81.36	C	1537.6
120-748B-10H-6, 41	84.01	C	1570.9
120-748B-11H-1, 122	86.82	C	1539.6
120-748B-11H-3, 126	89.86	C	1512.3
120-748B-11H-5, 44	92.04	C	1539.8
120-748B-11H-6, 25	93.35	C	1555.2
120-748B-12H-2, 119	97.79	C	1549.9
120-748B-12H-3, 129	99.39	C	1522.2
120-748B-12H-4, 136	100.96	C	1535.2
120-748B-12H-6, 36	102.96	C	1551.7
120-748B-13H-4, 57	109.67	C	1524.4
120-748B-13H-6, 59	112.69	C	1512.8
120-748B-14H-1, 134	115.44	C	1535.5
120-748B-14H-2, 15	115.75	C	1525.5
120-748B-14H-4, 68	119.28	C	1512.4
120-748B-15H-2, 127	126.37	C	1543.0
120-748B-15H-4, 126	129.36	C	1546.7
120-748B-15H-6, 126	132.36	C	1566.0
120-748B-16H-2, 20	134.63	C	1553.9
120-748B-16H-4, 20	137.63	C	1562.3
120-748B-16H-6, 20	140.63	C	1540.8
120-748B-17H-2, 130	145.40	C	1542.5
120-748B-17H-4, 130	148.40	C	1556.5
120-748B-17H-6, 130	151.40	C	1549.7
120-748B-18H-2, 130	154.90	C	1548.1
120-748B-18H-4, 134	157.94	C	1543.5
120-748B-18H-6, 132	160.92	C	1539.4
120-748B-19H-2, 132	164.42	C	1537.6
120-748B-19H-4, 132	167.42	C	1538.7
120-748B-19H-6, 52	169.62	C	1504.7
120-748B-20H-1, 59	171.69	C	1532.4
120-748C-1R-1, 77	173.77	C	1620.4
120-748B-20H-3, 84	174.94	C	1547.2
120-748C-1R-2, 99	175.49	C	1536.7
120-748B-22X-CC, 1	187.11	C	3726.1
120-748B-22X-CC, 1	187.11	A	3759.2
120-748B-22X-CC, 1	187.11	C	4509.4
120-748B-22X-CC, 1	187.11	A	4798.4
120-748B-22X-CC, 1	187.11	B	4226.9
120-748B-23X-2, 106	199.16	C	1547.7
120-748C-10R-1, 35	258.85	C	1649.1
120-748C-10R-2, 35	260.35	C	1990.2

Table 12 (continued).

Core, section, interval (cm)	Depth (mbsf)	DIR	Velocity (m/s)
120-748C-12R-1, 48	277.98	C	1734.8
120-748C-14R-1, 126	297.76	C	1554.6
120-748C-19R-1, 22	331.22	C	1785.8
120-748C-21R-1, 24	350.24	C	1787.3
120-748C-22R-1, 30	359.80	C	1753.8
120-748C-23R-CC, 20	369.20	C	1793.6
120-748C-24R-1, 1	378.51	C	2219.5
120-748C-24R-1, 35	378.85	C	1936.3
120-748C-24R-1, 62	379.12	C	2033.7
120-748C-25R-CC, 1	389.10	C	1789.1
120-748C-26R-CC, 20	397.70	C	3719.1
120-748C-27R-1, 1	407.01	C	3594.1
120-748C-27R-1, 110	408.10	C	2074.7
120-748C-29R-1, 8	426.08	C	3617.1
120-748C-29R-1, 9.0	426.09	C	3792.1
120-748C-30R-1, 93	436.43	C	3686.2
120-748C-30R-1, 96	436.46	C	3591.8
120-748C-30R-1, 7	435.57	C	2007.3
120-748C-31R-1, 7	435.57	C	4129.7
120-748C-31R-1, 7	435.57	C	4168.4
120-748C-32R-1, 27	454.77	C	4108.4
120-748C-33R-1, 105	465.05	C	3716.9
120-748C-34R-1, 137	474.87	C	3605.2
120-748C-35R-1, 92	483.92	C	2312.5
120-748C-36R-1, 36	492.86	C	3863.3
120-748C-36R-2, 121	495.21	C	3988.4
120-748C-37R-1, 77	502.77	A	3527.1
120-748C-37R-2, 67	504.17	C	2770.5
120-748C-38R-1, 75	512.25	C	3608.9
120-748C-38R-2, 8	513.08	C	3356.5
120-748C-39R-1, 23	521.23	C	3500.6
120-748C-39R-2, 55	523.05	C	2969.8
120-748C-40R-1, 45	530.95	C	2367.0
120-748C-41R-1, 18	540.18	C	3435.1
120-748C-42R-1, 77	550.27	C	3158.1
120-748C-43R-1, 81	559.81	C	3755.6
120-748C-44R-1, 49	568.99	C	3455.7
120-748C-45R-1, 130	579.30	C	2232.8
120-748C-46R-1, 124	588.74	C	2481.0
120-748C-46R-2, 13	589.13	C	3276.0
120-748C-47R-1, 35	597.35	C	3027.7
120-748C-48R-1, 26	606.76	C	2378.5
120-748C-48R-1, 55	607.05	C	2178.9
120-748C-49R-1, 19	616.19	C	2684.4
120-748C-50R-1, 76	626.26	C	2098.8
120-748C-50R-1, 82	626.32	C	2987.6
120-748C-51R-1, 129	636.29	C	2154.5
120-748C-52R-1, 25	644.75	C	2469.5
120-748C-53R-1, 63	654.63	C	2343.6
120-748C-53R-2, 60	656.10	C	2242.2
120-748C-54R-1, 26	663.76	C	2828.9
120-748C-54R-2, 58	665.58	C	2174.2
120-748C-54R-3, 22	666.72	C	2284.0
120-748C-55R-1, 14	673.14	C	2258.1
120-748C-55R-4, 29	677.51	C	2309.2
120-748C-55R-4, 29	677.51	A	2285.1
120-748C-55R-4, 29	677.51	B	2302.0
120-748C-56R-1, 96	683.46	C	2784.3
120-748C-56R-2, 107	685.07	C	2297.6
120-748C-56R-2, 107	685.07	B	2308.0
120-748C-56R-2, 107	685.07	A	2238.9
120-748C-61R-1, 57	728.07	C	2140.2
120-748C-61R-3, 57	731.07	C	2196.6
120-748C-62R-1, 27	732.77	C	2197.7
120-748C-62R-2, 28	734.28	C	2250.4
120-748C-62R-3, 29	735.79	C	2119.8
120-748C-62R-5, 108	739.58	C	2162.1
120-748C-63R-1, 55	742.55	C	2171.3
120-748C-64R-1, 56	752.06	A	2155.7
120-748C-64R-2, 90	753.90	A	2173.7
120-748C-64R-3, 94	755.44	A	2140.6
120-748C-64R-4, 69	756.69	A	2123.2
120-748C-65R-1, 21	761.21	C	1995.4
120-748C-66R-1, 57	771.07	C	1922.2
120-748C-67R-1, 12	780.12	A	1920.4
120-748C-67R-1, 12	780.12	C	1840.4
120-748C-68R-1, 55	790.05	A	2036.8
120-748C-68R-1, 55	790.05	C	1993.6

Table 12 (continued).

Core, section, interval (cm)	Depth (mbsf)	DIR	Velocity (m/s)
120-748C-69R-1, 70	798.20	A	2067.2
120-748C-70R-1, 46	807.46	A	2051.0
120-748C-70R-3, 63	810.63	A	2066.9
120-748C-70R-5, 16	813.16	A	2056.9
120-748C-71R-1, 113	817.63	C	2144.9
120-748C-71R-2, 94	818.94	C	2117.2
120-748C-71R-3, 115	820.65	A	2158.1
120-748C-71R-4, 111	822.11	A	2101.4
120-748C-71R-5, 72	823.22	A	2087.1
120-748C-71R-7, 48	825.98	C	1970.0
120-748C-72R-1, 79	826.79	A	2083.9
120-748C-72R-3, 123	830.23	A	2010.1
120-748C-72R-4, 126	831.76	C	2131.1
120-748C-73R-1, 93	836.43	C	2195.0
120-748C-73R-2, 25	837.25	A	2109.5
120-748C-73R-3, 35	838.85	A	2121.5
120-748C-73R-4, 34	840.34	C	2063.9
120-748C-73R-5, 128	842.78	A	2068.0
120-748C-73R-6, 57	843.57	A	1987.1
120-748C-74R-1, 62	845.62	C	2105.8
120-748C-74R-2, 69	847.19	C	2044.7
120-748C-74R-3, 69	848.69	A	1927.0
120-748C-74R-4, 96	850.46	A	2016.9
120-748C-75R-1, 52	855.02	A	2034.5
120-748C-75R-4, 8.0	859.08	A	2040.4
120-748C-75R-6, 27	862.27	A	2167.3
120-748C-76R-1, 39	864.39	A	2031.7
120-748C-76R-3, 30	867.30	A	1924.0
120-748C-76R-5, 91	870.91	A	2006.9
120-748C-77R-1, 90	874.40	A	2146.8
120-748C-77R-2, 124	876.24	A	2145.5
120-748C-77R-2, 124	876.24	C	2208.6
120-748C-77R-3, 138	877.88	A	3791.1
120-748C-77R-4, 62	878.62	A	1916.7
120-748C-77R-4, 117	879.17	A	3684.7
120-748C-77R-5, 58	880.08	A	2140.3
120-748C-77R-6, 41	881.41	A	4131.4
120-748C-78R-1, 64	883.64	A	1967.0
120-748C-78R-2, 67	885.17	A	2011.5
120-748C-78R-4, 131	888.81	A	2019.2
120-748C-78R-6, 25	890.75	A	2051.1
120-748C-79R-1, 24	892.74	C	2042.6
120-748C-79R-2, 119	895.19	A	2149.8
120-748C-79R-3, 50	896.00	A	2009.6
120-748C-79R-4, 29	896.40	A	1961.8
120-748C-79R-4, 78	896.89	A	3145.5
120-748C-79R-4, 123	897.34	A	3165.3
120-748C-79R-5, 16	897.75	C	4208.7
120-748C-79R-5, 19	897.78	C	4015.0
120-748C-79R-5, 19	897.78	A	3910.6
120-748C-79R-5, 88	898.47	A	4736.3
120-748C-79R-5, 112	898.71	C	4575.5
120-748C-79R-5, 112	898.71	A	4421.9
120-748C-79R-6, 15	899.14	C	4432.7
120-748C-79R-6, 15	899.14	A	4568.1
120-748C-79R-6, 44	899.43	A	4720.0
120-748C-79R-7, 66	900.98	A	4580.1

Note: DIR = direction of wave propagation; A = perpendicular to bedding; B = parallel to bedding; and C = perpendicular to split face of core.

Comparison of downhole compressional wave velocity and wet-bulk density profiles (Fig. 52) shows a general correlation between the two except in the ~400 to ~700 mbsf range. Wet-bulk density displays a slightly convex trend in this interval, whereas two trends are observed in the velocity profile: a slightly convex trend corresponding to unsilicified sediment, and a decreasing trend associated with silicified sediment. Although the degree of silicification has a strong influence on compressional wave velocity, its effect on wet-bulk density is minor. Downhole comparisons of velocity with water content and porosity (Fig. 52) show inverse relationships, common in marine sediment.

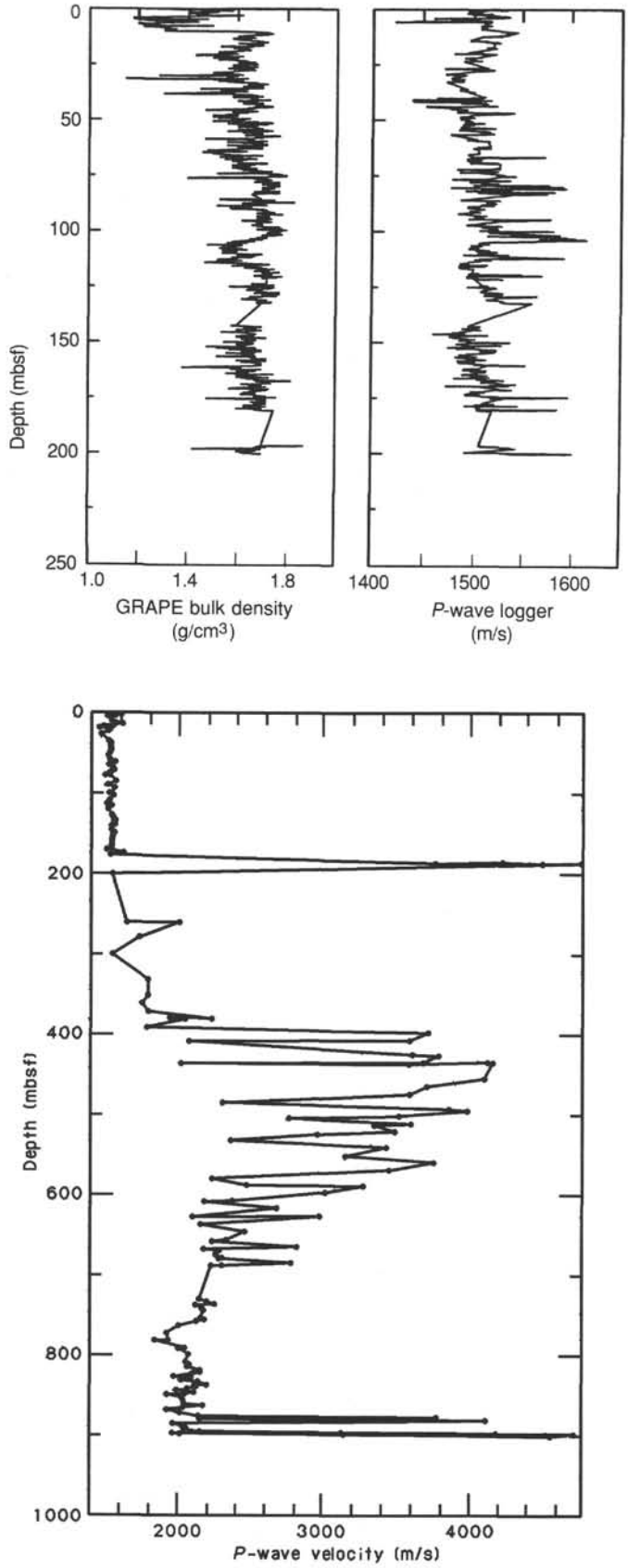

Figure 51. Downhole summary of compressional wave velocity (determined from Hamilton Frame measurements), Site 748, to 900 mbsf.

Again, the degree of silicification in the ~400 to ~700 mbsf interval has a major effect on velocity but little apparent effect on water content and porosity.

Undrained Shear Strength

Undrained shear strength (S_u) data were collected with the Wykeham-Farrance Vane device from the upper 200 m of the sediment column in undisturbed sections of APC and XCB cores. Downhole values are listed in Table 13 and are plotted in Figure 53. Values range from 3.5 kPa at 0.60 mbsf to 64.6 kPa at 6.65 mbsf. The data exhibit significant scatter from the seafloor to 10.45 mbsf, corresponding to the upper portion of the diatom ooze section (see "Lithostratigraphy and Sedimentology" section, this chapter).

From 10.45 to ~50 mbsf shear strength remains fairly constant with limited scatter, and between ~50 and ~100 mbsf values increase gradually. Beneath ~100 mbsf the low S_u values are unreliable; they are probably related to fracturing of brittle carbonate sediment and sediment disturbance. In the upper 100 m of the hole, the overall trend of the shear strength profile correlates with carbonate content and shows an inverse relationship to water content and porosity.

Thermal Conductivity, Downhole Temperature, and Heat Flow

Site 748 sediment cores were measured for thermal conductivity using a needle probe technique (Von Herzen and Maxwell, 1959). A probe was inserted and heated; resistance measurements were made over a 6-min interval. Only runs that displayed a temperature drift rate of $<0.04^{\circ}$C/min were retained for analysis. Downhole temperature was measured using the Uyeda temperature probe (T-probe) and standard operating procedures (see "Explanatory Notes" chapter, this volume).

The thermal conductivity data lie mainly in the upper 200 m of Site 748 (Fig. 54). Values range from 0.73 W/m · K near the seafloor to 1.69 W/m · K at 197.6 mbsf (Table 14). Thermal conductivity generally shows an inverse relationship to water content and porosity (Fig. 55). Values are lowest in the 0–11.2 mbsf interval, where water content and porosity are high. This interval consists of diatom ooze (see "Lithostratigraphy and Sedimentology" section, this chapter), and is underlain by nannofossil ooze. Thermal conductivity values increase gradually with depth below 11.4 mbsf, directly correlating with carbonate content.

The T-probe was deployed three times, twice in Hole 748B (85.6 and 133.1 mbsf), and once in Hole 748C (173.0 mbsf) (Figs. 56A–56C). The downhole temperatures determined from the T-probe data appear in Table 15. Variations in probe equilibration duration and the motion of the wireline during the measurements resulted in an unreliable sediment temperature at 173.0 mbsf and cast some uncertainty on the downhole temperature profile (Fig. 54). Post-cruise exponential decay curve-fitting to the T-probe data may allow determination of a 173.0-mbsf sediment temperature value, as well as permit refinement of the other temperature values. The average geothermal gradient of 71.2 °C/km calculated on board the ship is a reasonable value. The downhole temperature inversion between 85.6 and 133.1 mbsf suggests fluid circulation within the sediment, perhaps related to faulting observed to the west of Site 748. Mean heat flow is calculated to be 90 mW/m^2 at Site 748. An average thermal conductivity value (1.27 W/m · K) for the 0–133.1 mbsf interval was computed by taking the mean of weighted, equally spaced (0.5 m) values calculated from the discrete thermal conductivity data over the entire interval.

The heat flow observed on the earth's crust is the result of many processes, the most important of which are melting or

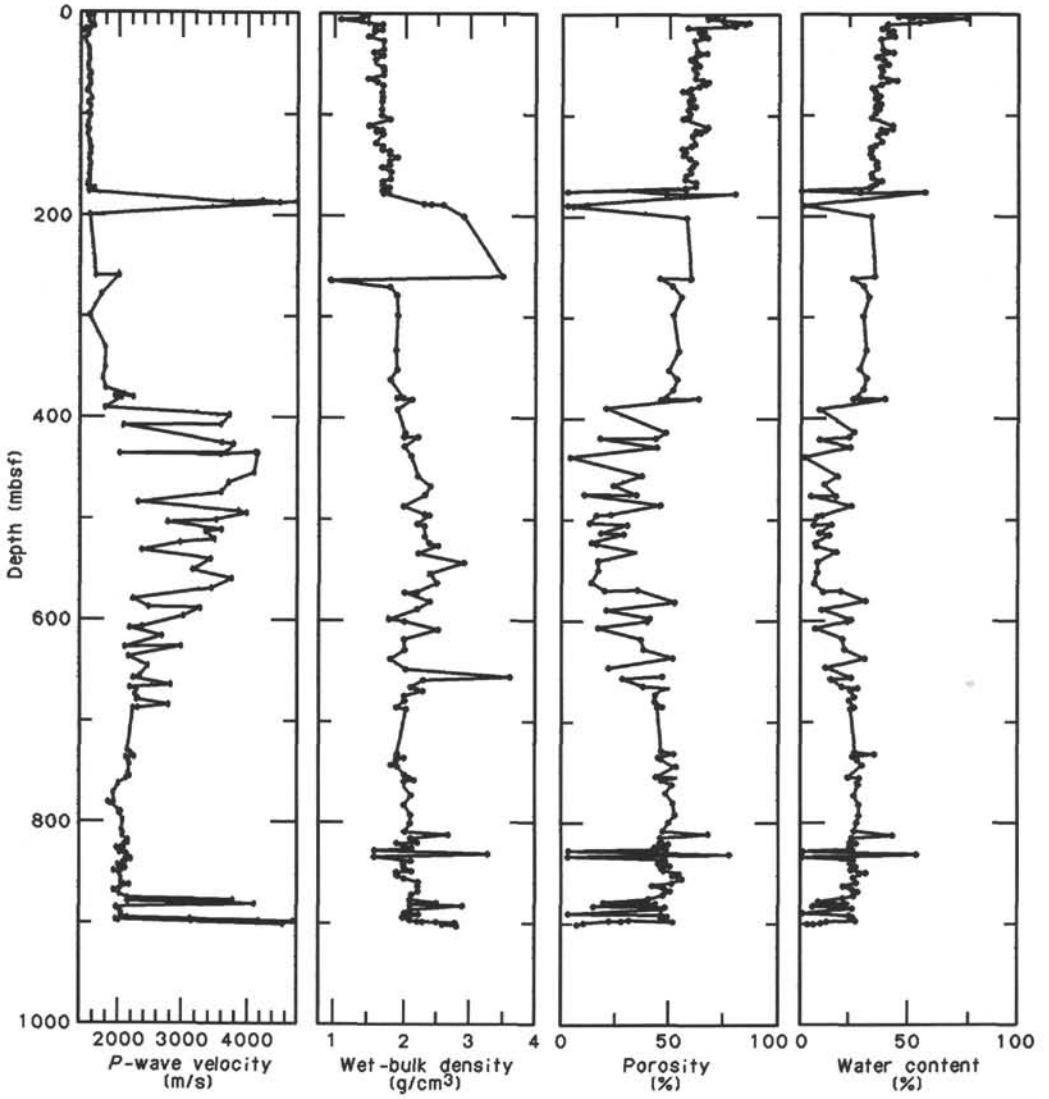

Figure 52. Comparison of downhole compressional wave velocity (Hamilton Frame) with wet-bulk density, porosity, and water content, Site 748, to 900 mbsf.

magma intrusion (including the seafloor-spreading process), crustal extension, erosion, and heat generation by radioactive decay. The flux of heat through oceanic crust is modeled well by exponential cooling from time of formation at spreading centers (Parsons and Sclater, 1977). The thermal evolution of continental crust is not as well understood, but a relation also exists between heat flow and age (Sclater et al., 1981).

Basins on continents (Sleep, 1971; Sleep and Snell, 1976) and on continental margins (Watts and Steckler, 1979) subside exponentially with time, beginning with a phase of regional subsidence, and regardless of the age of the continental crust. This regional subsidence has roughly the same time constant as that shown by the ocean floor (Sclater et al., 1981). Thermal studies indicate that heat decays exponentially in hot-spot swells on the ocean floor (Crough, 1978). Other studies (e.g., Detrick et al., 1981) indicate that the thermal "age" of the oceanic lithosphere may be reset by passing over a hot spot.

The Southern Kerguelen Plateau appears to have had a complex thermal history that is not fully explained by simple models describing exponential lithospheric cooling of a single thermal event. A model of the crustal structure of the Southern Kerguelen Plateau (Houtz et al., 1977) suggests that its crustal thickness lies between oceanic and continental values. Empirical heat flow vs. age curves are best developed for oceanic crust (Parsons and Sclater, 1977).

A comparison of the two mean heat flow values determined on Leg 120, 61 mW/m^2 at Site 747 and 90 mW/m^2 at Site 748, with heat flow vs. age curves for oceanic crust show that the crust at these two sites has a much higher heat flow than oceanic crust of Early Cretaceous age. Both sites lie less than 50 km from faults, and heat flow could be strongly influenced by tectonic events postdating the formation of the Southern Kerguelen Plateau.

Concluding Discussion

The geotechnical stratigraphy at Site 748, interpreted from index properties, compressional wave velocities, and thermal conductivity, consists of at least five units (Fig. 48):

Unit G1 (0–10.5 mbsf): Wet-bulk density is >1.65 g/cm^3; water content is $<40\%$; porosity is $>66\%$; carbonate content is commonly $<70\%$; compressional wave velocity averages ~ 1540 m/s; and thermal conductivity values are commonly <1.00 W/m · K.

Unit G2 (10.5–$\sim$400 mbsf): Wet-bulk density increases from ~ 1.60 to ~ 1.90 g/cm^3; water content decreases from $\sim 40\%$ to

Table 13. Undrained shear strength determined from Wykeham-Farrance Vane data, Site 748.

Core, section, interval (cm)	Depth (mbsf)	S_u (kPa)
120-748B-2H-1, 50	0.60	3.5
120-748A-1H-2, 109	2.59	3.7
120-748B-2H-3, 15	3.25	7.2
120-748A-1H-3, 140	4.40	25.7
120-748A-1H-4, 140	5.90	8.5
120-748B-2H-5, 55	6.65	64.6
120-748B-2H-7, 50	9.60	57.2
120-748A-1H-7, 85	9.85	14.9
120-748A-2H-1, 95	10.45	30.8
120-748B-3H-1, 126	10.86	11.9
120-748A-2H-3, 55	13.05	18.6
120-748B-3H-3, 55	13.15	11.1
120-748A-2H-5, 64	16.14	13.2
120-748B-3H-5, 55	16.15	4.5
120-748B-3H-7, 55	19.15	8.9
120-748B-4H-1, 130	20.40	13.4
120-748B-4H-3, 50	22.60	5.9
120-748B-4H-5, 130	26.40	10.4
120-748B-5H-5, 50	35.10	12.6
120-748B-5H-7, 50	38.10	20.0
120-748B-6H-2, 130	40.90	17.1
120-748B-6H-4, 50	43.10	8.9
120-748B-6H-6, 50	46.10	10.4
120-748B-7H-2, 113	50.23	12.6
120-748B-7H-4, 135	53.45	8.9
120-748B-7H-6, 76	55.86	8.9
120-748B-8H-3, 86	60.96	12.6
120-748B-8H-5, 93	64.03	20.0
120-748B-8H-6, 109	65.69	14.8
120-748B-9H-1, 58	67.18	14.1
120-748B-9H-3, 120	70.80	35.6
120-748B-9H-4, 125	72.35	45.3
120-748B-9H-5, 17	72.77	28.2
120-748B-9H-6, 19	74.29	17.8
120-748B-10H-1, 131	77.41	31.2
120-748B-10H-2, 85	78.45	20.8
120-748B-10H-4, 81	81.41	20.8
120-748B-10H-5, 73	82.83	21.5
120-748B-11H-1, 26	85.86	24.5
120-748B-11H-3, 123	89.83	50.5
120-748B-11H-5, 47	92.07	24.5
120-748B-11H-4, 21	90.31	39.4
120-748B-11H-5, 47	92.07	24.5
120-748B-12H-2, 117	97.77	24.5
120-748B-12H-3, 128	99.38	23.0
120-748B-12H-4, 133	100.93	26.0
120-748B-12H-6, 60	103.20	20.8
120-748B-13H-1, 107	105.67	7.4
120-748B-13H-4, 54	109.64	24.5
120-748B-13H-6, 49	112.59	20.0
120-748B-14H-1, 140	115.50	20.8
120-748B-14H-2, 12	115.72	38.6
120-748B-14H-4, 88	119.48	13.4
120-748B-14H-6, 12	122.00	15.6
120-748B-15H-2, 130	126.40	6.7
120-748B-15H-4, 130	129.40	17.8
120-748B-15H-6, 130	132.40	13.4
120-748B-16H-2, 25	134.68	8.2
120-748B-16H-4, 25	137.68	14.8
120-748B-16H-6, 25	140.68	11.9
120-748B-17H-2, 135	145.45	6.7
120-748B-17H-4, 140	148.50	12.6
120-748B-17H-6, 135	151.45	6.7
120-748B-18H-2, 130	154.90	3.7
120-748B-18H-4, 130	157.90	5.9
120-748B-18H-6, 130	160.90	14.8
120-748B-19H-2, 130	164.40	11.1
120-748B-19H-4, 130	167.40	10.4
120-748B-19H-6, 50	169.60	10.4
120-748B-20H-1, 63	171.73	10.4
120-748B-20H-3, 82	174.92	11.9
120-748C-1R-2, 87	175.37	11.9
120-748B-23X-1, 3	196.63	7.4

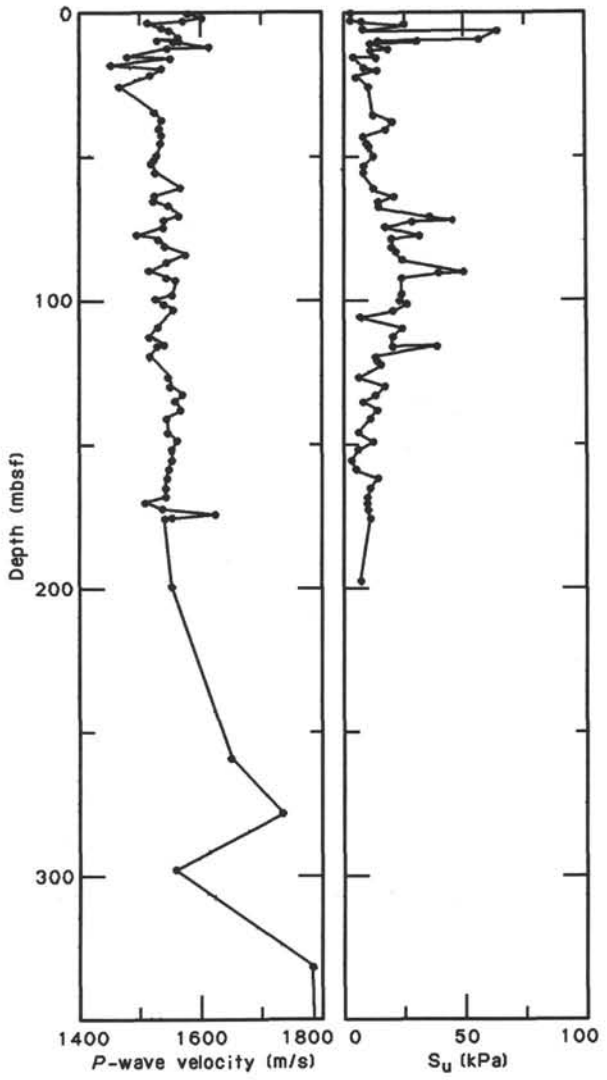

Figure 53. Comparison of downhole compressional wave velocity (Hamilton Frame) and undrained shear strength (S_u), determined from Wykeham-Farrance motorized vane measurements, Site 748, 0–350 mbsf.

~25%; porosity decreases from ~65% to ~50%; carbonate content ranges between ~70% and ~90%; compressional wave velocity is relatively uniform at ~1540 m/s between the seafloor and ~180 mbsf and increases from ~1550 to ~2000 m/s between ~180 and ~400 mbsf; and thermal conductivity is >1.00 W/m · K in the 10.5–~200 mbsf interval.

Unit G3 (~400–~700 mbsf): Wet-bulk density has a convex trend, ranging from ~1.90 to ~2.60 g/cm^3; water content and porosity have concave trends, varying from ~30% to ~5% and 50% to 10%, respectively; carbonate content decreases from >90% to <10% downhole; and compressional wave velocity shows two trends corresponding to silicified and unsilicified sediment: in the first, silicified sediment velocity decreases in the interval ranging between ~2800 and ~4800 m/s; and in the second, the velocity profile is convex in unsilicified sediment (varying between ~2100 and ~2400 m/s).

Unit G4 (~700–~875 mbsf): Wet-bulk density ranges between ~1.90 and ~2.25 g/cm^3; water content varies from ~20% to ~30%; porosity values lie between ~40% and ~55%; carbonate content varies from 0% to 5%; and compressional wave velocity generally decreases downhole from ~2200 to ~1900 m/s.

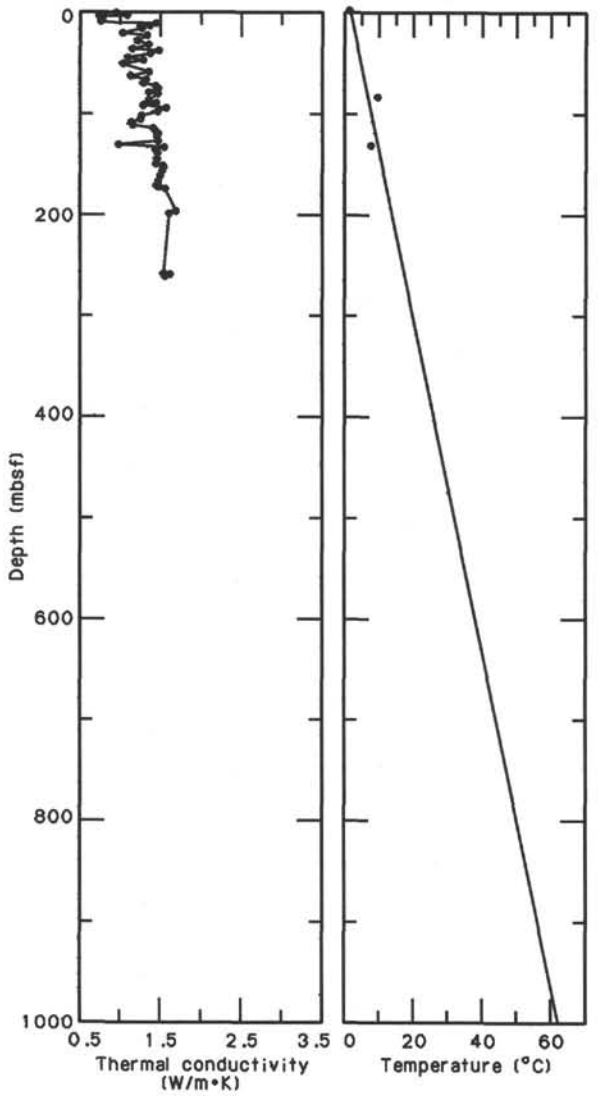

Figure 54. Downhole summary of thermal conductivity and temperature determinations, Site 748.

Unit G5 (below ~875 mbsf): Wet-bulk density varies widely, from 2.05 to 2.82 g/cm^3; water content lies between ~2% and ~26%; porosity ranges from <5% to >50%; no carbonate is present; and velocity varies widely between ~2000 and ~4700 m/s.

The individual contributions of several interrelated variables, such as sediment lithology, depth of burial, and diagenesis, are likely responsible for the physical state of the sediment and rock recovered at Site 748.

IGNEOUS PETROLOGY

Introduction

We encountered conglomerate consisting of basalt pebbles and boulders at a depth of 895.9 mbsf (Core 120-748C-79R-4, 60 cm), below Upper Cretaceous green glauconitic siltstones (part of Unit III; see "Lithostratigraphy and Sedimentology" section, this chapter). This conglomerate rests on a massive, analcite-bearing alkali-basalt lava flow at a depth of 898.8 mbsf some 150–200 m above the predicted basement (see "Site Geophysics" section, this chapter). A total of 4.5 m of basalt and basalt conglomerate was recovered.

Table 14. Thermal conductivity values for Site 748.

Core, section interval (cm)	Depth (mbsf)	Thermal conductivity (W/m · K)
120-748B-2H-2, 60	2.20	0.9460
120-748A-1H-3, 98	3.98	1.0770
120-748B-2H-4, 70	5.30	0.7810
120-748A-1H-4, 85	5.35	0.7330
120-748A-1H-5, 34	6.34	0.7370
120-748B-2H-6, 60	8.20	0.7900
120-748A-2H-2, 20	11.20	0.7620
120-748B-3H-2, 30	11.40	1.4380
120-748A-2H-4, 65	14.65	1.3520
120-748B-3H-5, 20	15.80	1.2480
120-748B-3H-6, 100	18.10	1.2640
120-748B-4H-2, 20	20.80	1.0290
120-748B-4H-4, 60	24.20	1.3220
120-748B-4H-6, 100	27.60	1.1990
120-748B-5H-2, 20	30.30	1.2120
120-748B-5H-4, 60	33.70	1.3450
120-748B-5H-6, 100	37.10	1.1480
120-748B-6H-2, 20	39.80	1.4760
120-748B-6H-4, 70	43.30	1.3710
120-748B-6H-6, 100	46.60	1.0900
120-748B-7H-2, 40	49.50	1.2790
120-748B-7H-4, 75	52.85	1.0380
120-748B-8H-4, 70	62.30	1.3570
120-748B-8H-6, 100	65.60	1.1230
120-748B-9H-2, 20	68.30	1.3130
120-748B-9H-4, 60	71.70	1.2940
120-748B-9H-6, 90	75.00	1.4280
120-748B-10H-2, 68	78.28	1.4800
120-748B-10H-4, 67	81.27	1.3450
120-748B-10H-5, 67	82.77	1.4570
120-748B-11H-3, 81	89.41	1.3500
120-748B-11H-4, 96	91.06	1.4300
120-748B-11H-6, 75	93.85	1.2860
120-748B-12H-2, 67	97.27	1.5660
120-748B-12H-4, 66	100.26	1.4510
120-748B-12H-6, 66	103.26	1.2680
120-748B-13H-2, 97	107.07	1.2540
120-748B-13H-4, 97	110.07	1.1390
120-748B-13H-6, 55	112.65	1.1720
120-748B-14H-2, 69	116.29	1.4000
120-748B-14H-4, 69	119.29	1.4320
120-748B-14H-6, 80	122.00	1.4730
120-748B-15H-2, 80	125.90	1.4430
120-748B-15H-4, 48	128.58	1.4760
120-748B-15H-6, 80	131.90	0.9840
120-748B-16H-2, 40	134.83	1.5350
120-748B-16H-4, 60	138.03	1.4300
120-748B-16H-7, 20	141.35	1.4670
120-748B-17H-4, 50	147.60	1.4440
120-748B-17H-6, 80	150.90	1.4410
120-748B-18H-2, 20	153.80	1.5160
120-748B-18H-4, 50	157.10	1.5110
120-748B-18H-6, 80	160.40	1.5000
120-748B-19H-2, 40	163.50	1.4690
120-748B-19H-4, 70	166.80	1.4740
120-748B-20H-2, 20	172.80	1.4390
120-748C-1R-1, 30	173.30	1.4920
120-748C-1R-2, 80	175.30	1.4900
120-748B-20H-4, 50	176.10	1.5420
120-748B-23X-1, 100	197.60	1.6870
120-748B-23X-3, 90	200.50	1.5970
120-748C-10R-1, 134	259.84	1.5340
120-748C-10R-2, 34	260.34	1.6070
120-748C-10R-3, 99	261.50	1.5550

Macroscopic Core Descriptions

Below the green glauconitic siltstones are 3 m of basaltic conglomerate. The conglomerate consists of well-rounded, light gray basalt pebbles and boulders in a calcareous sedimentary matrix containing abundant shell fragments. The pebbles and boulders range in size from 3 mm to >30 cm and are character-

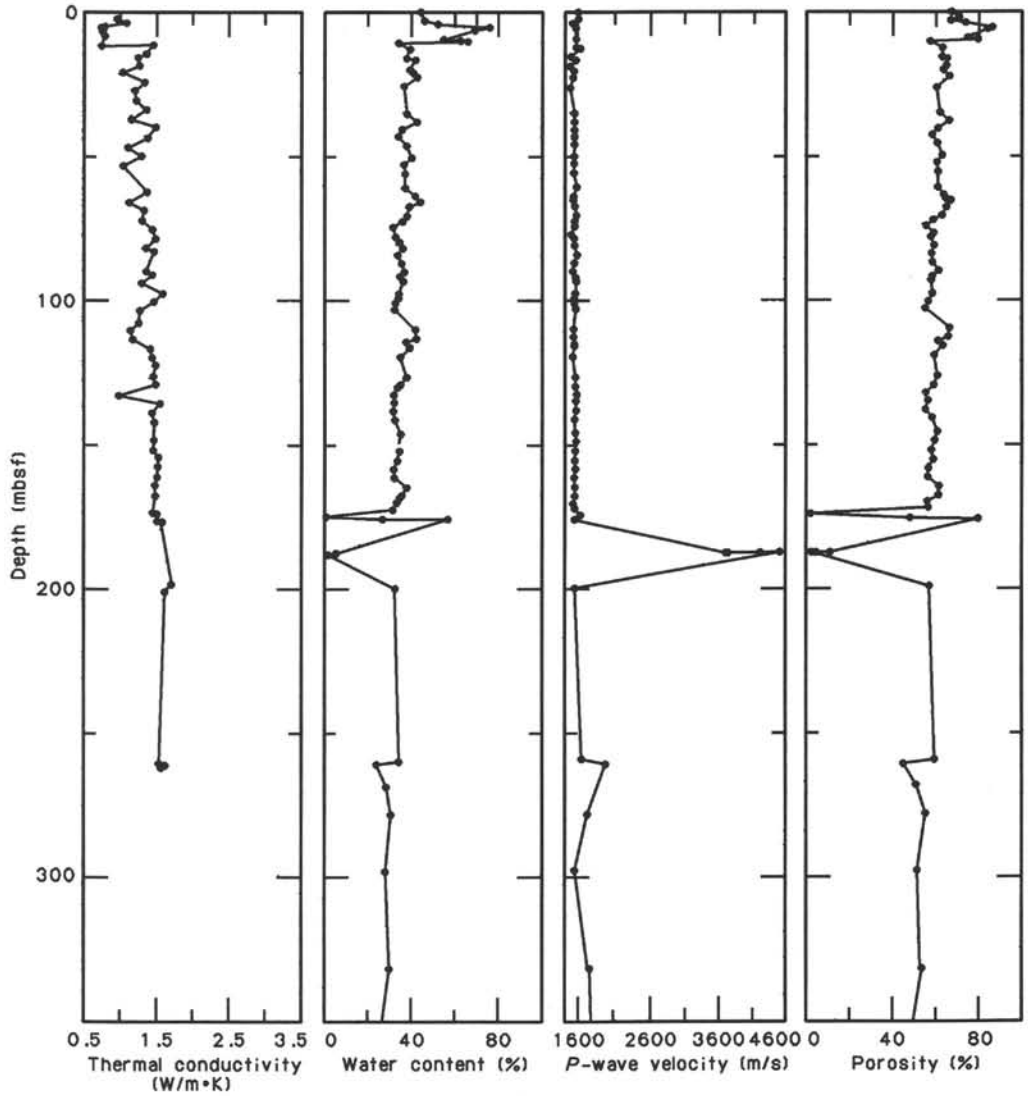

Figure 55. Downhole summary of thermal conductivity, water content, *P*-wave velocity, and porosity, Site 748, 0–350 mbsf.

ized by a 1–2-mm brown-colored rim that appears to be a weathering feature. Many pebbles have 1–3-mm calcite rims. Part of the conglomerate is illustrated in Figure 57.

The top 8–10 cm of the basalt underlying the conglomerate is strongly weathered and light gray-green in color. It contains a number of rounded structures, similar in dimensions to the pebbles in the overlying conglomerate (Fig. 57). They are sometimes rimmed by late-stage calcite. These are spheroidal weathering features that may have overprinted primary magmatic textures (e.g., brecciation of the lava flow produced by contraction during cooling). Dislocation of these spheroidally weathered structures provides a simple mechanism for the origin of the basalt conglomerates.

The remainder of the core consists of highly altered, brecciated, and massive, dark gray basalt. It contains round to oval amygdules that are occasionally cut by the numerous, near-horizontal carbonate-filled veins (Fig. 58). Angular inclusions up to 5 cm in size occur and are infilled by secondary minerals. Their shape suggests that they could be xenoliths.

Petrography

The massive flow consists of a sparsely clinopyroxene and plagioclase phyric basalt. Phenocrysts occur in an altered, intersertal to microcrystalline groundmass consisting of plagioclase laths, Fe-Ti oxides, and in some samples, altered clinopyroxenes. Clear, subhedral crystals of analcite constitute up to 40% of the rock (Fig. 59).

Subhedral clinopyroxene phenocrysts (0.5–2.0 mm) are most commonly pseudomorphed by clay minerals and only occasional relics of the original clinopyroxene remain. Plagioclase microphenocrysts (An_{55-60}) occur as euhedral laths (0.7–1.0 mm), which are generally fresh but are replaced by clay minerals when altered. Phenocrysts (0.5–1.0 mm) of brown to opaque spinel (picotite; up to 3%) were also observed. Clinopyroxene and plagioclase phenocrysts may show a glomeroporphyritic texture.

Olivine is not present as a phenocryst or groundmass phase. However, in one sample (120-748C-79R-6, 102–105 cm), olivine occurs as an oval, 5-mm xenocryst with a reaction rim of undetermined mineralogy. The olivine xenocryst exhibits mechanical twinning, which suggests that it may be of mantle origin.

Alteration

The basalt is highly altered by secondary minerals consisting mainly of zeolites, with lesser clays, carbonates, and quartz. The predominant zeolite is analcite, which may be either late-stage magmatic or the recrystallization of interstitial glass dur-

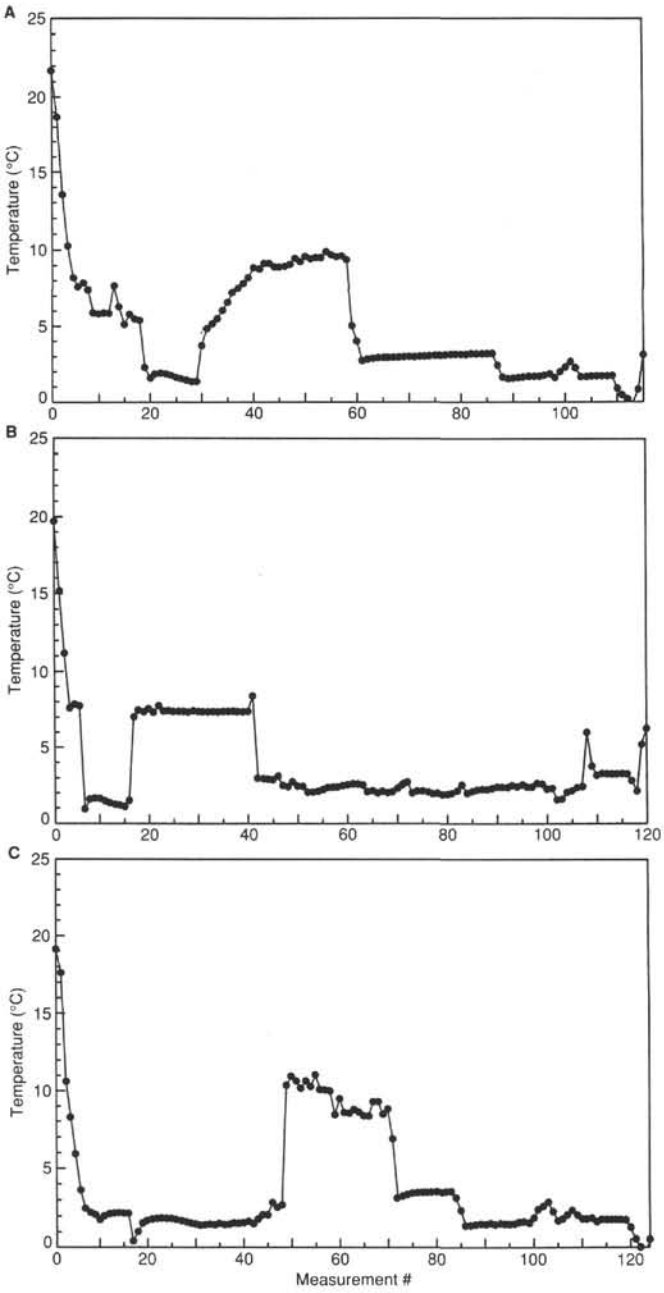

Figure 56. **A.** Downhole temperature run at 85.6 mbsf, Hole 748B (Core 120-748B-11H). **B.** Downhole temperature run at 133.1 mbsf, Hole 748B (Core 120-748B-16H). **C.** Downhole temperature run at 173 mbsf, Hole 748C (Core 120-748C-1R).

Table 15. Summary of downhole temperature measurements, Site 748.

Leg, hole, core	Depth (mbsf)	Mud line temperature (°C)	Bottom temperature (°C)
120-748B-11H	85.60	1.3	9.6
120-748B-16H	133.10	1.1	7.4
120-748C-1R	173.00	1.4	—

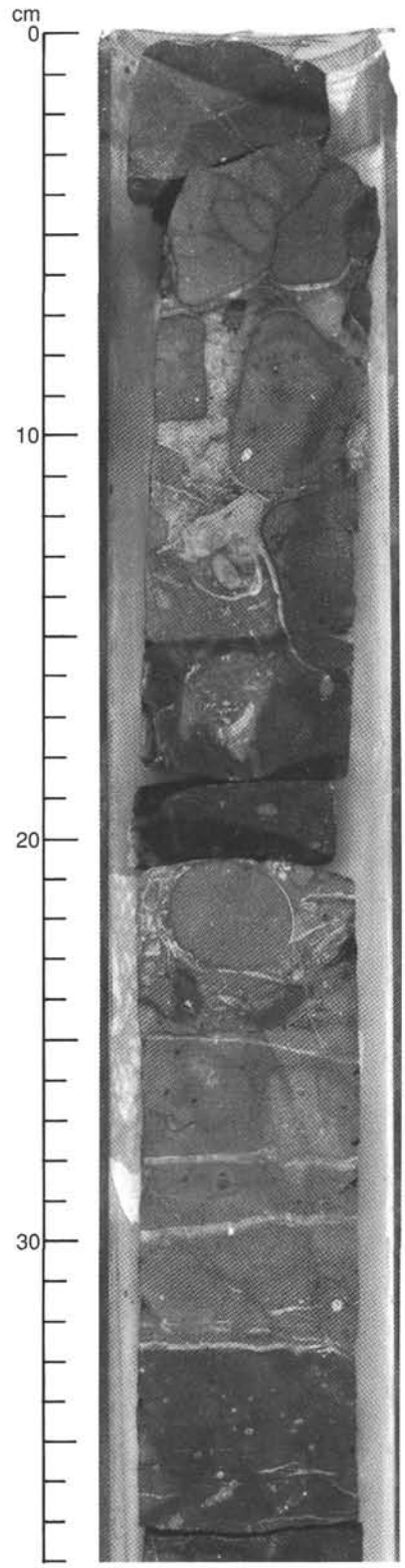

Figure 57. Contact between basalt conglomerate and analcite-bearing basalt flow. The upper 8–9 cm of the basalt flow is spheroidally weathered and shows an irregular contact with the conglomerate (Core 120-748C-79R-5, 0–38 cm).

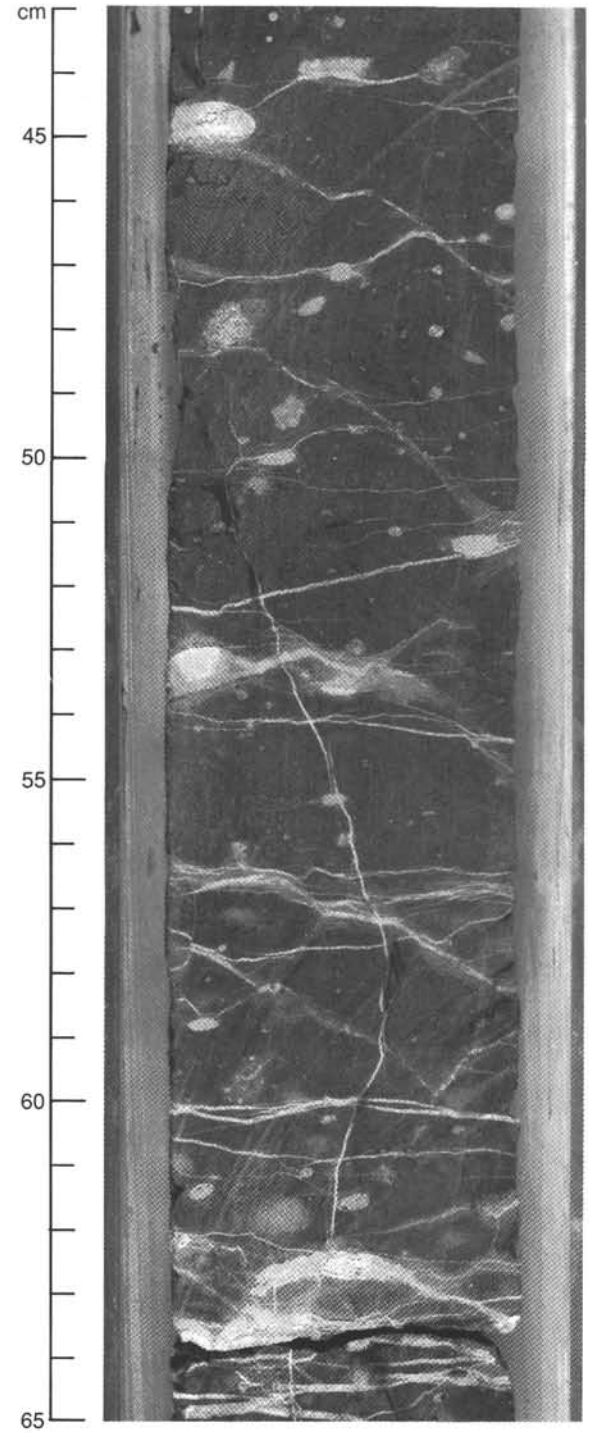

Figure 58. Macroscopic alteration of the massive basalt flow. The basalt and some amygdules are crosscut by near-horizontal, carbonate-filled veins (Core 120-748C-79R-5, 43–65 cm).

ing hydrothermal alteration. Smectites replace the phenocrysts and are also observed in the groundmass together with analcite and a fibrous mineral (undetermined zeolite). Vesicles and veins are infilled by smectite, calcite, and siderite(?). The angular inclusions are replaced by clays, quartz, calcite, and siderite.

Geochemistry

Four whole-rock major and trace element analyses representative of the basalt flow are given in Tables 16 and 17. The al-

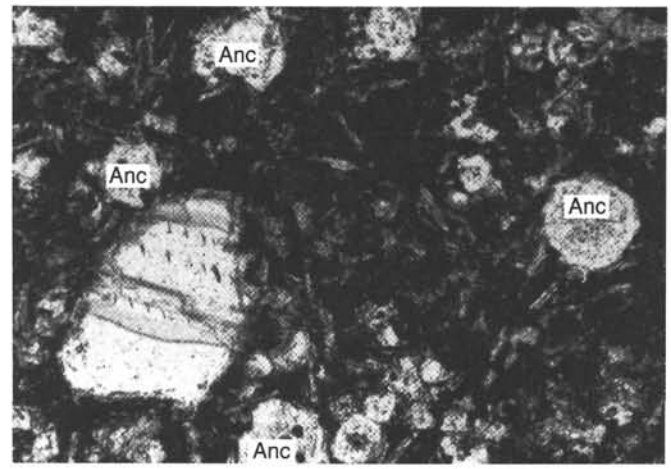

Figure 59. Photomicrograph of clear, subhedral crystals of analcite (Anc) in an altered, fine-grained intersertal groundmass. Width of field of view = 2.5 mm, plane polarized light.

Table 16. Major element analyses and normative composition of basalts from Hole 748C.

Core, section, interval (cm)	79R-4 140–142	79R-6 121–123	79R-7 45–48	79R-7 65–67
SiO_2	52.37	47.07	47.28	48.46
TiO_2	3.62	2.61	2.53	2.66
Al_2O_3	20.68	16.78	16.55	17.07
Fe_2O_3	5.79	9.38	9.32	8.04
MnO	0.04	0.12	0.08	0.07
MgO	2.50	8.74	9.00	7.25
CaO	7.21	6.77	7.01	7.55
Na_2O	3.85	5.39	5.02	5.50
K_2O	1.17	0.53	0.54	0.99
P_2O_5	1.25	1.05	1.04	1.09
Total	98.49	98.45	98.38	98.68
LOI	7.50	6.83	6.00	4.89
Mg#	NC	62.09	63.05	61.44
Qz	8.91	0	0	0
Ne	0	6.93	4.98	7.53
Or	7.06	3.21	3.27	5.98
Ab	33.21	33.86	34.30	33.54
An	29.04	20.48	21.52	19.32
Di	0	6.12	6.32	9.93
Hy	8.11	0	0	0
Ol	0	20.06	20.45	14.49
Ap	2.78	2.35	2.33	2.43
Il	7.02	5.08	4.93	5.16
Mt	1.18	1.91	1.90	1.63
Co	2.69	0	0	0

Note: LOI = loss on ignition and NC = not calculated.

Table 17. Trace element analyses of basalts from Hole 748C.

Core, section, interval (cm)	Rb	Ba	Nb	Sr	Zr	Y	Zn	Cu	Cr	Ni
120-748C-										
79R-4, 140–142	6	1716	113	1248	611	27	51	31	228	67
79R-6, 121–123	5	1095	123	1035	596	28	83	27	178	152
79R-7, 45–48	4	1097	122	1097	597	27	79	31	154	167
79R-7, 65–67	7	1216	126	1236	606	30	81	31	167	165

tered nature of the basalts is reflected in their high loss on ignition (4.9–7.6 wt%). The basalts are alkaline, as evidenced by nepheline normative compositions and high TiO_2 and P_2O_5 abundances. The high Mg# (61–63), high nickel (150–170 ppm), and chromium (150–180 ppm) abundances indicate that the basalts have undergone little crystal fractionation.

Relative to mid-ocean ridge basalts (MORB) and transitional basalts from Hole 747C, basalts from Hole 748C are strongly enriched in the highly incompatible elements (e.g., Zr and Nb). The concentration of incompatible elements in Hole 748C basalts is greater than the enriched "hot-spot" basalts from Heard and Kerguelen islands (Storey et al., 1988). The "enriched" basalts from Heard and Kerguelen islands and Hole 748C do, however, have similar Zr/Nb ratios (i.e., Zr/Nb = 5–8; see also "Site 749" chapter, Fig. 35, this volume).

Summary

An alkaline, analcite-bearing basalt lava flow was encountered above basement, probably interlayered with sediments. This lava is sparsely clinopyroxene and plagioclase phyric and is characterized by the presence of clear, subhedral crystals of analcite. It contains olivine xenocrysts of probable mantle origin. It is highly altered and secondary minerals are clays, zeolites, quartz, calcite, and siderite(?). The basalt has undergone relatively little fractionation and is strongly enriched in incompatible elements. It has compositional characteristics similar to intraplate, oceanic-island alkaline basalts.

SEISMIC STRATIGRAPHY

The seismic profiles in the Raggatt Basin across Site 748 (Figs. 2, 7, and 8) show two strong reflectors that correspond to the top of the lower Sequence K1, and to the boundary between Sequences K3 and P1. At Site 748 these two reflectors are clear and can easily be traced on the *Rig Seismic* and the *JOIDES Resolution* seismic records at 0.83 s and 0.41 s TWT, respectively (Fig. 7). The basement, just below Reflector K1, lies at 0.92 s TWT and can only be resolved precisely on the *Rig Seismic* multichannel seismic reflection profile. The other reflectors at 0.61, 0.29, 0.16, and 0.09 s TWT, which were deduced from seismic stratigraphic interpretation, cannot be scaled on the *JOIDES Resolution* seismic line (see "Site Geophysics" section, this chapter).

The two reflectors observed at 0.83 and 0.41 s TWT on the seismic records at Site 748 are related to major changes in the lithology or in the corresponding physical properties. Core descriptions indeed revealed several clear lithologic events. From top to bottom, the first lies at the top of Subunit IIB at 180.6 mbsf and corresponds to the first occurrence of porcellanite and chert. Farther down, three important changes are recorded in Unit III; the first is at the top of Subunit IIIA at 389.1 mbsf, the second at the top of Subunit IIIB at 692.0 mbsf, and the third at the top of Subunit IIIC at 897.6 m. Subunits IIIA and IIIB consist of glauconitic rudstones, grainstones, packstones, wackestones, sandstones, siltstones, and claystones and are distinguished by a change in carbonate content and components. Subunit IIIC consists of a basalt cobble conglomerate.

Unit III extends from 389.1 to 898.8 mbsf. The deepest event corresponds to a basalt flow at the top of Unit IV between 898.8 and 902.2 mbsf, and it corresponds to Subunit IVA (see "Lithostratigraphy and Sedimentology" section, this chapter). The physical properties (index properties, compressional wave velocities, and thermal conductivity) measured at Site 748 roughly follow the lithologic subdivisions already discussed. Based on water content, porosity, wet-bulk density, and compressional wave velocity, the sedimentary section was divided into five geotechnical units. From top to bottom, the major changes are at ~400, ~700, and ~875 mbsf and can easily be correlated with the tops of Subunits IIIA, IIIB, and IVA, respectively (see "Physical Properties" section, this chapter).

Taking into account the seismic data, lithology, and physical properties, the seismic reflectors at 0.41 s (P1/K3 boundary) and 0.83 s (K2/K1 boundary) must be correlated with the tops of Subunits IIIA (389.1 mbsf) and IIIC (897.6 mbsf) or IVA (898.8 mbsf), respectively. Subunit IIA is characterized by relatively uniform index properties and a constant compressional wave velocity of 1.54 km/s. Between ~180 and ~400 mbsf (Subunit IIB), the compressional wave velocity increases from ~1.55 to ~2.00 km/s and reaches in some places (e.g., chert) values as high as 4.8 km/s (Fig. 51).

Because of very poor recovery, only a few measurements were obtained for Subunit IIB, and the mean velocity cannot be evaluated for this sequence. As the bottom of Subunit IIB (389.1 mbsf) is clearly correlated with the seismic reflector at 0.41 s TWT, it is possible, assuming a mean velocity of 1.54 km/s for Subunit IIA, to calculate a mean compressional wave velocity of 2.37 km/s for Subunit IIB. This value appears rather high but may be explained by a large proportion of chert.

Subunit IIIA shows two velocity trends corresponding to silicified and unsilicified sediments; a mean compressional wave velocity of 2.9 km/s can be estimated from the data points (Fig. 51). This value is in good agreement with the value of 3.03 km/s calculated by assuming that the seismic reflector at 0.61 s (K3/K2 boundary) correlates with the top of Subunit IIIB. For Subunit IIIB the mean compressional wave velocity can be estimated from the velocity measurements made between ~700 and ~875 mbsf or can be calculated on the basis of the seismic-lithologic correlations, which show that the reflector at 0.83 s (K2/K1 boundary) can be associated with the top of Subunit IIIC or IVA. The measured velocity values range between 1.90 and 2.20 km/s (Fig. 51), and the calculated value for Sequence K2 is 1.88 km/s.

The clear inversion of compressional wave velocity observed in Unit III is unusual and needs to be documented by complementary shore-based analysis. Below the basalt flow, recovery was extremely poor, and compressional wave velocity measurements were impossible in the lowermost cored section. Moreover, since the basement traced at 0.92 s TWT on the seismic record was not reached, no mean velocity can be estimated for Unit IV. The interpreted seismic section (*Rig Seismic*) at Site 748 is given in Figure 60.

Based upon these correlations, a vertical velocity distribution model that relates the different seismic sequences with the lithologic units can be established for the sedimentary column at Site 748 in the western Raggatt Basin on the Southern Kerguelen Plateau (Fig. 61).

Site 748 is located about 15 km to the northeast of a major normal fault, trending north 100°–110°, facing to the southwest, and showing a vertical throw of about 1500 m (Fig. 4). To the southwest, toward the north-trending 100°–110° normal fault, the seismic sequences thin by onlap and toplap and the basement outcrops about 10 km west of the site (see "Site Geophysics" section, this chapter).

Close to Site 748, the basement corresponds to a weakly defined reflector overlying a series of dipping reflectors that almost parallel the basement reflector and dip to the northeast (Figs. 8 and 60). The lowermost Sequence K1 resting upon the basement is essentially confined to the deepest part of the Raggatt Basin and is characterized by high-amplitude reflectors with poor continuity that drape the preexisting basement topography. Sequence K2 thins toward the southwest by offlap and is characterized by low-amplitude reflectors with moderate to poor continuity.

Sequences K1 and K2 are overlain by a thick K3 sequence, which corresponds to medium- to low-amplitude and high-con-

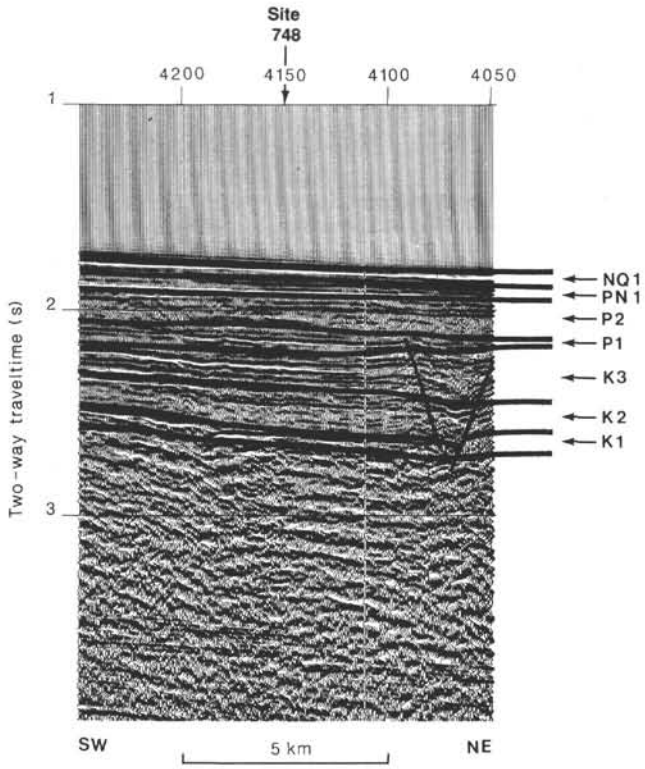

Figure 60. Interpretation of the *Rig Seismic* (RS02-27) seismic reflection profiles at Site 748 with identification of the seismic sequences. The uninterpreted seismic section is shown in Figure 8. The correlation of the seismic sequences with the lithologic units is given in Figure 61.

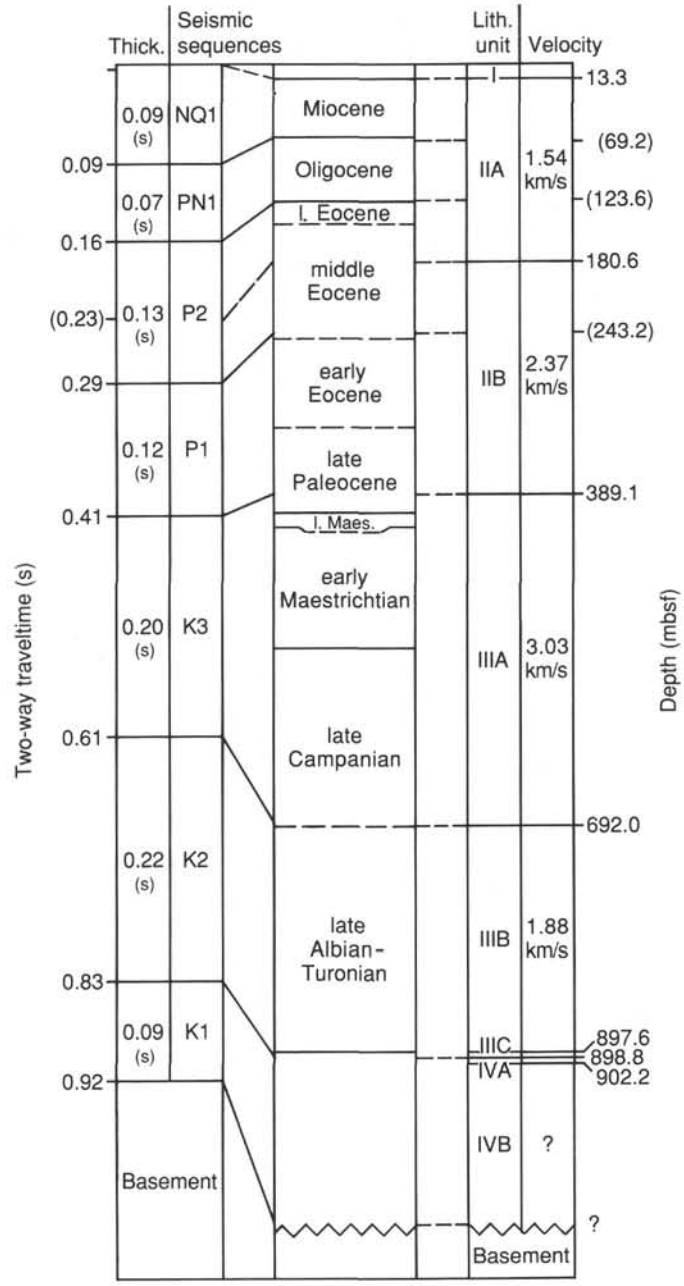

Figure 61. Vertical velocity distribution model for the sedimentary column at Site 748, showing correlation of the seismic sequences with the different lithologic units.

tinuity reflectors. Sequence K3 disappears toward the southwest between Sequences K2 and P1 by toplap and is characterized to the northeast by mounds of probable volcanic or carbonate origin. The mounds appear to be developed at the base of Sequence K3 but extend into the overlying Sequence P1.

Sequences P1 and P2 are relatively uniform and correspond to low-amplitude reflectors of high continuity; the two sequences disappear to the southwest by offlap. The two uppermost Sequences PN1 and NQ1 are separated from Sequence P2 by a high-amplitude unconformity. Close to the site these two sequences are relatively thin and disappear abruptly by toplap near the basement outcrop (Colwell et al., 1988; Schlich et al., 1988; Coffin et al., in press; see also "Background and Objectives" and "Site Geophysics" sections, this chapter).

The basalt flow cored between 898.8 and 902.2 mbsf forms the entire Subunit IVA. It has compositional characteristics similar to intraplate, oceanic-island alkaline basalts and probably represents the last and the youngest of a series of basalt flows that form Unit IV in part. True basement probably lies 150–200 m below the TD of Hole 748C.

The evolution of the central part of the Southern Kerguelen Plateau, as derived from all these observations (see "Lithostratigraphy and Sedimentology" and "Biostratigraphy" sections, this chapter) and from seismic stratigraphy, can be summarized as follows:

1. Prior to the late Albian–Turonian (K1, Unit IV), basalt flows covered the plateau over the region close to the site. These flows are strongly weathered and appear to be interlayered with siltstones and claystones derived from that weathering. Wood fragments, if in place, denote the development of soils and vegetation on some of these flows. During this time span, the site was probably subaerial or at very shallow depth and subsidence was necessarily slow.

2. From the late Albian–Turonian to the late Maestrichtian (K2–K3, Unit III), sedimentation rates were about 46 m/m.y. The area close to the site remained at shallow depth (50–200 m) throughout this period of time. The lower part of the sedimentary section (K2, Subunit IIIC and IIIB) consists of a basalt cobble conglomerate overlain by glauconitic sandstones, siltstones, and claystones, with no or rare silicified bioclastic debris. The upper part of the section (K3, Subunit IIIA) consists of rudstones, grainstones, packstones, and wackestones that are intermittently silicified.

3. An important hiatus of at least 6 m.y. occurred between the late Maestrichtian and the late Paleocene (~62 Ma). This

event is related to a major tectonic episode that affects the entire Raggatt Basin and probably the entire Southern Kerguelen Plateau. This tectonic event corresponds, close to Site 748, to a large northwest-southeast uplift that abuts the southern end of the 77°E Graben to the west. During this time span, the area at Site 748 subsided rapidly from 50–200 to 1000 m, at a rate of about 150 m/m.y.

4. From late Paleocene (~62 Ma) to middle Eocene (P1 and the lower part of P2, Subunit IIB) times, sedimentation was continuous with a rate of about 18 m/m.y., and the site subsided slowly at about the same rate. The sedimentary section consists of nannofossil ooze and chalk with chert and porcellanite. During this period of time, mounds developed at the base of Sequence K3 (Subunit IIIA) and extended into Sequence P1 (lower part of Subunit IIB). The major faulting episode that started during the deposition of Sequence K3 (Subunit IIIA) extended into Sequence P1 (lower part of Subunit IIB).

5. A hiatus of at least 2 m.y. occurred during the middle Eocene. If confirmed by complementary shore-based studies, this event could be related to the separation by seafloor spreading of the Northern Kerguelen Plateau and Broken Ridge dated at 43–42 Ma (Munschy and Schlich, 1987).

6. Since the late Eocene (~39 Ma), the sedimentation, mainly nannofossil ooze, has been essentially continuous with the exception of a hiatus of about 6 m.y. in the middle Miocene, which is probably related to a paleoceanographic event. The sedimentation rate varies throughout this period of time between 4 and 6 m/m.y.

SUMMARY AND CONCLUSIONS

Site 748 (proposed site SKP-3C; 58°26.45′S, 78°58.89′E; water depth = 1290 m) is a short-term reentry site located on the Southern Kerguelen Plateau in the western part of the Raggatt Basin, east of Banzare Bank. The site was intended to recover an expanded section of Paleogene and Cretaceous sediments in order to decipher the tectonic and geologic history of this portion of the plateau. A second objective was to recover basement samples from the Raggatt Basin to compare with other Kerguelen Plateau basement sites (Sites 738, 747, and 748).

A 930-m-thick late Albian–Turonian through lowermost Pleistocene sedimentary section with basalt flows near the base was cored in three holes using the APC, XCB, RCB, and ultimately a reentry minicone to achieve deep penetration. The Mesozoic sediments have a remarkably high glauconite content and are of shallow-water origin. As at Site 747, the depositional environment deepened sharply near the close of the Mesozoic, signaling a major tectonic event that affected much of the Kerguelen Plateau. A major discovery in the Cenozoic section is the occurrence of ice-rafted debris near the base of the Oligocene, which provides the most direct and compelling physical evidence yet for the existence of a continental ice sheet on East Antarctica at this time.

Operations

The upper 180.6 m of the section was cored via APC until refusal with 100% recovery. Upon switching to the XCB, cherts were encountered almost immediately and recovery dropped sharply to 12%. The reentry hole was initiated using the RCB and was drilled with poor recovery through partially silicified sediments to 550 mbsf, at which point a model LH (Hayes) reentry minicone was deployed in order to take advantage of a window of relatively calm weather for that operation.

The hole was continued to 742 mbsf, whereupon a successful reentry procedure was conducted to change the bit. The hole was then drilled to a total depth of 935 m, where a failed flapper valve allowed massive backflow of sediments into the BHA, thereby preventing further operations at this site, including logging. Aside from the sediment recovered from the BHA, little material was trapped in cores (i.e., in core-catcher socks) taken over the basal 27 m of the hole, perhaps due to the malfunction of the flapper valve and/or to excessive ship heave. Nevertheless, average core recovery in nonsilicified sediments over the last 95 m prior to these problems was 70%, and this is the deepest penetration yet achieved via reentry using a Hayes minicone.

Geophysics

Site 748 is located on Australian MCS line RS02-27 (time mark 100.2340, shot point 4150) trending northeast across the Raggatt Basin, where the basement lies between 1100 and 1300 mbsf and where an almost complete sedimentary section, ranging from Cretaceous to Holocene, is present. To the west the Raggatt Basin terminates abruptly against faults associated with the 77°E Graben, or farther to the south against the basement outcrop of the Banzare Bank. To the east the Raggatt Basin corresponds to a scarp or slope merging into the deep Labuan Basin. The sediment cover in the Raggatt Basin reaches 2500–3000 m and rests upon a weakly defined basement reflector.

Seven distinct seismic sequences, which can be grouped into two megasequences, have been identified in the Raggatt Basin. The upper megasequence is divided into three sequences (NQ1, PN1, and P2), and the lower megasequence into four sequences (P1, K3, K2, and K1). The NQ1 and PN1 sequences are only observed in the central part of the basin and are truncated in all directions by toplap. Sequence P2 filled the relief of the lower megasequence by onlap. Sequences P1 and K3 are characterized by mounds; the thickness of Sequence P1 remains fairly uniform whereas Sequence K3 shows significant variations in thickness. Sequence K2 and K1 filled up the center of the basin and disappeared in all directions by onlap. A major tectonic episode occurred between Sequences K3 and P1 and corresponds to the shift of the depocenter, which moves from west (K1, K2, and K3) to east (P1, P2, PN1, and NQ1).

At Site 748 the basement reflector lies at about 0.92 s TWT below seafloor, and two major reflectors corresponding to the top of the lower Sequence K1 and to the boundary between Sequences K3 and P1 can be traced at 0.83 and 0.41 s TWT below seafloor, respectively. From seismic stratigraphy studies, it is possible to scale several other seismic reflectors at 0.61, 0.29, 0.16, and 0.09 s TWT below seafloor at Site 748. The reflectors at 0.92, 0.83, and 0.41 s TWT are visible on the *JOIDES Resolution* survey line, although it is almost impossible to scale the minor reflectors observed on the MCS line; these reflectors are masked by the noise level and the bubble pulse of the seismic source. The vertical velocity distribution was estimated from previous sonobuoy experiments (*Marion Dufresne* cruise 47) and from seismic reflection stack velocities. These values were later readjusted by taking into account the drilling results at Site 747. Basement was expected to be at about 1130 mbsf (0.92 s TWT) and the K3/P1 boundary at about 370–390 mbsf (0.41 s TWT).

Lithobiostratigraphy and Igneous Petrology

Lithologic units (Figs. 9 and 10; Table 2) recognized at Site 748 are presented as a composite section from the seafloor down as follows:

Unit I: depth, 0–13.3 mbsf; age, late Pleistocene to early Pliocene; diatom ooze with radiolarian and foraminifer-enriched intervals, dropstones, and ice-rafted debris.

Unit II: depth, 13.3–389.1 mbsf; age, late Miocene to late Paleocene; nannofossil ooze, chalk, porcellanite, and chert, generally well bioturbated and divisible into two subunits.

Subunit IIA: depth, 13.3–180.6 mbsf; age, late Miocene to middle Eocene; nannofossil ooze with biosiliceous enriched in-

tervals; abundant ice-rafted debris (mostly quartz) in a short (37 cm) early Oligocene interval.

Subunit IIB: depth, 180.6–389.1 mbsf; age, middle Eocene to late Paleocene; nannofossil ooze, chalk, porcellanite, and chert.

Unit III: depth, 389.1–898.8 mbsf; age, late Paleocene to late Albian; glauconitic bioclastic and nonbioclastic sediment, in part silicified. In general, carbonate content in this unit decreases downhole from a high of about 96% near the top of the unit to a low near 1% by 728 m. Organic carbon content, which is negligible in the overlying units, fluctuates between about 0.2% and 0.6% (maximum, 1.0%). Two hiatuses that presumably represent disconformities are present at the top of the sequence. The most important of these separates the Cretaceous from the overlying upper Paleocene and spans at least 6 m.y.; the other occurs between the upper and lower Maestrichtian and spans perhaps up to 5 m.y. The unit is tentatively divided into three subunits.

Subunit IIIA: depth, 389.1–692.0 mbsf; age, late Paleocene to late Campanian; glauconitic rudstones, packstones, and grainstones all intermittently partly silicified. Glauconite grains compose from 5% to 58% of the sediment; pyrite is pervasive but never greater than 5%. Clay content increases downhole, whereas carbonate decreases. Angular, clear sand-size quartz and clear, untwinned feldspar are rare components. Basalts clasts are present in the lower Maestrichtian (Sample 120-748C-31R-CC), and clay rip-up clasts are present at 626 mbsf.

The bioclastic material is composed of fine sand- to granule-size debris of bryozoans, inoceramids, benthic foraminifers, echinoid spines, siliceous sponge spicules, molluscs, radiolarians, crinoid columnals, red algae, and possible brachiopods. Between 483 and 550 mbsf, inoceramid debris occurs in rock-forming proportions (20%–85% of the sediment). Bryozoans, broken and displaced, may also be strongly enriched in these lower Maestrichtian packstones. An intact irregular echinoid was found at 635 mbsf. Occasional phosphatic vertebrate debris include teeth, scales, and bones.

Subunit IIIB: depth, 692.0–897.6 mbsf; age, upper Albian–Turonian; glauconitic sandstones, siltstones, and claystones. This subunit is distinguished from Subunit IIIA by the absence of carbonate bioclasts. The upper boundary is uncertain because of the minuscule recovery between 692 and 727.5 mbsf plus the fact that what was recovered could be cavings. As determined from sedimentology, the boundary is placed at the base of Core 120-748C-56R (Fig. 10), although if taken from paleontology it could be placed at the base of Core 120-748C-58R (Fig. 34). In the absence of better core recovery and any logging data, the exact placement is arbitrary. It appears, however, that a disconformity representing a hiatus of at least 10 m.y. must separate the two subunits. For purposes of these reports, we arbitrarily place that disconformity at the base of Core 120-748C-58R.

Age determinations for this unit are centered around three points. The 5 cm of material recovered in the core catcher of Core 120-748C-58R are dated as late Campanian by nannofossils and planktonic foraminifers, but this material may not be in place. Shore-based palynological studies (D.P.C. Hos, telex comm., 28 April 1988, and B. Mohr, written comm., 23 March 1988) indicate a Cenomanian to Turonian age for Core 120-748C-62R and a late Albian to Cenomanian age for Cores 120-748C-70R through -78R.

The top of Subunit IIIB consists of glauconitic sandstones (down to 732.5 mbsf). The sand grains consist primarily of glauconite (chips, peloids, and bulbous dark particles) and silicified fossils (including molds of radiolarians, foraminifers, and sponge spicules with some of the latter replaced by fibrous chalcedony). Pyrite, phosphatic vertebrate debris, foraminifers, terrestrial plant spores, quartz, and untwinned feldspar may also be present. Although present throughout the Cretaceous section, bone fragments peak at about 742 m, where they are a significant rock-forming component.

Below 732.5 mbsf the siltstones contain between 5% and 96% glauconite and may be massive, bioturbated, current laminated, or cross-bedded. Rip-up clasts are present at 841 mbsf. Zeolites of the clinoptilolite-heulandite family are an important component between 742 and 826.5 mbsf (up to 30% in Core 120-748C-64R), as are quartz and clear, untwinned feldspar (up to 10% of the sediment). Also appearing within this interval is an alteration product (possibly palagonite or devitrified ash), which increases downhole and makes up 5%–100% of some samples between 798 and 902 mbsf.

Siderite is present as burrow fills by 790 mbsf; it becomes more abundant downhole where it develops into concretions. Pyritized wood fragments, either disseminated within massive beds or concentrated along bedding planes, first appear downhole at 816 m and include some larger (2–4 mm) pieces. Although calcareous microfossils are conspicuously absent from this subunit below 711 mbsf, an unusual macrofauna consisting of serpulid worms and current-aligned bivalves are present at 843 m (Fig. 35).

Slickensided fractures with green sparry calcite fillings up to 1 cm thick are present in the basal 60 m. In Core 120-748C-78R, they occur as a conjugate pair.

Subunit IIIC: depth, 897.6–898.8 mbsf; basalt cobble conglomerate consisting of rounded, altered basalt cobbles and boulders, broken thick-walled mollusc fragments, and a matrix of glauconitic, calcareous siltstone; no baked contact evident, but sparry calcite veins common.

Unit IV: depth, 897.6–935.0 mbsf; altered basalt flow and underlying lithologies, undated but subdivided into two units.

Subunit IVA: depth, 898.8–902.2 mbsf; sparsely clinopyroxene and plagioclase phyric basalt, strongly weathered and altered.

Subunit IVB: depth, 902.2–935.0 mbsf; predominantly downhole cavings from Unit III plus some lithologies not encountered above. All of this material was recovered only as fragments in core-catcher socks or the BHA; no intact cores were retrieved. Lithologies not observed previously are (1) red and green smectitic clay with goethite and hematite stains; (2) brown smectitic clay with fine calcite and siderite veins; and (3) highly altered pieces of basalt with vesicles filled with alteration minerals.

Physical Properties and Heat Flow

Trends in index physical properties, plus changes in compressional wave velocity, allow the section at Site 748 to be divided into at least five geotechnical units, which correspond closely with the lithologic units and changes in key sedimentary components such as carbonate content. These units are:

Unit G1 (0–10.5 mbsf; equivalent to lithologic Unit I).

Unit G2 (10.5–~400 mbsf; equivalent to lithologic Unit II): wet-bulk density increases, water content decreases, porosity decreases, and compressional wave velocity increases beginning at ~180 mbsf.

Unit G3 (~400–~700 mbsf; equivalent to lithologic Unit IIIA): wet-bulk density has a convex trend whereas water content and porosity have concave trends; most striking, compressional wave velocity has a convex trend in nonsilicified sediment and decreases in silicified layers.

Unit G4 (~700–875 mbsf; equivalent to lithologic Unit IIIB): compressional wave velocity continues to decrease downhole.

Unit G5 (below ~875 mbsf): values vary widely without discernible trends.

The velocity inversion between ~400 m and 875 m is striking, and one not commonly observed in marine sediments. This trend corresponds to decreases in carbonate and biogenic silica contents, and an increase in clay content. It could result, therefore, from a general decrease in carbonate and silica cementation downhole and the consequent diminution of sediment rigidity.

Three downhole temperatures were measured using the Uyeda temperature probe at 85.6, 133.1, and 173 mbsf. An average geothermal gradient of 71.2°C/km and an average thermal conductivity of 1.27 W/m · K were used to calculate a mean value for heat flow equal to 90 mW/m^2. This plus the mean heat flow value of 61 mW/m^2 at Site 747 are much higher than the expected values for oceanic crust of Early Cretaceous age. Both sites lie less than 50 km from faults, and heat flow could be strongly influenced by tectonic and magmatic events that postdate the formation of the plateau. Circulation of fluids within the sediment, perhaps related to faulting, may also explain a downhole temperature inversion noted in the geothermal gradient (Fig. 54).

Seismic Stratigraphy, Depositional and Tectonic History

The two major reflectors, observed above basement at 0.41 and 0.83 s TWT on the seismic records at Site 748 are related to major changes in the lithology and physical properties. The seismic reflectors at 0.41 s (P1/K3 boundary) and 0.83 s (K2/K1 boundary) must be correlated with the tops of Subunits IIIA (389.1 mbsf) and IIIC (897.6 mbsf) or IVA (898.8 mbsf), respectively.

Subunit IIA is characterized by relatively uniform index properties and a constant compressional wave velocity of 1.54 km/s. Subunits IIA and IIB do not correspond to any obvious seismic reflectors. Due to very poor recovery, only a few velocity measurements were obtained for Subunit IIB; thus, the mean velocity cannot be calculated. Values increased from ~1.55 and ~2.00 km/s and reached values as high as 4.8 km/s in some places (e.g., chert). Since the bottom of Subunit IIB (389.1 mbsf) is clearly correlated with the seismic reflector at 0.41 s TWT (P1/K3 boundary), it is possible, assuming a mean velocity of 1.54 km/s for Subunit IIA, to calculate a mean compressional wave velocity of 2.37 km/s for Subunit IIB. This value is rather high, but it can be explained by the large proportion of chert.

The seismic reflector at 0.61 s TWT (K3/K2 boundary) can be correlated with the top of Subunit IIIB. On the basis of this correlation, the calculated mean velocities are 3.03 km/s for Subunit IIIA and 1.88 km/s for Subunit IIIB. These values are in good agreement with the measured compressional wave velocities of 2.9 km/s for Subunit IIIA and 1.90–2.20 km/s for Subunit IIIB. These results corroborate the unusual observed velocity inversion. Since basement at 0.92 s TWT was not reached and recovery was very poor, the mean velocity for Unit IV cannot be estimated. Based upon these correlations, a vertical velocity distribution model relating the different seismic sequences to the lithologic units has been established for the sedimentary column at Site 748 in the western Raggatt Basin (Fig. 61).

The basalt cored at 898.8 mbsf has compositional characteristics similar to intraplate, oceanic-island alkaline basalts and is believed to represent the last of a series of basalt flows that, for lack of core recovery, can only be inferred to lie within Subunit IVB. The Unit IV basalts are necessarily younger than those that form the true basement of the Raggatt Basin. These younger flows are strongly weathered, and some appear to be interlayered with siltstones and claystones derived from that weathering. Wood fragments, if in place, denote the development of soils and vegetation on some flows.

A further indication of the presence of organic matter in this subaerial or shallow subaqueous environment may be the presence of sideritic clay. The suspected presence of sediments interstratified with basalt flows plus the regional seismic analysis outlined above indicate that true basement (located at 0.92 s TWT) was not penetrated at this site, but lay 150–200 m below the TD of Hole 748C.

Beginning with the basal conglomerate of Subunit IIIC, the first unquestioned marine sediments deposited in this portion of the Raggatt Basin are glauconitic with up to 0.5% organic matter, denoting a restricted marine environment. The high-energy conditions that produced the conglomerate gave way to a more tranquil depositional environment, and upper Albian–Cenomanian silts began to accumulate. Current activity is evident, however, from the occasional cross-laminated sediments and rip-up clasts. Associated with these are a rare megafauna consisting of serpulid worms and delicate, current-oriented bivalves that, if in place, may suggest a shallow (inner-shelf depth?), low-energy environment of deposition.

The prevalence of alteration products (palagonite?) and the accumulation of iron-rich glauconite suggests subaerial weathering and erosion of basalt, which must have formed the margin of the restricted site of deposition. This land margin supported vegetation, as indicated by the terrestrial wood fragments, pollen, and spores, and it served as a source for the fine clastic sediments. The physical or ecological barriers that restricted the site of deposition were sufficient to exclude both the benthic foraminifer fauna and the calcareous pelagic fauna and flora that flourished at this time in the open marine waters beyond this site (e.g., at Site 738 drilled on Leg 119). This phase of deposition is interrupted by a significant hiatus with a disconformity suspected within the poorly recovered interval at about 692 mbsf. There is no record of Santonian or lower Campanian sediments at this site.

High glauconite contents characterize the remainder of Unit III as do total organic contents between 0.2% and 0.6% (maximum 1.0%). These are mostly type III hydrocarbons composed of terrestrial and highly oxidized marine organic matter. Datable calcareous microfossil assemblages appear at 711 mbsf and are soon followed upcore in Subunit IIIA by a host of invertebrates, whose skeletal remains incorporated in the sediment dramatically increased the proportion of carbonate preserved. Some fossils, such as coralline red algae and encrusting bryozoans, indicate periods of quite shallow-water deposition along banks or "reefs" (up to inner shelf environments). Most of the skeletal material has been fragmented and redeposited by wave action or currents. Nevertheless, the inoceramid remains, which compose up to 85% of some intervals, appear to be little affected by diagenesis and should provide reliable isotopic paleotemperature data. Some recovered vertebrate teeth belong to sharks and possibly to mosasaurs (giant swimming lizards).

Sedimentation rates in this shallow environment were high, up to 60 m/m.y., and easily kept pace with subsidence. Biogenic productivity was quite high in the shallow banklike environment represented by the carbonate section (Subunit IIIA), and compensated for the diminishing input of clastic sediments. In addition, siliceous sponges, radiolarians, diatoms, and silicoflagellates contributed abundant biogenic silica that was ultimately responsible for the silicified layers in Unit III. The amount of glauconite produced over the entire 500-m-thick Unit III section, however, is extraordinary, particularly in view of the high sedimentation rate. Because glauconite forms most abundantly in water depths between 50 and 200 m, this site of deposition was maintained close to such depths for an exceedingly long period of time (over 30 m.y.). The geographic extent of these deposits on the plateau and processes and paleoenvironmental

conditions that led to their formation are major unanswered questions raised by this discovery.

Mesozoic calcareous nannofossil and planktonic foraminifer assemblages have an even stronger austral affinity than those at Site 747 to the north. The incursion noted at Site 747 of transitional planktonic foraminifer and coccolith taxa during the Campanian is not recorded at Site 748 (e.g., *Quadrum trifidum, Q. gothicum,* and *Q. sissinghi* are absent). Sedimentation was apparently continuous from the late Campanian into the early Maestrichtian, but a portion of the middle Maestrichtian is missing. The uppermost Maestrichtian and Danian are also missing (hiatus = ~6–7 m.y.).

The Cretaceous/Tertiary hiatus corresponds to a widespread regional disconformity, noted as the prominent reflector at 0.41 s TWT below seafloor on our seismic records, and thought to mark a major tectonic and erosional event that affected much of the Kerguelen Plateau (i.e., see "Summary and Conclusions" in the Site 747 chapter and references therein). Subsidence of Site 748 following this erosional event was quite rapid, bringing the paleodepth of the site of deposition from 50–200 m during the late Maestrichtian to ~1000 m by the beginning of the late Paleocene.

As in the case of Site 747, this rapid subsidence may have occurred as a result of extensional tectonics and/or the dissipation of a thermal anomaly beneath the plateau. In the present case, the 77°E Graben lies 120 km west of Site 748; a smaller but similar feature lies just 25 km to the west (Fig. 2). These features were active during this late Maestrichtian tectonic event. In contrast to Site 747, however, we did not core any debris-flow sequences associated with this event.

The upper Paleocene through middle Eocene pelagic carbonate and chert sequence is apparently continuous and was deposited in water depths similar to the present day since subsidence had far outstripped the high sedimentation rate of 20 m/m.y. Regional seismic analysis shows that by Eocene times, the depocenter for the basin had shifted considerably toward the east as a consequence of the profound Maestrichtian tectonic event.

Full (100%) recovery in the upper 180 m of the section in Hole 748B provides an excellent Neogene calcareous-biosiliceous section with good paleomagnetic control that complements the one obtained at Site 747. The main elements of the magnetic polarity record from Anomaly Correlatives 1 to 18 (Pleistocene to late Eocene) have been recognized. Both the upper and lower epoch boundaries of the thick (65–70 m) Oligocene section are clearly defined by bio- and magnetostratigraphy (Anomaly Correlatives 6C and 13).

The striking occurrence of abundant angular quartz sand, heavy minerals, and micas within the lower Oligocene nannofossil ooze between Sections 120-748B-14H-1, 137 cm, to 120-748B-14H-2, 24 cm, was attributed by the shipboard scientists to ice rafting (Leg 120 Scientific Drilling Party, 1988). This interpretation has been confirmed by shore-based scanning electron microscope and energy-dispersive X-ray studies (Breza et al., 1988). These studies document fresh conchoidal fractures and surface textures on the quartz that indicate a glacial origin and the presence of a heavy mineral suite characteristic of metamorphic or plutonic source rocks rather than a suite derived from the devitrification of a volcanic ash. According to the planktonic foraminifer, diatom, and nannofossil biostratigraphy, the IRD interval can be dated between 35 and 36 Ma (between paleomagnetic Chrons 12 and 13).

The direct physical evidence of appreciable lower Oligocene IRD this far north of the Antarctic continent (the lowest latitudinal occurrence known) is highly significant and proves unequivocably, in our opinion, the existence of an early Oligocene ice sheet on the Antarctic continent at this time, a topic that until now has been strongly debated (see review by Wise, et al., 1985). To date, the strongest arguments for the existence of such an ice cap have been based on interpretations of the stable isotope records of the world's oceans (Matthews and Poore, 1980; Miller and Fairbanks, 1983, 1985; Keigwin and Keller, 1984; Shackleton et al., 1984; Wise et al., 1985; Miller et al., 1987).

Wise et al. (1985) discuss the probable location, mode of formation, and possible extent of such an ice sheet. The proxy evidence from the deep-sea stable isotope record has been bolstered by drilling along the margins of Antarctica where lower Oligocene tills and/or ice-rafted sediments have been dated in the Weddell Sea (Leg 113 Shipboard Scientific Party, 1987), Ross Sea (Barrett et al., in press), and Prydz Bay (Leg 119 Shipboard Scientific Party, 1988), which is located directly south of the Kerguelen Plateau. All of these occurrences indicate grounded ice at sea level, and it has been argued that the Weddell Sea and Prydz Bay occurrences necessitate the existence of an early Oligocene ice cap (Wise et al., 1987, and Leg 119 Shipboard Scientific Party, 1988, respectively).

On the other hand, it can be argued that all of these occurrences may indicate only local glaciation, perhaps of nearby highlands or mountains, and such an interpretation has been made for the Ross Sea occurrences (Leg 119 Shipboard Scientific Party, 1988). No such argument can reasonably be made for the occurrence of IRD at Site 748, which lies nearly 1000 km north of Prydz Bay. Ice rafting to localities this far removed from the Antarctic continent into waters that during the early Oligocene were probably warmer than those in the region today, must, in our opinion, have been supported by the presence of a continental ice sheet, however ephemeral and short lived its existence may have been.

Several minor hiatuses are present in the Oligocene, and parts of the lower and middle Miocene are missing (hiatus = ~1–3 m.y.). Major hiatuses are identified in the upper Miocene–lower Pliocene (~4.0–8.5 Ma) and in the middle Miocene (12–17 Ma). The Pleistocene is condensed and discontinuous. At other sites in the region, the diminution of carbonate in this part of the section corresponds with the deterioration of late Cenozoic climates. Site 748 is located some 900 km south of the present-day Polar Front, and only Antarctic microfossil assemblages are recorded through most of the Pliocene-Pleistocene sediments. Silicoflagellate assemblages point to an amelioration of climates during the early Pliocene, suggesting that the ancestral Polar Front may have migrated south of the site at that time.

These shipboard results indicate that this site, in conjunction with others cored on the plateau, will be quite valuable for paleoceanographic studies. Taking the Neogene together with the Paleogene and Cretaceous sequences, we have an essentially complete record of the events that highlight the evolution of this portion of the Raggatt Basin on the Southern Kerguelen Plateau.

In summary, the primary tectonic and depositional events recorded at Site 748 (see "Lithostratigraphy and Sedimentology," "Biostratigraphy," and "Sedimentation Rates" sections in this chapter) and derived from seismic stratigraphy (see "Seismic Stratigraphy" section, this chapter) can be outlined as follows:

1. Drilling results at Site 748 and from earlier dredging along the 77°E Graben (Leclaire et al., 1987a) indicates that the Southern Kerguelen Plateau basement consists of basalts erupted during Early Cretaceous times. The basalts are compositionally akin to other oceanic flood basalts and transitional MORB (T-MORB). In the western Raggatt Basin, this phase was followed by a series of apparently younger eruptions of lavas more closely related in composition to oceanic-island alkaline ("hot-spot") basalts. Strong subaerial or subaqueous weathering, and the possible development of vegetation and sediment accumula-

tions on some of these flows, apparently produced the interstratified sequence mapped in the central and western part of the Raggatt Basin as seismic Sequence K1, which in turn corresponds to lithologic Unit IV.

2. Subsidence of the western Raggatt Basin began by late Albian–Cenomanian times and allowed the accumulation of glauconitic, predominantly siliciclastic sediments in a restricted, shallow-water marine environment (seismic Sequence K2; lithologic Subunits IIIC and IIIB).

3. The onset of more open-marine, albeit shallow-water (inner- to outer-shelf depth) conditions apparently followed a prolonged Santonian–early Campanian hiatus. It caused an influx of calcareous planktonic faunas and floras and allowed benthic invertebrate communities to flourish. The rapid accumulation of skeletal carbonate debris compensated for the diminished input of detrital clastics, but the production of glauconite continued at a remarkably high rate. All of this accounts for a high sedimentation rate of about 35–45 m/m.y. for Unit IIIA sediments (equivalent to seismic Sequence K3), and their accumulation easily kept up with subsidence.

4. The first discernible break in sedimentation occurs in the Maestrichtian, where an early to middle Maestrichtian hiatus spans up to 5 m.y. This is followed by a disconformity between the upper Maestrichtian and upper Paleocene that spans at least 6 m.y. and corresponds to the major tectonic event that affects the entire Raggatt Basin and probably the entire Southern Kerguelen Plateau. Associated with uplift, erosion, volcanism(?), and rifting, this event saw the regional development of an irregular, "mounded" topography at the top of seismic Sequence K3. Also associated with this event is the uplift of basement 25 km west of Site 748 and the formation of the 77°E Graben 120 km to the west. Finally, extensional tectonics and related processes resulted in the rapid subsidence of Site 748 from 50–200 m in the Maestrichtian to ~1000 m by the late Paleocene, at a rate of about 150 m/m.y.

5. Pelagic sedimentation during the remainder of the Paleogene was nearly continuous at a rate of about 18 m/m.y., which balanced the slow subsidence rate. A possible hiatus of at least 2 m.y. in the middle Eocene could correspond with rifting to the north of the Northern Kerguelen Plateau and Broken Ridge (Munschy and Schlich, 1987).

6. Ice-rafted debris in the lowermost Oligocene corresponds to other drilling and geochemical evidence for the early Oligocene continental glaciation of East Antarctica and provides the most compelling evidence yet for such an event.

7. The low accumulation rate (4–6 m/m.y.) of dominantly nannofossil oozes of Subunit IIA above the chert horizons of Subunit IIB has been essentially continuous, except for a 1–3-m.y. hiatus in the middle Miocene, which probably corresponds to an oceanographic event. A similar explanation would account for the hiatus in the late Pliocene, which corresponds roughly with the onset of Northern Hemisphere glaciation, which in turn is probably linked to Antarctic glaciations.

REFERENCES

Alietti, A. 1972. Polymorphism and crystal-chemistry of heulandites and clinoptilolites. *Am. Mineral.,* 57:1448–1462.

Barker, P. F., Kennett, J. P., et al., 1988. *Proc. ODP, Init. Repts.,* 113: College Station, TX (Ocean Drilling Program).

Barr, F. T., 1970. The foraminiferal genus Bolivinoides from the Upper Cretaceous of Libya. *J. Paleontol.,* 44:642–654.

Barrett, P. J., Hambrey, M. J., and Robinson, P. H., in press. Cenozoic glacial and tectonic history of CIROS-1, McMurdo Sound. *In* Thompson, M.R.A., Crame, J. A., and Thompson, J. W. (Eds.), *Geological Evolution of Antarctica:* Cambridge (Cambridge Univ. Press).

Barron, J. A., Nigrini, C. A., Pujos, A., Saito, T., Theyer, F., Thomas, E., and Weinreich, N., 1985. Synthesis of biostratigraphy, central equatorial Pacific, Deep Sea Drilling Project Leg 85: refinement of Oligocene to Quaternary biochronology, *In* Mayer, L., Theyer, F., et al., *Init. Repts. DSDP,* 85: Washington (U.S. Govt. Printing Office), 905–934.

Belford, D. J., 1960. Upper Cretaceous foraminifera from the Toolonga Calcilutite and Gingin Chalk, Western Australia. *Bull. Bur. Miner. Resour., Geol. Geophys. Aust.,* 57:1–198.

Berggren, W. A., Aubry, M.-P., and Hamilton, W. N., 1983. Neogene magnetobiostratigraphy of Deep Sea Drilling Project Site 516 (Rio Grande Rise, South Atlantic). *In* Barker, P. F., Dalziel, I.W.D., et al., *Init. Repts. DSDP,* 72: Washington (U.S. Govt. Printing Office), 939–948.

Berggren, W. A, Kent, D. V., and Flynn, J. J., 1985a. Jurassic to Paleogene: Part 2, Paleogene geochronology and chronostratigraphy. *In* Snelling, N. J. (Ed.), *The Chronology of the Geological Record.* Geol. Soc. Mem. (London), 10:141–195.

Berggren, W. A., Kent, D. V., Flynn, J. J., and Van Couvering, J. A., 1985b. Cenozoic geochronology. *Geol. Soc. Am. Bull.,* 96:1407–1418.

Berggren, W. A., Kent, D. V., and Van Couvering, J. A., 1985c. The Neogene: Part 2, Neogene geochronology and chronostratigraphy. *In* Snelling, N. J. (Ed.), *The Chronology of the Geological Record.* Geol. Soc. Mem. (London), 10:211–260.

Berggren, W. A., and Miller, K. G., 1988. Paleogene tropical planktonic foraminiferal biostratigraphy and magnetochronology. *Micropaleontology,* 34:362–380.

Boyce, R. E., 1976. Definitions and laboratory techniques of compressional sound velocity parameters and wet-water content, wet-bulk density, and porosity parameters by gravimetric and gamma ray attenuation techniques. *In* Schlanger, S. O., Jackson, E. D., et al., *Init. Repts. DSDP,* 33: Washington (U.S. Govt. Printing Office), 931–955.

_____, 1977. Deep Sea Drilling Project procedures for shear strength measurements of clayey sediment using modified Wykeham-Farrance laboratory vane apparatus. *In* Barker, P. F., Dalziel, I.W.D., et al., *Init. Repts. DSDP,* 36: Washington (U.S. Govt. Printing Office), 1059–1068.

Breza, J. R., Wise, S. W., and Ocean Drilling Program Leg 120 Shipboard Scientific Party, 1988. Lower Oligocene ice-rafted debris on the central Kerguelen Plateau, ODP Leg 120: evidence for East Antarctica Continental Glaciation. *Geol. Soc. Am. Abstr. Programs,* 20(7):A69.

Chen, P. H., 1975. Antarctic radiolaria. *In* Hayes, D. E., Frakes, L. A., et al., *Init. Repts. DSDP,* 28: Washington (U.S. Govt. Printing Office), 437–513.

Ciesielski, P. F., and Weaver, F. M., 1974. Early Pliocene temperature changes in the Antarctic seas. *Geology,* 2:511–515.

Clement, B. M., Kent, D. V., and Opdyke, N. D., 1982. Brunhes-Matuyama polarity transition in three deep-sea sediment cores. *Philos. Trans. R. Soc., London, Ser. A,* 306:113–119.

Coffin, M. F., Munschy, M., Colwell, J. B., Schlich, R., Davies, H. L., and Li, Z. G., in press. Seismic stratigraphy of the Raggatt Basin, Southern Kerguelen Plateau: tectonic and paleoceanographic implications. *Geol. Soc. Am. Bull.*

Colwell, J. B., Coffin, M. F., Pigram, C. J., Davies, H. L., Stagg, H.M.J., and Hill, P. J., 1988. Seismic stratigraphy and evolution of the Raggatt Basin, Southern Kerguelen Plateau. *Mar. Pet. Geol.,* 5: 75–81.

Crough, S. T., 1978. Thermal origin of mid-plate hot-spot swells. *Geophys. J. R. Astron. Soc.,* 55:451–470.

Deroo, G., Herbin, J. P., and Huc, A. Y., 1984. Geochemistry of organic carbon in South Atlantic sediments from Deep Sea Drilling Project Leg 75. *In* Hay, W. W., Sibuet, J.-C., et al., *Init. Repts. DSDP,* 75: Washington (U.S. Govt. Printing Office), 983–1000.

Detrick, R. S., Von Herzen, R. P., Crough, S. T., Epp, D., and Fehn, U., 1981. Heat flow on the Hawaiian swell and lithospheric reheating. *Nature,* 292:142–143.

Drever, J. I., 1982. *The Geochemistry of Natural Waters:* London (Prentice-Hall).

Gieskes, J. M., and Peretsman, G., 1986. Water chemistry procedures on SEDCO 471—some comments. *ODP Tech. Note,* No. 5.

Gombos, A. M., Jr., and Ciesielski, P. F., 1983. Late Eocene to early Miocene diatoms from the southwest Atlantic. *In* Ludwig, W. J., Krasheninnikov, V. A., et al., *Init. Repts. DSDP,* 71, Pt. 2: Washington (U.S. Govt. Printing Office), 583–634.

Helby, R., Morgan, R., and Partridge, A. D., 1987. A palynological zonation of the Australian Mesozoic. *Mem. Assoc. Australas. Paleontol.,* 4:1–94.

Houtz, R. E., Hayes, D. E., and Markl, R. G., 1977. Kerguelen Plateau bathymetry, sediment distribution and crustal structure. *Mar. Geol.,* 25:95–130.

Jenkins, D. G., 1985. Southern mid-latitude Paleocene to Holocene planktic foraminifera. *In* Bolli, H. M., Saunders, J. B., and Perch-Nielsen, K. (Eds.), *Plankton Stratigraphy:* Cambridge (Cambridge Univ. Press), 263–282.

Keigwin, L. D., and Keller, G., 1984. Middle Oligocene climatic change from equatorial Pacific Site 77. *Geology,* 12:16–19.

Kennett, J. P., and Srinivasan, M. S., 1983. *Neogene Planktonic Foraminifera: A Phylogenetic Atlas:* Stroudsburg, PA (Hutchinson Ross).

Kent, D. V., and Gradstein, F. M., 1985. A Cretaceous and Jurassic geochronology. *Geol. Soc. Am. Bull.,* 96:1419–1427.

Lambe, T. W., and Whitman, R. V., 1969. *Soil Mechanics:* New York (Wiley).

Leclaire, L., Bassias, Y., Denis-Clocchiatti, M., Davies, H., Gautier, I., Gensous, B., Giannesini, P. J., Patriat, P., Segoufin, J., Tesson, M., and Wannesson, J., 1987a. Lower Cretaceous basalts and sediments from the Kerguelen Plateau. *Geo-Mar. Lett.,* 7:169–176.

Leclaire, L., Denis-Clocchiatti, M., Davies, H., Gautier, I., Gensous, B., Giannesini, P. J., Morand, F., Patriat, P., Segoufin, J., Tesson, M., and Wannesson, J., 1987b. Nature et âge du plateau de Kerguelen-Heard, secteur sud. Résultats préliminaires de la campagne "N.A.S.K.A.—MD48". *C. R. Acad. Sci., Ser. 2,* 304:23–28.

Leg 113 Shipboard Scientific Party, 1987. Glacial history of Antarctica. *Nature,* 328:115–116.

Leg 119 Shipboard Scientific Party, 1988. Early glaciation of Antarctic. *Nature,* 333:303–304.

Leg 120 Scientific Drilling Party, 1988. ODP at Kerguelen Plateau, Leg 120 explores origins and history. *Geotimes,* 33:12–16.

McRae, S. G., 1972. Glauconite. *Earth Sci. Rev.,* 8:397–440.

Matthews, R. K., and Poore, R. Z., 1980. Tertiary ^{18}O record and glacio-eustatic sea-level fluctuations. *Geology,* 8:501–504.

Miller, K. G., and Fairbanks, R. G., 1983. Evidence for Oligocene–middle Miocene abyssal circulation changes in the western North Atlantic. *Nature,* 306:250–253.

_____, 1985. Oligocene-Miocene global carbon and abyssal circulation changes. *In* Sundquist, E., and Broeker, W. S. (Eds.), *The Carbon Cycle and Atmospheric CO_2: Natural Variations Archean to Present:* Washington (American Geophysical Union). Geophys. Monogr. Ser., 469–486.

Miller, K. G., Fairbanks, R. G., and Mountain, G. S., 1987. Tertiary oxygen isotope synthesis, sea level history, and continental margin erosion. *Paleoceanography,* 2:1–19.

Munschy, M., and Schlich, R., 1987. Structure and evolution of the Kerguelen-Heard Plateau (Indian Ocean) deduced from seismic stratigraphy studies. *Mar. Geol.,* 76:131–152.

Nigrini, C. A., 1985. Radiolarian biostratigraphy in the central equatorial Pacific, Deep Sea Drilling Project Leg 85. *In* Mayer, L., Theyer, F., et al., *Init. Repts. DSDP,* 85: Washington (U.S. Govt. Printing Office), 511–551.

Parsons, B., and Sclater, J. G., 1977. An analysis of the variation of ocean floor bathymetry and heat flow with age. *J. Geophys. Res.,* 82:803–827.

Perch-Nielsen, K., 1979. Calcareous nannofossils from the Cretaceous between the North Sea and the Mediterranean. *Int. Union Geol. Sci., Ser. A,* 6:223–272.

_____, 1985. Mesozoic calcareous nannofossils. *In* Bolli, H. M., Saunders, J. B., and Perch-Nielsen, K. (Eds.), *Plankton Stratigraphy:* Cambridge (Cambridge Univ. Press), 329–426.

Petrushevskaya, M. G., 1975. Cenozoic radiolarians of the Antarctic, Leg 29, DSDP. *In* Kennett, J. P., Houtz, R. E., et al., *Init. Repts. DSDP,* 29: Washington (U.S. Govt. Printing Office), 541–675.

Pichon, J. J., Labracherie, M., Labeyrie, L. D., and Duprat, J., 1987. Transfer functions between diatom assemblages and surface hydrology in the Southern Ocean. *Palaeogeogr., Palaeoclimatol., Palaeoecol.,* 61:79–95.

Pujos, A., 1985. Cenozoic nannofossils, central equatorial Pacific, Deep Sea Drilling Project Leg 85. *In* Mayer, L., Theyer, F., et al., *Init. Repts. DSDP,* 85: Washington (U.S. Govt. Printing Office), 581–607.

Saito, T., 1985. Planktonic foraminiferal biostratigraphy of eastern equatorial Pacific sediments, Deep Sea Drilling Project Leg 85. *In* Mayer, L., Theyer, F., et al., *Init. Repts. DSDP,* 85: Washington (U.S. Govt. Printing Office), 621–653.

Schlich, R., 1975. Structure et âge de l'océan Indien occidental. *Mem. Hors Ser. Soc. Geol. Fr.,* 6:1–103.

_____, 1982. The Indian Ocean: aseismic ridges, spreading centers, and oceanic basins. *In* Nairn, A.E.M., and Stehli, F. G. (Eds.), *The Ocean Basins and Margins: The Indian Ocean* (Vol. 6): New York (Plenum Press), 51–147.

Schlich, R., Coffin, M. F., Munschy, M., Stagg, H.M.J., Li, Z. G., and Revill, K., 1987. *Bathymetric Chart of the Kerguelen Plateau.* [Jointly edited by Bureau of Mineral Resources, Geology and Geophysics, Canberra, Australia; Institut de Physique du Globe, Strasbourg, France; and Territoires des Terres Australes et Antarctiques Françaises, Paris, France.]

Schlich, R., Munschy, M., Boulanger, D., Cantin, B., Coffin, M. F., Durand, J., Humler, E., Li, Z. G., Savary, J., Schaming, M., and Tissot, J. D., 1988. Résultats préliminaires de la campagne océanographique de sismique réflexion multitraces MD47 dans le domaine sud du plateau de Kerguelen. *C. R. Acad. Sci., Ser. 2,* 305:635–642.

Sclater, J. G., Parsons, B., and Jaupart, C., 1981. Oceans and continents: similarities and differences in the mechanisms of heat loss. *J. Geophys. Res.,* 86:11535–11552.

Shackleton, N. J., Hall, M. A., and Boersma, A., 1984. Oxygen and carbon isotope data from Leg 74 foraminifers. *In* Moore, T. C., Rabinowitz, P., et al., *Init. Repts. DSDP,* 74: Washington (U.S. Govt. Printing Office), 599–644.

Shaw, C. A., and Ciesielski, P. F., 1983. Silicoflagellate biostratigraphy of middle Eocene to Holocene subantarctic sediments recovered by Deep Sea Drilling Project Leg 71. *In* Ludwig, W. J., Krasheninnikov, V. A., et al., *Init. Repts. DSDP,* 71, Pt. 2: Washington (U.S. Govt. Printing Office), 687–737.

Sissingh, W., 1977. Biostratigraphy of Cretaceous calcareous nannoplankton. *Geol. Mijnbouw,* 56:37–65.

Sleep, N., 1971. Thermal effects of the formation of Atlantic continental margins by continental breakup. *Geophys. J. R. Astron. Soc.,* 24: 325–350.

Sleep, N., and Snell, N. S., 1976. Thermal contraction and flexure of mid-continent and Atlantic marginal basins. *Geophys. J. R. Astron. Soc.,* 45:125–154.

Storey, M., Saunders, A. D., Tarney, J., Leat, P., Thirlwall, M. F., Thompson, R. N., Menzies, M. A., and Marriner, G. F., 1988. Geochemical evidence for plume-mantle interactions beneath Kerguelen and Heard Islands, Indian Ocean. *Nature,* 336:371–374.

Taylor, E., 1984. Oceanic sedimentation and geotechnical stratigraphy: hemipelagic carbonates and red clays [Ph.D. dissert.]. Texas A&M Univ., College Station.

Tissot, B. P., and Welte, D. H., 1984. *Petroleum Formation and Occurrence:* Berlin-Heidelberg-New York (Springer-Verlag).

Tjalsma, R. C., and Lohmann, G. P., 1983. Paleocene-Eocene bathyal and abyssal benthic foraminifera from the Atlantic Ocean. *Micropaleontol. Spec. Publ.,* 4:1–90.

Toumarkine, M., and Luterbacher, H., 1985. Paleocene and Eocene planktic foraminifera. *In* Bolli, H. M., Saunders, J. M., and Perch-Nielsen, K. (Eds.), *Plankton Stratigraphy,* Cambridge (Cambridge Univ. Press), 87–154.

Van Morkhoven, F.P.C.M., Berggren, W. A., and Edwards, A. S., 1986. Cenozoic cosmopolitan deep-water benthic foraminifera. *Bull. Cent. Rech. Explor. Prod. Elf-Aquitaine,* Mem. 11.

Von Herzen, R. P., and Maxwell, A. E., 1959. The measurement of thermal conductivity of deep-sea sediments by a needle probe method. *J. Geophys. Res.,* 65:1557–1563.

Watts, A. B., and Steckler, M. S., 1979. Subsidence and eustasy at the continental margin of eastern North America. *In* Talwani, M., Hay, W., and Ryan, W.B.F. (Eds.), *Deep Drilling Results in the Atlantic Ocean: Continental Margins and Paleoenvironment:* Washington (American Geophysical Union). Maurice Ewing Ser., 3:235–248.

Wise, S. W., Jr., Gombos, A. M., and Muza, J. P., 1985. Cenozoic evolution of polar water masses, southwest Atlantic Ocean. *In* Hsü,

K. J., and Weissert, H. J. (Eds.), *South Atlantic Paleoceanography:* Cambridge (Cambridge Univ. Press), 283–324.

Wise, S. W., Jr., Hay, W. W., O'Connell, S., Barker, P. F., Kennett, J. P., Burckle, L. H., Egeberg, P. K., Fütterer, D. K., Gersonde, R. E., Golovchencko, X., Hamilton, N., Lazarus, D. B., Mohr, B., Nagao, T., Pereira, C.P.G., Pudsey, C. J., Robert, C. M., Schandl, E., Spiess, V., Stott, L. D., Thomas, E., and Thompson, K.F.M., 1987. Early Oligocene ice on the Antarctic continent. *Geol. Soc. Am. Abstr. Programs,* 19:893.

Ms 120A-110

NOTE: All core descriptions forms ("barrel sheets") and core photographs have been printed on coated paper and bound as Section 3, near the back of the book, beginning on page 377.

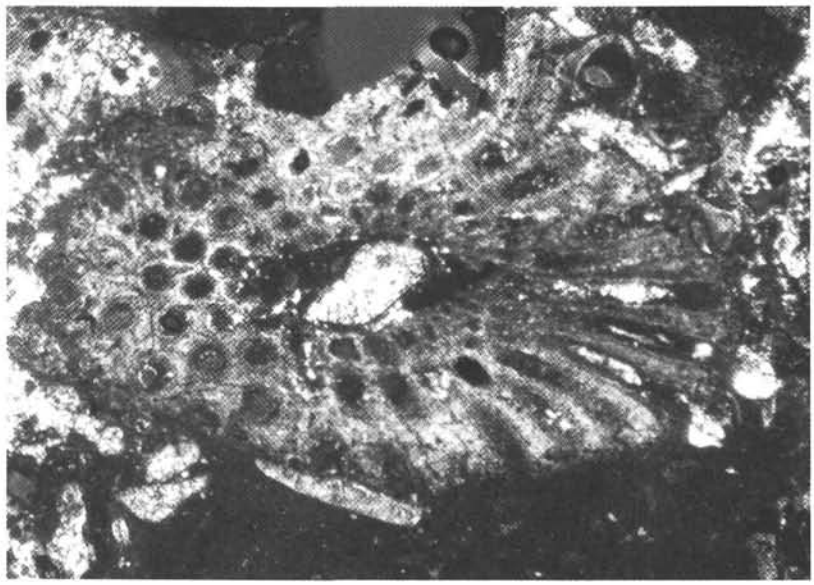

1

2

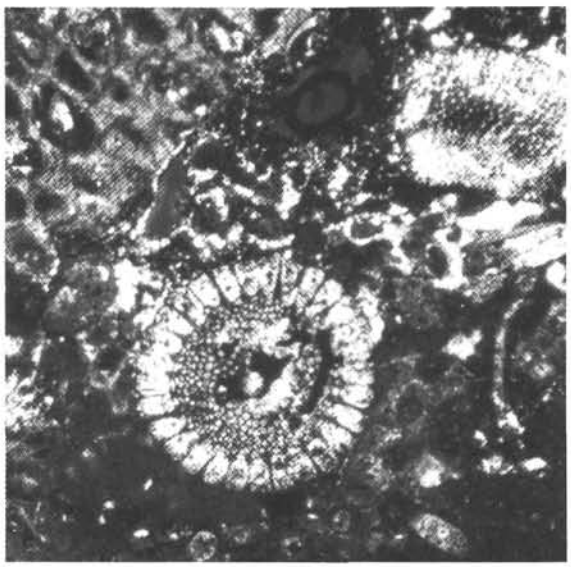

3

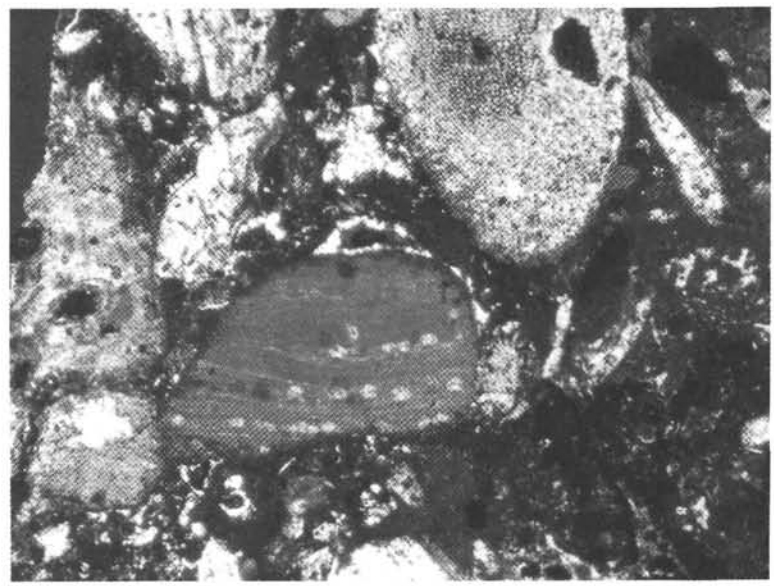

4

Plate 1. Sample 120-748C-32R-1, 32–38 cm. Thin sections of bioclastic packstone to rudstone with fragmented, densely packed bioclasts in a micrite matrix, partially silicified. Includes algal, echinoid, crinoid, and bryozoan fragments with some glauconite. Scale for each micrograph is 36× or 1 cm = 0.3 mm. **1.** Bryozoan with well-preserved rows of zooecia in cross nicols showing zones of partial silicification. **2.** Bryozoan zoaria section and an echinoid spine. **3.** Complex echinoid spine section. **4.** Fragment of coralline red algae showing rows of sporangia and dense cellular laminations. Micrograph also shows ovid section from a crinoid.

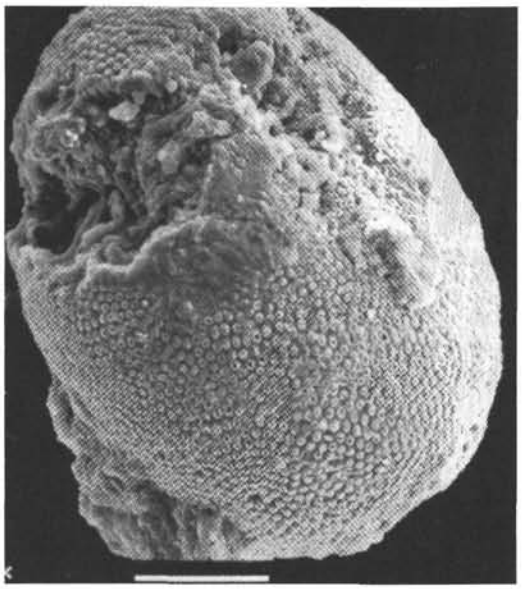

1

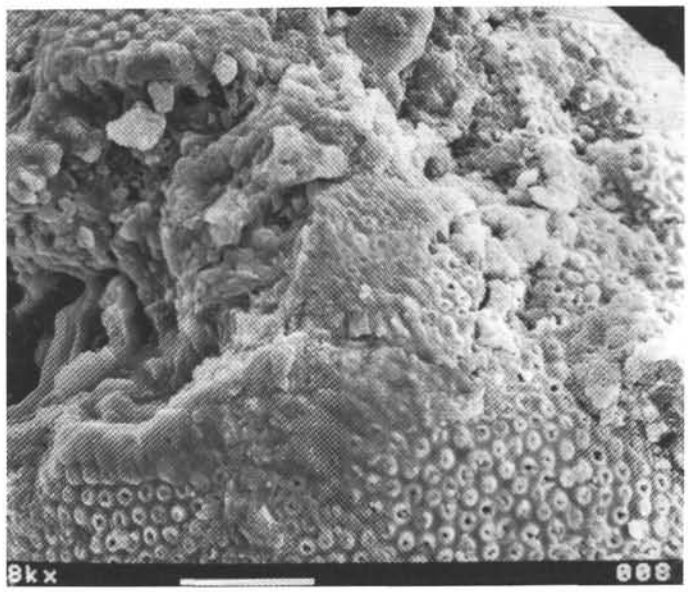

2

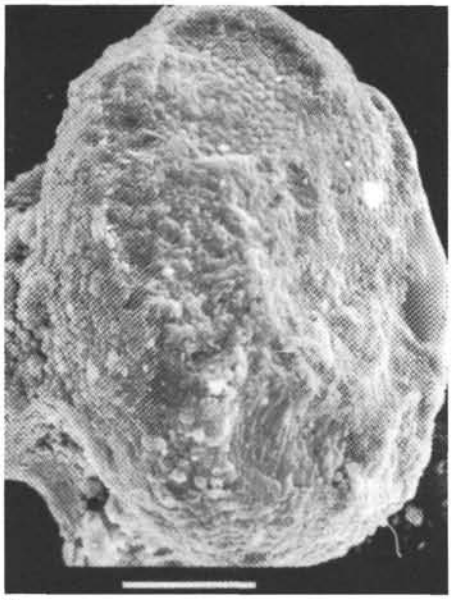

3

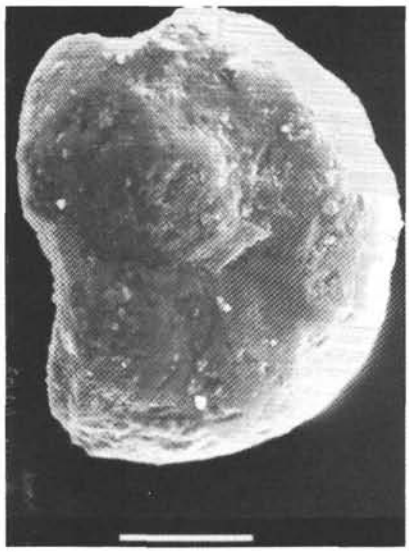

4

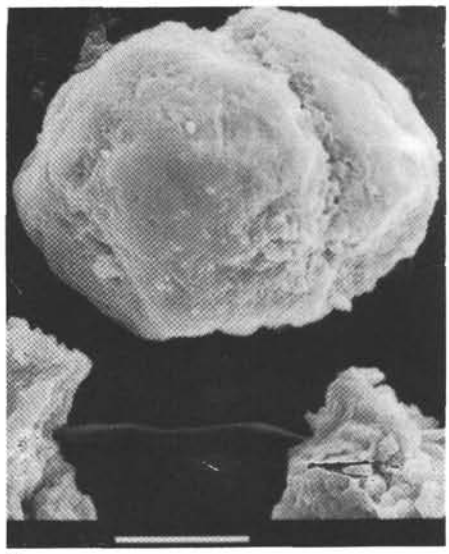

5

Plate 2. Sample 120-748C-47R-CC. Electron micrographs of sand-size siliceous particles that are common in Cretaceous cores from Site 748. **1.** Sterraster-type sponge microsclere with polyaxon having a spheroid surface and very short ray protrusions and internal radiating spine structures. Whole fossil replaced and filled with microcrystalline chalcedony. Scale = 300×, or bar = 0.06 mm. **2.** Close up of Plate 2, Fig. 1, at 558×, or bar = 0.035 mm. **3.** View of sterraster polyaxon microsclere mold with outer surface removed. Scale = 300×, or bar = 0.06 mm. **4, 5.** Chalcedonic molds from possible foraminifers. Scale for Fig. 4 = 840×, or bar = 0.020 mm; for Fig. 5 = 300×, or bar = 0.06 mm.